INVESTIGATION OF Ba, BaO, Sr AND SrO
PULSED LASER-INDUCED VAPOR PLUMES IN N_2,
O_2, MICROWAVE DISCHARGED O_2, AND VACUUM
AT LOW LASER FLUENCE

THESIS

David L. Byers, Captain, USAF

AFIT/GAP/ENP/96D-4

19970519 032

DEPARTMENT OF THE AIR FORCE
AIR UNIVERSITY
AIR FORCE INSTITUTE OF TECHNOLOGY

Wright-Patterson Air Force Base, Ohio

INVESTIGATION OF Ba, BaO, Sr AND SrO
PULSED LASER-INDUCED VAPOR PLUMES IN N_2,
O_2, MICROWAVE DISCHARGED O_2, AND VACUUM
AT LOW LASER FLUENCE

THESIS

David L. Byers, Captain, USAF

AFIT/GAP/ENP/96D-4

DTIC QUALITY INSPECTED 3

AFIT/GAP/ENP/96D-4

INVESTIGATION OF Ba, BaO, Sr AND SrO

PULSED LASER-INDUCED VAPOR PLUMES IN N_2,

O_2, MICROWAVE DISCHARGED O_2, AND VACUUM

AT LOW LASER FLUENCE

THESIS

Presented to the Faculty of the Graduate

School of Engineering Air Education and

Training Command In Partial Fulfillment

of the Requirement for the Degree of

Master of Science in Applied Physics

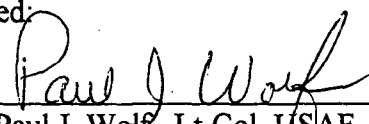David L. Byers, B.S.

Captain, USAF

October 1996

DTIC QUALITY INSPECTED 3

INVESTIGATION OF Ba, BaO, Sr AND SrO

PULSED LASER-INDUCED VAPOR PLUMES IN N_2,

O_2, MICROWAVE DISCHARGED O_2, AND VACUUM
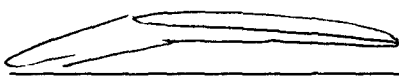
AT LOW LASER FLUENCE

David L. Byers, B.S.

Captain, USAF

Approved:

Paul J. Wolf, Lt Col, USAF
Chairman, Advisory Committee

27 NOV 96

Glen P. Perran, Maj, USAF
Member, Advisory Committee

27 Nov 96

David E. Weeks
Member, Advisory Committee

27 Nov 96

Acknowledgments

I would like to first thank my thesis adviser, Col. Paul J. Wolf, for the opportunity to work on an experimental thesis. His endless patience and encouragement when all looked hopeless are greatly appreciated. I would also like to express my gratitude to my committee members, Major Glen P. Perran and David E. Weeks, for their advice and support in troubleshooting the obstacles which continuously impeded progress in my laboratory work.

I am indebted to Dr. William F. Bailey for the numerous calculations made on the backs of his envelopes. I would also like to thank Jim Reynolds, Greg Smith, and Belinda Johnson for their assistance in building this project.

Most of all, I thank my wife for her tireless support in keeping the family together during these months of my nearly total absence. I apologize to my children for missing baseball and soccer games, school activities and other special times. I hope to make up for it in the coming year.

Finally, I am grateful to the Air Force for giving me this opportunity to expand my knowledge and advance my career.

David L. Byers

Table of Contents

List of Figures

AFIT/GAP/ENP/96D-4

Abstract

Ba, BaO, Sr and SrO were ablated by 248 nm laser pulses at fluences ranging from 270 $mJ-cm^{-2}$ to 575 $mJ-cm^{-2}$ in vacuum and in 25 mtorr atmospheres of N_2 , O_2 and microwave-discharged O_2. The spectral emissions of these plumes were compared for indications of ionization due to Ba or Sr collisions with each gas. The addition of a background gas increased the ion and neutral signature across the spectrum. SrO band emission was observed at 16,600-16,900 cm^{-1} and possible BaO band emissions were observed in the 18,250-18,400 cm^{-1}, 19,000-19700 cm^{-1} and 19,800-20,000 cm^{-1} regions. A screened plate ion probe was use to establish the ion content of the Ba plume. A time of flight study established low-pressure (1 to 35 mtorr) and low-fluence (40 to 160 $mJ-cm^{-2}$ relationships on Ba^+ velocity and population. Observed ion velocities ranged fron 3.1 km/sec. To 4.5 km/sec. Results indicate the addition of a background gas at pressures less than 25 mtorr quenches Ba^+ in the plume and retards the plume expansion.

INVESTIGATION OF Ba, BaO, Sr AND SrO PULSED LASER-INDUCED VAPOR PLUMES IN N_2, O_2, MICROWAVE DISCHARGED O_2, AND VACUUM AT LOW LASER FLUENCE

I. Introduction

1.1 Justification

As we reach out into space with satellites and even manned flight, we find we must have a thorough understanding of the relationships governing the physical and chemical processes in the vicinity of the spacecraft, especially in the ionosphere where most military and civilian space operations occur. To increase our knowledge, we continually test new theories to better use our technology and to further our capabilities.

On the March 1996 Space Shuttle mission, astronauts performed the Tethered Satellite System Reflight (TSS-1R) experiments testing the possibility of generating electricity by sweeping a stretched-out cable through the Earth's magnetic field. Although the experiment was cut short by a catastrophic failure of the cable (it broke causing the loss of the satellite), many important results

1

were obtained proving the feasibility of the system. Among the results, the astronauts observed that when the satellite's maneuvering thrusters fired, releasing a neutral gas into space, the potential of the satellite dropped several hundred volts accompanied by a sharp increase in current flow (NASA, 1996). NASA attributed this effect to the rapid ionization of the thruster gases near the satellite, creating a highly conductive plasma which acted as an additional current path.

The ionization processes creating this effect, though theorized and well studied in the laboratory, fail to explain, let alone predict, events occurring in the near-Earth region of space, the ionosphere.

1.2 Defining the Problem

Ionospheric experiments have attempted to prove these theoretical ionization processes , especially Alfven's critical ionization velocity hypothesis (Liou, 1995), yet the results don't give a definite "this is what's going on" answer. These experiments involve injecting Ba, Sr, and/or other elements as a vapor into the space environment from a rocket or satellite platform and looking at the resulting reactions by three methods: optically observing atomic emissions remotely, counting ions with a probe, and through

mass spectroscopy, the latter two of these methods requiring the instruments actually fly through the injected vapor (Lai et al., 1992). Ba is most often selected as one of the elements for these experiments because it is easily ionized and both Ba and its ion Ba^+ emit in the visible spectrum thus simplifying the problem of remote sensing (Bernhardt, 1992). Sr is also often used for the same reason.

One popular theory explaining the high Ba^+ counts observed in these tests is the charge exchange model

$$Ba + O^+ \rightarrow Ba^+ + O \qquad (1.1)$$

If this process is a dominant source for Ba^+, then the ionization rate should relate to the O^+ density. This doesn't occur (Stenbaek-Nielsen, 1993). Likewise, even higher Ca^+ counts should be observed due to the larger $Ca-O^+$ cross section but again, this is not the case.

Timothy M. Shadid attempted to give a complete accounting for the Ba^+ and Sr^+ counts from the G-1 and G-11b chemical releases from the Combined Release and Radiation Effects Satellite (CRRES), the latest of these space-based experiments, but found he could only partially explain the ions' source because many of the building blocks of the existing theories remain undiscovered (Shadid, 1995). The conditions for the two chemical releases were nearly the same; the differences being that the G-1 release was at 495

km altitude on the sunlit side of the dawn terminator and the G-11b release was at 478 km altitude on the dark side of the dawn terminator (Bernhardt, 1992). Shadid accounted for the Ba^+ in the sunlit region due to photo-ionization (Shadid, 1995), but found photo-ionization was not a major source of ionization of Sr in the sunlight (Shadid, 1995) and that cross sections were too small for both charge exchange and electron impact ionization to generate the ion counts (Shadid, 1995). Shadid did show that for cross sections on the order of 10^{-17} cm^2, charge stripping could explain the remaining ion counts (Shadid, 1995). He emphasized 'could' since charge stripping cross sections for Ba in ambient O were only theoretical ranging from 10^{-18} cm^2 to 10^{-16} (approximately the right size but no experimental results are available to back these numbers up) and no Sr in ambient O cross section were available.

Comparing the data of other CRRES releases, Wolf noticed an altitude dependence on ionization rates for Ba and Sr (1996b). Over the 200km depth of the ionosphere where this relationship held, the dominant atmospheric specie was atomic oxygen (O). He suggested that collisions with O may cause collisional ionization to occur resulting in the high ion counts. In searching the literature, no experimental data for Ba-O and Sr-O collisional cross sections has been published.

1.3 The Problem

The purpose of this thesis is to take a first look at
Ba-O and Sr-O collisional interaction at hyper thermal
energies to determine if collisional ionization can be
detected. The results of this study should answer yes or no
as to whether ionization of Ba and Sr is observed in
collisional interaction with O and should lead to a better
experiment design aimed at measuring the associated
ionization cross sections.

1.4 Background

From the start, Ba has been used in chemical release
experiments in the upper atmosphere and in space (Neynaber
et al., 1972) which has sparked some interest in Ba
reactions with atmospheric constituents. These studies
generally involve reaction with molecular species and not O
which is the dominant gas throughout most of the ionosphere.
The reason for the lack of data on O reactions is the
difficulty in maintaining a reliable source of O. Because
of the extremely reactive nature of O, it quickly reacts
with surfaces of tubing, chamber walls, etc. to either
oxidize the surface or recombine to form O_2 (the surface
providing the third body to remove the excess energy)
(Kaufman, 1961).

1.4.1 Collisional Cross Sections of Neutral-Ion Pairs

A merging beam experiment measured reaction cross sections of Ba with the atmospheric molecular ions O_2^+, N_2^+, and NO^+ (Neynaber et al., 1972). In the reactions

$$Ba + O_2^+ \xrightarrow{\quad k_1 \quad} BaO^+ + O \qquad (1.2)$$

$$Ba + N_2^+ \xrightarrow{\quad k_2 \quad} BaN^+ + N \qquad (1.3)$$

$$Ba + NO^+ \xrightarrow{\quad k_3 \quad} \begin{cases} BaO^+ + N \\ BaN^+ + O \end{cases} \qquad (1.4)$$
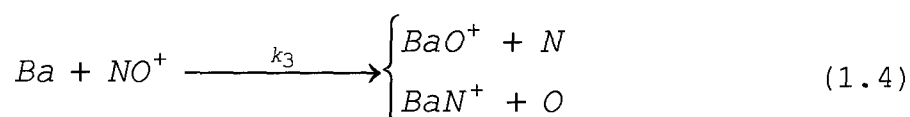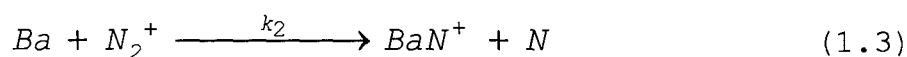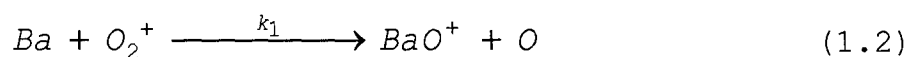
the relative cross sections were found at hyper thermal relative energies ranging from 0.1 eV to about 20 eV. The results showed that $\sigma_{O2} > \sigma_{NO} > \sigma_{N2}$ and that the cross sections decreased exponentially with increasing relative energy.

In another experiment, the reaction of Ba^+ with O_2 and H_2O was studied to better understand the transport mechanism of meteor metals from the ionsphere to the ground. The reaction

$$Ba^+ + O_2 \rightarrow BaO^+ + O \qquad (1.5)$$
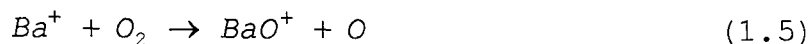
was found to have a threshold of about 0.4 eV (endothermic reaction) and the cross section for the reaction reached an

6

apparent maximum of about 10^{-16} cm^2 over a relative
collisional energy range of 3 to 7 eV.

In both of these experiments, one of the collision
partners was ionized to facilitate energy input to hyper
thermal energies. The bulk of information (over 95%) found
involved Ba collisionally reacting with O_2 in the process of
growing high-temperature-superconducting films. In these
experiments a target of yttrium(Y)-Ba-Copper(Cu)-oxide is
generally laser ablated or sputtered to form fast moving
vapor pulse which sprays a thin layer of these constituents
onto a surface. By repeating the process a film is grown
(Geohegan, 1994). Ablating in an ambient O_2 gas is a means
of incorporating more oxygen in the resulting film which
changes the conductive characteristics of the film. BaO
concentration in the plume is sometimes measured via
absorption spectroscopy to help determine the amount of
oxygen being taken up in the film (Blair et al., 1992).

1.4.2 Associative Ionization of Ba, Sr and Ca

The background research to set up this experiment
uncovered (with amazing luck in an unpublished document)
only one experiment actually involving Ba and Sr reacting
with O, specifically, Ba, Sr and Ca reactions with O and O_2^*
that result in associative ionization through the following
processes:

7

$$M + O \rightarrow MO^+ + e \qquad\qquad (1.6)$$

$$M + O_2 \rightarrow MO_2^+ + e \qquad\qquad (1.7)$$

$$MO_2^* + M \rightarrow (MO)_2^+ + e \qquad\qquad (1.8)$$

$$MO^* + M \rightarrow M_2O^+ + e \qquad\qquad (1.9)$$

where M is a metal atom (Ba, Sr or Ca) and N is a third body (Dyke, 1995). In this experiment a beam of Ba, Sr or Ca atoms at thermal kinetic energies (<0.2 eV) cross a beam of microwave discharged O_2 [a mixture of O, O_2 and O_2^* ($X^3\Sigma_g^-$, $a^1\Delta_g$)] and the products of reaction were observed with an ion mass spectrometer. The ion products observed were O^+, O_2^+, M^+, MO^+, M_2O^+ and $(MO)_2^+$. When the O was deactivated to find the reaction with only O^*, the ion signals were completely quenched to levels below the detection limits of the mass spectrometer for Sr and Ca reaction but not for Ba. For Ba reaction no change was observed in the ion signals.

Associative ionization, that of Equ. 1.9 in particular, has been suggested as a source of positive ion in the CRRES experiments and also in the CRIT 11 experiment, another ionosphere-based experiment involving the injections of Ba into the environment and looking for ionization products (Lai et al., 1992). Such molecular ions would be

indistinguishable in experiment since the ion probe used detects any positive charge.

1.4.3 Collisional Ionization

One form of collisional ionization is ion-pair formation as described quantum mechanically by the Landau-Zener-Stueckelberg (LZS) model discussed below. This model has been confirmed experimentally for alkali-halogen and alkali-O reactions (Baede, 1975). Dr. Paul Wolf postulates that this theory can be extended to alkali-earth metals to produce Ba^+ or Sr^+ (Wolf, 1996a).

The basis of this model is solving the time independent Hamiltonian wave equation

$$\hat{H}\Psi = E\Psi \tag{1.10}$$

can be simplified by applying the Born-Oppenheimer approximation to separate the relatively slow nuclear motion from the much faster electronic motions (Baede, 1975). Diagonalizing the resulting Hamiltonian matrix for a two-state system gives the solutions

$$E_1 = \tfrac{1}{2}\left\{ H_{11} + H_{22} + \left[\left(H_{22} - H_{11}\right)^2 + 4H_{12}^2\right]^{1/2} \right\} \tag{1.11}$$
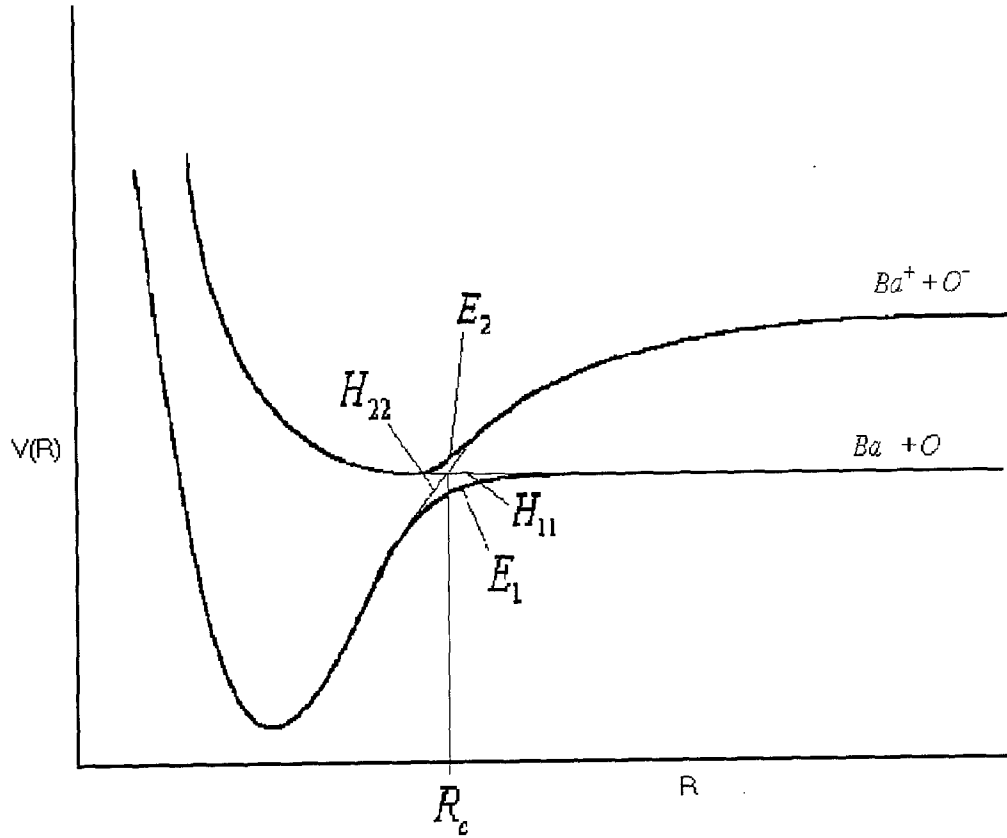
Figure 1. Potential curve of two adiabatic states (heavy lines) and the adiabatic states (thin lines) for Ba and O (Beade, 1975).

$$E_2 = \frac{1}{2} \left\{ H_{11} + H_{22} - \left[\left(H_{22} - H_{11} \right)^2 + 4H_{12}^2 \right]^{1/2} \right\} \tag{1.12}$$

where magnetic interaction is neglected such that H_{12} is equal to H_{21} (Baede, 1975) and

$$H_{ij} = \left\langle \varphi_i \left| H_{el} \right| \varphi_j \right\rangle \tag{1.13}$$

given φ_i is the electronic wave function of the ith state and H_{el} is the electronic Hamiltonian operator. If the wave functions are symmetric, then the off diagonal terms of the matrix are non zero and the potential curves described by E_1 and E_2 never cross (Landau and Lifshitz, 1981) giving rise to adiabatic states shown in Figure 1 as the heavy lines.

In the BO approximation, the terms involving the operation of the nuclear kinetic energy operator on the electronic wave functions were assumed to be very small and were thus neglected. Because they are non zero, diabatic states arise giving a transition path between the adiabatic states (Baede, 1975) shown in Figure 1 as the thin lines. The LZS model predicts the probability of the system transitioning between the adiabatic states.

In the approximation that H_{11} is a constant covalent potential between the neutral atoms and H_{22} is the coulombic potential between the ions, then the crossing distance, R_c, is given by

$$R_c = \frac{e^2}{\Delta E} \qquad (1.14)$$

$$\Delta E = I - EO \qquad (1.15)$$

where e is the charge of an electron, I is the ionization potential of Ba and EO is the electron affinity of O (Lacmann, 1980).

The LZS model assumes in the region $R \approx R_c$, the radial velocity, v_r, is approximately constant (over an extremely small distance v_r doesn't change much), the diabatic states are approximately linear with respect to R (thus linear with respect to time since v_r is approximately constant) and that H_{12} is approximately constant near R_c (Baede, 1975). These approximations give a transition probability of (Lacmann, 1980)

$$p = \exp\left\{ \frac{-2\pi H_{12}^2}{v_r \left| \frac{d}{dr}(H_{22} - H_{11}) \right|} \right\}$$
(1.16)

For a constant H_{11} and

$$H_{22} = \frac{-e^2}{R}$$
(1.17)

$$v_r = v\left(1 - \frac{b^2}{R_c^2}\right)^{1/2}$$
(1.18)

where v is the relative velocity of the atoms and b is the impact parameter,

$$p = \exp\left\{\frac{-2\pi H_{12}^2 R_c}{v}\left[1 - \frac{b^2}{R_c^2}\right]^{1/2}\right\}$$ (1.19)

This shows the transition probability increases exponentially as the collision velocity increases (Lacmann, 1980). Based on this theory, Wolf calculated an estimated Ba-O cross section of approximately 10^{-19} cm^2 at 10 eV, 5 x 10^{-21} cm^2 at 6eV, and 10^{-22} cm^2 at 3ev (Wolf, 1996).

A similar development can describe an atom-molecule collision but it is much more complex because the problem is no longer a two-body problem but a multi-body problem instead. An example of this might be (Lacmann, 1980)

$$Ba + O_2 \rightarrow Ba^+ + O_2 + e$$ (1.20)
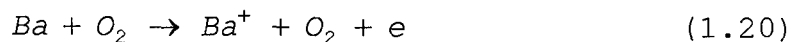
II. Experimental Methods

In this experiment, Ba- and Sr-based targets were laser ablated to generate plumes of high kinetic energy Ba and Sr atoms in a low pressure (1 to 25 mtorr) atmosphere of N_2, O_2 and microwave discharged O_2 with the goal of extracting collisional data on Ba + O and Sr + O. Since a microwave discharge only produces a fraction of O leaving a mixture of O and O_2 (discharged O_2), the O_2 background was to give information on Ba/Sr + O_2 collisional reactions which, when removed from the Ba/Sr + discharged O_2 results, would leave the Ba + O collisional interaction. N_2 was also used to compare the O_2 results with those of a relatively inert diatomic molecule to identify reactions specific to O_2.

2.1 Vacuum Chamber and Gas-Flow System

Figure 2 is a diagram of the plumbing system used in this experiment. The vacuum chamber in this experiment has a volume of approximately three liters. The pumping system, a Varian Turbo V80 vacuum pump with a Varian SD 300 forepump, is rated at 75 liters per second pumping speed and maintained chamber pressure at about 5×10^{-7} torr throughout the time of this experiment. In the chamber, an MKS 1.0 torr Baratron measured pressures down to 10^{-4} torr with the output displayed on an MKS Type 270 signal
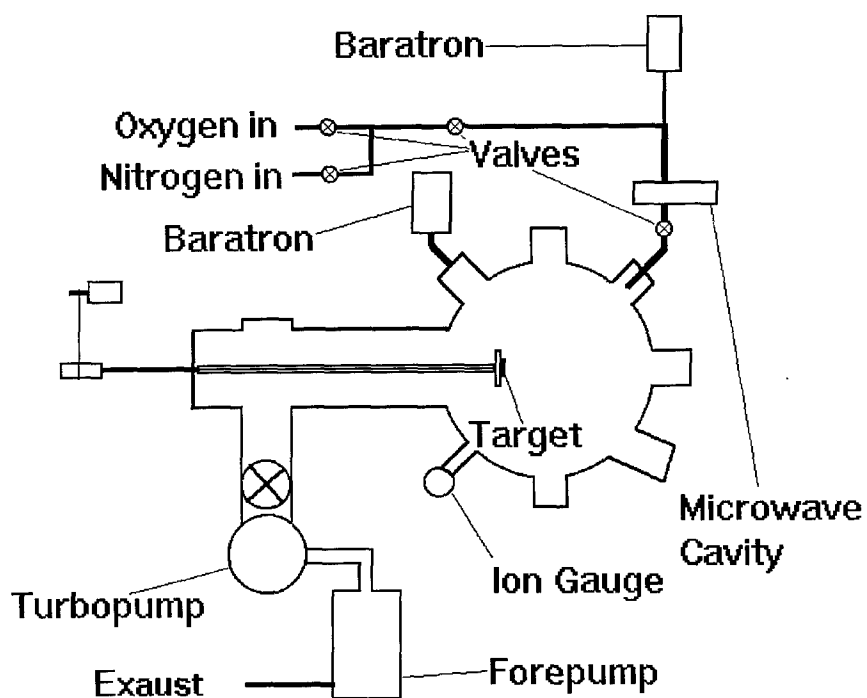
Figure 2. Diagram of experimental setup.

conditioner/display. Below this pressure, an MDC 432023 ion gauge with an IG4400 Ionization Gauge Controller provided the measurements. Additionally, a Teledyne Type DV-6M thermocouple vacuum gauge tube allowed monitoring of the fore line pressure.

The gas-flow system used a needle valve to control the flow of O_2 or N_2 into an Opthos Instruments microwave discharge cavity. The microwave discharge cavity generated the atomic oxygen in this experiment by discharging the O_2 before it flowed into the chamber. The typical discharge

had at least 70 watts of forward power and less than 2 watts

reflected power. To minimize deactivation of the O on metal

surfaces, a Teflon fitting connected the ceramic tube

running through the discharge cavity to the quartz glassware

valve, controlling the flow out of the discharge cavity and

into the vacuum chamber. The glassware valve in the wide

open position provided enough restriction to maintain a

pressure of 0.5 to 1.0 torr (ideal for the cavity operation)

in the discharge cavity while the chamber pressure remained

at or below 25 mtorr.

2.2 Determining the Flow Rates Through the Chamber

To understand the processes occurring in the vacuum

chamber it is necessary to know the flow rates into the

system. Flow rates were measured with a Unit Instruments

200 standard cubic centimeter per minute (sccm) flow meter

controlled by a Sierra Instruments Flow Box Controller.

This flow meter system was calibrated using a calibrated

flow meter, accurate to within 0.001%, at the Precision

Measurement Equipment Laboratory on Wright-Patterson AFB.

N_2 gas flowed through the flow meter which was connected in

series with the calibration instrument to compare their

readings. Consistent with the manufacturers' literature, the

resulting data fit was linear. A simple linear regression

resulted in the following expression for converting the Flow Box Controller output to a flow rate:

$$F = .113x + 2.53 \qquad (2.1)$$

where F is the flow rate in sccm and x is the output from the Flow Box Controller. This fit gives flow rates within 1.5 sccm of the calibration source flow rate which is much better than the manufacturer's warranty of 4% of full scale or 8 sccm.

Flow rates were then correlated with the associated chamber pressures to establish the relationship. Since the chamber pressure is dependent not only on the flow rate into the chamber and the pump capacity, but also the size of the exhaust lines, the pump efficiency, foreline pressure and a myriad of other factors, the relation is very complex and therefore the data was fit with a fourth order polynomial. Fourth order was chosen because it gave smooth, tight fit to the data and was well behaved at the end points. The fifth order polynomial had no significant overall improvement in fit and wasn't well behaved near the end points. The resulting polynomial regression is

$$F(p) = -5.187 * 10^{-7} * p^4 + 2.219 * 10^{-4} * p^3 - 0.03584 p^2 + 2.996 p - 0.9164$$

$$(2.2)$$

The regression gives an accuracy of 3.5 sccm at 12.5 mtorr but comparing the fit to the data, it looks good to within about 2.0 sccm.

A chamber pressure of 25.0 mtorr equates to a flow rate of 55 sccm or 0.917 scc per sec. At 25 mtorr, 0.917 scc would fill a volume of about 28 l. This suggests the pumping speed at 25 mtorr is only 28 l-sec^{-1} and the average residence time in the chamber is the pumping speed divided by the chamber volume or 0.107 sec.

2.3 Mounting and Positioning Ablation Targets Inside the Vacuum Chamber

Ablation targets (Ba, BaO, Sr and SrO) were epoxied with Torr Seal™ to copper disks cut to fit in a target holder. The target holder mounted on a mechanical feed-through in the vacuum chamber that allowed 15 cm of linear movement and rotation of the target. A 1 RPM motor was connected to the feed-through to rotate the target during the ablation process.

A Questek Series 2000 KrF Excimer laser provided 50 to 300 mJ, 28 nsec pulses at a wavelength of 248 nm that were focused on the targets to generate ablation plumes.

A HeNe laser was used to align the optics by centering and leveling the beam on the windows of the chamber. The

lenses, mirrors and spectrometer were then centered on the beam. The target mounted in the chamber was moved forward until half of the HeNe laser beam was blocked by the target. The length of the feed-through arm was measured and set as the reference or target zero position. The target position was then determined by subtracting the reference length from the length of the arm. Likewise, the ion probe position was set by moving it forward until it just touched the target at the zero position and the length of the rod sticking out of the chamber was recorded as the reference.

2.4 Determining Laser Fluence on the Target

The characterization of the ablation plume (neutral atom density, ion density, population of excited states, temperature, etc.) is strongly dependent on the fluence of the laser pulse (Nishikawa, 1994). Assuming the laser beam has uniform intensity, dividing the total energy available on target by the area of the laser spot on target determines the fluence of the ablation laser pulse.

The total energy output of the Excimer laser was measured with a Ophir model PE-50-S-BB power meter connected to a LeCroy 9450A digital oscilloscope. The peak voltage of 20 pulses (averaged together) was divided by the power meters conversion factor, 1.867 V/J, to give the laser
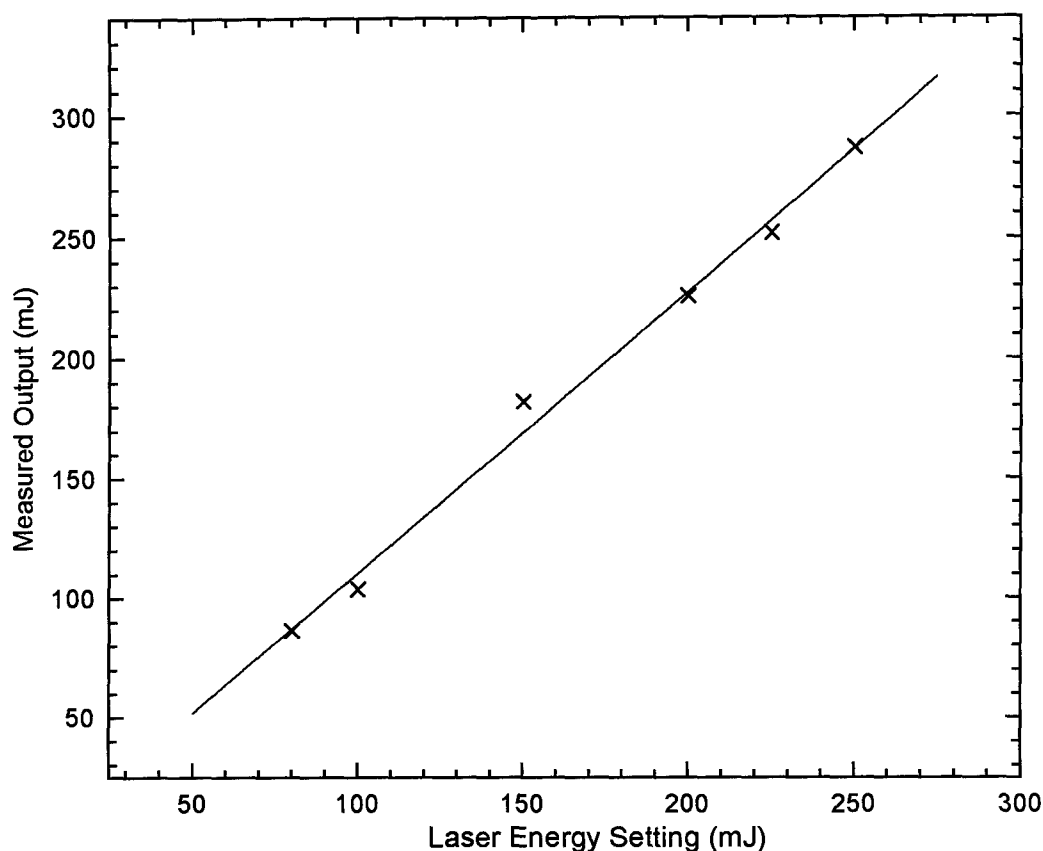
Figure 3. Laser output calibration curve to correlate the
laser energy setting with the actual output pulse energy. A
linear regression resulted in the relation
"output" = 1.77 x "setting" - 6.64 mJ.

output. Figure 3 shows a comparison of the laser's

indicated output with the actual power measured.

To create a uniformly shaped beam, the laser beam

passed through an aperture, clipping it to 1.06 cm x 2.17 cm

and was focused onto the target by an ARC100-02-1000 (1 m

focal length) lens and a KRF-1537-45 UNP UV-coated mirror.

A MgF window passed the ultraviolet (UV) light into the

vacuum chamber. Losses due to the window, mirror and lens amounted to only 14% whereas the aperture reduced the cross-sectional area of the beam, and thus the power on target, by 60%. Additionally, a Ba film slowly deposited on the inside of the chamber window further reducing the transmission of the laser pulse. The change in transmittance over approximately 25,000 shots was 13%. It is assumed that most of this deposition occurred during the spectral runs since the fluence was much higher than during the ion probe runs. To compensate, the fluence was reduced an additional 13% during the ion probe measurements. In this thesis, it is therefore assumed that 34% of the original laser energy reached the target during the spectral data runs and 30% during the ion probe runs.

An UV-sensitive paper was placed in the chamber at 2.72 cm from the target zero position to measure the spot size on target. The lens was positioned at a point on a rail designated as 20 cm (a metric scale was taped to the rail to give a relative reference position). The laser pulses were then projected onto the photo sensitive paper making an image of the laser spot. This process was repeated at 5 cm intervals along the rail. The dimensions of these laser spots were measured with a vernier caliper and multiplied to get the area. Defining x as the sum of the relative lens

position and the target position, a least squares fit of the reciprocal of the area with x gives

$$k(x) = 0.00176x^2 - 0.0264x + 1.38 \qquad (2.3)$$

The fluence on the target as a function of x, becomes

$$\varphi(x) = \tau k(x) E_L \qquad (2.4)$$

where τ is a system transmission coefficient (equal to 0.34 or 0.30) and E_L is the output energy from the laser.

As the target is moved inside the chamber, the lens is moved proportionally to maintain a relatively constant path length between the target and lens and thus a constant fluence on the target.

As the target moves farther away from the mirror, the angle of incidence of the laser beam, measured from the target normal, decreases reducing the area and thereby increasing the fluence. Over the full range of target positions, the angle of incidence changed not more than 1.5 degrees thereby changing the spot size and fluence up to 1.7%. Moving the lens in increments of 1.06 cm instead of 1.0 cm for each 1.0 cm the target moves would compensate for the increased fluence but was beyond the lens position tolerance limit of 0.2 cm. The lens was moved in even 1.0

22

cm increments ignoring this small correction factor thus introducing a small systematic error in the results.

2.5 NO Titration to Determine the Presence of Atomic Oxygen in the Chamber.

An NO titration was employed to determine if O atoms, produced in the microwave cavity were present in the vacuum chamber. The reactions occurring in the titration are

$$O + NO \xrightarrow{k_1} NO_2 + h\nu \qquad (2.5)$$

$$O + NO + M \xrightarrow{k_2} NO_2 + M \qquad (2.6)$$

$$O + NO_2 \xrightarrow{k_3} O_2 + NO \qquad (2.7)$$
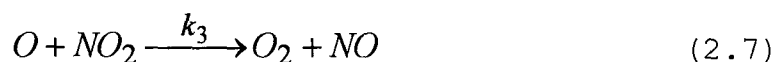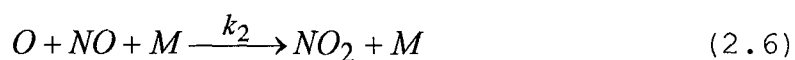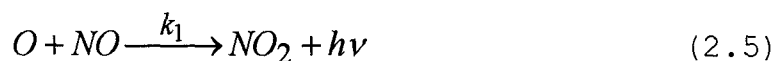
where k_1 = 2.5x10^{-17} cm^3-sec^{-1} , k_2 = 6.90x10^{-32} cm^6-sec^{-1} , and k_3 = 3.5x10^{-13} cm^3-sec (Kaufman, 1961). The associated rate equations are

$$\frac{d[O]}{dt} = -k_1[NO][O] - k_2[M][NO][O] - k_3[NO_2][O] \qquad (2.8)$$

$$\frac{d[NO]}{dt} = -k_1[NO][O] - k_2[M][NO][O] + k_3[NO_2][O] \qquad (2.9)$$

$$\frac{d[NO_2]}{dt} = k_1[NO][O] + k_2[M][NO][O] - k_3[NO_2][O] \qquad (2.10)$$

$$\frac{d[O_2]}{dt} = k_3[NO_2][O] \qquad (2.11)$$

$$I \propto k_1[NO][O] \qquad\qquad (2.12)$$

where I is the observed intensity of the emission due to the radiative combination reaction (Kaufman,1961) of Eqn (2.5). Integrating Eqn (2.8) gives

$$[O]=[O]_0 \exp\left\{\left[-\left(k_1 + k_2[M]\right)[NO] - k_3[NO_2]\right]t\right\} \qquad (2.12)$$

Since k_3 is much greater than both k_1 and $k_2[NO]$, the reaction of Eqn (2.7) is much faster than that of both (2.5) and (2.6). Assuming it occurs immediately after an NO_2 molecule is formed, Eqn (2.12) simplifies to

$$[O]=[O]_0 \exp\left[-2\left(k_1 + k_2[M]\right)[NO]t\right] \qquad (2.13)$$

In this experiment $[M] \sim [O_2] \sim 10^{15}$ cm^{-3} (assuming only a small fraction of O is generated). If $[NO] = [O_2]$, then (2.13) is

$$[O] = [O]_0 \exp\left[- 0.19t\right] \qquad\qquad (2.14)$$

and the e-folding time is over 5 sec. Ideally, in a titration, if the reaction occurs in a limited space such that the photo emissions from the initial mixing of NO with O to the point where nearly all the O is reacted away, then the peak in the emissions occurs when [NO] added to the system equals [O] in the system and [O] is measured by metering the NO flow rate. Since the flow through the chamber replaces the atmosphere in about 0.1 sec., this

reaction is far too slow and most of the reactants are pumped out of the chamber before having a chance to react. Therefore in this experiment, the titration indicated only the presence of O in the chamber and gave no indication of [O].

The photo emission was observed with a photo-multiplier tube (PMT) and measured with respect to the NO flow rate. Typical PMT currents observed were 250 nA to 400 nA above dark current (-1nA). Two additional tests were performed to ensure the photo emission was due to Eqn. 2.5 and not some other reaction involving O_2 or an excited state of O_2 (O_2^* is also generated in the microwave discharge). The first was to shut off the microwave discharge cavity while the photo emission was maximum. The photo emission extinguished almost immediately proving that the emissions were a result of a reaction with a product from the microwave cavity (O or O_2^*). In the second test, silver wool was placed in the tubing between the microwave cavity and the chamber to absorb any O generated and pass O_2 and O_2^* into the chamber. In this second test, the PMT current increased only 0.3 nA above the dark current thus showing that O was responsible for the emission by reacting with NO.
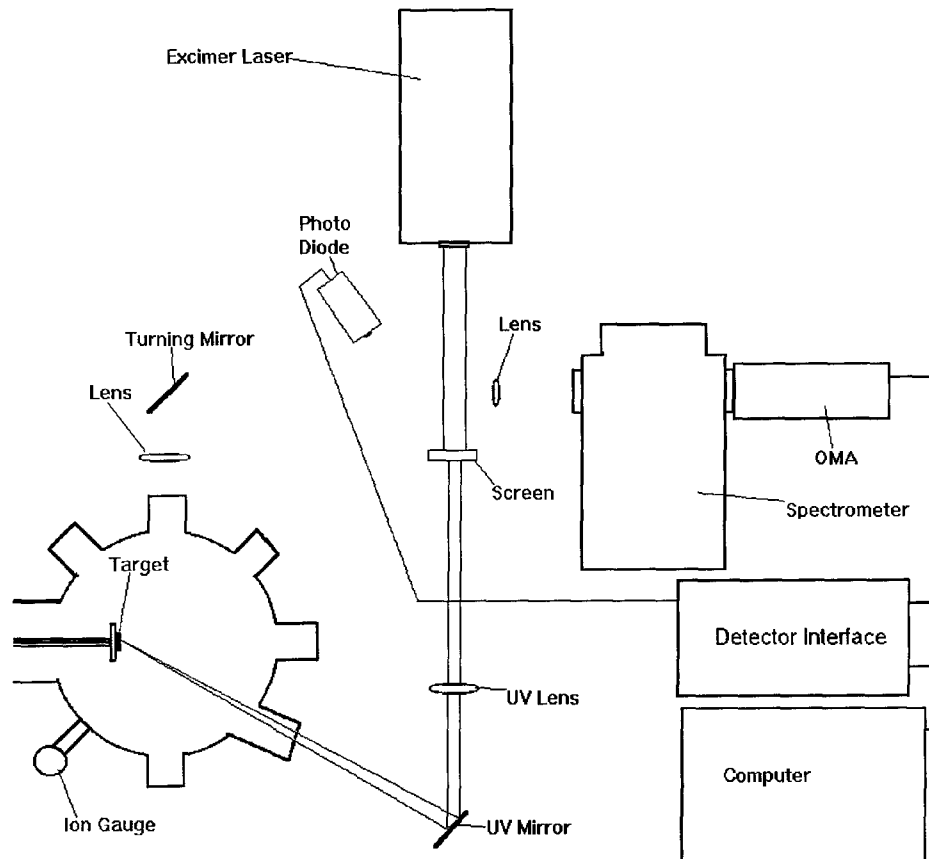
Figure 4. The experimental setup to observe spectral emissions from the plume.

2.6 Setup for Observing Ablation-Plume Emission and

Measuring the Plume Ion Densities

Figure 4 shows the spectrometer setup. The spectral

emissions of the plume were observed with an EG&G Parc model

1420 Intensified Silicon Photo diode array detector (Optical

Multichannel Analyzer or OMA) on an ARC Spectra Pro 500, 0.5

meter spectrometer. The OMA interfaced to a 486 computer

through a 1461 Detector Interface for output. The spectral

information was time-integrated over 16.6 msecs, much longer than the duration of the plume, and thus temporal spectral data wasn't available. Emissions from the plume were collected by a 2" (f/4.0) lens turned by a mirror and focused on the spectrometer slit by a 1" (f/6.9) lens (matching the spectrometer's (f/6.9) optics). The turning mirror used to collect the BaO and SrO spectra was a rear-surface-coated glass mirror thus limiting the shorter wave length spectra to about 400 nm. For collecting the Ba and Sr spectra, a UV Al coated mirror with a band reflectivity of 250-600 nm was used, allowing spectral data below 400 nm. Spectra was obtained above 600 nm for Ba and Sr but the response of the mirror above 600 nm is assumed to be below 50% thus decreasing the observed signal. Spectra were obtained at 20 nm intervals from 320 nm to 800 nm for Ba and Sr and from 400 nm to 780 nm for BaO and SrO. Each interval or display contains about 28 nm of spectral data. The spectrometer slit width was 100 nm and gave a minimum resolution of about 0.3 nm determined by observing the Hg 365.02 nm and 365.48 nm lines and the Ne 534.11 and 534.33 nm lines. Spectra from 120 laser shots were summed at laser repetition rates of 2 to 5 shots per second to improve the signal-to-noise ratio.
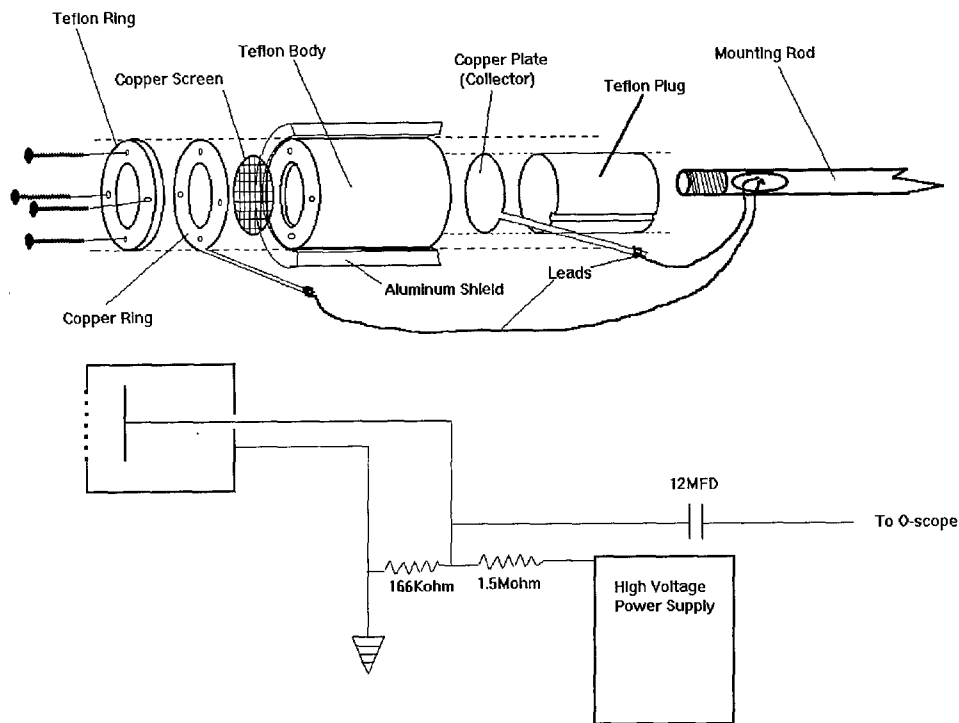
Figure 5. Exploded diagram of the ion probe along with a schematic of the bias circuit.

To supplement the spectral information, a screened plate ion probe, shown in Figure 5, patterned after one used by D.N. Mashburn and D.B. Geohegan to study laser-ablation plume dynamics in thin film deposition experiments (Mashburn, 1989), was used to determine time of flight (TOF) and ion content in the plume. The probe housing is machined out of Teflon, the plate and screen are of copper and the outer shield is of aluminum. Once assembled, the entire structure except for the opening was wrapped in Teflon tape
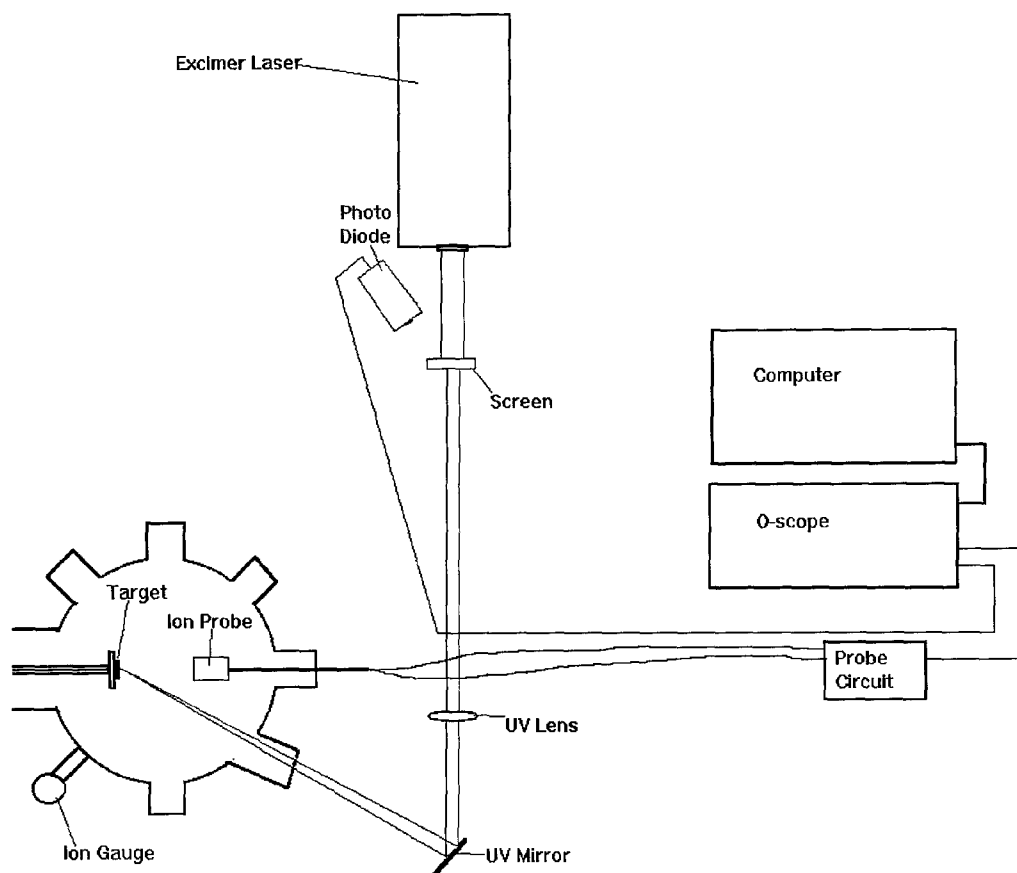
Figure 6. Diagram of the lab setup for collecting data with the ion probe.

to minimize erroneous signals caused by the electrical

connectors collecting free electrons and ions in the

chamber. The probe was mounted on an 8-inch piece of 1/4"

stainless steel tubing through which electrical wires were

run to connect to the probe. This was sealed with Torr Seal

to prevent air leaks into the chamber. The tubing fit

through a Cajon fitting on a face plate on the chamber with

the excess tubing protruding out of the chamber. This setup

allowed the probe to be pushed forward into the chamber

(closer to the target) or pulled out (away from the target) without breaking the vacuum in the chamber. A negative bias was maintained on the collector by a Stanford Research Systems PS-325 low-noise, high-voltage power supply stepped down across a 10 to 1 voltage divider. A 12 MFD feed-through capacitor isolated the oscilloscope from the power supply. The resulting large RC time constant (18 sec) between the ion probe and the power supply blocked virtually all the AC ion probe signal from feeding back into the power supply while the short RC time constant (0.6 msec) between the probe and the o-scope set on 50Ω input impedance readily passed 1 Mhz signals.

The collector has an effective area of 1.06 cm^2 (area of the collector minus the area covered by the screen wires) and is 2 mm away from the screen. The target-to probe distance is defined as the distance between the target and the collector. Data was obtained in this experiment at target-to-probe distances of 3.0 cm to 8.0 cm with typical fluences of about 75 $mJ-cm^{-2}$.

III. Discussion of Ion Probe and Spectral Data

3.1 Ion Probe Results and Analysis

The purpose for using the ion probe was to quantify the characteristics of the ablation plume. To determine the optimum bias to apply to the collector of the probe, voltages of -10 to -160V were applied in 10V increments. The amplitude of the peaks is plotted in Fig. 7. The initial explanation of Fig. 7 was that as the negative bias increased, more of the electrons were swept out of the plume until they were all removed thus the curve levels off. This would leave only the ions to be detected by the probe. Then as the bias further increased, secondary-emission electrons from the impacting ions would be swept away causing the signal to increase again. Accordingly, the bias was set at -120V, a point where all ions are collected but secondary electrons are not repelled from the plate. Now take a step back and look at the big picture. How many 90 eV electrons are generated in the ablation process? Not many! In fact, the electrons energies are expected to be less than or equal to the energies of the Ba^+ in the plume (less than 10 eV for Ba^+ as calculated in the next section). If this is the case, why does the signal continue to increase, what story
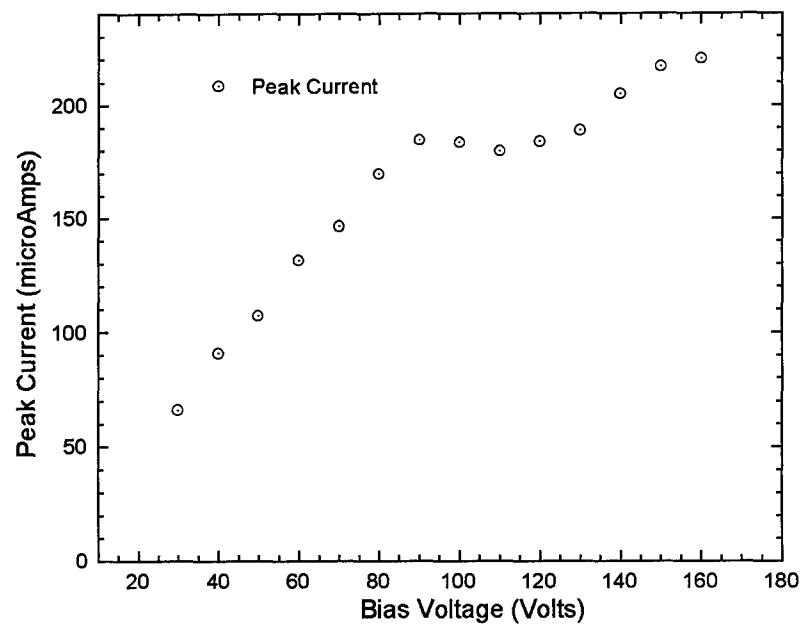
Figure 7. A plot of the ablation-plume peak current verses the ion probe screen to plate bias voltage.
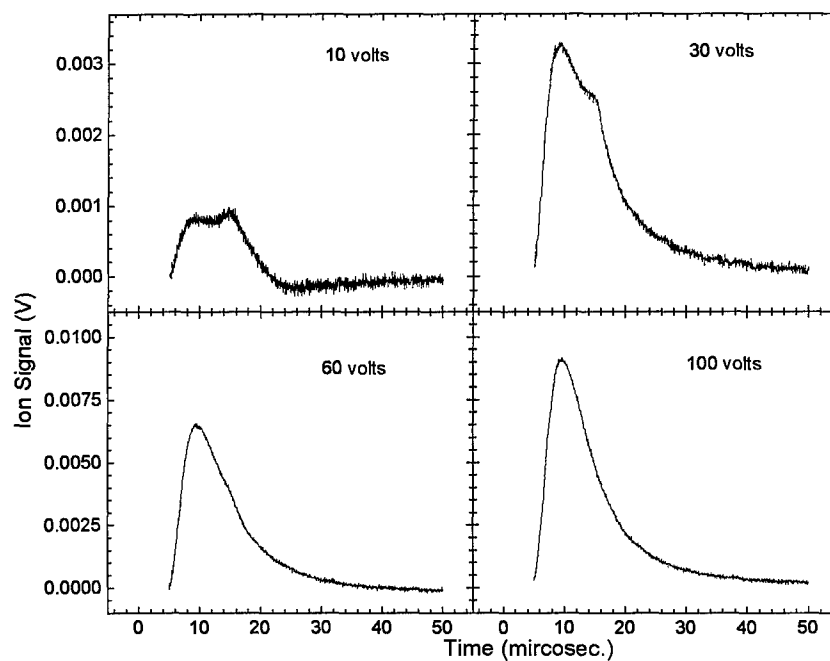
Figure 8. Ion probe signals obtained with voltages ranging from -10 to -160 V on the collector.

is the probe really telling and what is the optimum bias to interrogate the ablation plume? Looking at Fig. 8, a lot of structure stands out at potentials below 60V. It is beyond the scope of this thesis to perform and in-depth study to determine the optimum bias for this probe. In this experiment, -120V was used for all the tests with the knowledge that the quantitative results may have an undetermined systematic error.

Fig. 9 shows the ion probe output at 5.0 cm from the target in vacuum. This shows a good fit to the Maxwell Boltzmann distribution expressed as

$$n(t) = At^{-4} \exp\left(\frac{m}{2k_bT}\left(\frac{d}{t} - u_0\right)^2\right) + B \qquad (3.1)$$

for $n(t)$ defined as the ion density observed at time t, A is a constant of proportionality, B is an arbitrary constant that set the zero line for the function, m is the ion mass, d is the target-to-collector distance, k_6 is Boltzmann's constant, T is temperature and u_0 is the center of mass velocity (Nishikawa, 1994).

A, B, T and u_0 were variable parameters in the fitting process and the results are plotted as the thin solid line in Fig. 9. The results of this fit gave a temperature of 8600K. At high laser fluence, the ion probe response
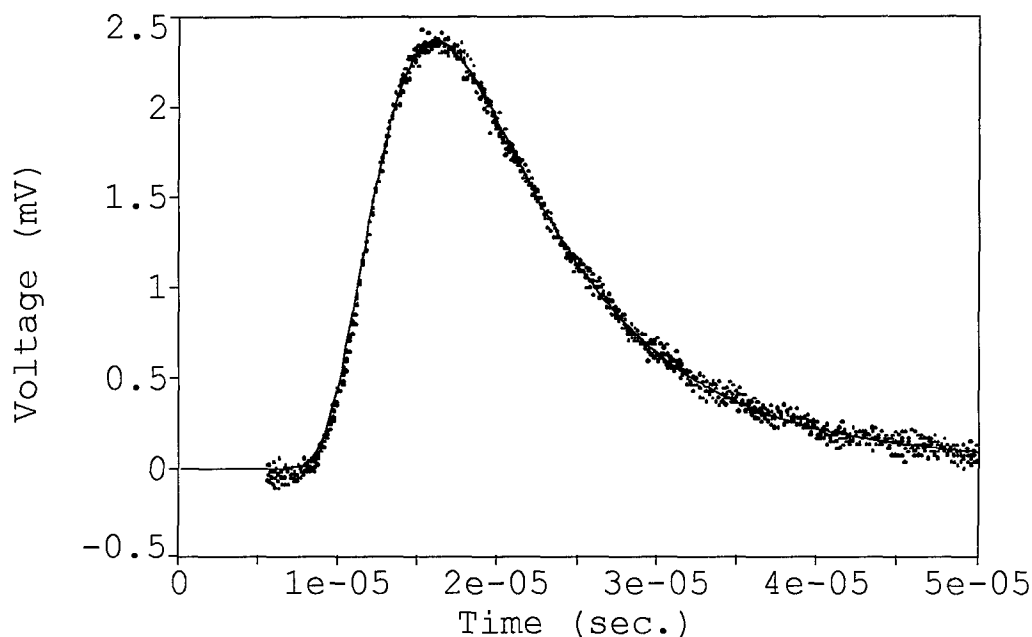
Figure 9. Ion probe signal at 5.0 cm from the target in a vacuum.

was no longer peaked as shown in Fig. 9 but instead the top

was flattened by high plasma densities saturating the probe

(Witanachi, 1996). Low laser fluence (less than $150mJ/cm^2$)

was used to prevent ion probe saturation. The effects of

pressure on the time of flight procedures were performed

five times establishing a small sample from which an

estimate of error could be determined. The error bars in

the following plots were determined by dividing the

amplitude and standard error by the average amplitude at

each given distance. This resulted in a uniform average

value of 1.0, a variance of 0.09, and a standard error of
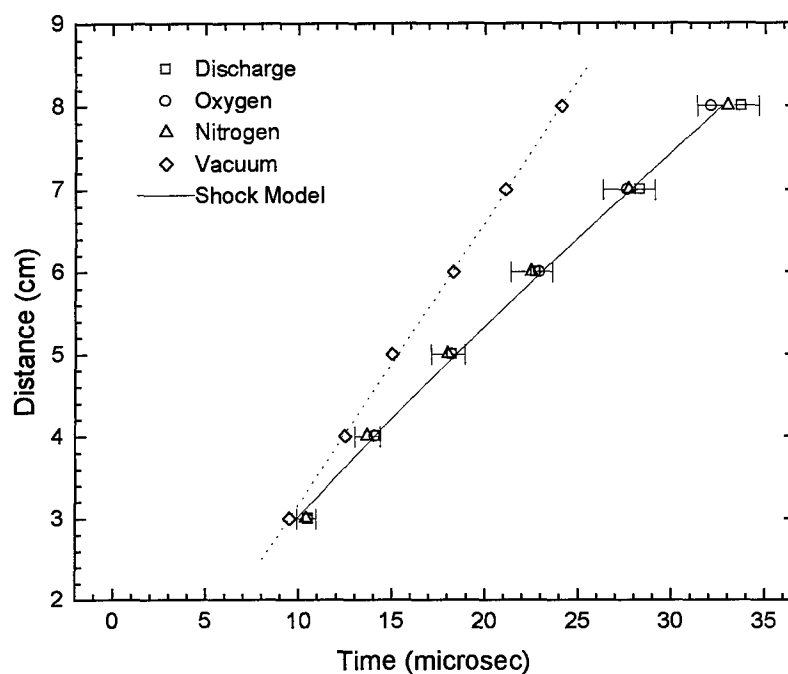
Figure 10. Time of flight in vacuum and 12.5 mtorr background.

0.3 for all of the data points independent of distance. The standard error, then, for a data point is 0.3 times the magnitude of that point. Similarly, the standard error for time of flight was determined to be 0.05 times the time of flight for the given point.

3.1.1 Time of Flight

The time of flight was defined as the time of arrival of the ion signal's peak. Fig. 10 shows the time of flight in 12.5 mtorr background gas and in vacuum. The plot in vacuum is very linear as expected, showing no deceleration.
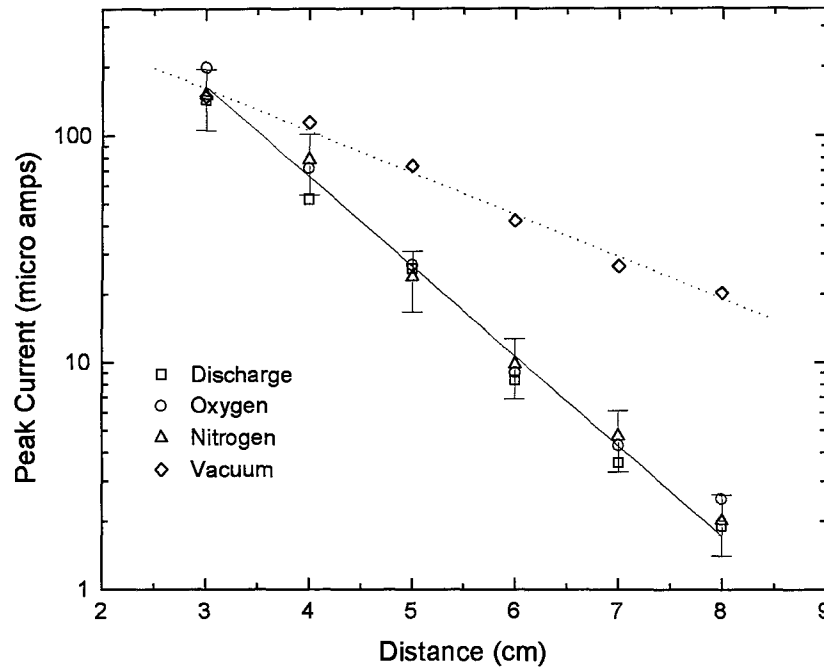
Figure 11. Plot of time of flight peak current in vacuum and 12.5 mtorr.

The slope of this line was calculated to be 3.5 km/sec. The tight grouping of the three gases indicates little dependence on the type of gas. These data points were fit to the shock model given by

$$d = at^b \tag{3.2}$$

where d is the distance from target and t is the time of flight (Geohegan, 1994); a and b were variable fit parameters which were determined to be 2.6 cm-μsec$^{-1.22}$ and 1.22, respectively. Figures 11 and 12 show the dependence of the peak current and total charge detected by the probe, respectively. Although this plot is over a limited range,

36

the linearity of the semilog plot indicates an exponential decay in the signal with increased distance which is in agreement with earlier studies (Geohegan, 1994). The steeper slope in the background gases as compared to the vacuum plot indicates a quenching of the ions. The presence of a background gas may confine the plume's plasma cloud allowing a higher rate of recombination which reduces the ion signal. Figures 13, 14, and 15, show the time of flight, peak ion current and total ion charge detected by the probe, respectively, at 25.0 mtorr. These plots show the same general results as those at 12.5 mtorr, only more pronounced. The fit parameters for the shock model, a and b, were determined to be 3.0 cm-μsec$^{-1.21}$ and 1.21, respectively.

3.1.2 Affect of Fluence on Ion Signal

The fluence tests were at a distance of 5.0 cm in vacuum and 12.5 mtorr background. Fig. 16 shows a decrease in time of flight and a corresponding increase in velocity with an increase in fluence. Fig. 17 shows a nearly linear increase in the peak signal above what seems to be a threshold at about 85 mJ/cm^2. Fig. 18 shows a similar characteristic for the total charge detected. The total
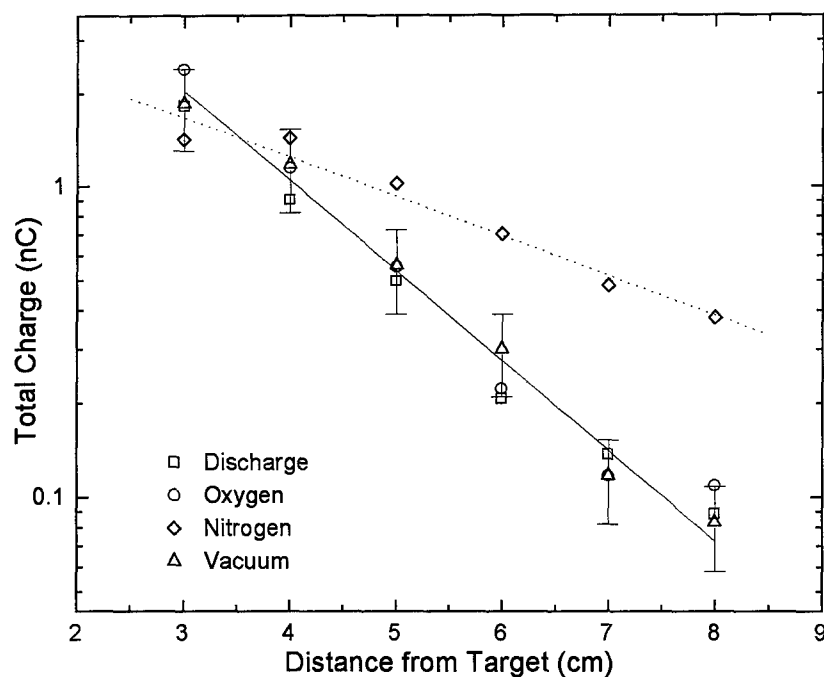
Figure 12. Total charge detected by the ion probe in a 12.5 mtorr background.

charge detected did not decrease as much as the peak current in the 12.5 mtorr atmosphere. This indicates that drag due to the background gas tends to broaden the Maxwell Boltzmann distribution.

3.1.3 Pressure Effect on Ion Signal

Figures 19, 20, and 21, show a linear relation between time of flight, peak current and total charge detected in
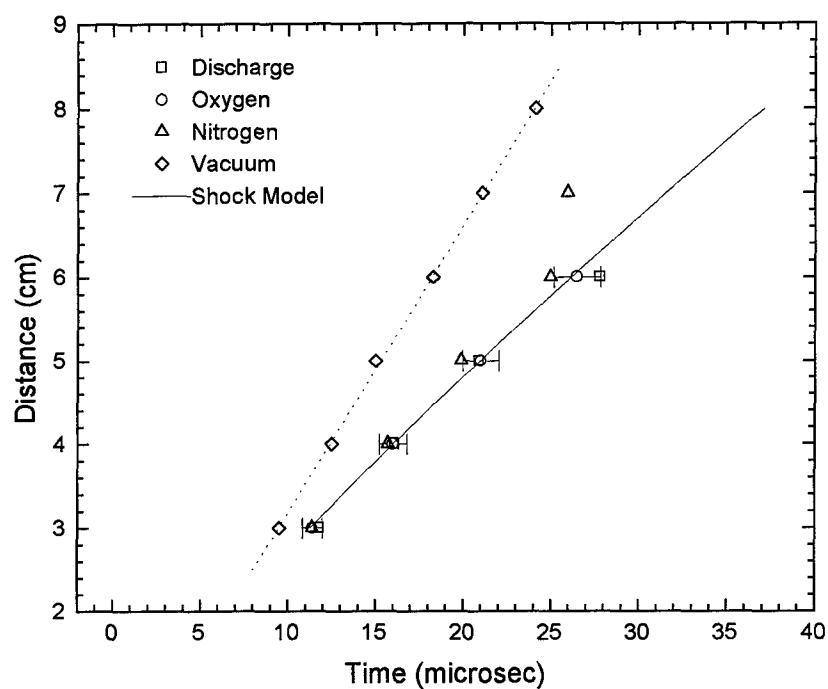
Figure 13.   Time of flight in 25.0 mtorr.
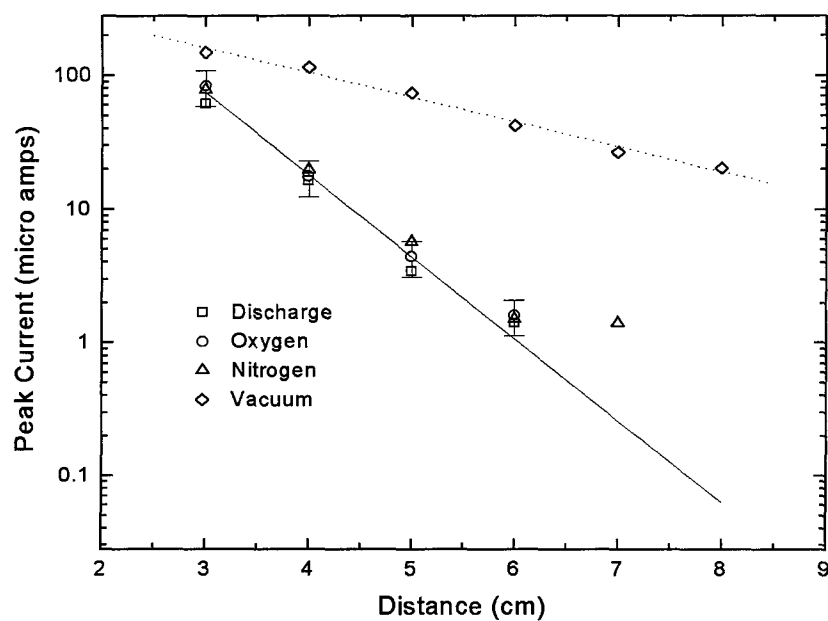
Figure 14.   Time of flight peak current detected in vacuum and in 25.0 mtorr background.
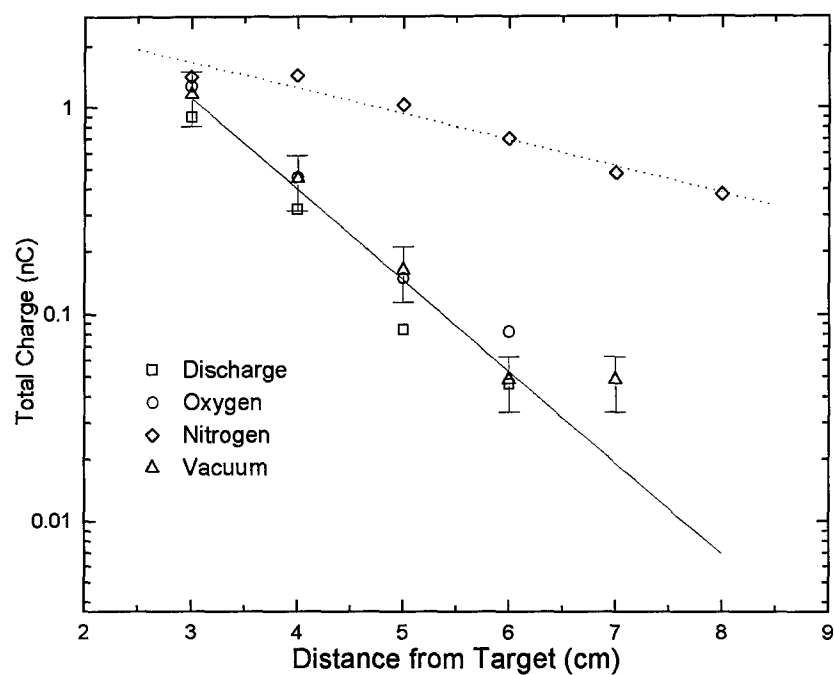
Figure 15. Total charge detected in 25.0 mtorr background.
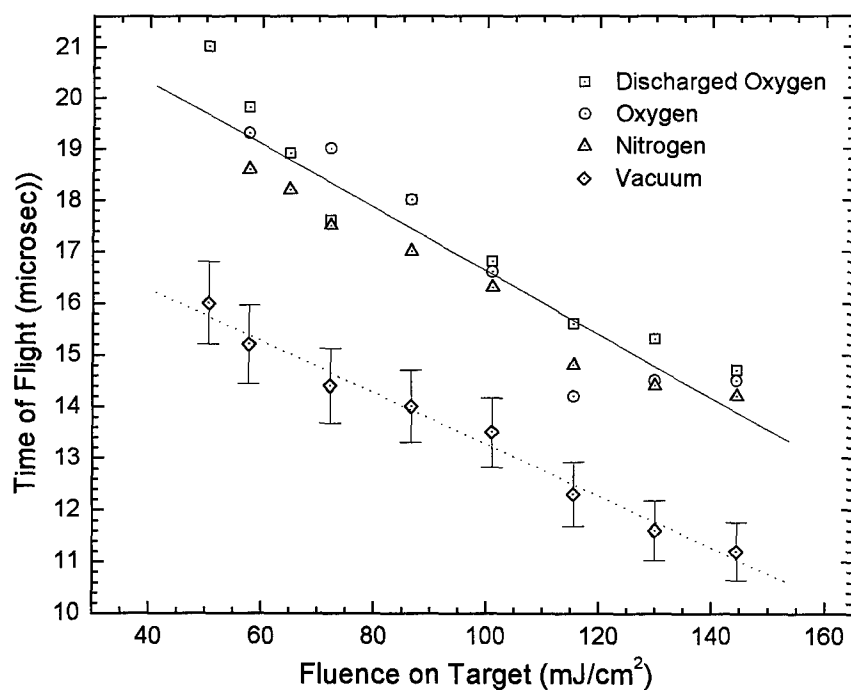
Figure 16. Time of flight dependence on fluence at 5.0 cm
from the target in 12.5 mtorr background.
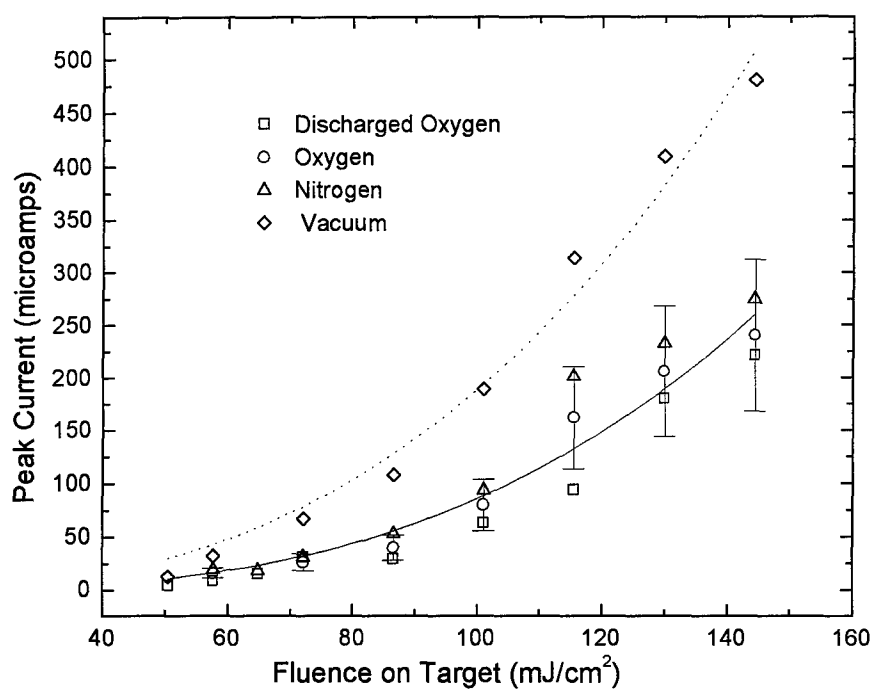
Figure 17. Dependence of peak current on fluence.
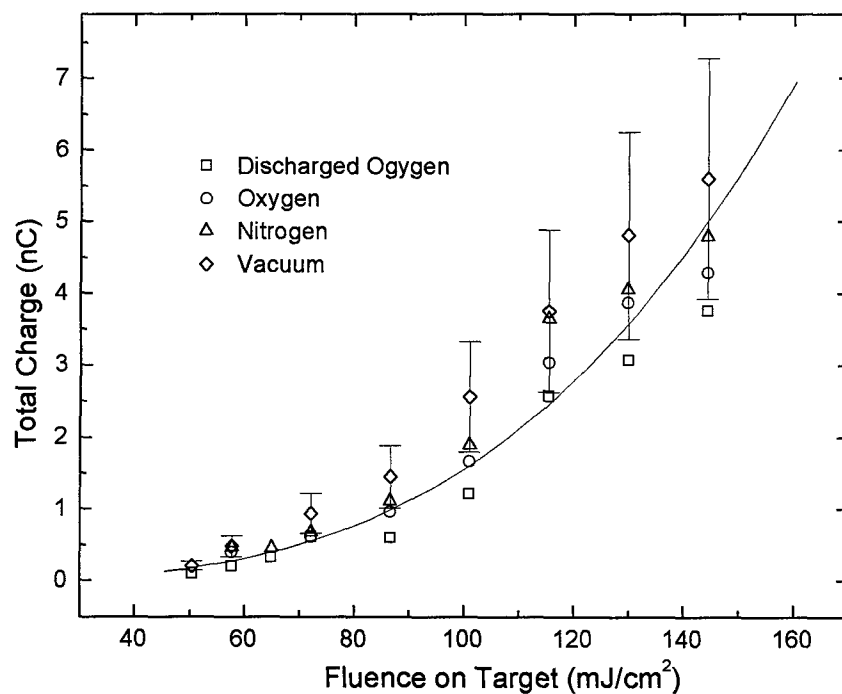
Figure 18. Total charge detected in relation to fluence.
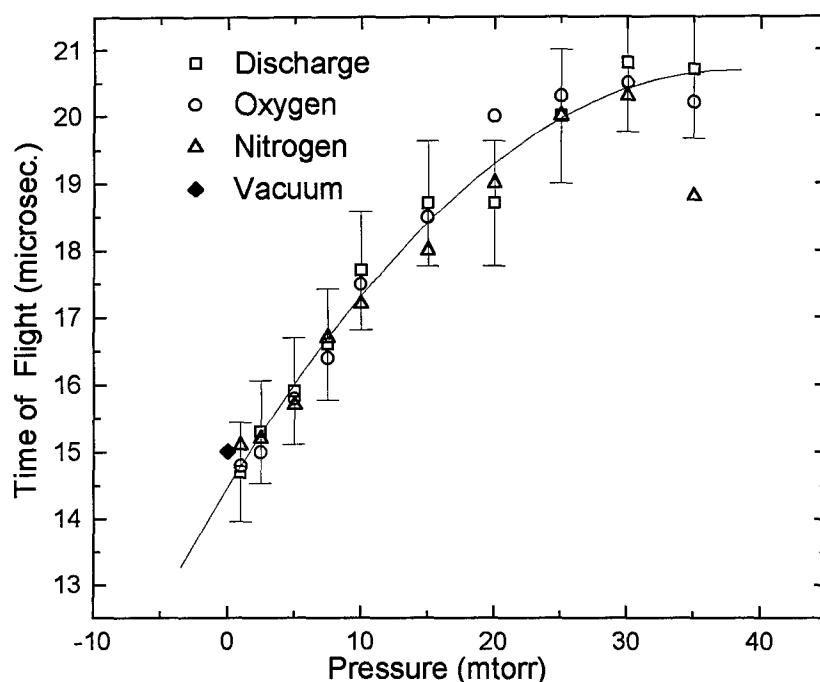
Figure 19. Effect of pressure on time of flight at 5.0 cm.

relation to changes in pressure. Generally, the time of flight increases with an increase in pressure and the peak current and total charge decreases with an increase in pressure.

Two anomalies are seen in these plots. The first is a decrease in time of flight in all three gases as pressure increases from 30 to 35 mtorr. This is not believed to be an actual phenomena but is assumed to be within the error limits of the system. The curve fitted to the data is a

42
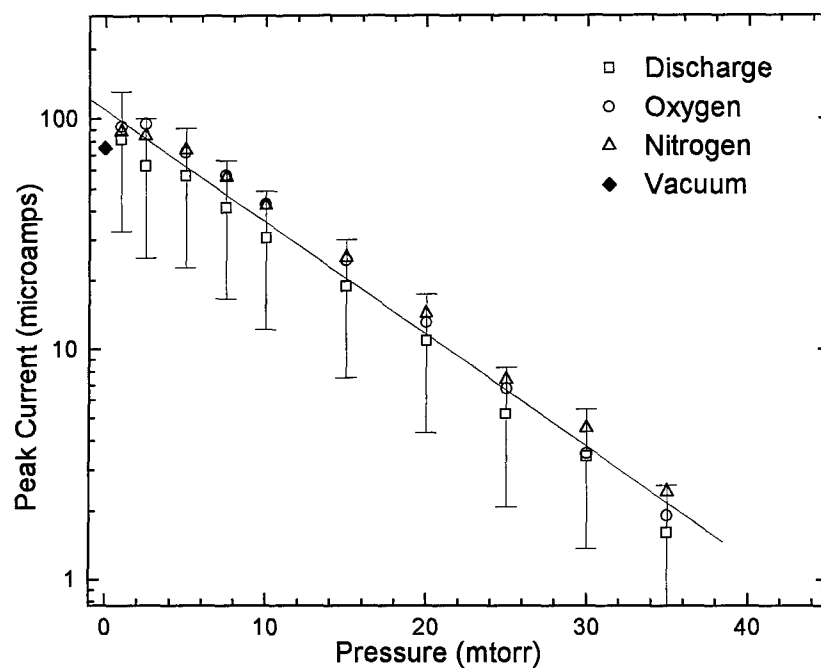
Figure 20. Effect of pressure on peak current.
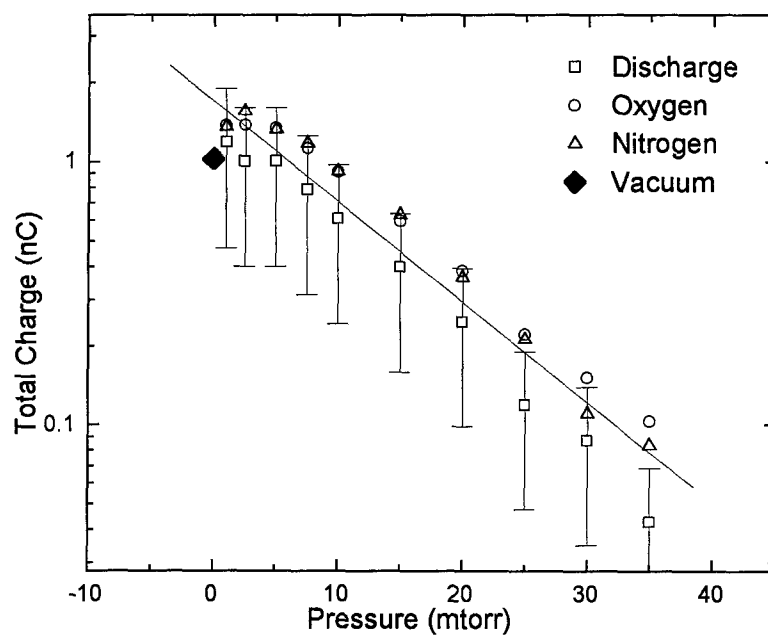
Figure 21. Pressure effect on total charge detected at 5.0 cm.

fourth-order polynomial and is only shown for clarity and is not meant to reflect physical properties.

The second anomaly is the apparent increase in total current detected as the pressure increases from 1.0 to 2.5 mtorr in O_2 and N_2 atmospheres. Similarly, this is within the error limits of the system and the current actually remains constant or even decreases as background gas is added.

3.1.4 Upper Bound on Total Ba-O Collisional Ionization Cross Section

Because an increase in the total charge in the plume was not detected in the discharged O_2 background gas as compared to the O_2 background gas, a rough estimate on the upper bound can be set by the fact that any increase in the ion number density (n_i) due to collisions with O was less than the minimum detectable signal. Given the rate change in n_i as

$$\frac{dn_i}{dt} = kn_O n_{Ba} \qquad (3.3)$$

$$k = \sigma_i v \qquad (3.4)$$

where n_O is [O], n_{Ba} is [Ba], σ_i is ionization cross section and v is relative velocity of the atoms, the total change in n_i is

$$\Delta n_i = \int_{t_O}^{t_f} \sigma_i v n_O n_{Ba} dt \qquad (3.5)$$

Assuming $v \cong v_{Ba}$ (neutral Ba velocity) $\cong v_i$ (ion

velocity) $\gg v_O$ (O atom velocity), that v_{Ba} is constant over

the path from the target to the ion probe, that n_O is

constant and uniform throughout the chamber and that Δn_i is

the minimum discernible signal, then Eqn. (3.5) becomes

$$\Delta n_i \geq \sigma_i v_{Ba} n_O \int_{t_O}^{t_f} n_{Ba} dt \qquad (3.6)$$

Assuming that the atoms in the plume expand uniformly

outward from the ablation sight through the solid angle Ω

such that

$$\Omega \cong \frac{A_a}{x_O^2} = \frac{A_p}{\left(x_O + d\right)^2} \qquad (3.7)$$

and

$$x_0 = \frac{d}{\left(\sqrt{\dfrac{A_p}{A_a}} - 1\right)} \qquad (3.8)$$

where A_a is the area of the ablation site, x_O is the

distance from the vertex of Ω to the ablation site, A_p is

the area of the probe and d the target to probe distance.

The n_i detected by the probe is

$$n_i = \frac{I_p}{A_p v_i} \qquad (3.9)$$

where I_p is the current detected by the probe. Assuming

$\gamma = \frac{n_{Ba}}{n_i}$ is constant, then

$$n_{Ba} = \frac{\gamma I_p}{A_p v_i} \qquad (3.10)$$

at the ion probe and, because the plume expands uniformly, the Ba flux through any surface in Ω is independent of the distance from the target given by

$$F = \gamma I_p \qquad (3.11)$$

and

$$n_{Ba} = \frac{\gamma I_p}{\Omega (x + x_0)^2 v} = \frac{\gamma I_p (x_0 + d)^2}{A_p (x + x_0)^2 v} \qquad (3.12)$$

which parameterized in terms of time by $x = vt$ gives

$$n_{Ba} = \frac{\gamma I_p (x_0 + d)^2}{A_p (vt + x_0)^2 v} \qquad (3.13)$$

Integrating Eqn. (3.6) gives

$$\Delta n_i \geq \frac{\gamma \sigma_i n_o I_p (x_0 + d) d}{A_p v_i^2 x_0} \qquad (3.14)$$

and for $\Delta n_i = \frac{I_{min}}{A_p v}$

$$\sigma_{max} \leq \frac{x_0 v_i I_{min}}{\gamma n_o I_p (x_0 + d)d} \qquad (3.15)$$

For $A_p = 1.06$ cm^2 $A_a = 0.43$ cm^2 , I_p (in vacuum) = 72 μA,

$v_i = 3.5 \times 10^5$ cm/sec, $n_o = 8.2 \times 10^{12}$ cm^{-3} at 25 mtorr., $\gamma = 100$

(Geohegan, 1994) and $d = 5.0$ cm, the above derived equation

gives $x_o = 8.77$ cm and $\sigma_{max} = 7.6 \times 10^{-13}$ cm^2.

3.1.5 Analysis of the Signal-to-Noise Ratio

This experiment looked for a small change in the total integrated charge of the ablation plume in O_2 and discharged O_2 background gases to determine if collisional ionization was occurring between Ba and O. Assume this change is 1% of the total signal. How large of a sample is needed to distinguish this change using the current experimental setup?

In this experiment 300 samples (the charge in one ablation plume or pulse is one sample) were averaged to estimate the parent distribution mean (the actual average charge per pulse). From the pressure effects on time of flight tests discussed in Sec. 3.1, the normalized sample average was 1.0 and the variance, S^2, was 0.09, giving a standard error, S, of 0.3. From the Central Limit Theorem,

the variance of each sample set, σ^2, is related to S^2 by the relation

$$s^2 = \frac{\sigma^2}{n} \qquad\qquad (3.16)$$

assuming each sample set is the same size and where n is the number of sample sets (in this case, 5). From this relation, $\sigma^2 = 0.45$.

By Eqn. (3.16), to reach the goal of reducing the standard error to less than 1% ($S^2 \le 0.0001$) requires $n \ge$ 4500. This means to reduce the standard error to less than 1% of the total signal requires 4500 sets of 300 shots each or 1.35×10^6. This shows that the method employed in this experiment has far too much noise to effectively measure ionization cross sections on the order of 10^{-20} cm^2.

3.2 Analysis of Ablation Plume Emission Spectra

The following discussion of the spectral data is not a complete accounting of the data from this experiment. The purpose for this analysis of the ablation plume emissions is to qualitatively identify species present in the plume. Since the ion probe does not differentiate between different positive species, this analysis gives a clue to which ions the probe detects. This analysis only identifies those

species transitioning from excited states and gives no indication of, for example, ground-state atomic species. A few samples of the data will be presented as examples of the spectra observed and to highlight some of the more interesting features. The complete set of spectral data taken in this project is included in the appendices to this thesis.

In general, with the exception of the Ba plume emissions, the overall emissions observed in the background gases were of higher intensity than those in vacuum. This phenomena is attributed to the background gases restricting the expansion of the plume and thereby confining it to a smaller volume for a longer period of time (Wolf, 1996). Not only does the intensity increase due to the higher density of emitting atoms but also because the ion-electron recombination rate is higher in the denser plasma.

3.2.1 Spectral Analysis of Plume Emission from Ba-Based Target Ablations

The plume emission resulting from the ablation of the Ba target was observed over the spectra ranging from 310 nm to 810 nm. The emission from the BaO target ablation plume was observed over the spectral range of 390 nm to 790 nm. The laser fluence on target was 220 mJ/cm^2 for the Ba target and 425 mJ/cm^2 for the BaO target.

Figures 22(a) and 22(b) show spectra for Ba and BaO, respectively, in the region around 400 nm. In both figures BaI spectral lines are seen at 389.3 nm, 391.0 nm, 393.7 nm and 399.3 nm. The shoulder observed at the base of the 393.4 nm line in the Ba spectra corresponds with a weak BaII spectral emission at 394.3 nm. The lines at 394.5 nm, 395.4 nm and 397.3 nm in the BaO spectra correspond to OII(^2P-$^2p^0$) transitions. Because these lines are present in all the BaO spectra and absent from the Ba spectra, the ablation of oxygen atoms from the BaO target is assumed to be the source of these excited O ions.

The transition to the ground state of BaII at 455.4 nm is shown in Fig. 23 along with another BaII line at 452.5. The other lines in these spectra are due to BaI transitions. Note the relative intensity of the emissions of the Ba plume decreases significantly in the oxygen backgrounds as compared to the emissions in vacuum and nitrogen, while the emissions from the BaO plume increase with respect to the emissions in vacuum. This phenomena is attributed to the oxygen atoms, ablated from the BaO target, having a higher velocity than the barium atoms.

Assuming each particle in the plume has approximately equal kinetic energy, the ratio of velocities of O to Ba would be inversely proportional to the square root of the ratio of their mass. This appears to be a conservative estimate

based on experimental results from the ablation of SiO which showed the ratio of velocity is more closely proportional to the inverse of the mass ratio. Although the velocity of the oxygen atoms was not measured in this experiment, based on this assumption that velocity goes as the inverse of the square root of the ratio of the mass, O atom velocity is 2.5 times higher than that of the Ba atoms. This would cause O to dominate the leading edge of the expanding plume and sweep the ambient O_2 out of the path ahead of the Ba atoms, thereby preventing any Ba - O_2 reactions.

This observation, along with Dyke's results when O was removed from the discharged oxygen (discussed in Section 1.4.2), indicate Ba + O_2 reactions have much larger cross sections than do Ba + O reactions. It is not known if molecular species are formed or if Ba - O_2 collisions are inelastic resulting in quenched excited states, either of which would effectively reduce the BaI* and BaII* emissions.

Figure 24(a) shows a broad spectral feature between about 478.5 nm and 486.5 nm in Ba plume emission in an oxygen and discharged oxygen background which does not appear in the nitrogen or vacuum backgrounds or in any of the BaO spectra (Figure 24(b)). The shape of this feature is that of a molecular type species and indicates a reaction of Ba and the ambient oxygen, however, the wavelength of
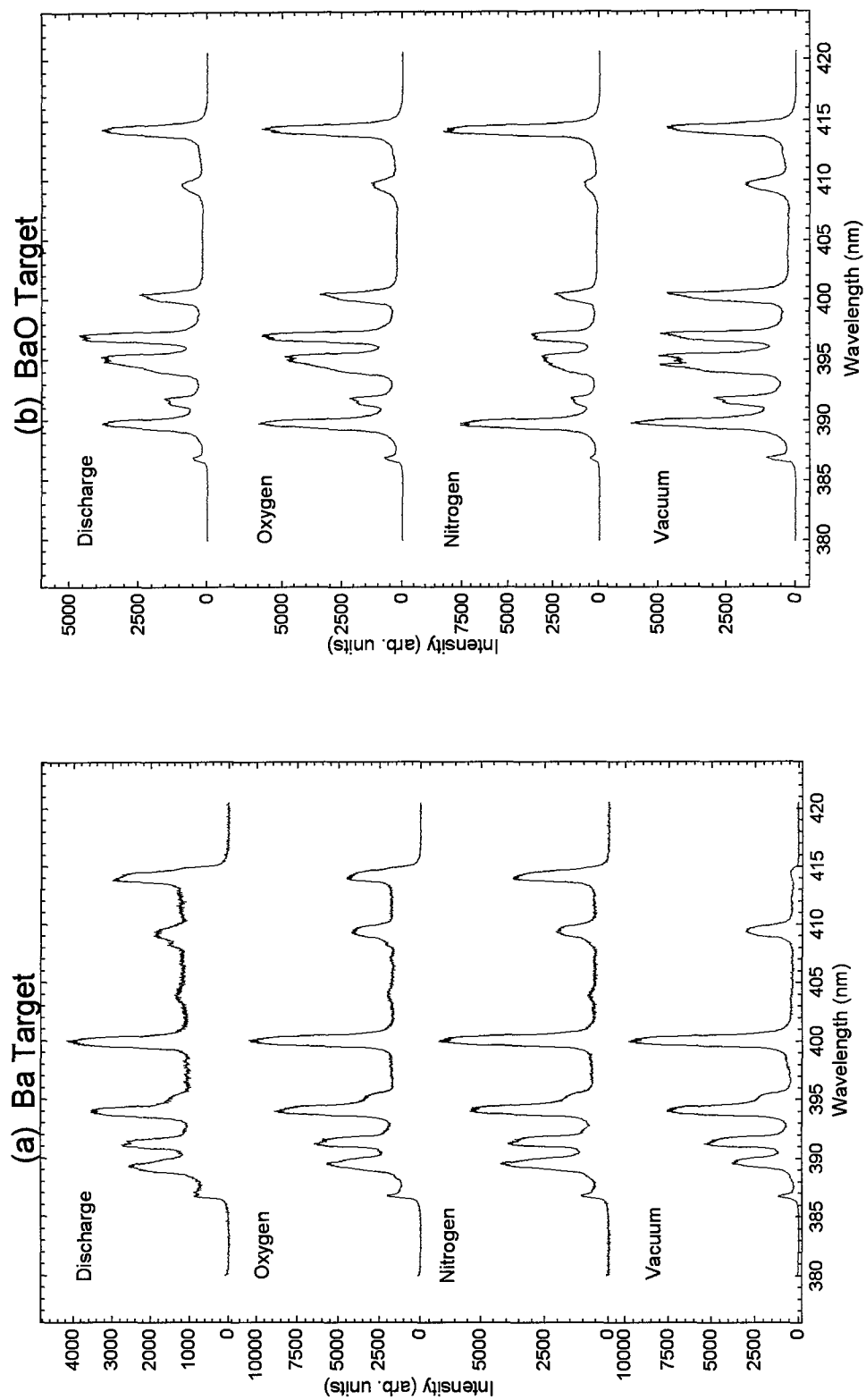
Figure 22. Ba (a) and BaO (b) ablation plume spectra near 400 nm in 25 mtorr background gases and in vacuum.
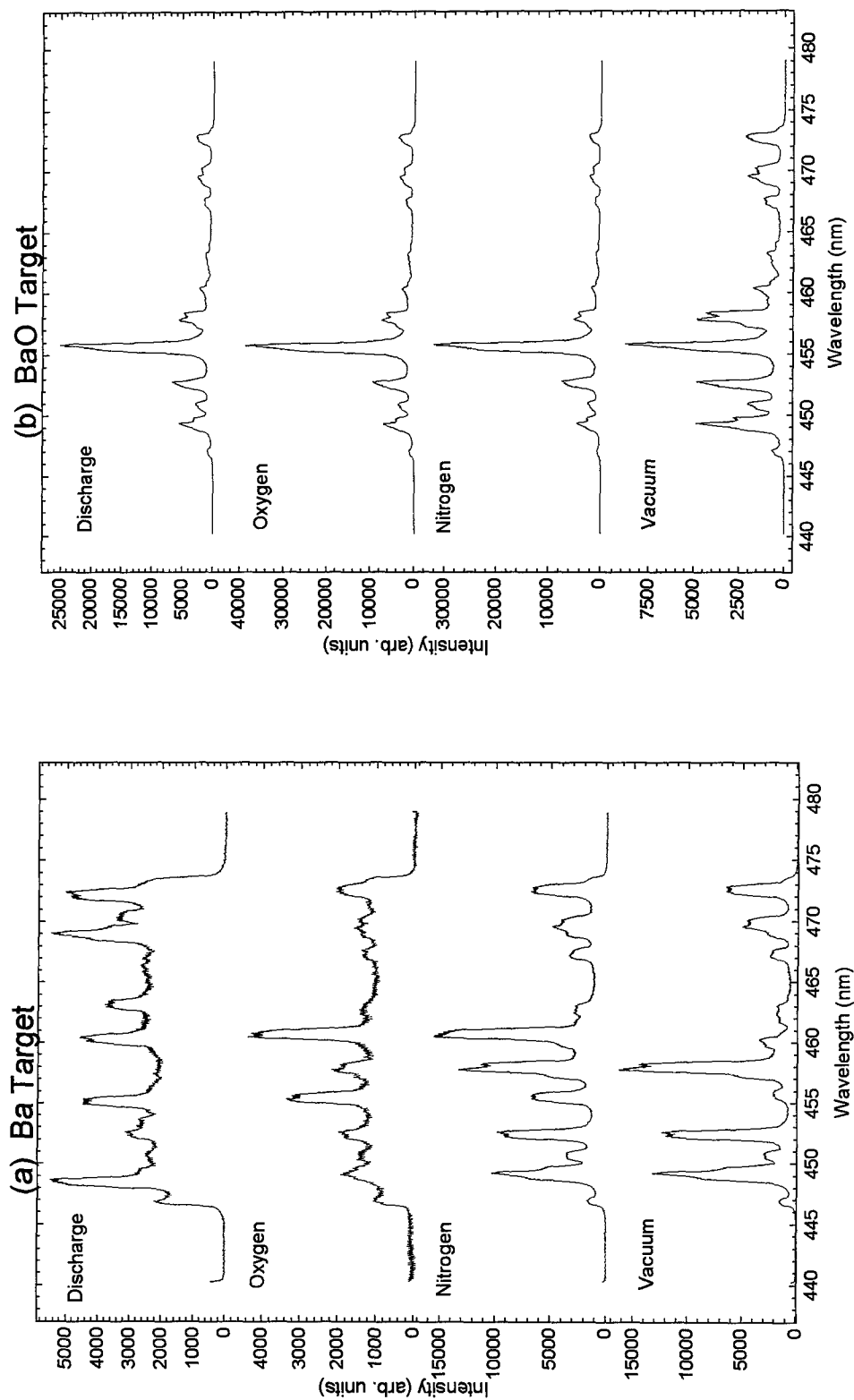
Figure 23. Ba (a) and BaO (b) ablation plume spectra near 460 nm in 25 mtorr background gases and in vacuum.
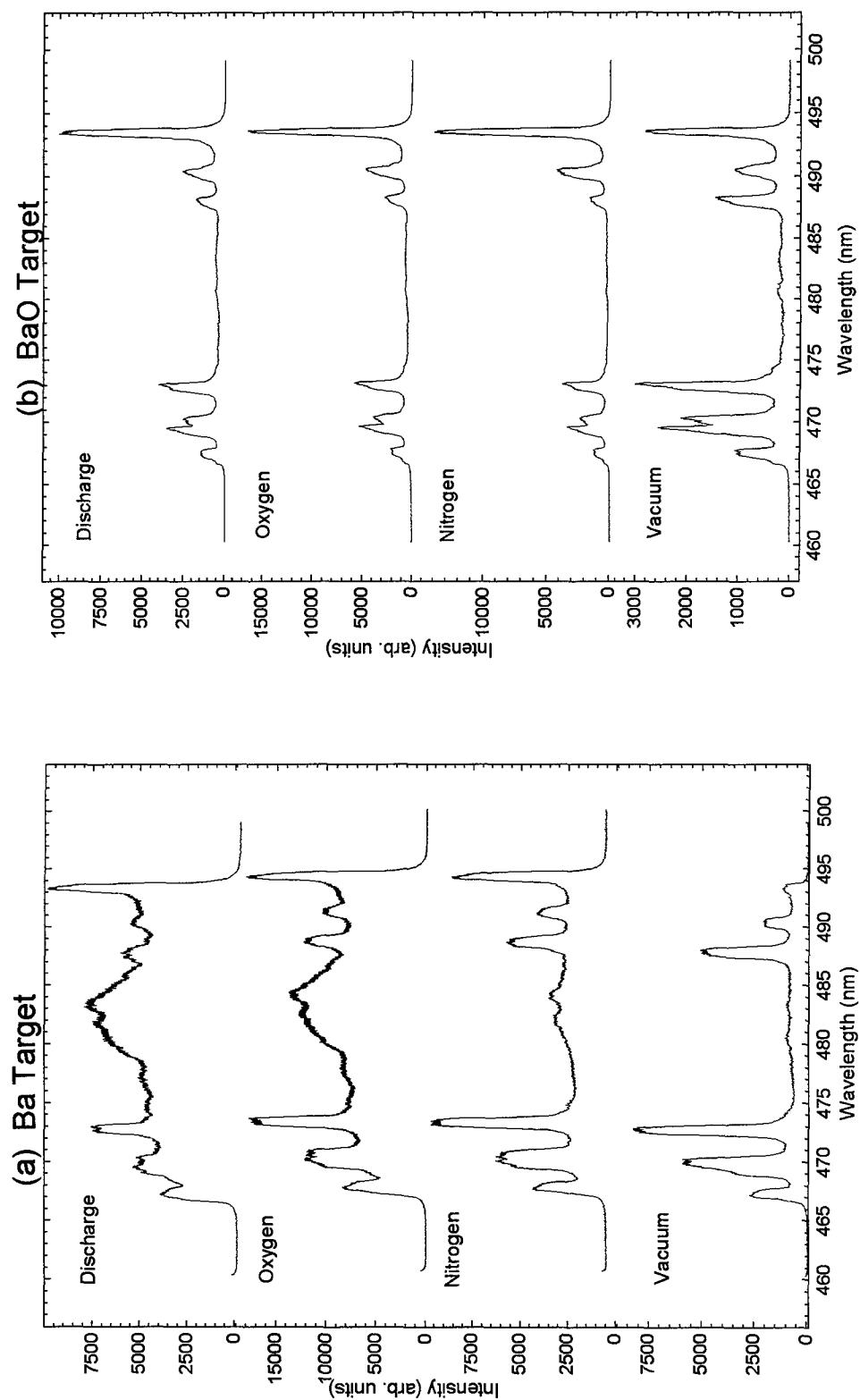
Figure 24. Ba (a) and BaO (b) ablation plume spectra near 480 nm in 25 mtorr background gases and in vacuum.
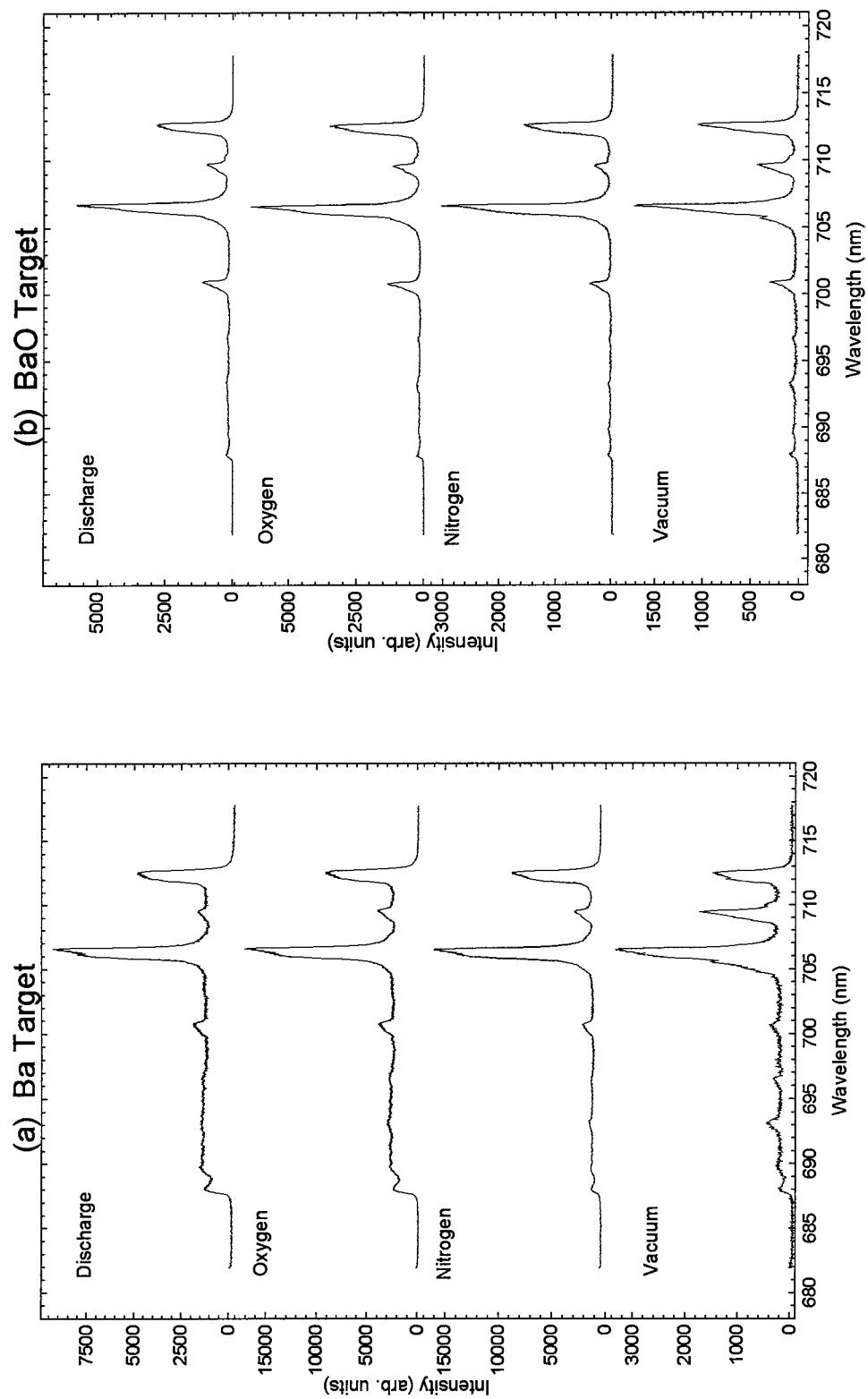
Figure 25. Ba (a) and BaO (b) ablation plume spectra near 700 nm in 25 mtorr background gases and in vacuum.

this band does not correlate with known BaO* emission bands. That the signal in discharged O_2 is 50% weaker and that the feature is absent in the BaO spectra indicates the reaction proceeds faster with ground state or collisionally excited O_2 than with O or $O_2(^1\Delta)$. Another prominent feature shown in Figure 24(a) is the high base line of the Ba plume emissions in the oxygen atmospheres compared to the other spectra. This high base line begins from about 420 nm and runs through about 550 nm. This continuous emission is typical of electron-ion recombination. Again, the absence of this continuous emission from the BaO plume is due to O ablated from the BaO target dominating the leading edge of the expansion plume.

Fig. 25 shows a BaIII line at 709.6 nm and BaI lines at 706.0 and 712.0 nm on both the Ba and BaO spectra. In laser ablation plumes, the recombination rate for multiple ionized atoms is very high and therefore do not exist beyond a few millimeters from the target (Geohegan, 1994). This will be discussed in greater detail in Section 3.2.3.

3.2.2 Spectral Analysis of Plume Emissions from Sr-Based Target Ablations

The plume emissions resulting from the ablation of the Sr target were observed over the spectrum ranging from 330

nm to 790 nm. The laser fluence on the Sr target was 385 mJ-cm^{-2}. Emissions from the SrO target were observed over the spectral range from 390 nm through 790 nm at two positions: 1.0 cm from the target and 3.0 cm from the target. The laser fluence on the SrO target was 575 mJ-cm^{-2} at 1.0 cm and 2.0 J-cm^{-2} at 3.0 cm. Fig. 26 shows spectra for Sr and SrO in the region near 420 nm. SrII lines are seen at 407.7 nm, 416.2 nm, 421.6 nm and 430.5 nm. SrIII lines are seen at 409.0 nm and 433.6 nm. A sharp increase in intensity of the 407.7 nm and 421.6 nm SrII lines in the SrO plume is seen with the addition of background gases while a moderate increase is observed in the Sr plume. An OI line at 423.3 nm is only seen in the SrO plume and shows a sharp increase in intensity with the addition of background gases. An SrIV line is present at 467.9 nm in both spectra (Fig. 27) and like the BaIII line discussed earlier does not exist beyond a few millimeters from the ablation site.

Three OI lines exist in a tight group at 777.2 nm, 777.4 nm, and 777.5 nm. These are shown in Fig. 28b, the SrO plume emissions at 3.0 cm, in vacuum, and in the oxygen backgrounds but are nearly non-existent in the nitrogen background. These same lines are non-existent in the Sr plume emissions except in the discharged oxygen background (Fig. 28a). The presence of the lines in the SrO plume
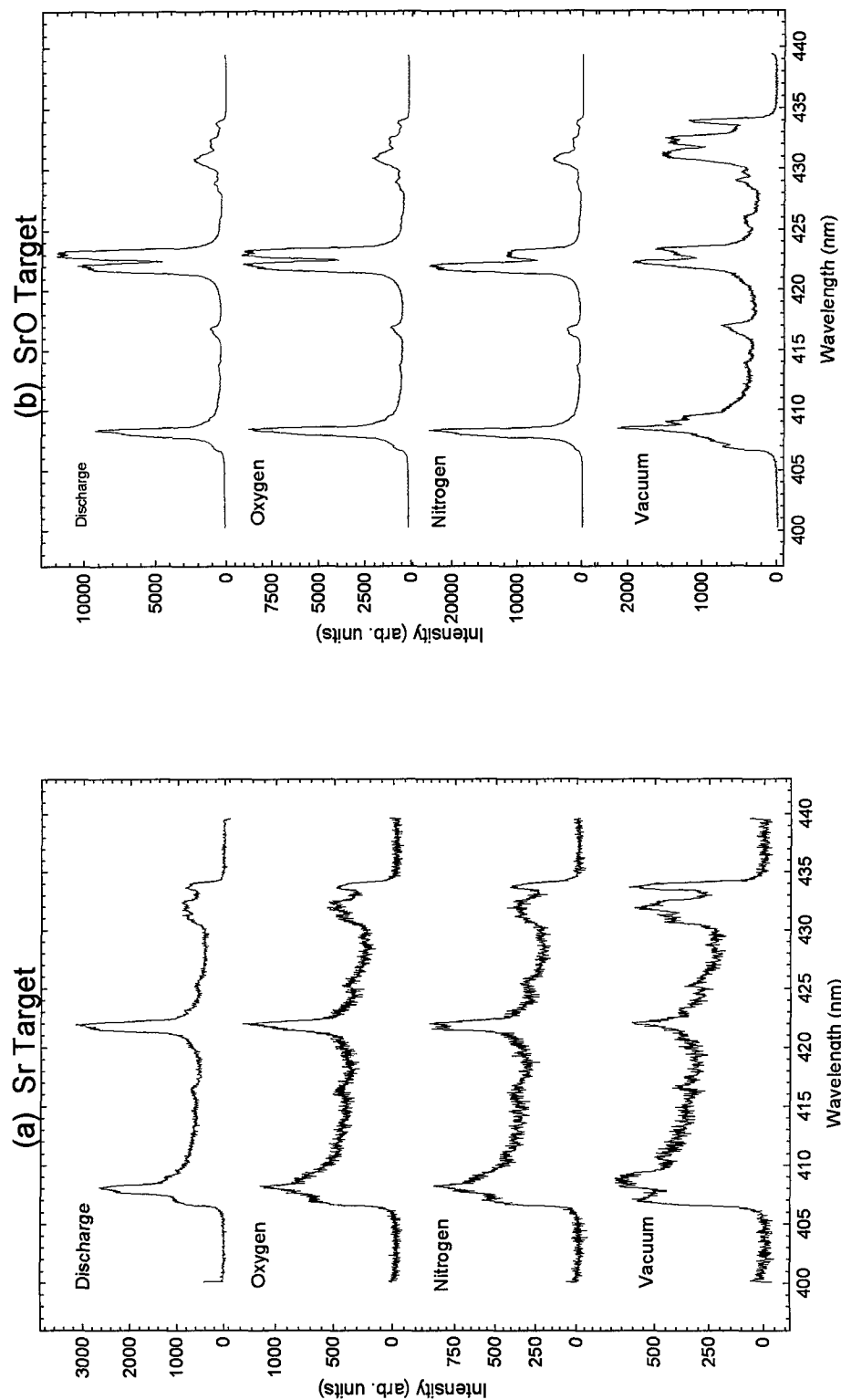
Figure 26. Sr (a) and SrO (b) ablation plume spectra near 420 nm in 25 mtorr background gases and in vacuum.
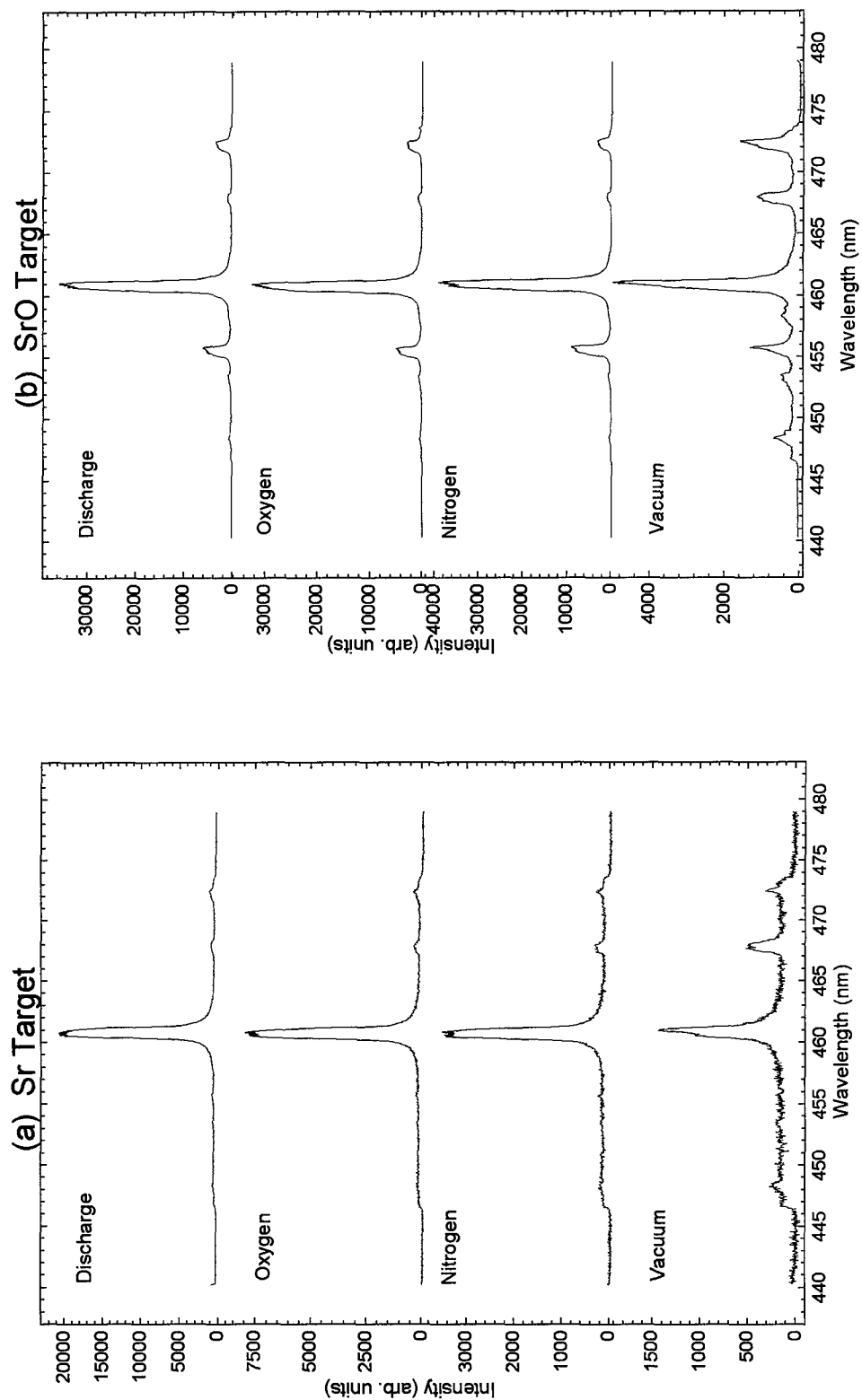
Figure 27. Sr (a) and SrO (b) ablation plume spectra near 460 nm in 25 mtorr background gases and in vacuum.
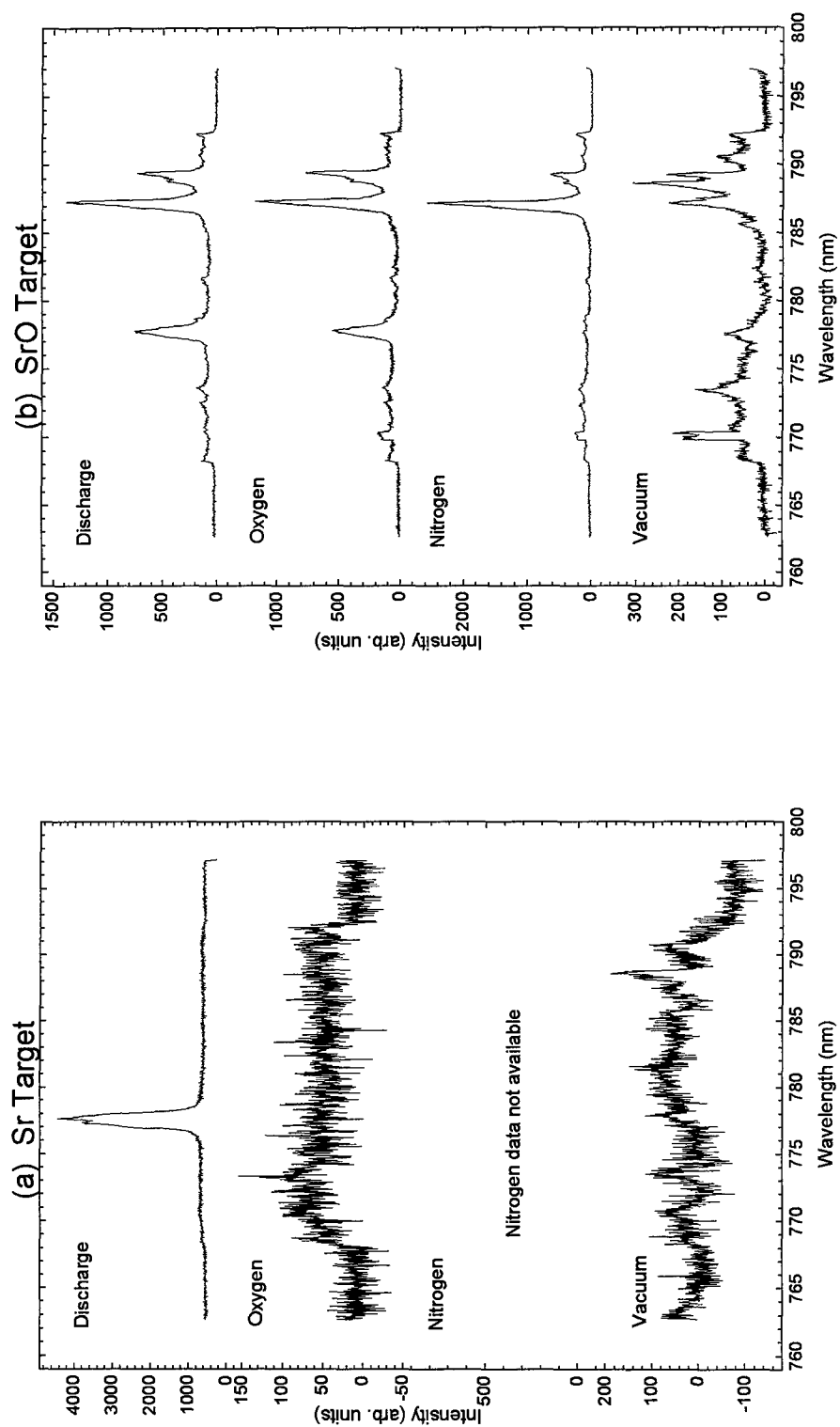
Figure 28. Sr (a) and SrO (b) ablation plume spectra near 780 nm in 25 mtorr background gases and in vacuum.

emissions is probably due to O, ablated from the SrO target, being excited during the ablation process. The absence of these lines in nitrogen background indicates a highly efficient, possibly even resonant, O^* - N_2 collisional process deactivating the O^*. The energy of this emission is 1.60 eV which is close to the $N_2(X\ {}^1\Sigma_g^+ - X\ {}^2\Pi_g)$ transition (Rees, 1989) and is the most likely candidate since the N_2 background gas flows into the chamber in ground state.

The absence of these lines in all but the discharged oxygen background gas in the Sr plume emissions indicates a possible Sr-O or $O_2(a\ {}^1\Delta)$ reaction.

3.2.3 Spectral Analysis of the Sr Ablation Plume Emissions in Oxygen and Discharged Oxygen Backgrounds at 12.5 mtorr and 25 mtorr

Plume emissions resulting from the ablation of the Sr target were observed at 340 nm, 400 nm, 420 nm, and 600 nm center wavelengths for O_2 and discharged O_2 ambient gases at 12.5 and 25.0 mtorr. This gave a unique look at the plume emissions in oxygen background gases at different pressures. These regions of the spectrum were chosen because they cover all the strong SrII emission lines within the optical limits of this system.
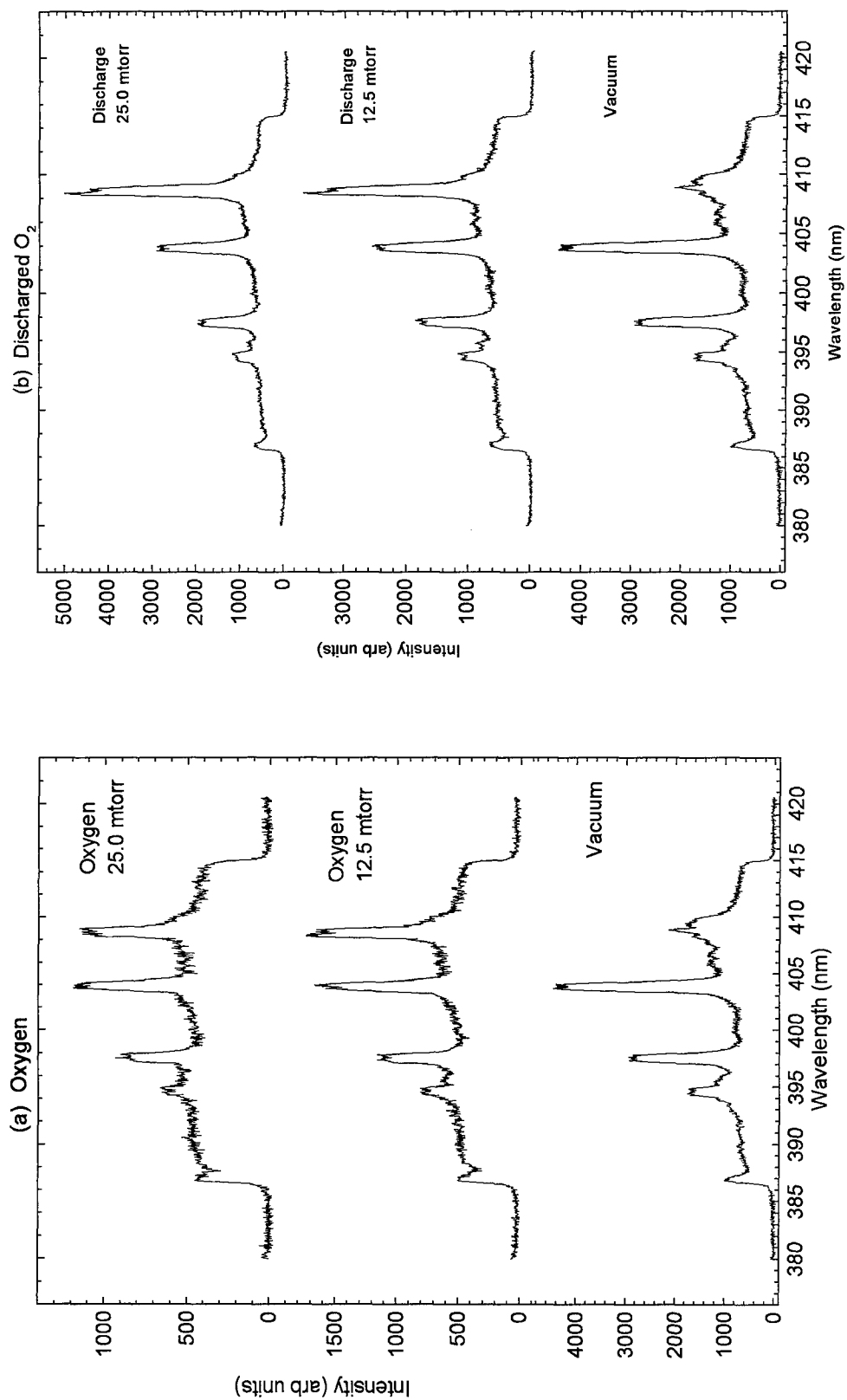
Figure 29. Sr ablation plume spectra in O_2 (a) and in discharged O_2 (b) near 400 nm in 12.5 and 25 mtorr background gases and in vacuum.
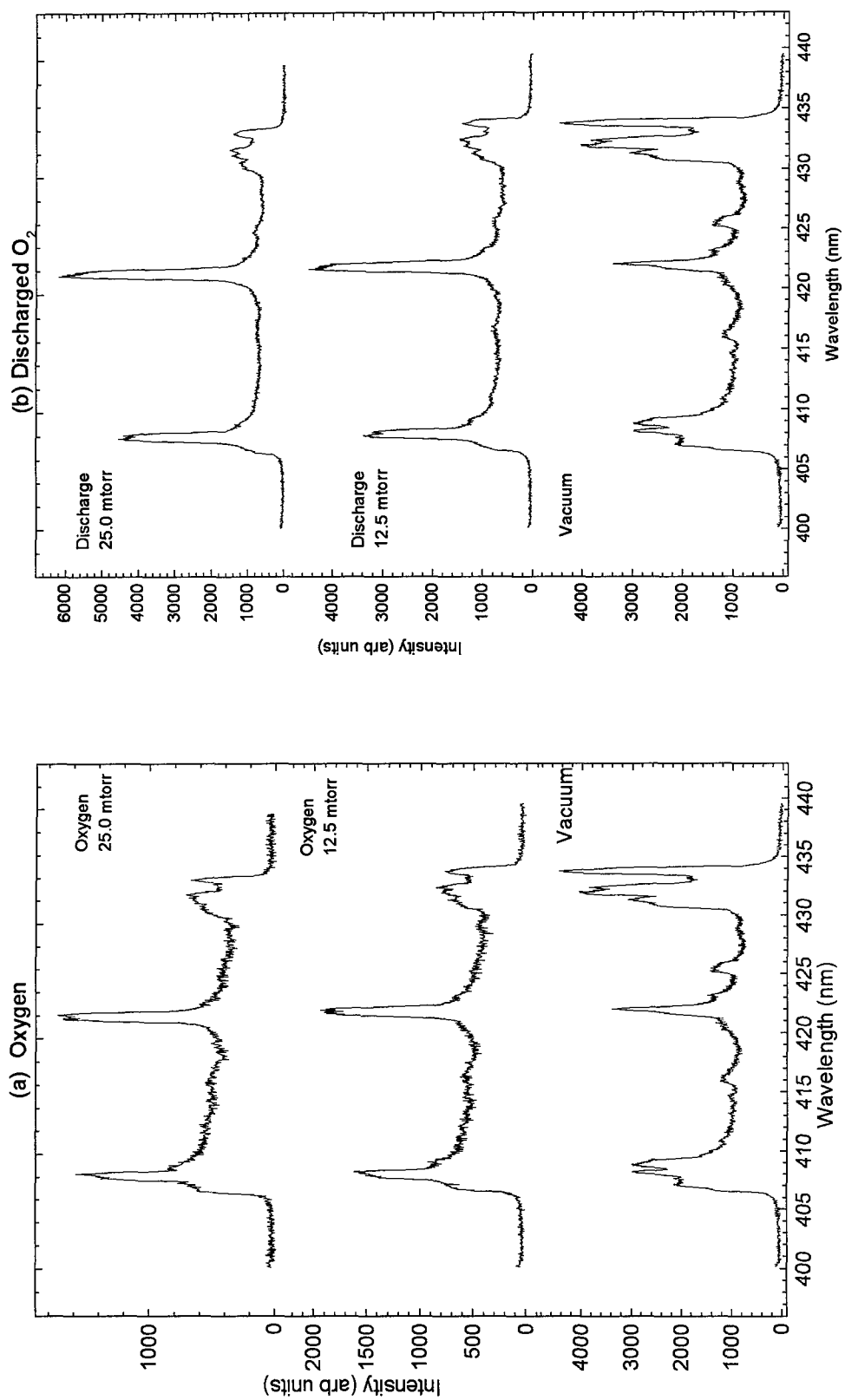
Figure 30. Sr ablation plume spectra in O_2 (a) and in discharged O_2 (b) near 420 nm in 12.5 and 25 mtorr background gases and in vacuum.
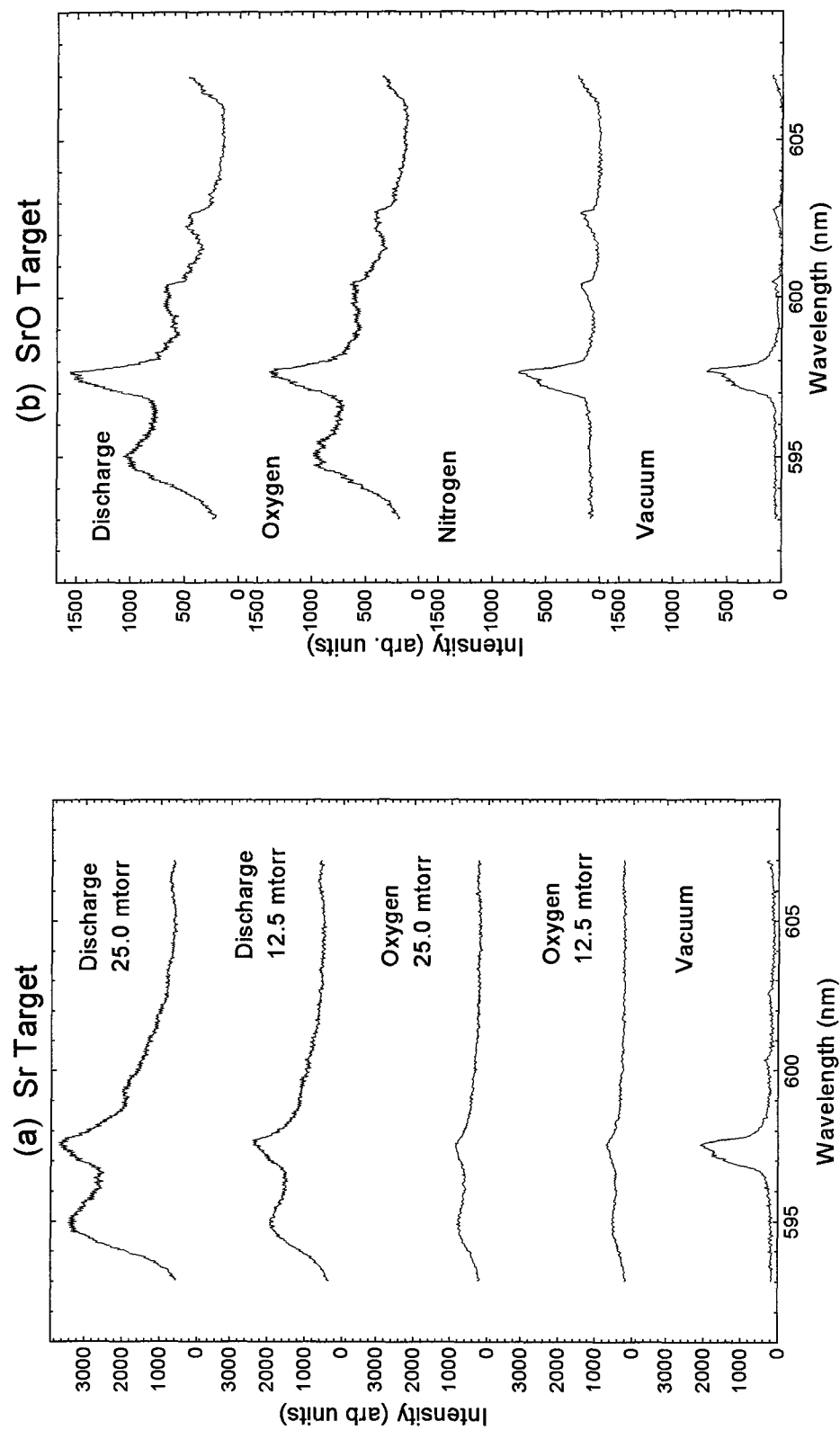
Figure 31. (a) Sr ablation plume spectra in O_2 and in discharged O_2 near 600 nm in 12.5 and 25 mtorr background gases and in vacuum and (b) SrO ablation plume spectra in 25 mtorr background gases and in vacuum.

Figures 29, 30, and 31 show spectra for SrO in oxygen and discharged oxygen at 400, 420, and 600 nm wavelengths, respectively. In Fig. 29(a), with the addition of O_2 gas, the OII line at 408.8 nm appears as before but is relatively unaffected by the change in pressure. The SrI lines decrease in intensity with the addition of the O_2 with only a slight decrease in intensity with doubling of pressure. In contrast, the discharged oxygen background SrI spectral lines decrease in intensity with the addition of a background gas and show no relative change with respect to the increase in pressure but the OII line increases significantly with the increase in pressure. The intensity of the SrII transition-to-ground state spectral line at 421.6 nm is relatively unchanged with the addition of O_2 while it increases in intensity with the addition and increase in pressure of the discharged oxygen background.

Between 594 and 601 nm is a broad feature resembling a molecular spectra (Fig. 31) which coincides with an unclassified SrO band (Huber, 1979). Because this feature is present in all the Sr-based target ablation plume emissions in oxygen background gases and non-existent in vacuum and nitrogen background (even for SrO plumes), this feature is due to an Sr + O_2 reaction with SrO as a product. The intensity of this feature increases nearly linearly with an increase in O_2 or discharged O_2 pressure. This feature is

four times more intense in the discharged background than in the O_2 background indicating the reaction cross section is four times larger with O_2(a $^1\Delta$) than with ground-state O_2.

3.2.4 Spectral Analysis of the Wide Spectral Lines

The most striking feature of all the spectral data taken in this experiment is the unusually wide lines. The lines coincide with the expected atomic spectra but are on the order of one nanometer wide. To eliminate the possibility of equipment malfunction causing the lines to appear broader than normal, a xenon calibration lamp was placed opposite the spectrometer such that its light would travel through the chamber and along the same path as the plume emissions. Fig. 32 shows the plume emissions both with and without the Xe lamp. The Ba spectral lines are approximately 1 nm wide while the narrow (0.2 nm) Xe lines are clearly visible at 462.4 nm and 467.1 nm, superimposed on the ablation plume spectra in both the O_2 and N_2 background gas. This demonstrates the equipment was properly aligned and the broad lines were an actual characteristic of the observed spectral emissions.

To eliminate the possibility of the lens system being focused on or near the ablation sight instead of 1.0 cm away from the target surface, the SrO target was moved an
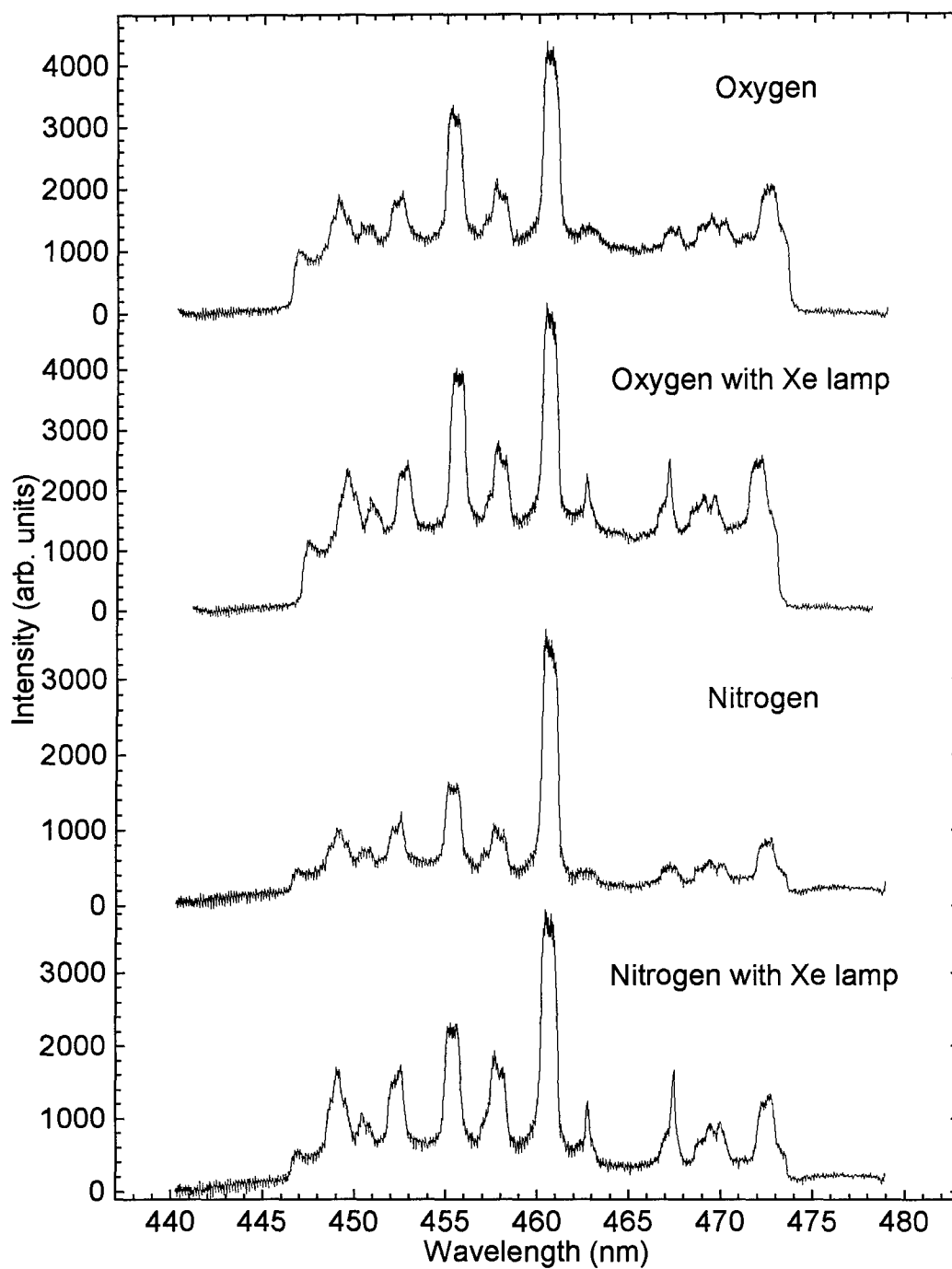
Figure 32.   Ba spectra in O_2 and N_2 with and without Xe calibration lines.
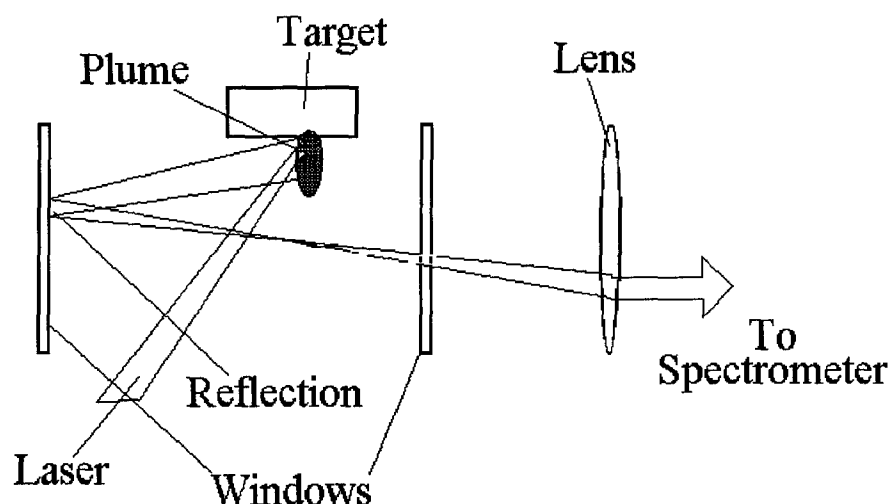
Figure 33. **Diagram of experiment depicting how the reflection of the laser spot is within the field of view of the spectrometer.**

additional 2.0 cm out of the optical system's field of view.

The resulting SrO spectra, taken 3.0 cm from the target surface,

has the same broad spectral lines. This eliminated the

possibility the lens system was inadvertently focused on the

ablation site.

Reassessment of the equipment setup uncovered the

possibility that the reflection of the ablation sight off the

chamber window was within the field of view of the spectrometer

as show in Fig. 33. Within the first few millimeters of the

target, high temperatures and plasma densities contribute to

Stark broadening due to electron-ion collisions. This would

account for the very broad spectral lines. Additional evidence

to support this theory was the existence of BaIII, SrIII, and

SrIV lines in the respective spectra.

IV. Conclusion and Recommendation

4.1 Summary of the Ion Probe Results

The results of measuring the ion content of Ba ablation plumes found at the ion cloud time of flight in a background gas fits the shock model (Eqn. 3.2) and that the total integrated charge in the plume decreases exponentially with respect to distance from the target and with respect to increasing background gas pressure. This is in agreement with earlier studies. An increase in Ba ion density due to collisional ionization was not detected because signal noise was more than an order of magnitude larger than the expected change (assuming a change of 1% and a standard error of 0.3). An upper bound on total ionization cross section was found to be 7.6×10^{-13} cm^2 which is 7 to 8 orders of magnitude larger than the expected values for Ba-O ion pair formation.

The nature of the ablation process (its strong dependence of fluence and target surface condition) leads to large pulse-to-pulse variations in the ablation plume ion density. This large variation in plume ion density makes it impossible to measure tiny changes in total charge due to collisional ionization. By removing the charged particles from the plume prior to injecting the plume into the

background gas would result in an ion signal due to collisional processes only.

4.2 **Summary of the Spectral Data**

The spectral data taken in this thesis shows Stark broadening of the spectral lines and spectral lines from multiply-charged ions, characteristic of ablation plume emissions very near the target surface. The most probable cause for this is the reflection of the bright emissions at the target surface off the vacuum chamber window opposite the optical system collecting light for the spectrometer. Because of this, ion species in the plume cannot be determined for distances greater than a few millimeters from the target.

This experiment did find a SrO spectral feature between 593 nm (1863 cm^{-1}) and 602.5 nm (16598 cm^{-1}) which coincides with the unclassified SrO band in the 16600-16900 cm^{-1} region (Huber, 1979, 630). Because this molecular signal is present in both O_2 and discharged O_2 spectra for both Sr and SrO ablation plumes and not in the SrO vacuum or N_2 spectra which is expected to contain O from the ablation of SrO, it is concluded that the SrO* is formed by the collision of Sr with O_2. The five-fold increase in this signal in discharged O_2 over O_2 indicates the reaction is more

efficient with excited O_2 giving the most probable reaction as

$$Sr + O_2^* \rightarrow SrO^* + O \qquad\qquad (4.1)$$

The Ba spectra has broad molecular-like features in regions 500-506 nm (19,800-20,000 cm^{-1}), 508-526 nm (19,700-19,000 cm^{-1}), and 544-548 nm (18,250-18,400 cm^{-1}). These features were not found to coincide with known BaO bands and no Ba, Ba^+ or Ba^{++} lines are known to be near these features (Reader, 1980, 13). The presence of these features in O_2 (strongest) and discharged O_2 indicates a possible Ba + O_2 reaction. As briefly discussed in Section 1.4, these reactions can be complex (Dyke, 1995).

4.2 Recommendations for Future Study

As often happens with experimental projects, more questions were raised than answered in this project. As a result, several areas of further study are recommended here.

First, to fully understand what the ion probe detects, a probe needs to be calibrated with a known ion source to shed light on the observed increase in ion current as bias voltage increased well beyond potentials high enough to strip out all the electrons.

Investigations into the SrO band near 600 nm could lead to classifying the emissions source. The broad features in the Ba spectra should be studied to determine if they are indeed emission bands from BaO, BaO_2, or some other molecular form of Ba and to determine what limits the reaction in the BaO ablation plume.

Finally, this experiment should be redesigned to eliminate the charged particles from the plume before injection into the ambient gases to study the collisional ionization. A suggested method is to use dual vacuum chambers. Pump the first chamber to high vacuum wherein the target is ablated, a narrow beam of expanding ablation plasma is skimmed off and the charged particles stripped-out electrostatically. The resulting beam of neutral particles would pass through a small orifice into the second chamber containing low pressure atmospheres of O and O_2. Use mass spectroscopy to investigate byproducts of the collisional interactions at hyper thermal energies.
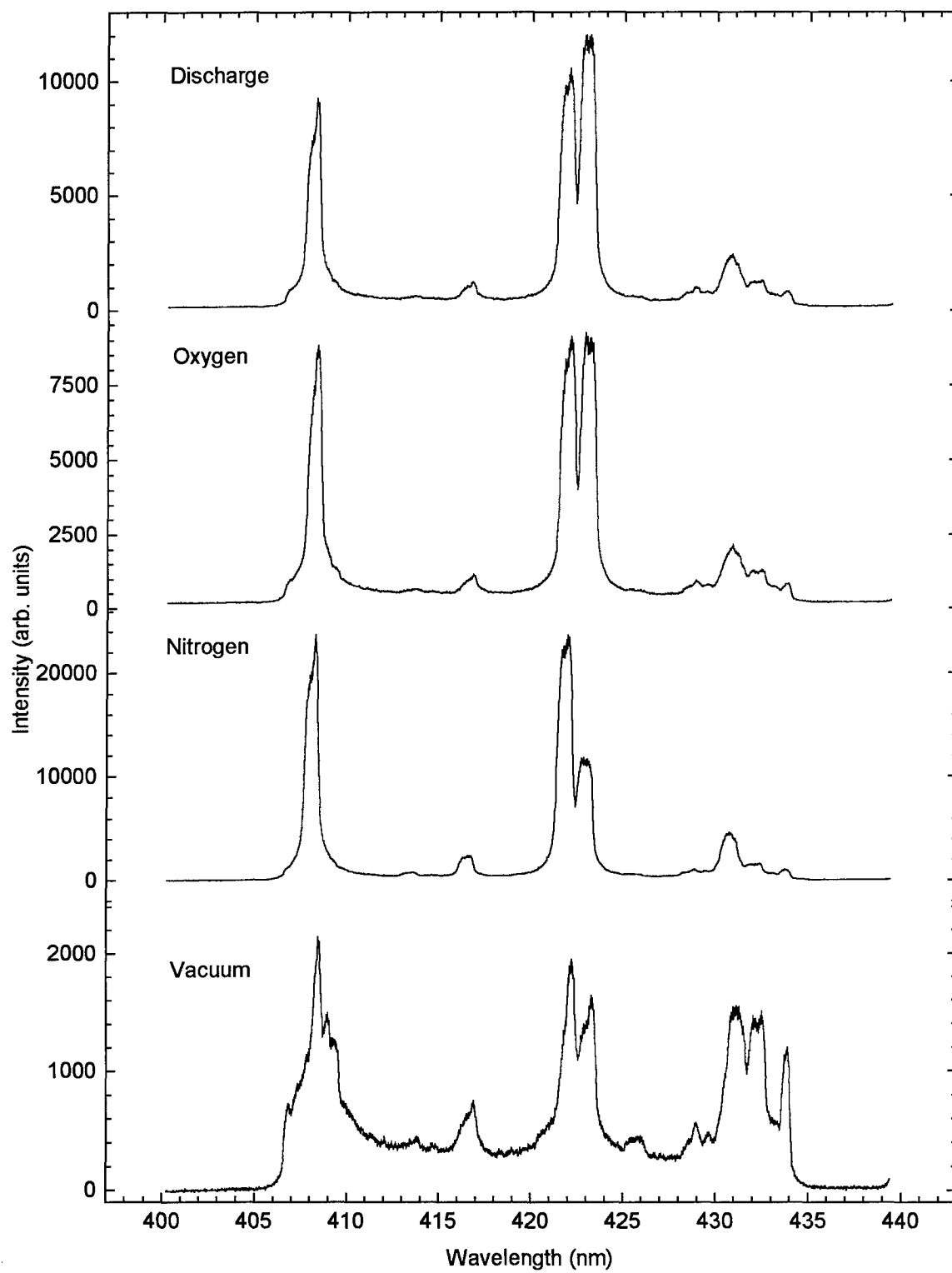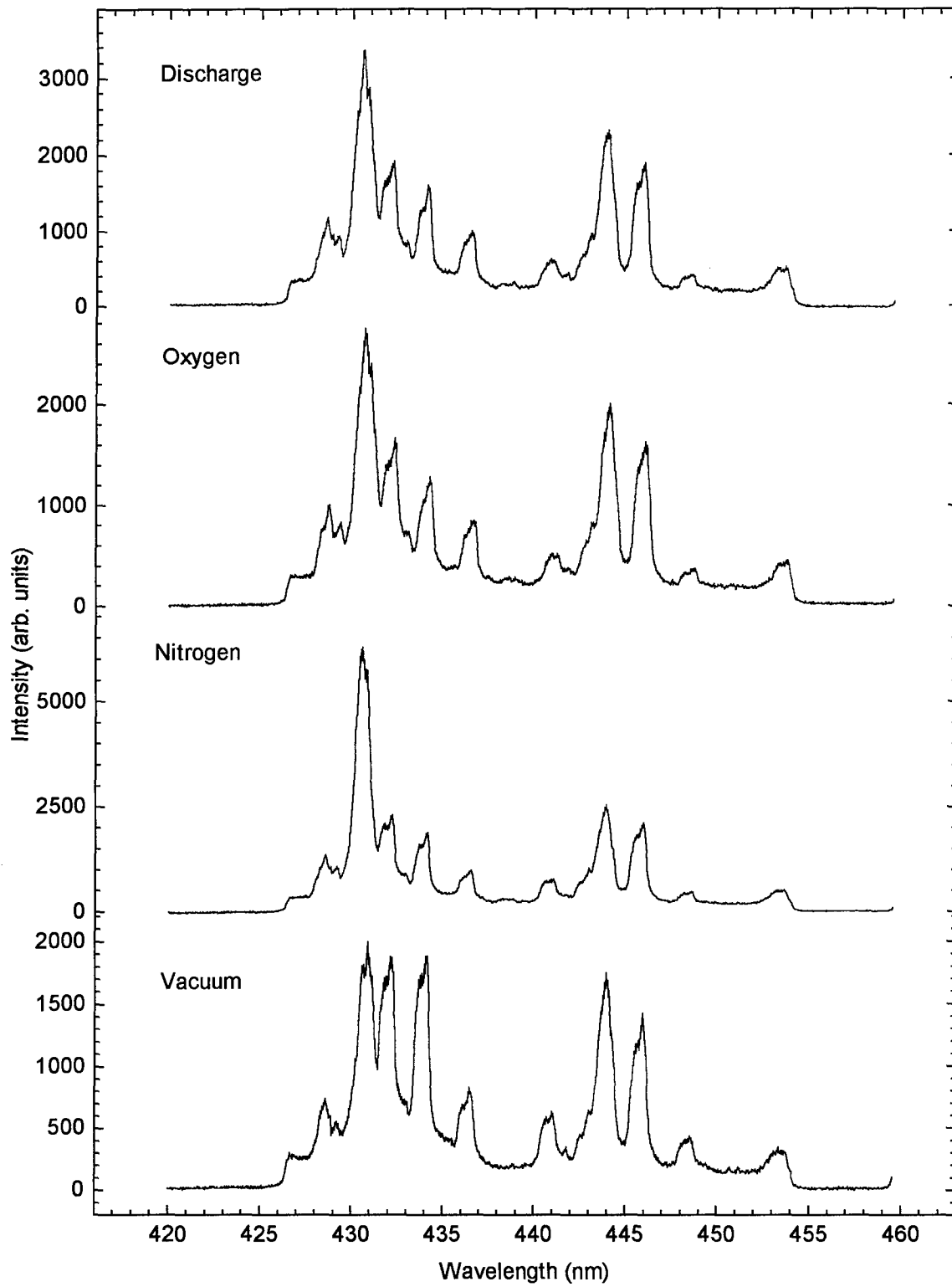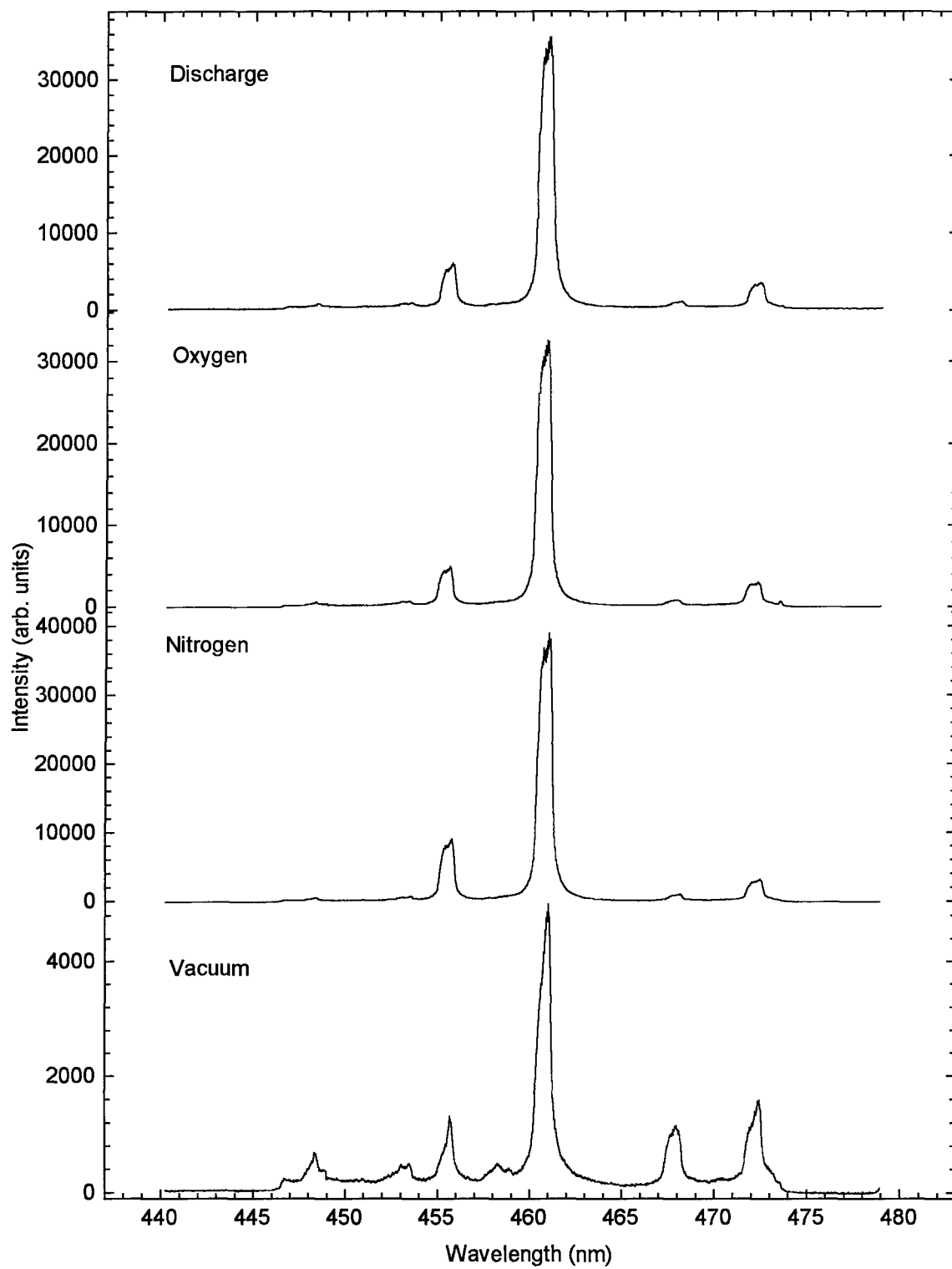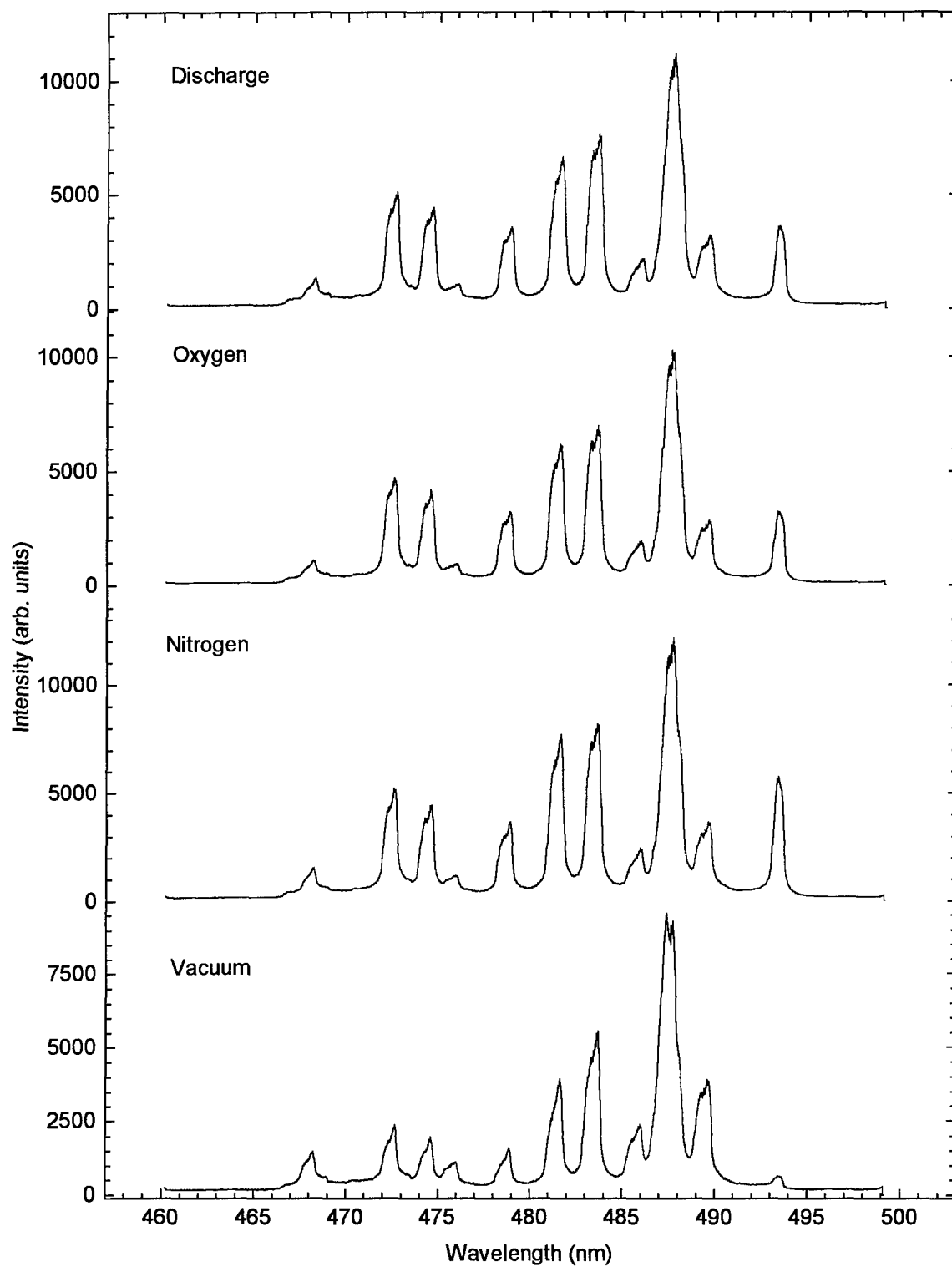
Appendix A: Spectral Data from Ba Target

Appendix A contains spectral data of laser-ablation plumes from a Ba target. Background gases were at 25.0 mtorr. Data was taken 1.0 cm from the target. Laser fluence was 270 mJ-cm^{-2}. Data was taken using a 0.5 m spectrometer with a 1200g/mm grating, 100μm slit and an Oma linear array. The signal was integrated over 16.6 msec and 120 pulses were summed to get this output.

Intensity (arb. units)

Wavelength (nm)
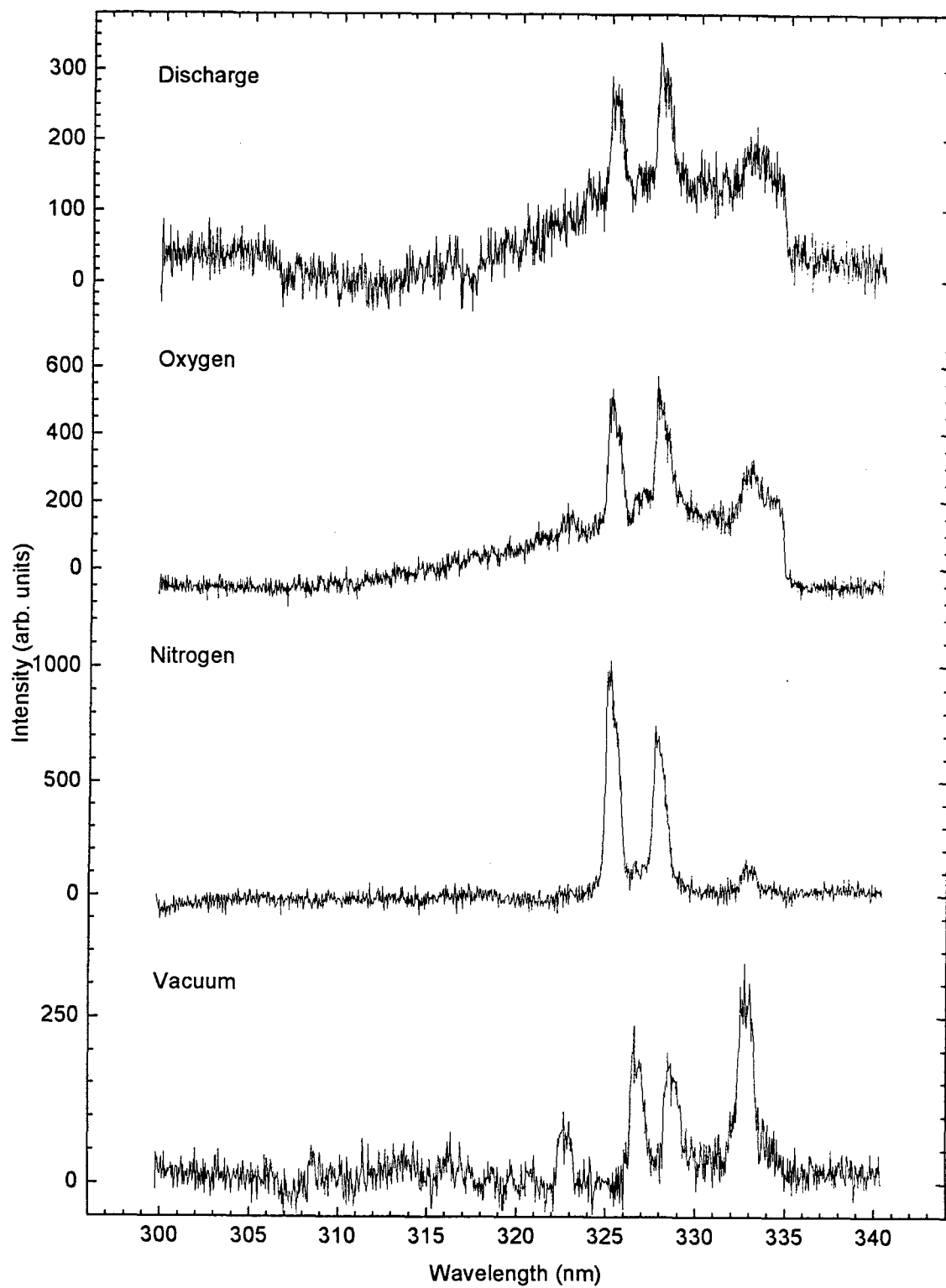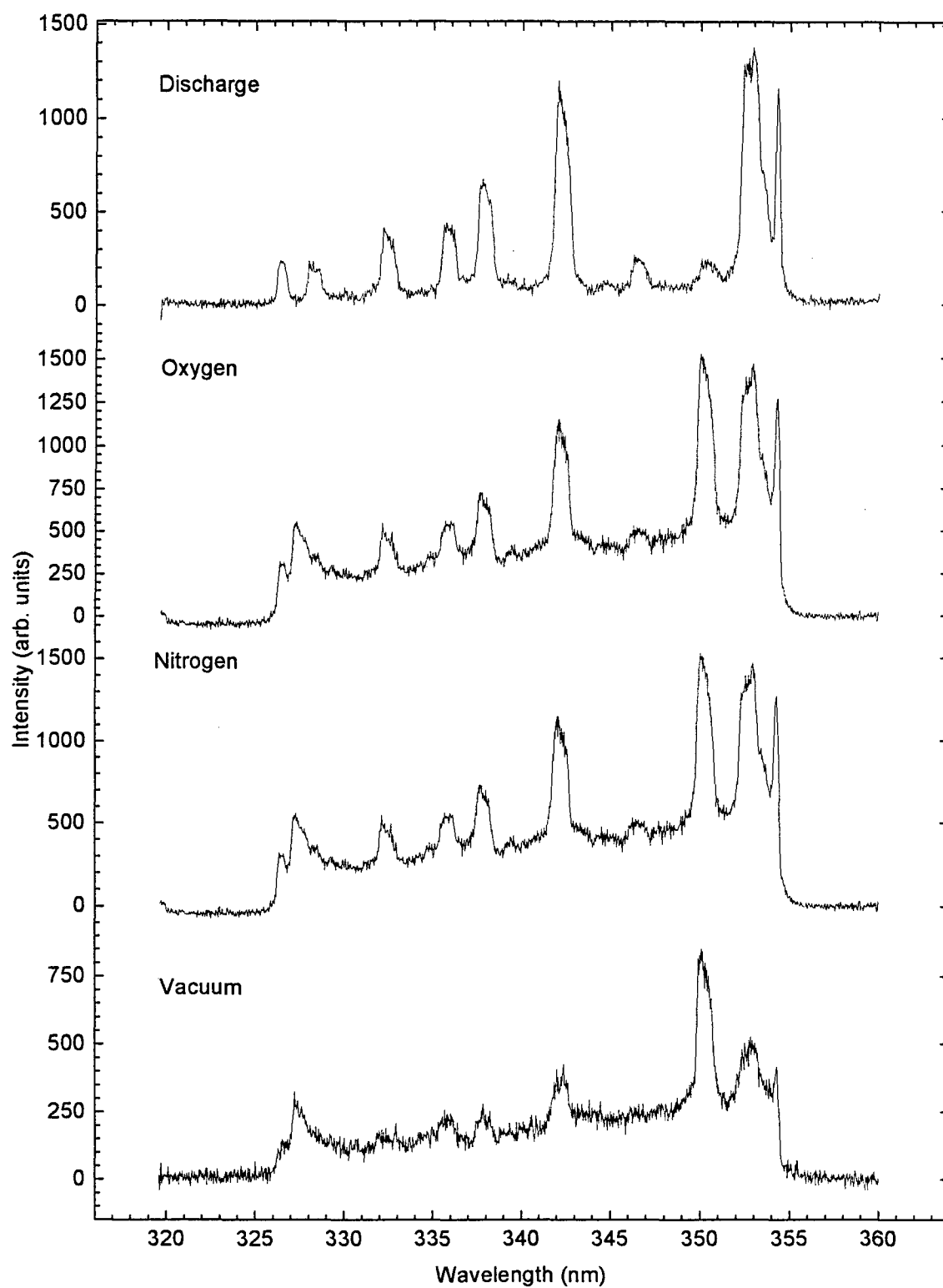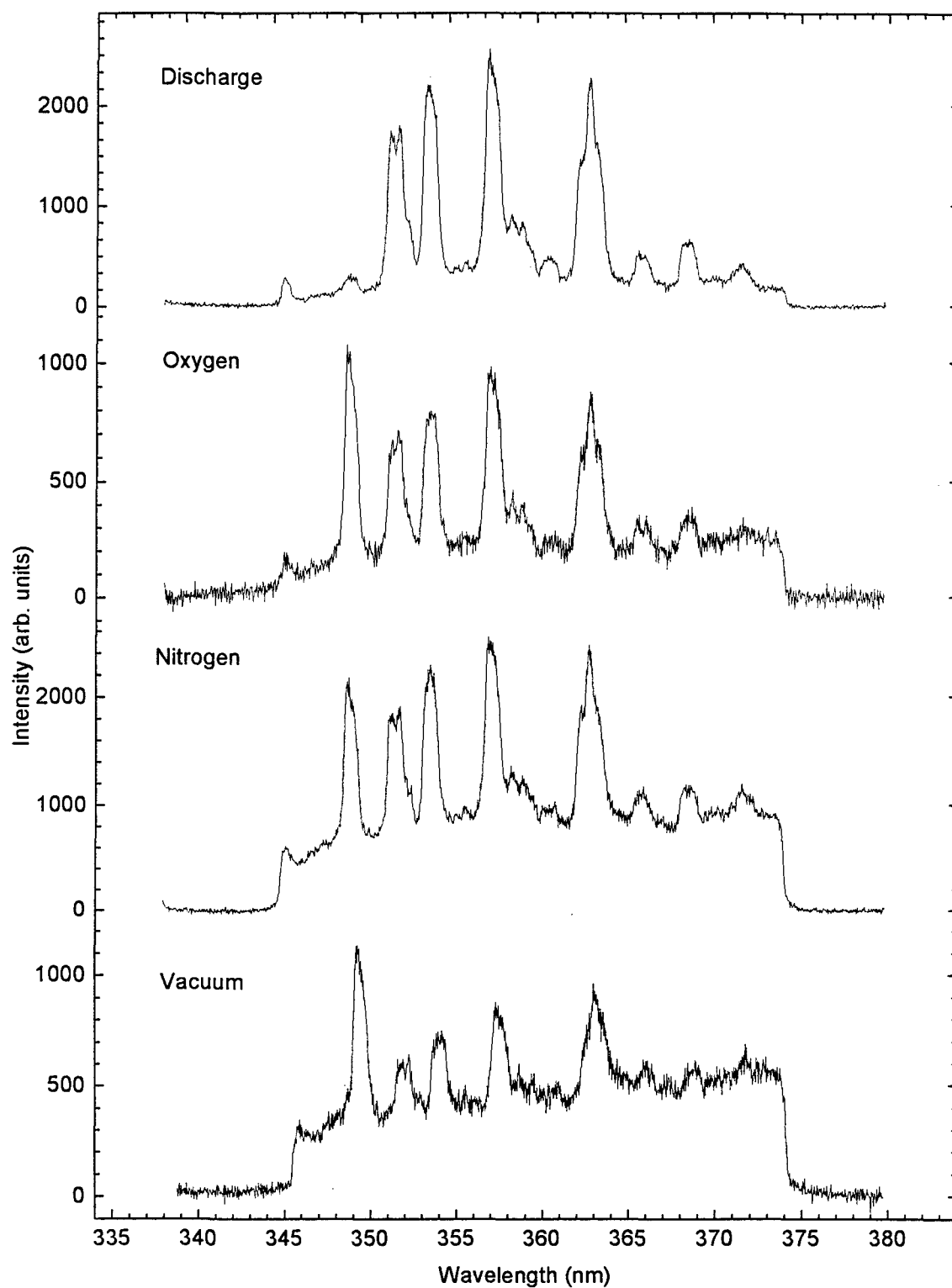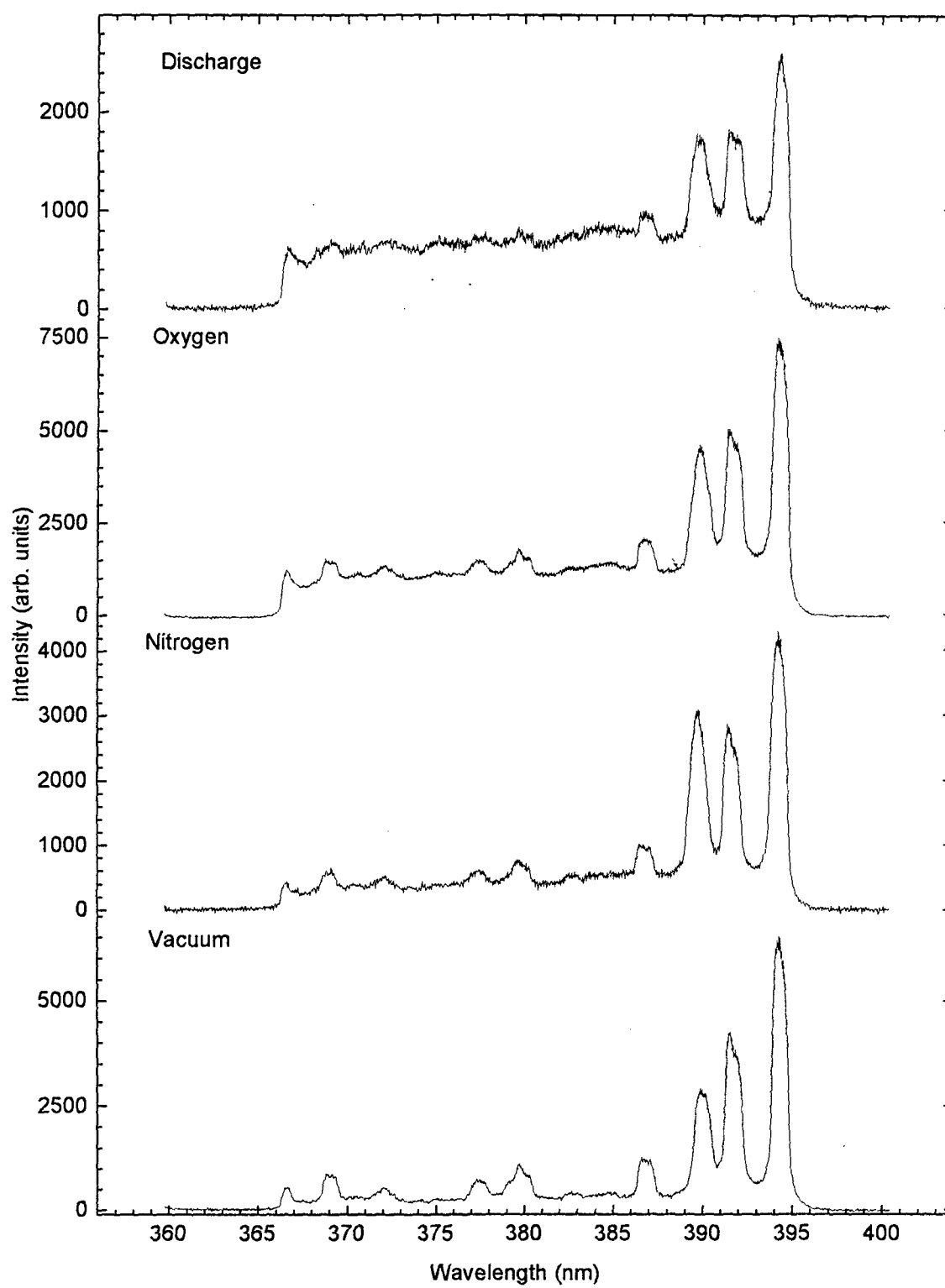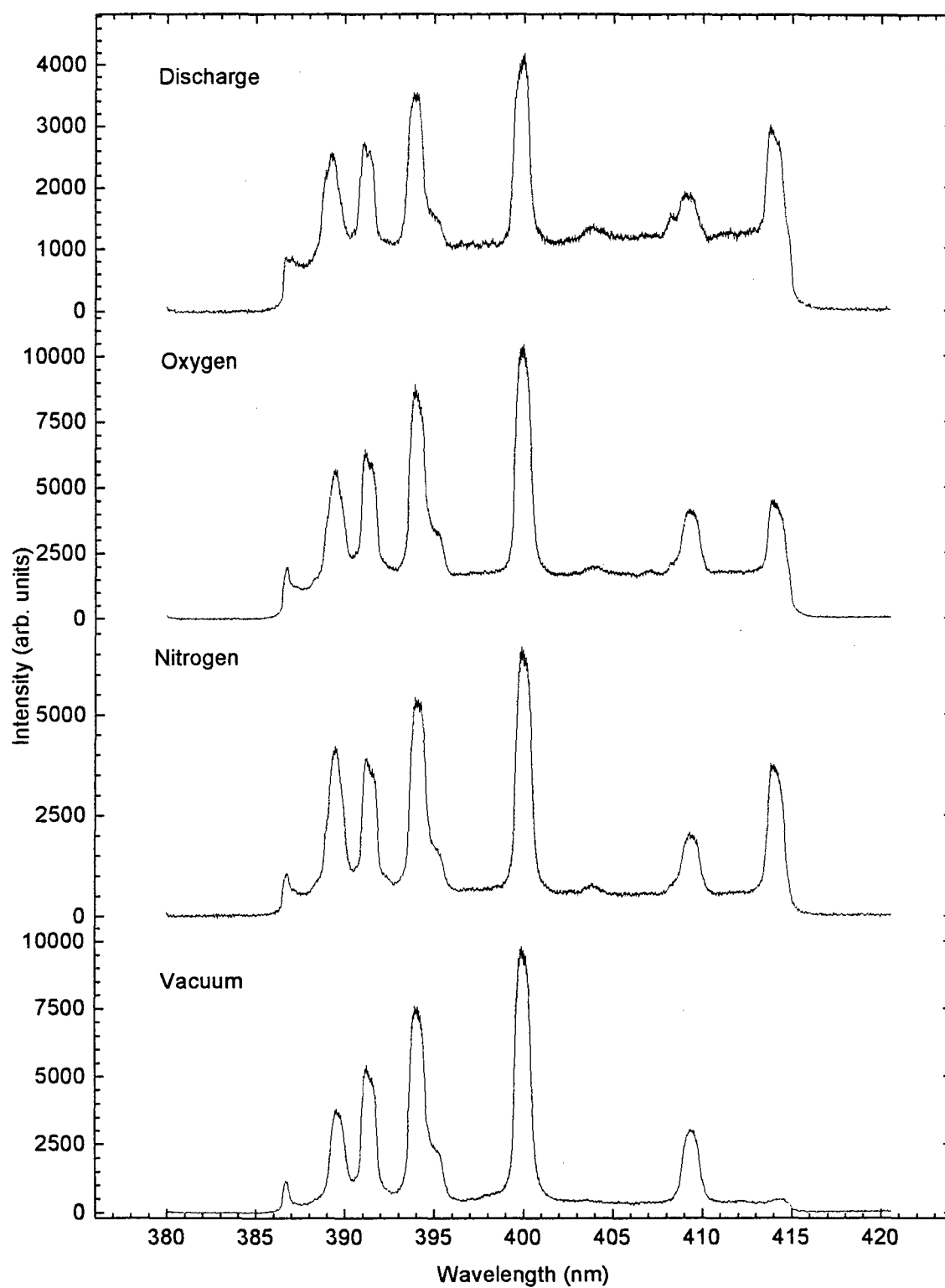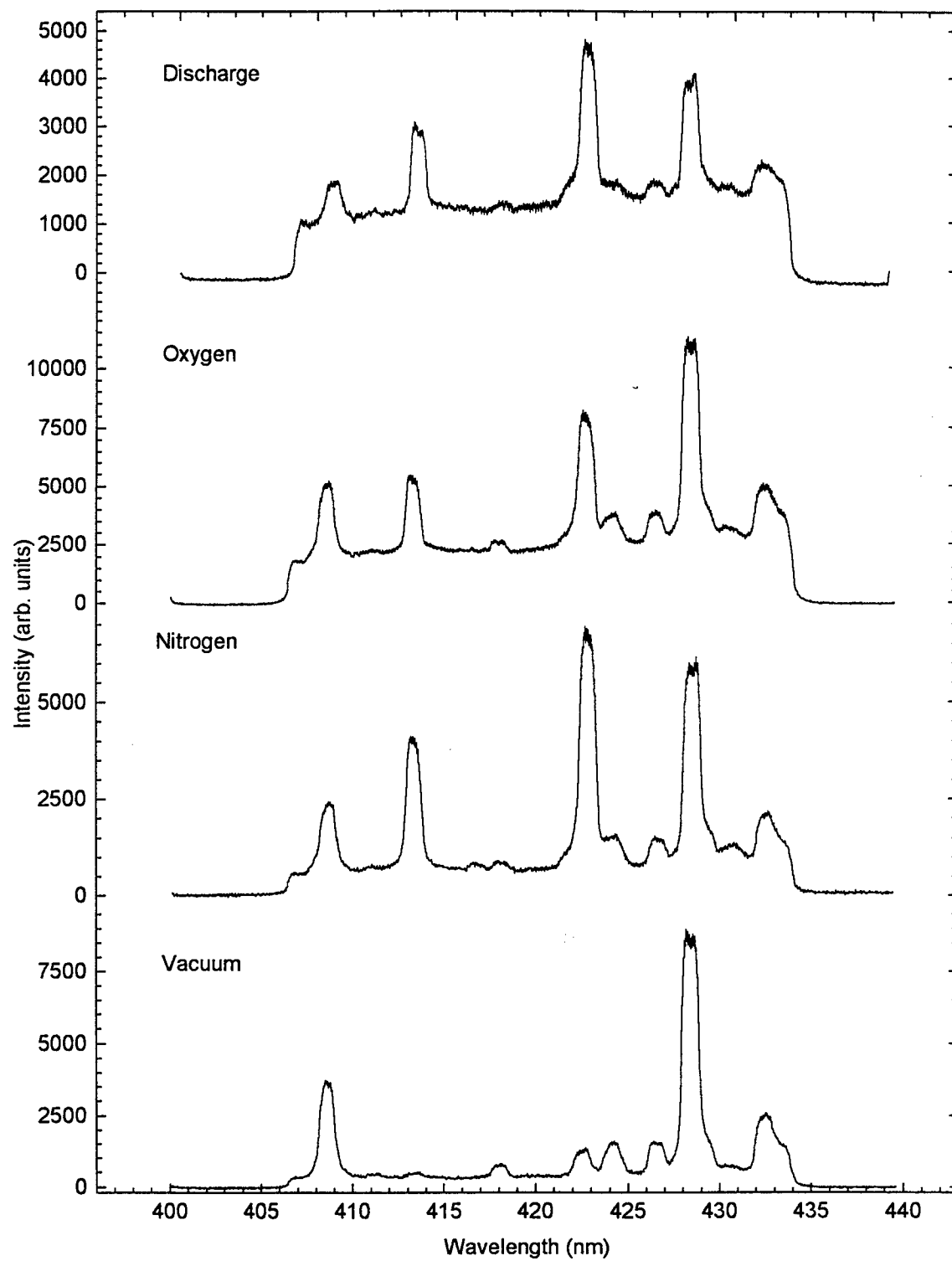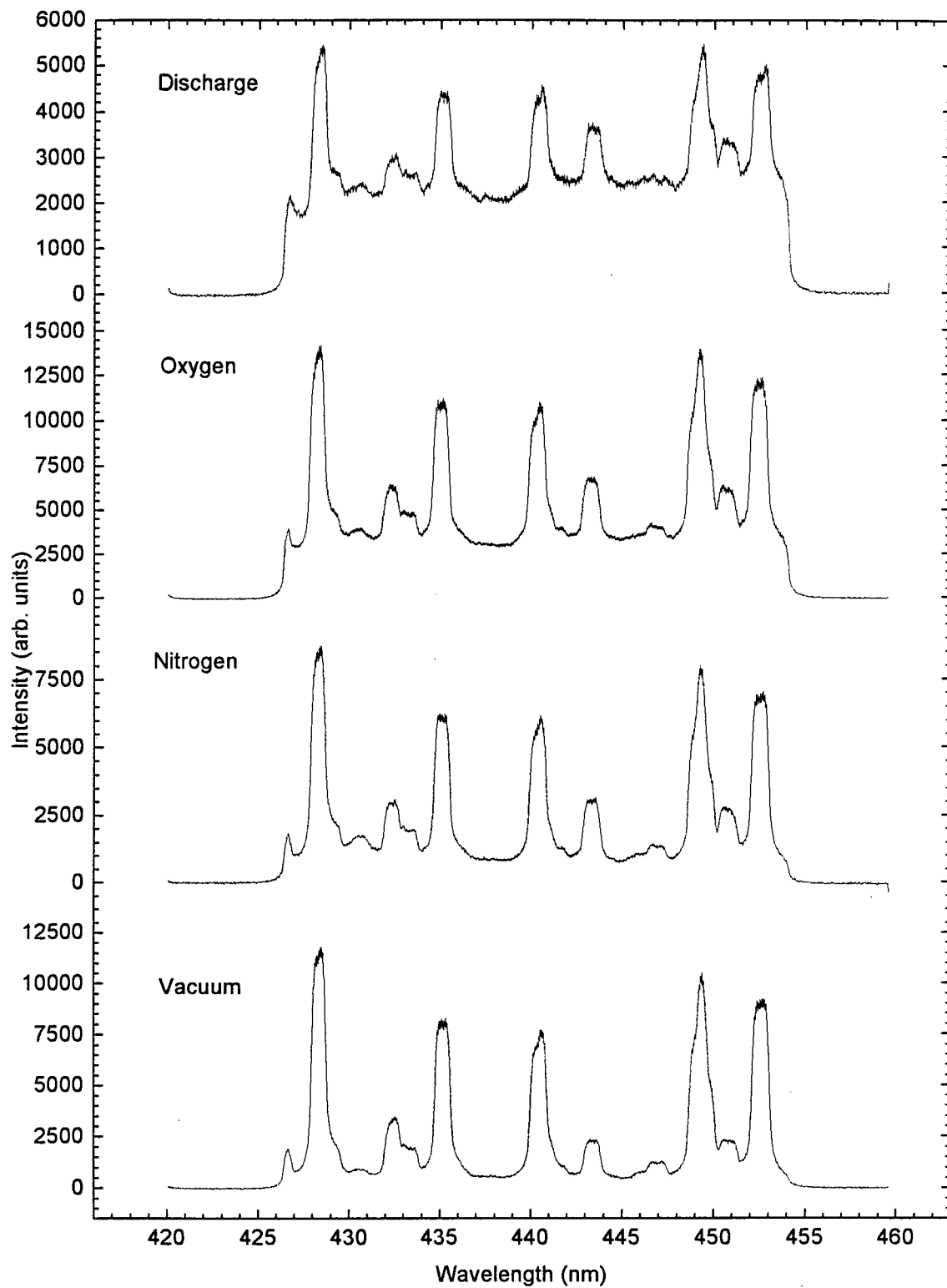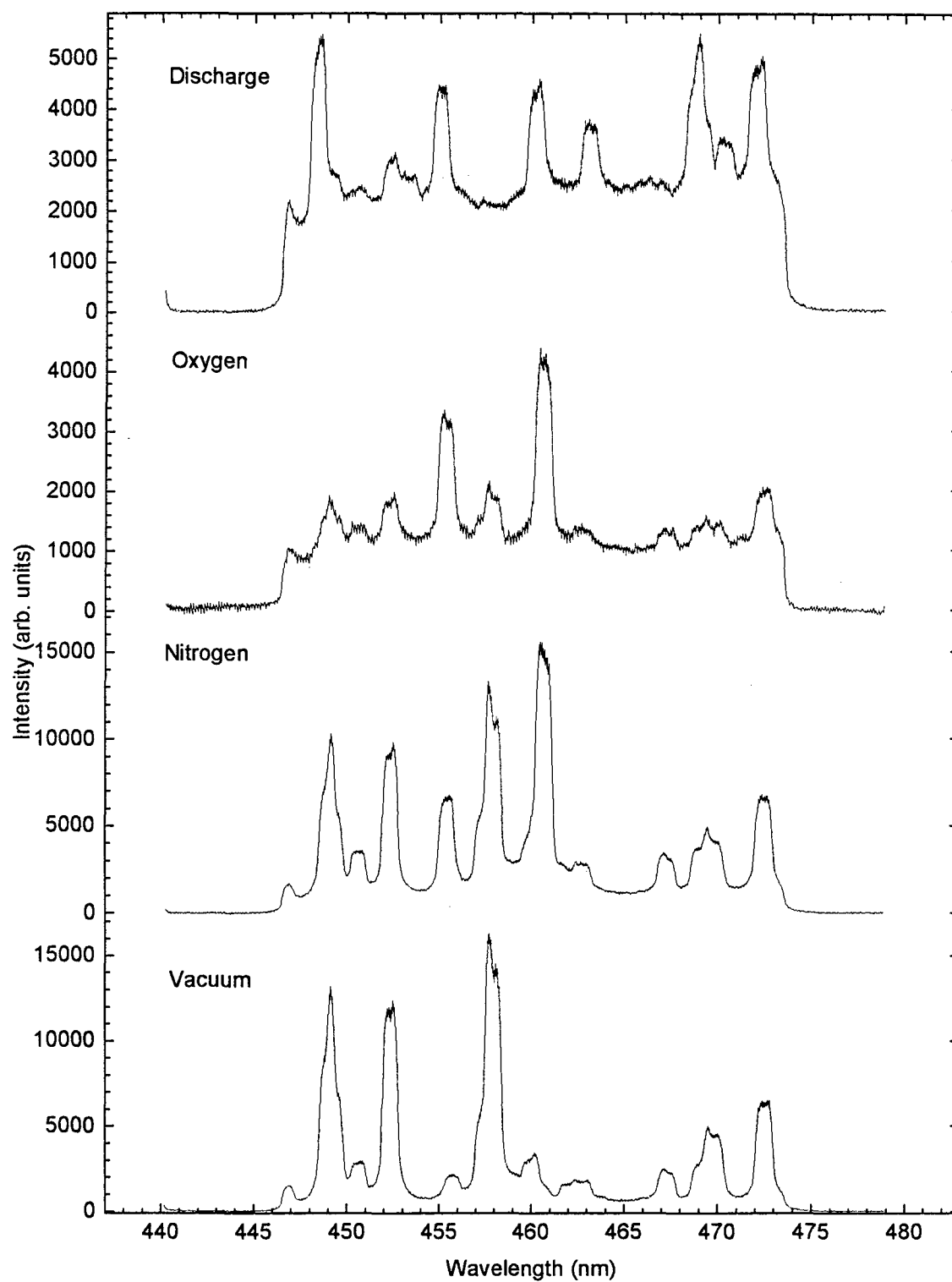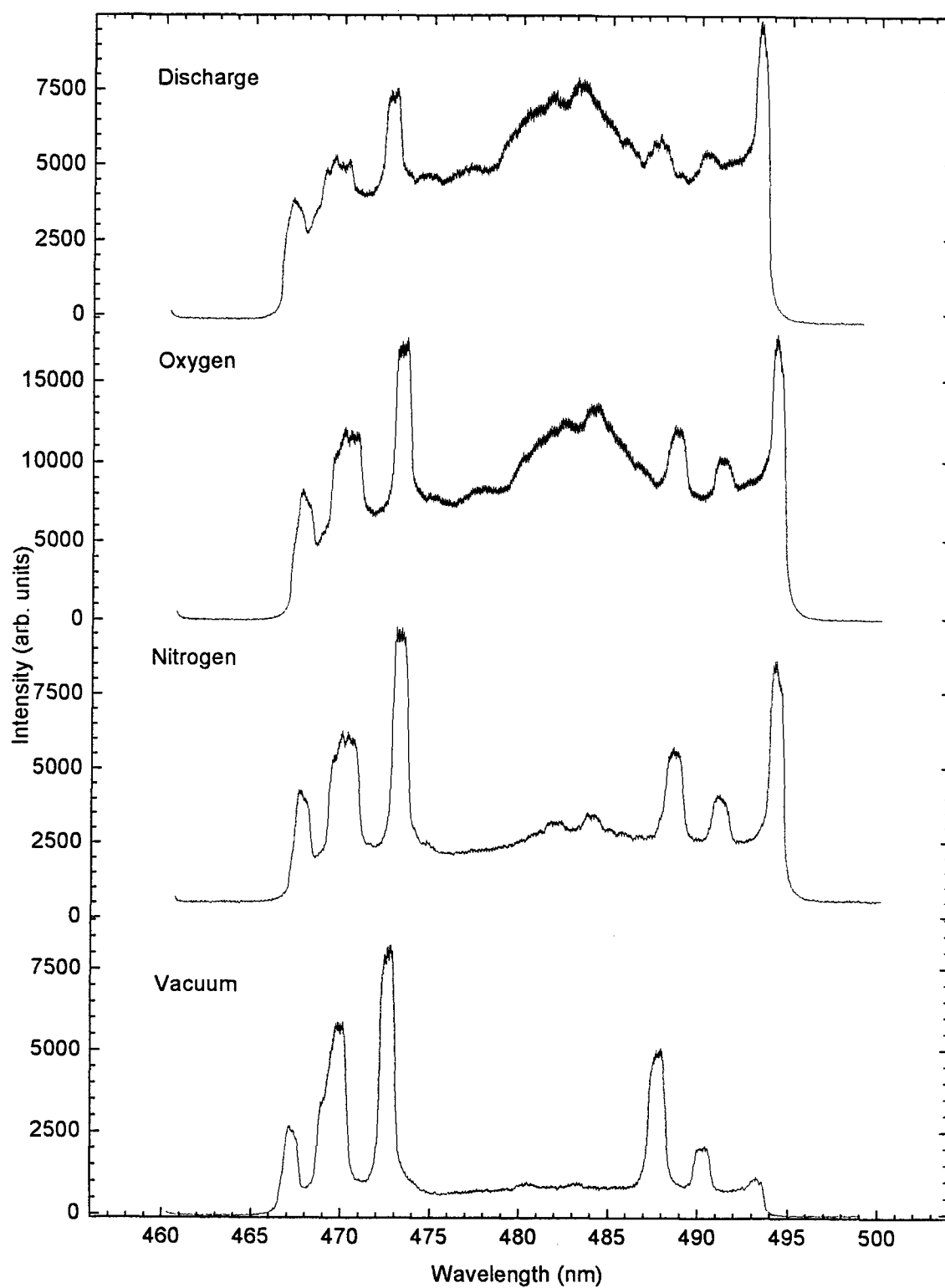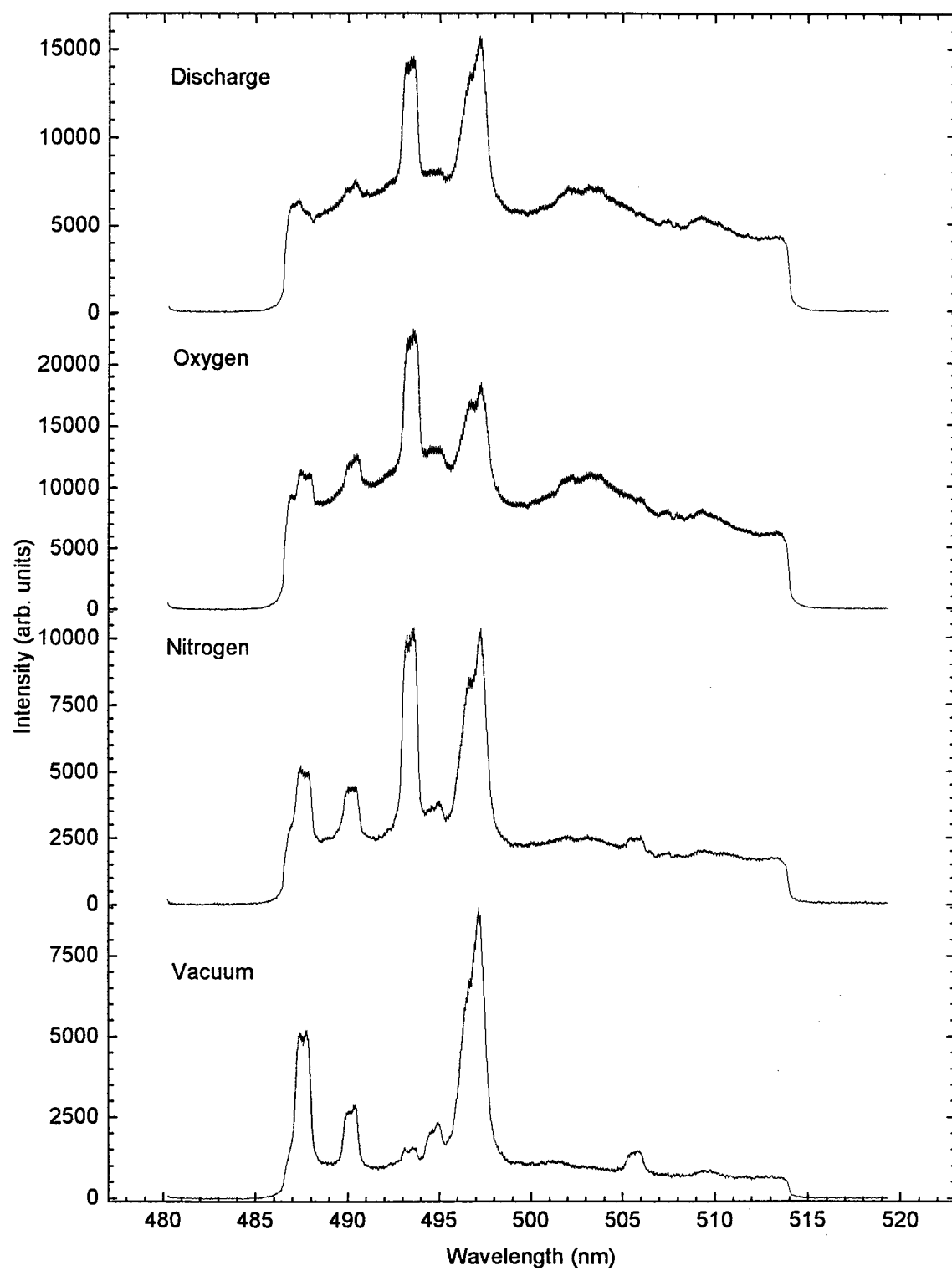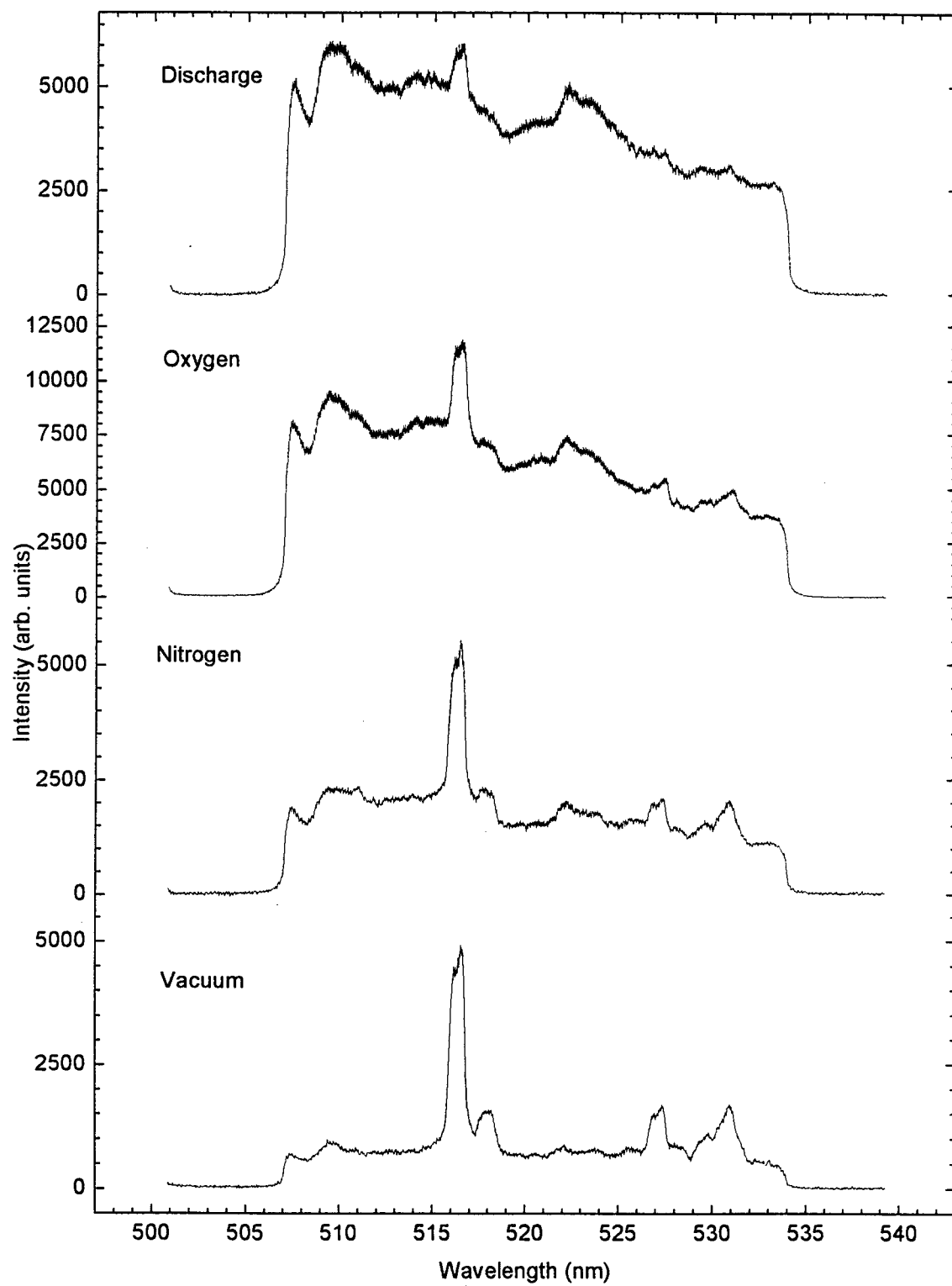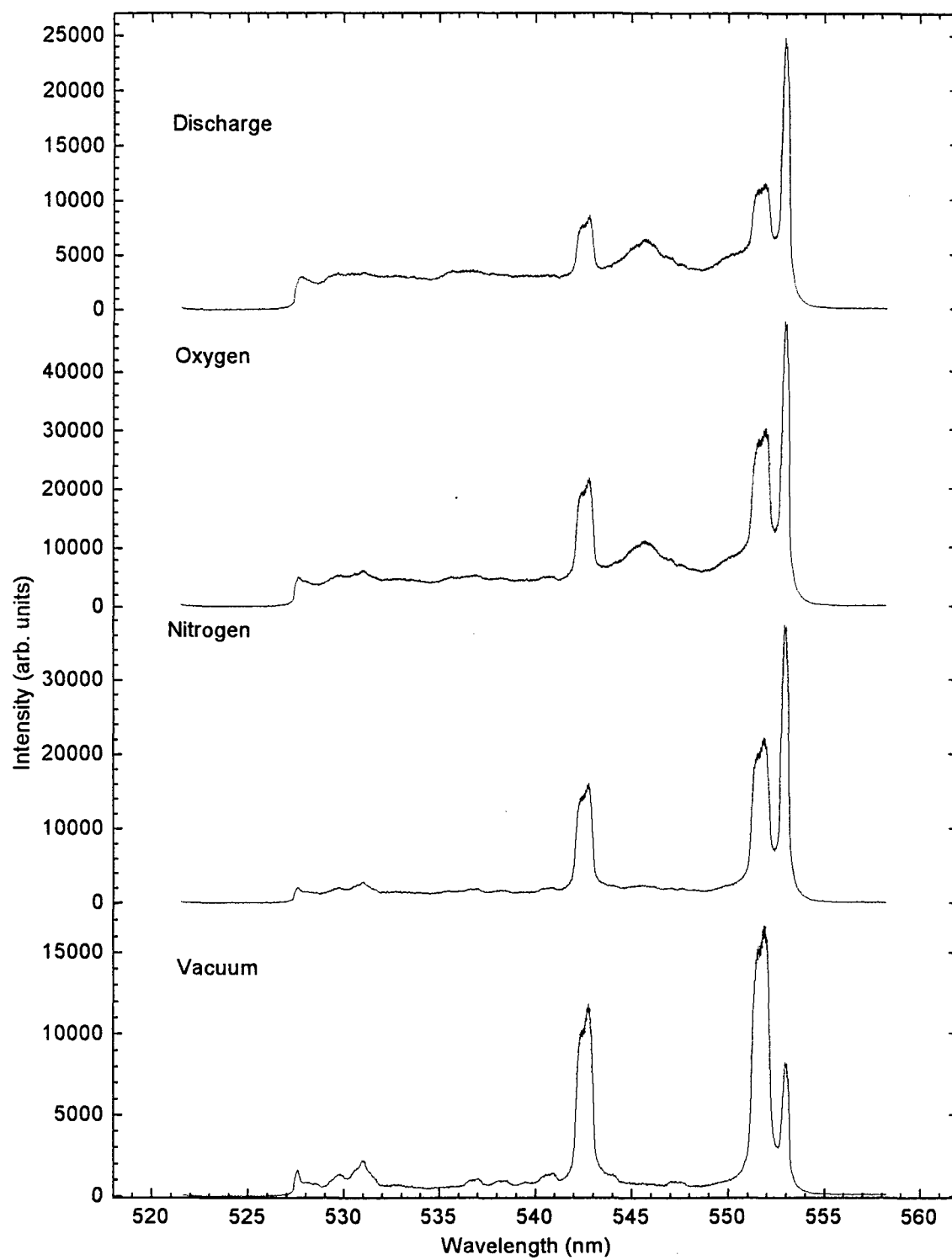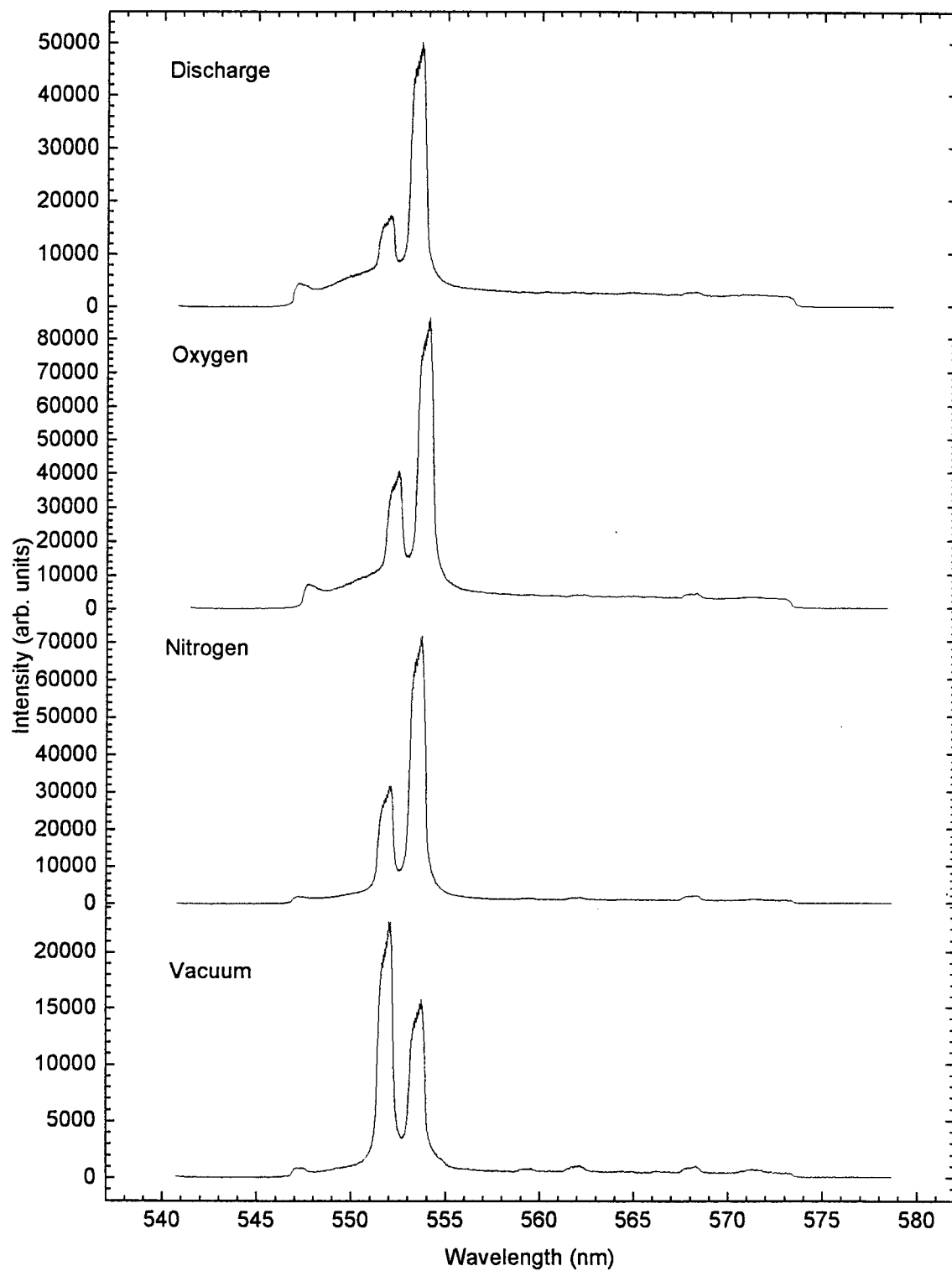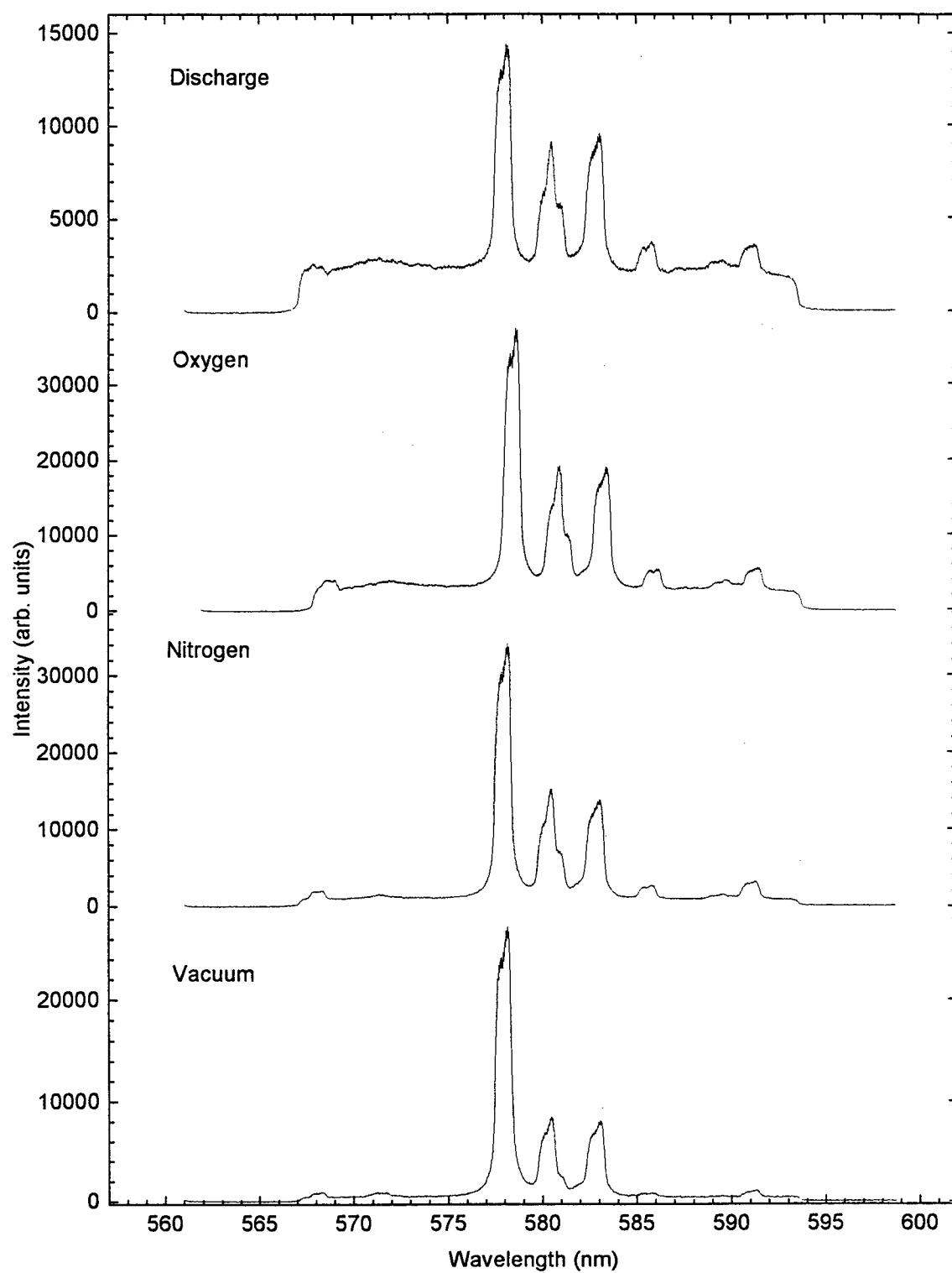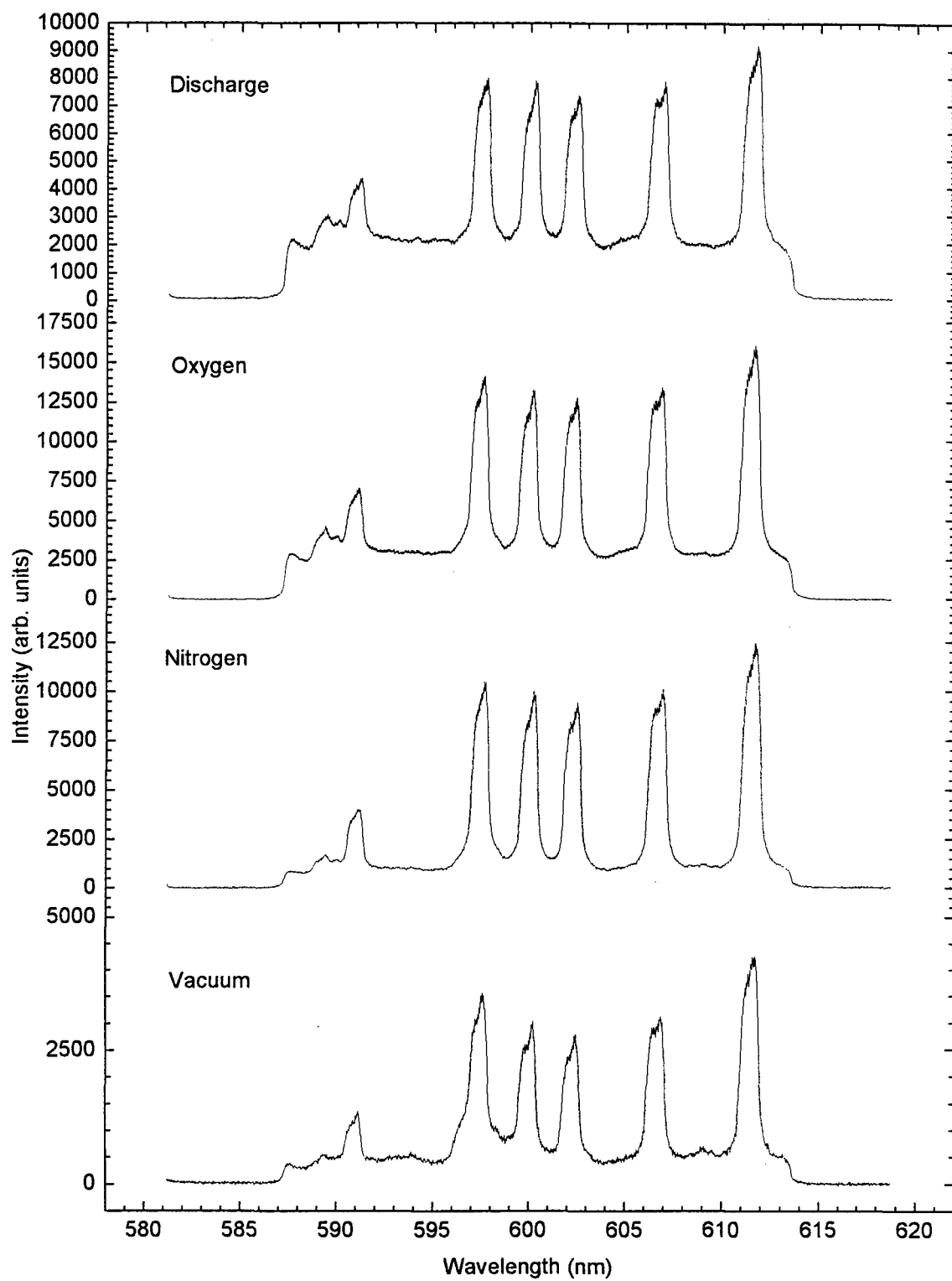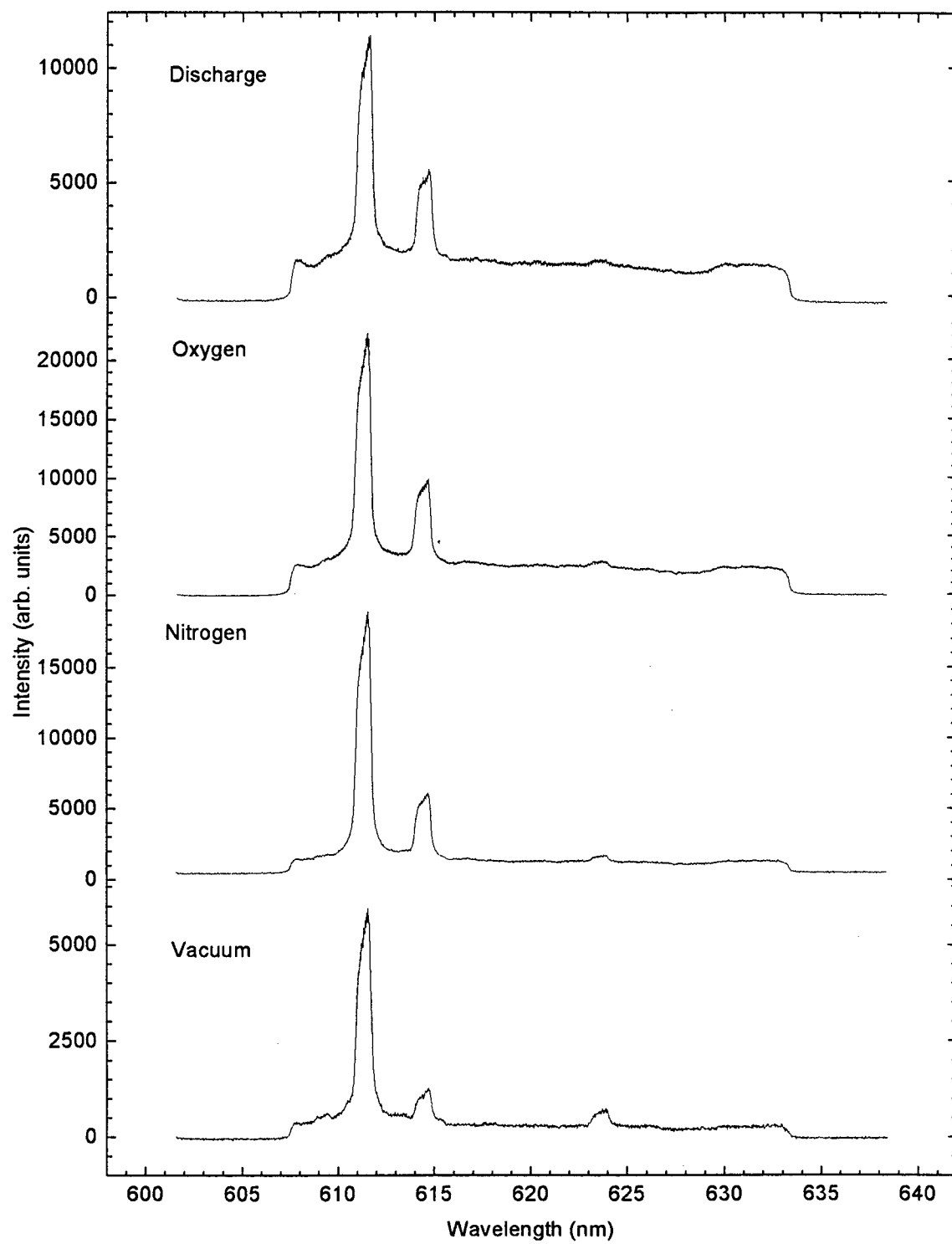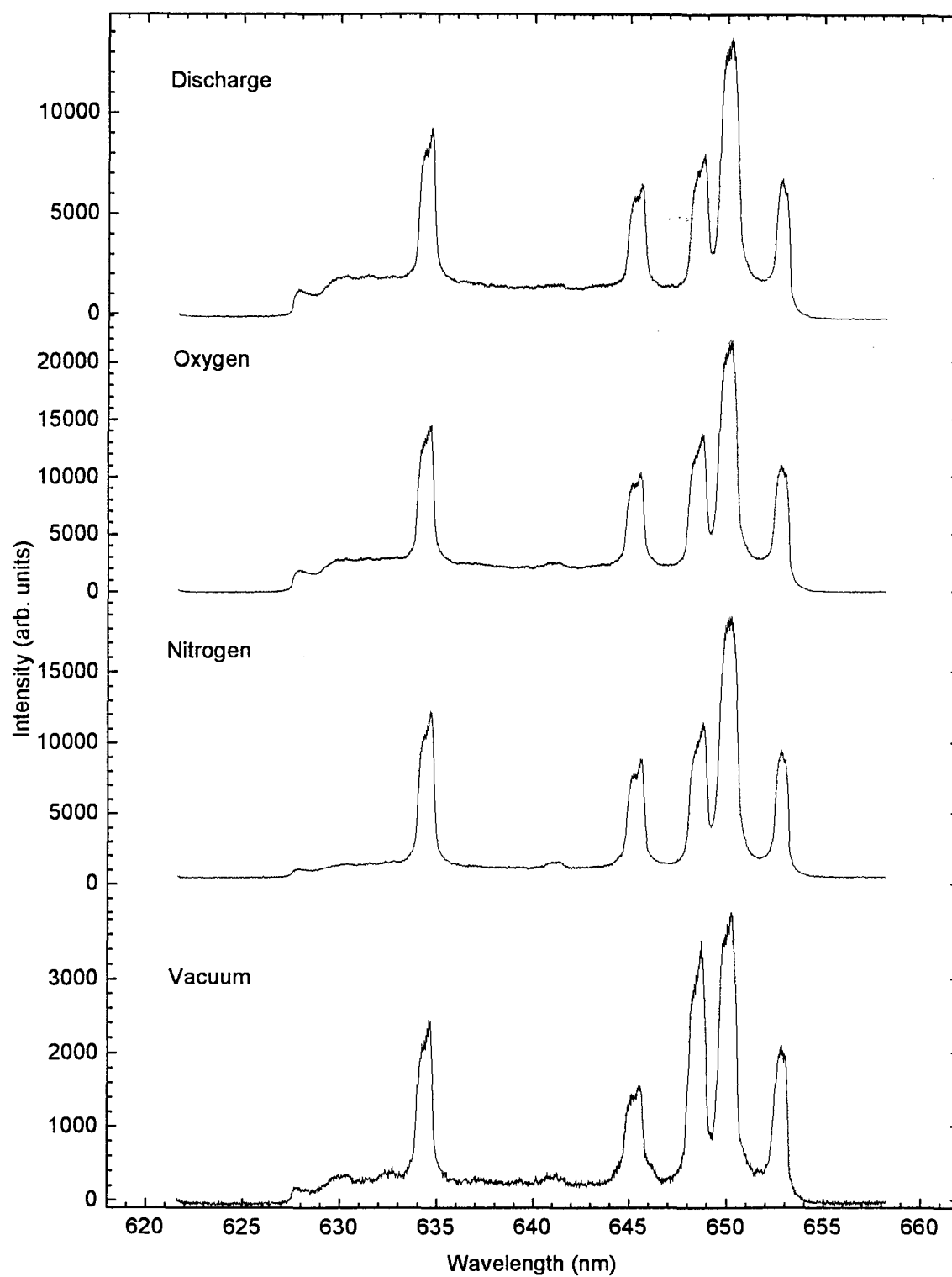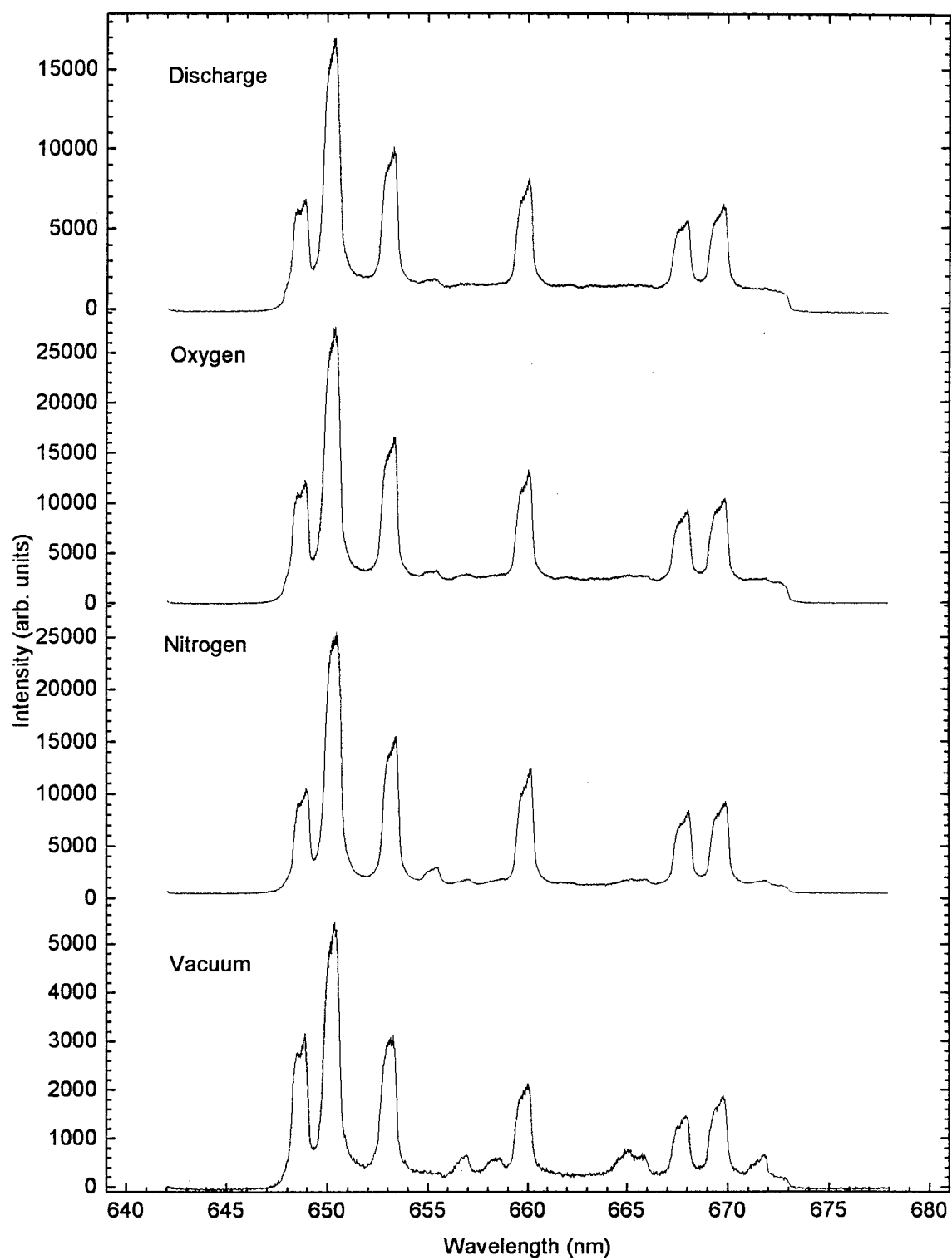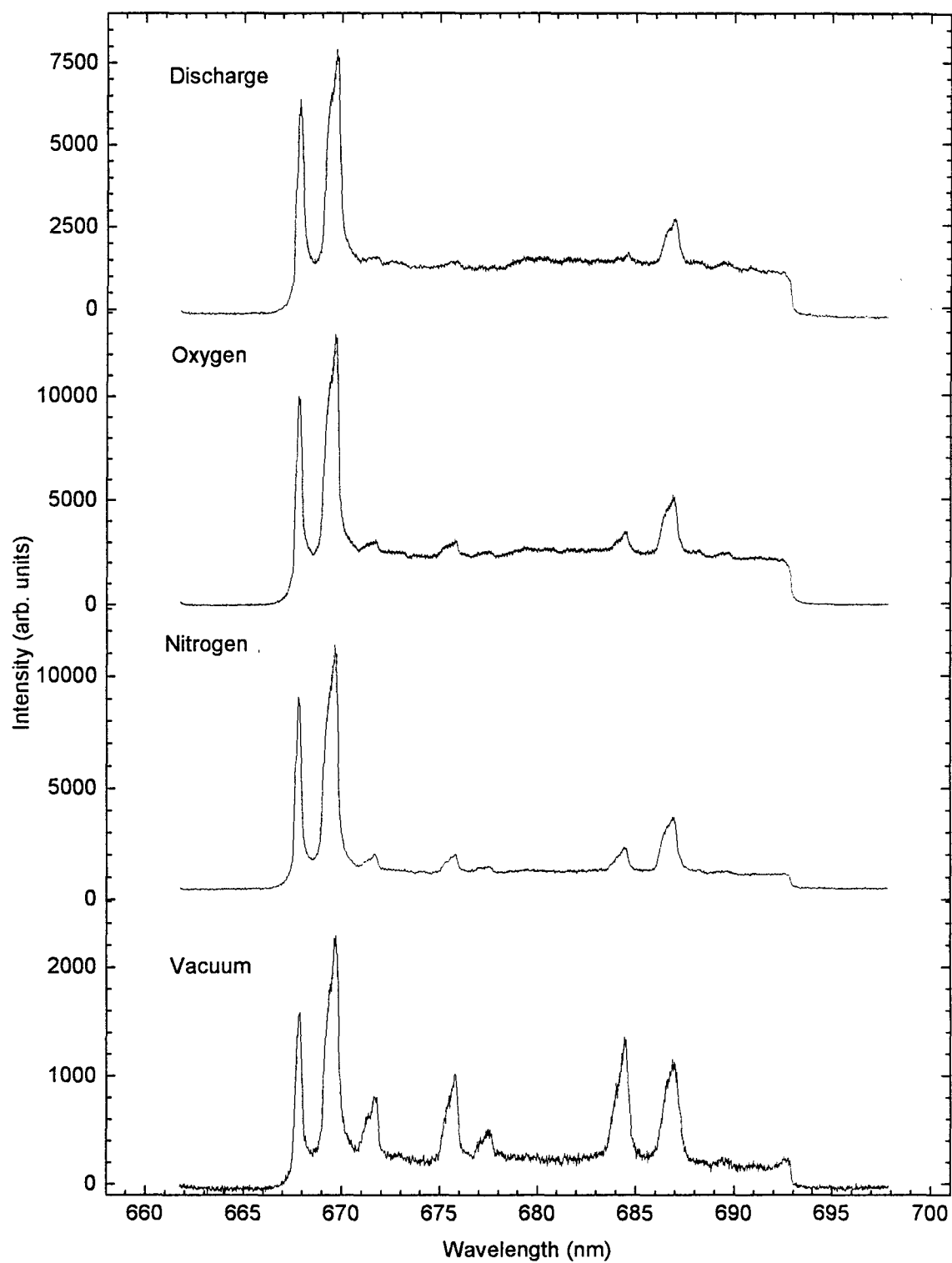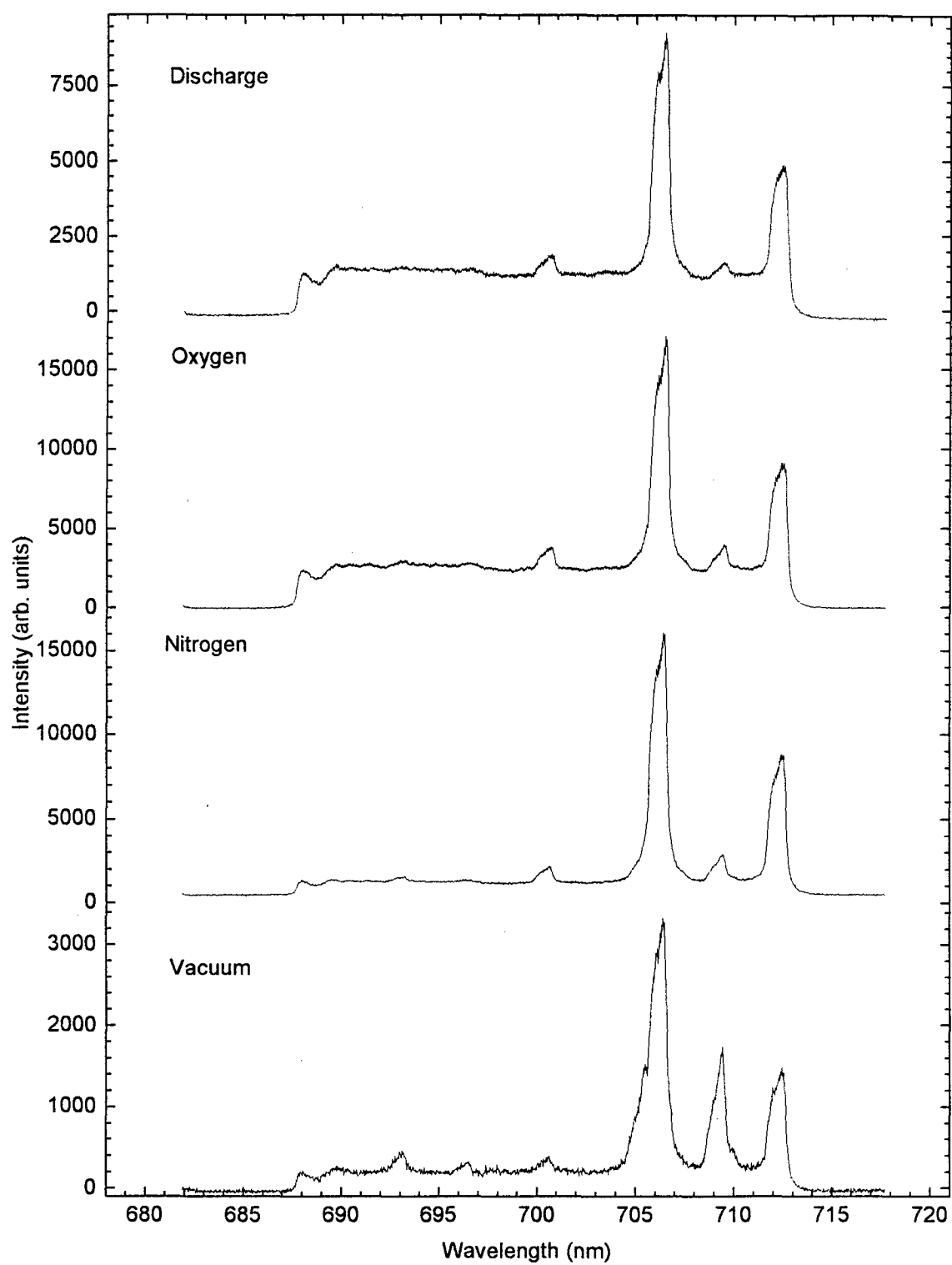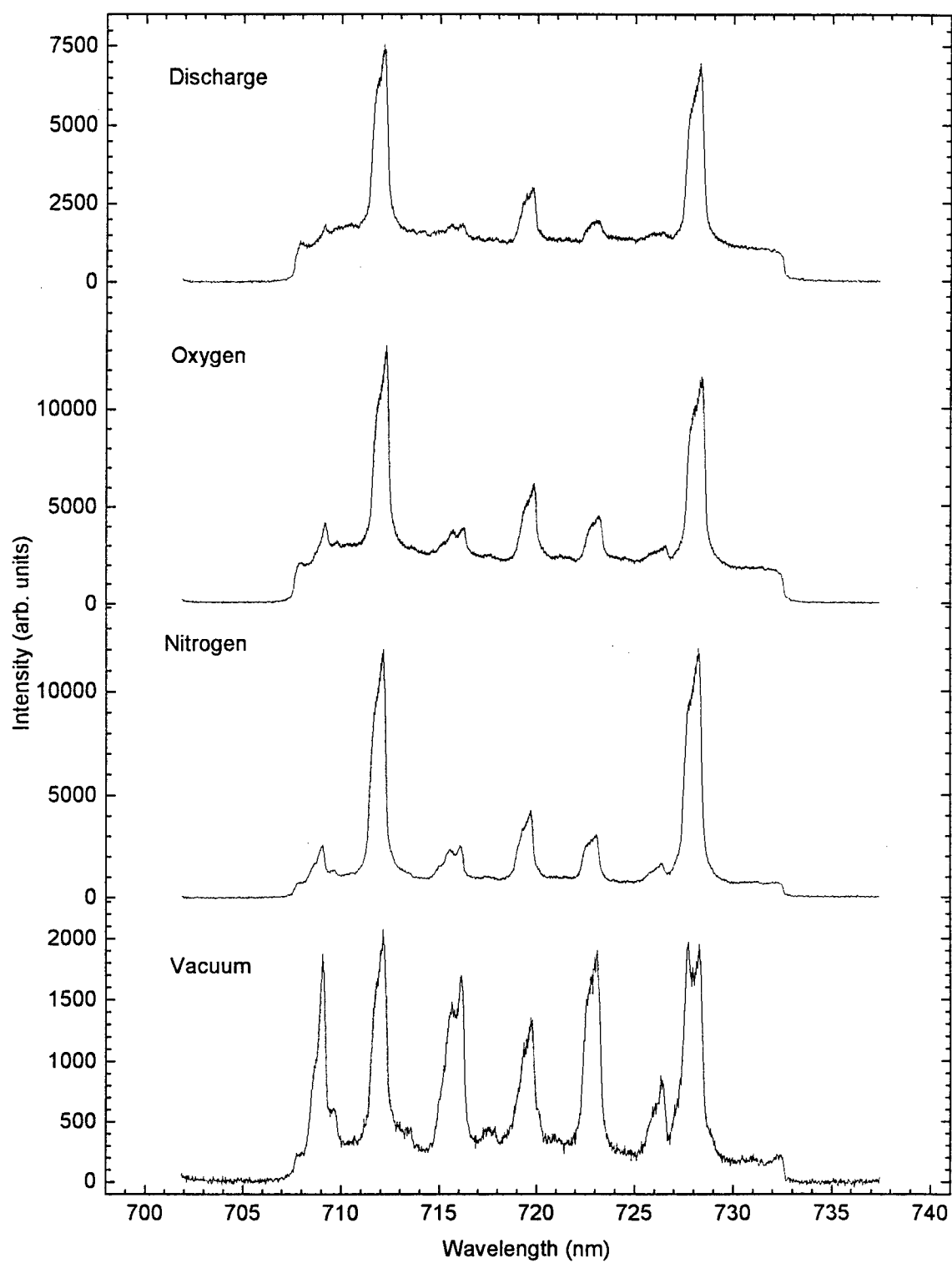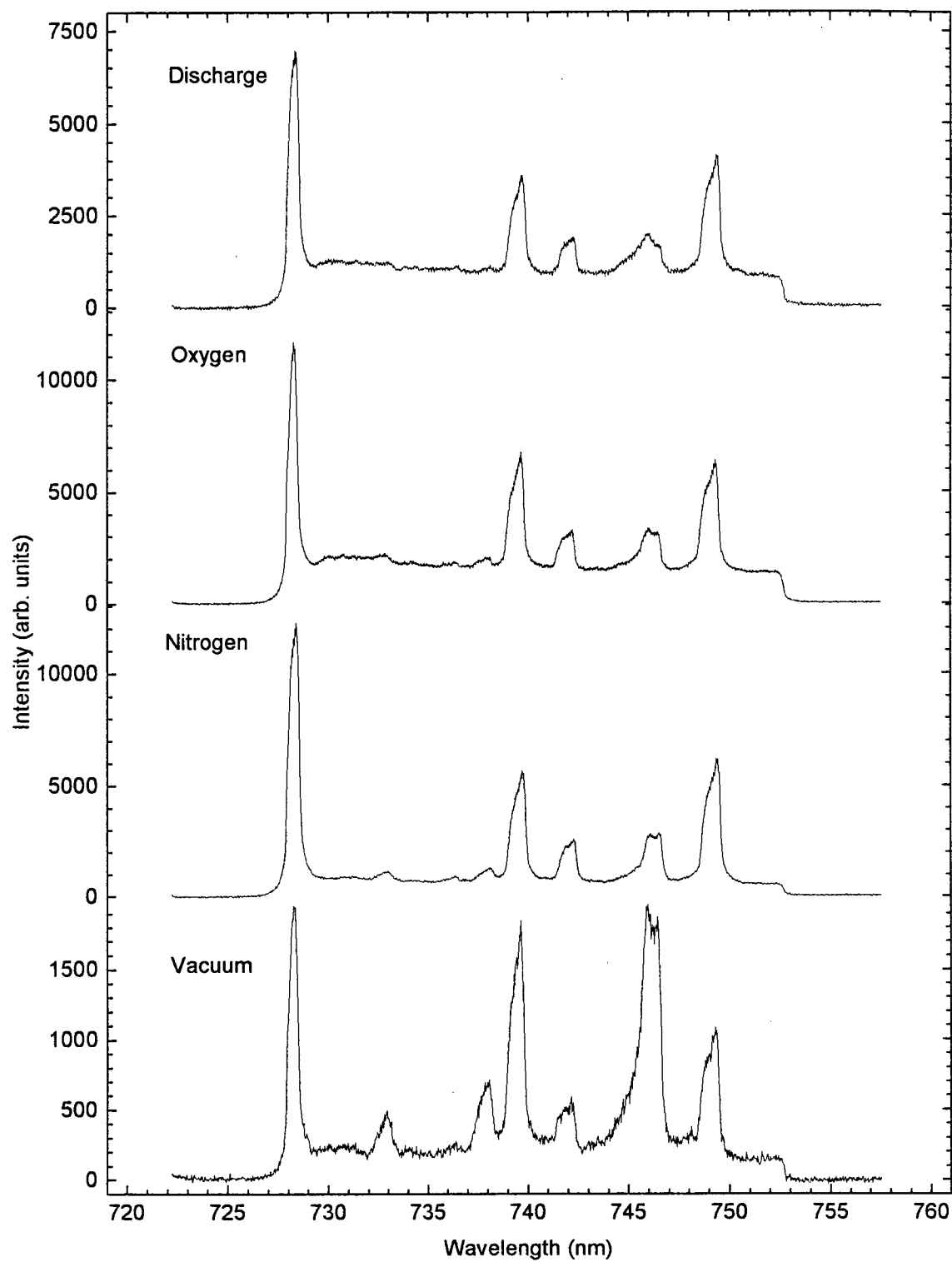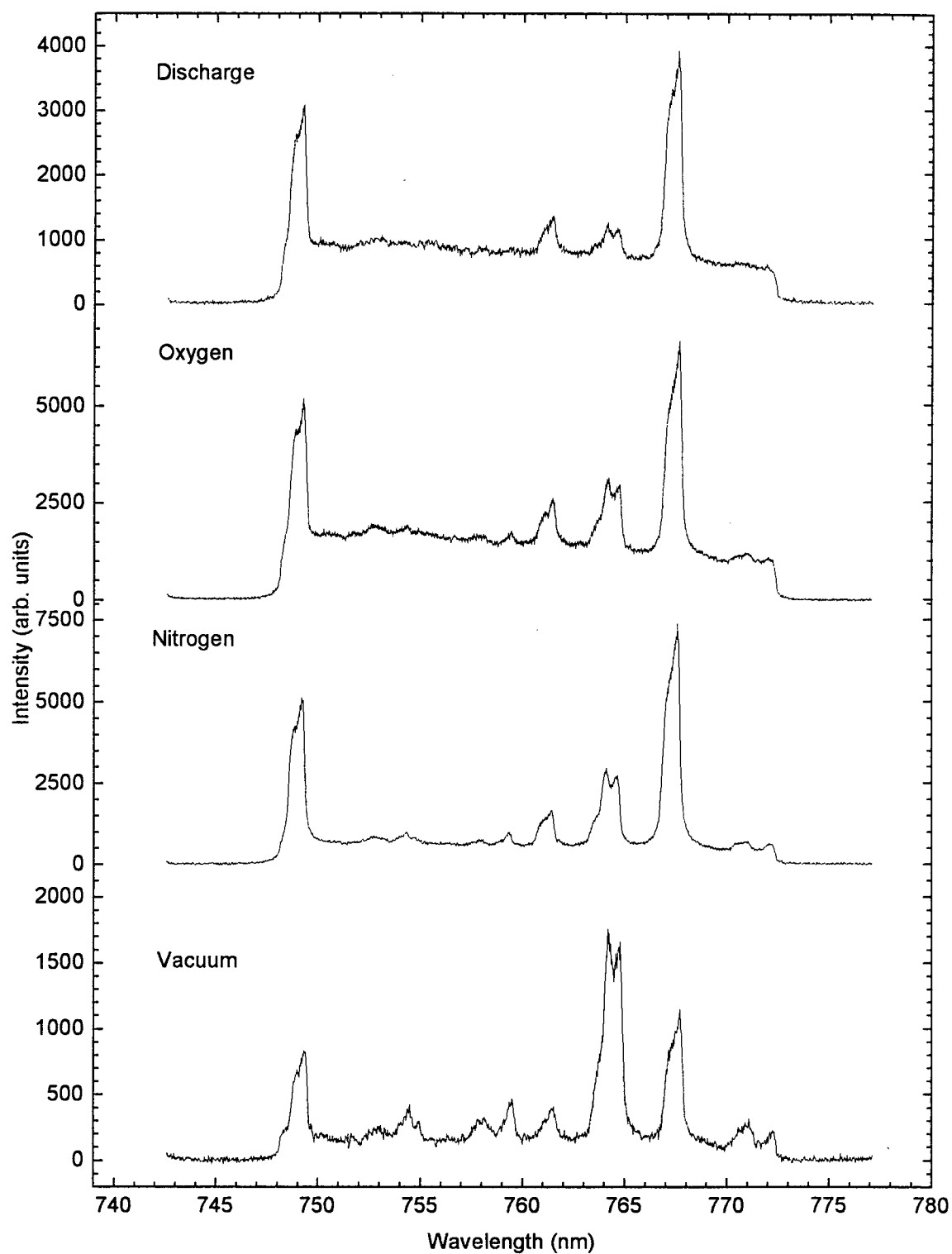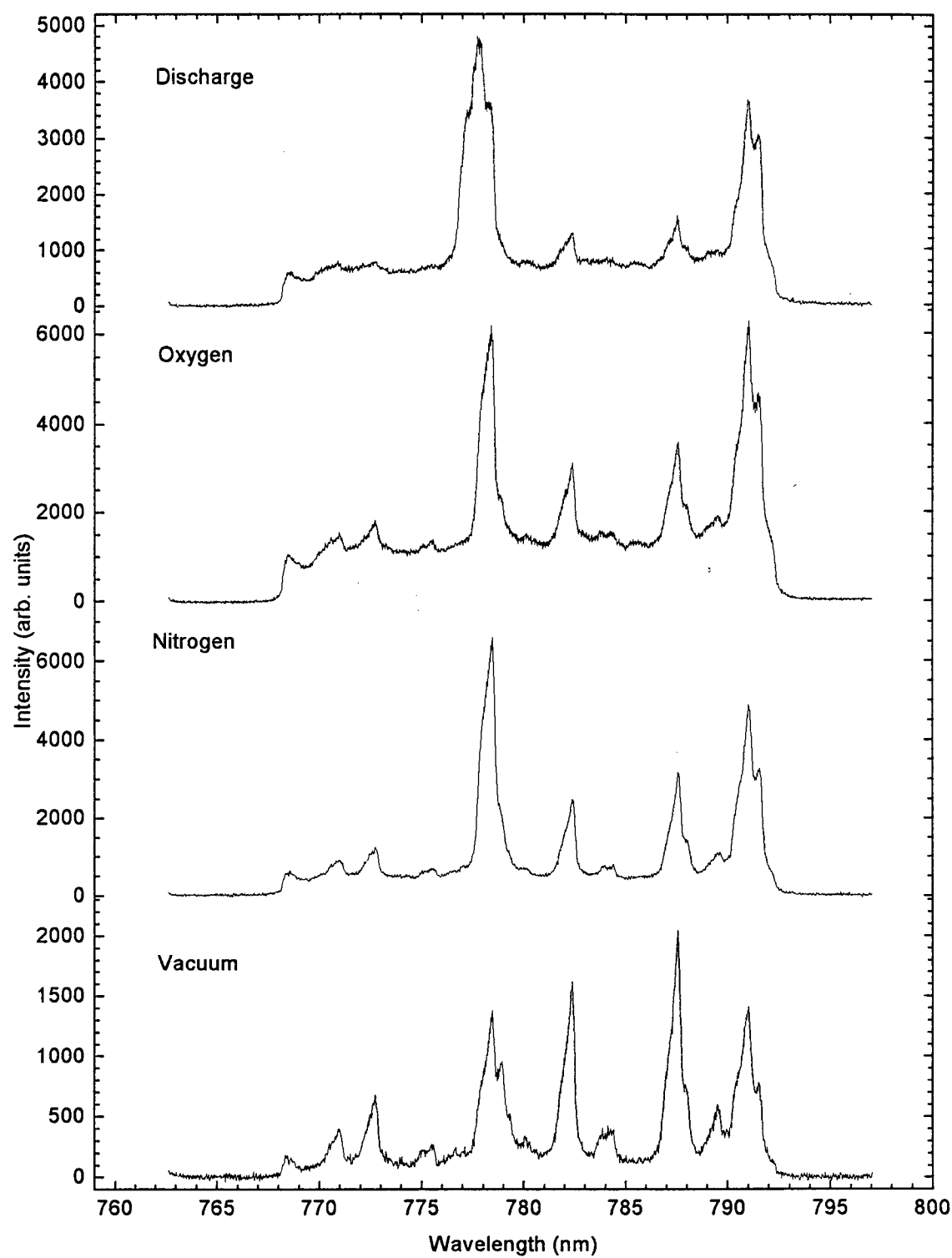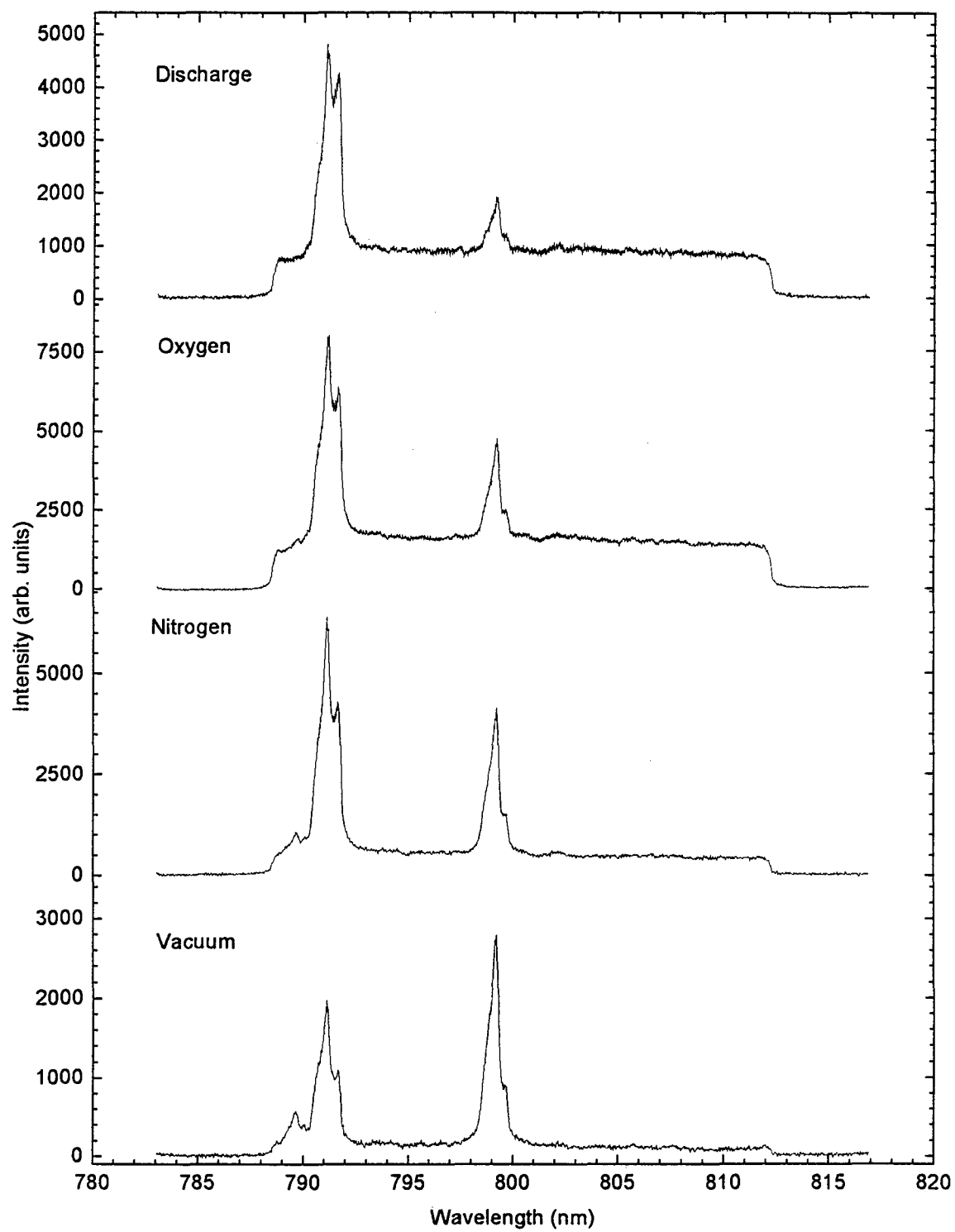
Appendix B: Spectral Data from BaO Target

Appendix B contains spectral data of laser-ablation plumes from a BaO target. Background gases were at 25.0 mtorr. Data was taken 1.0 cm from the target. Laser fluence was 425 $mJ-cm^{-2}$. Data was taken using a 0.5 m spectrometer with a 1200g/mm grating, 30μm slit and an Oma linear array. The signal was integrated over 16.6 msec and 120 pulses were summed to get this output.
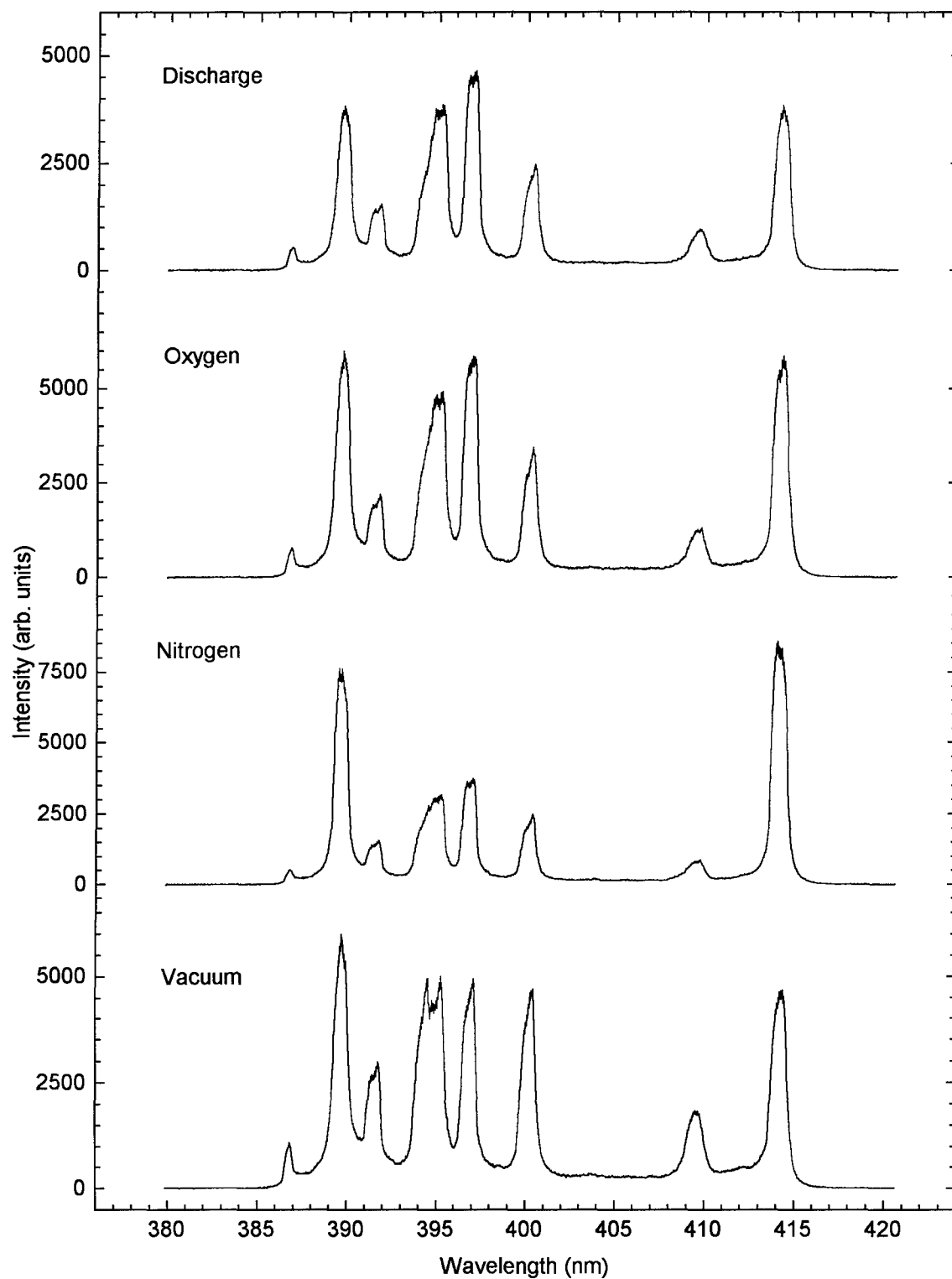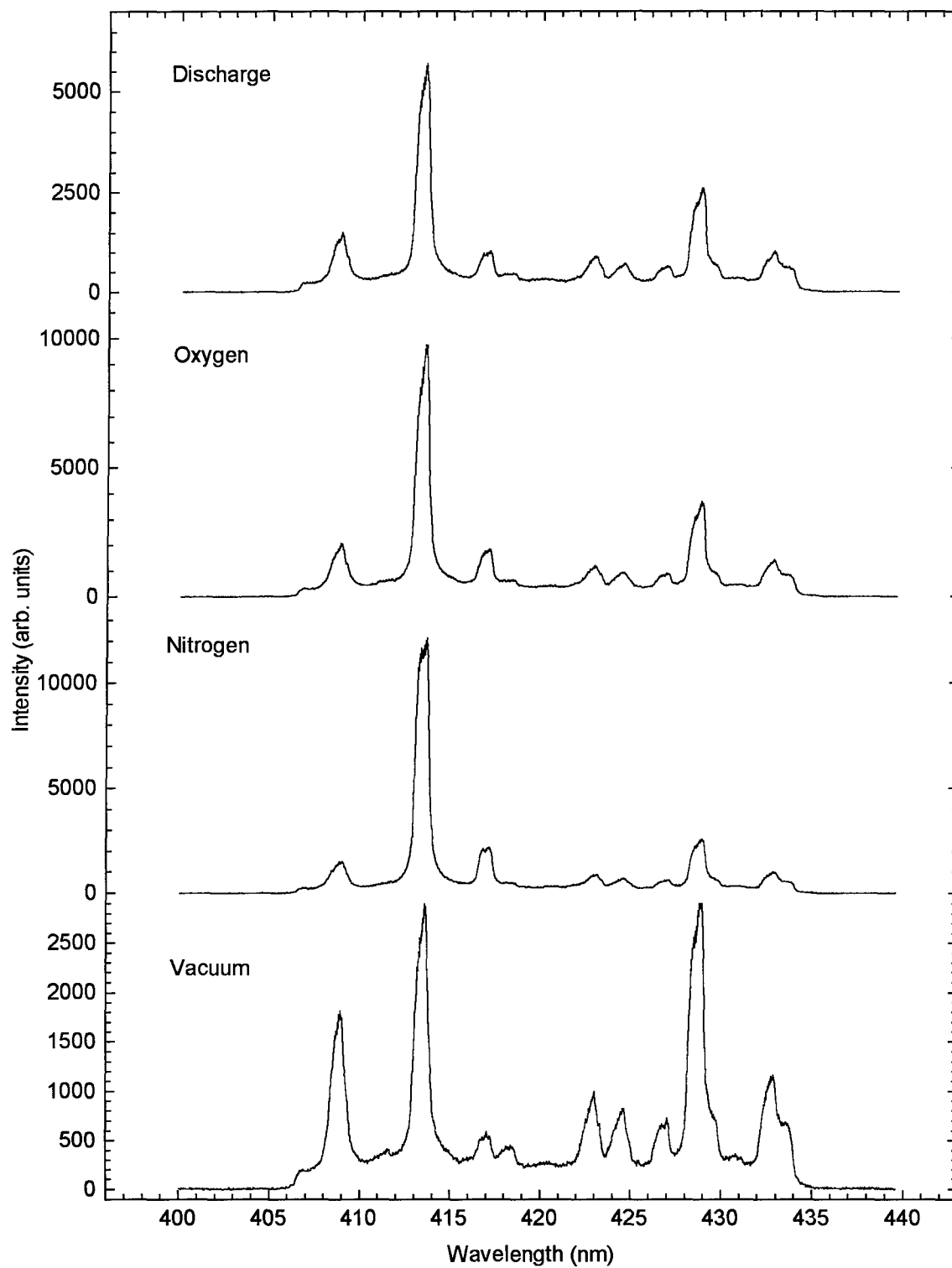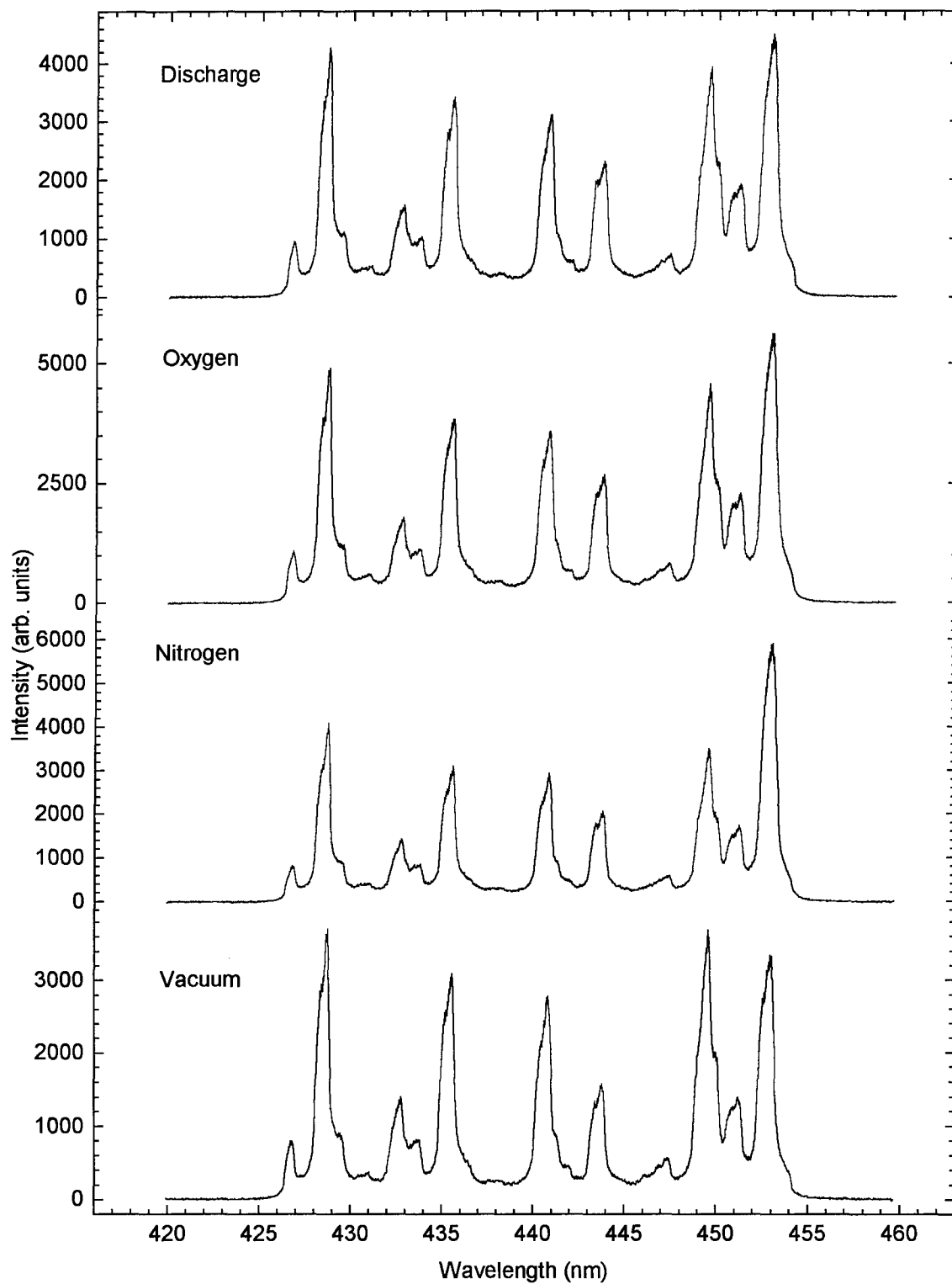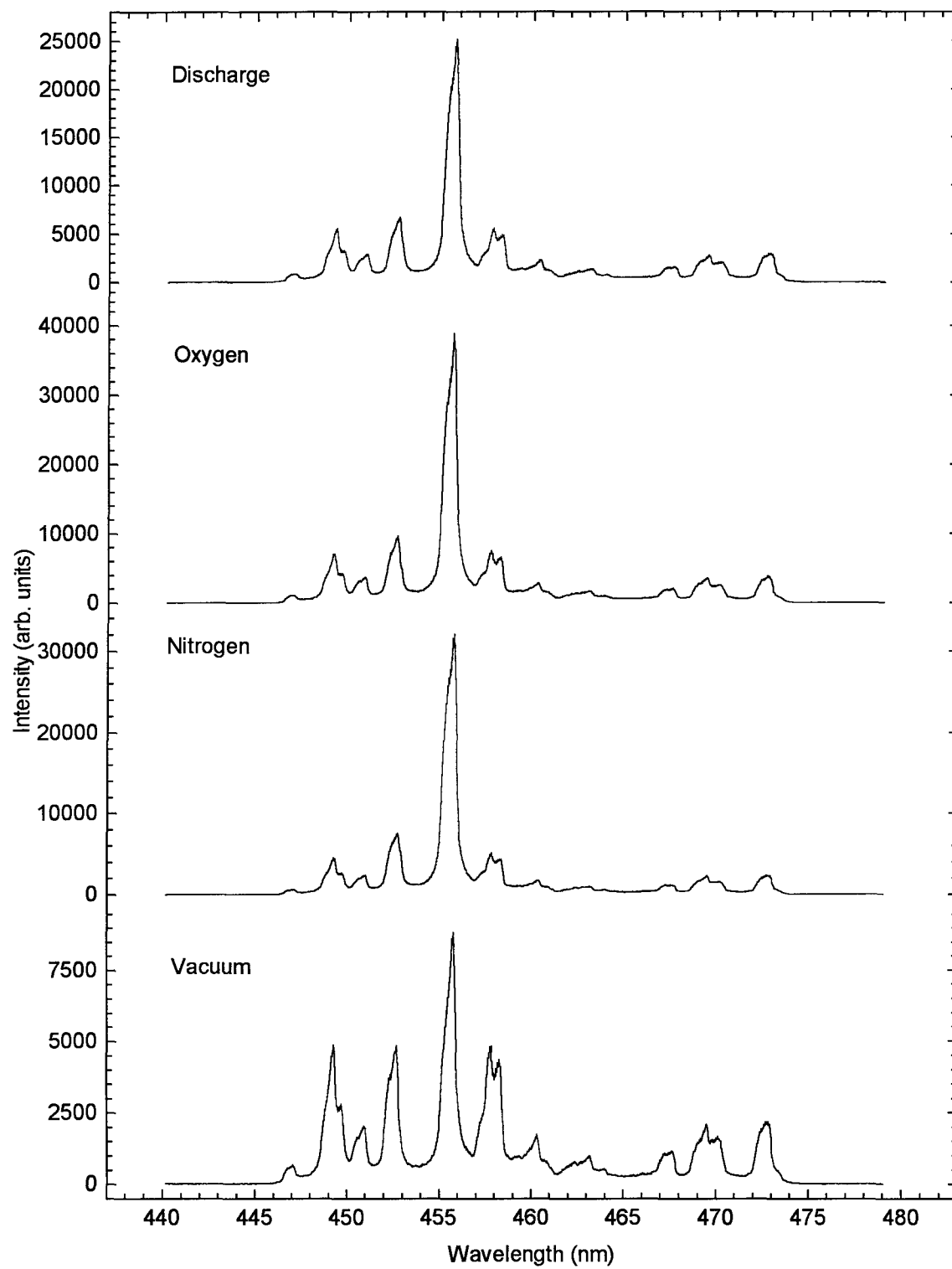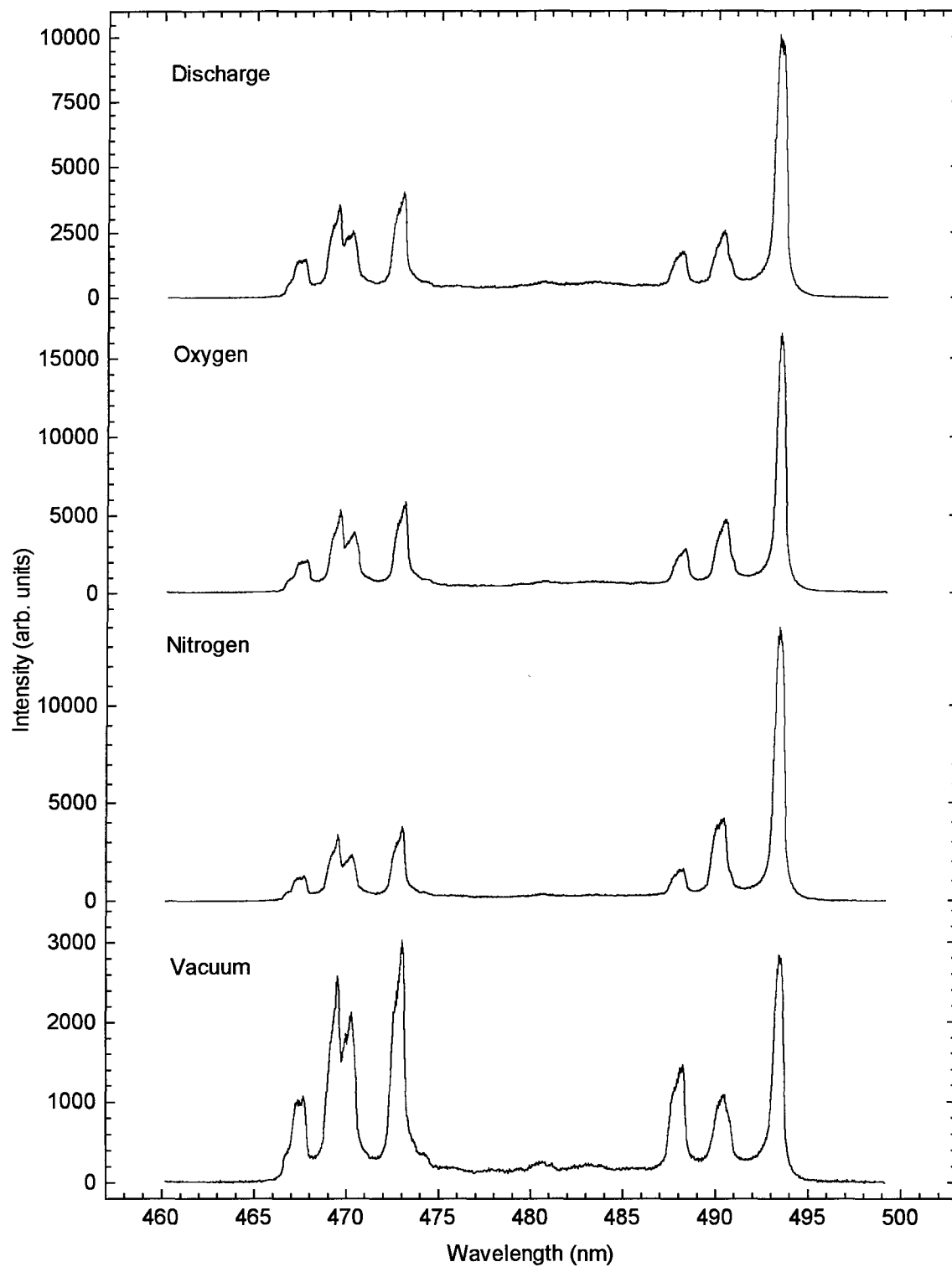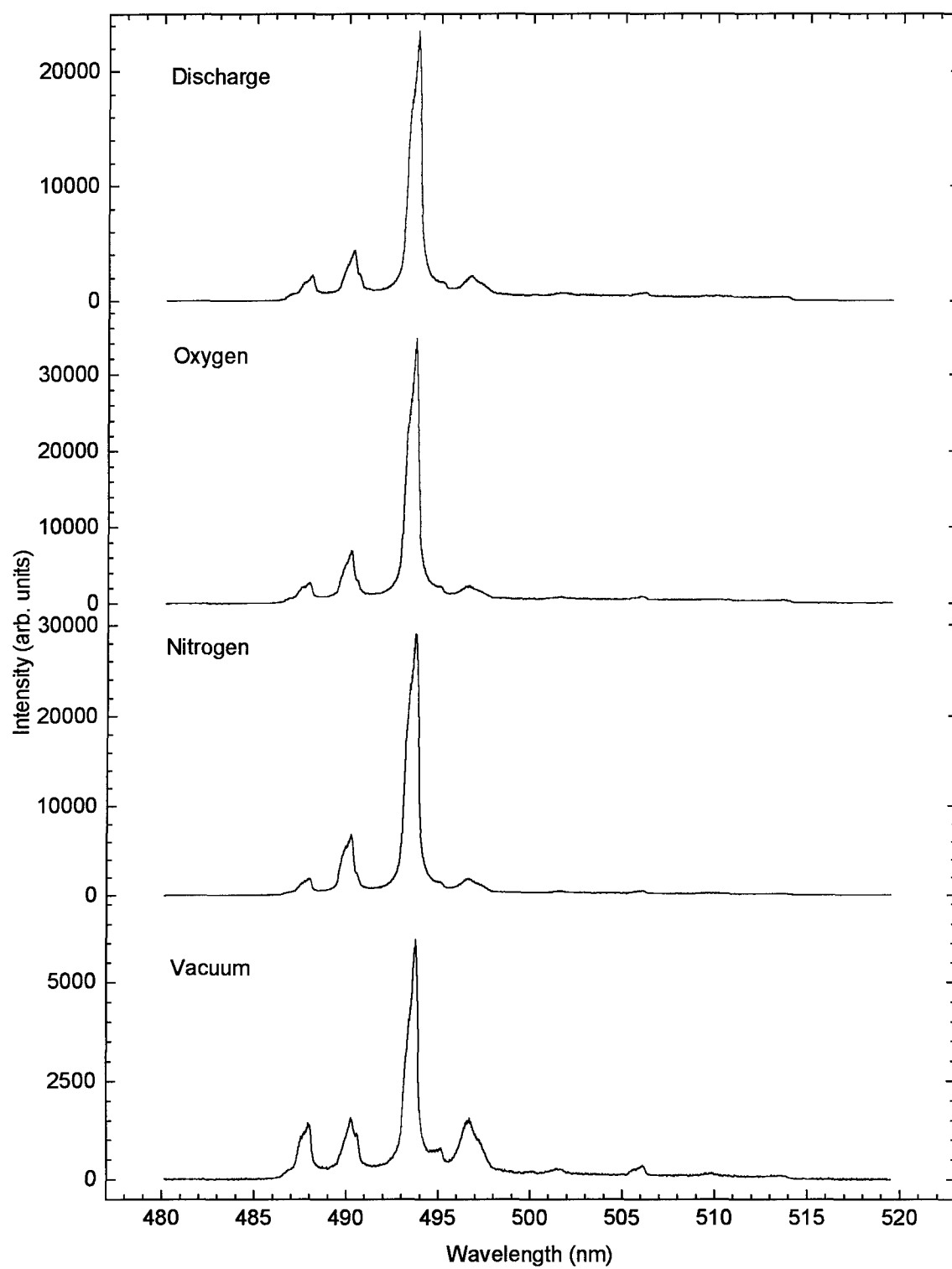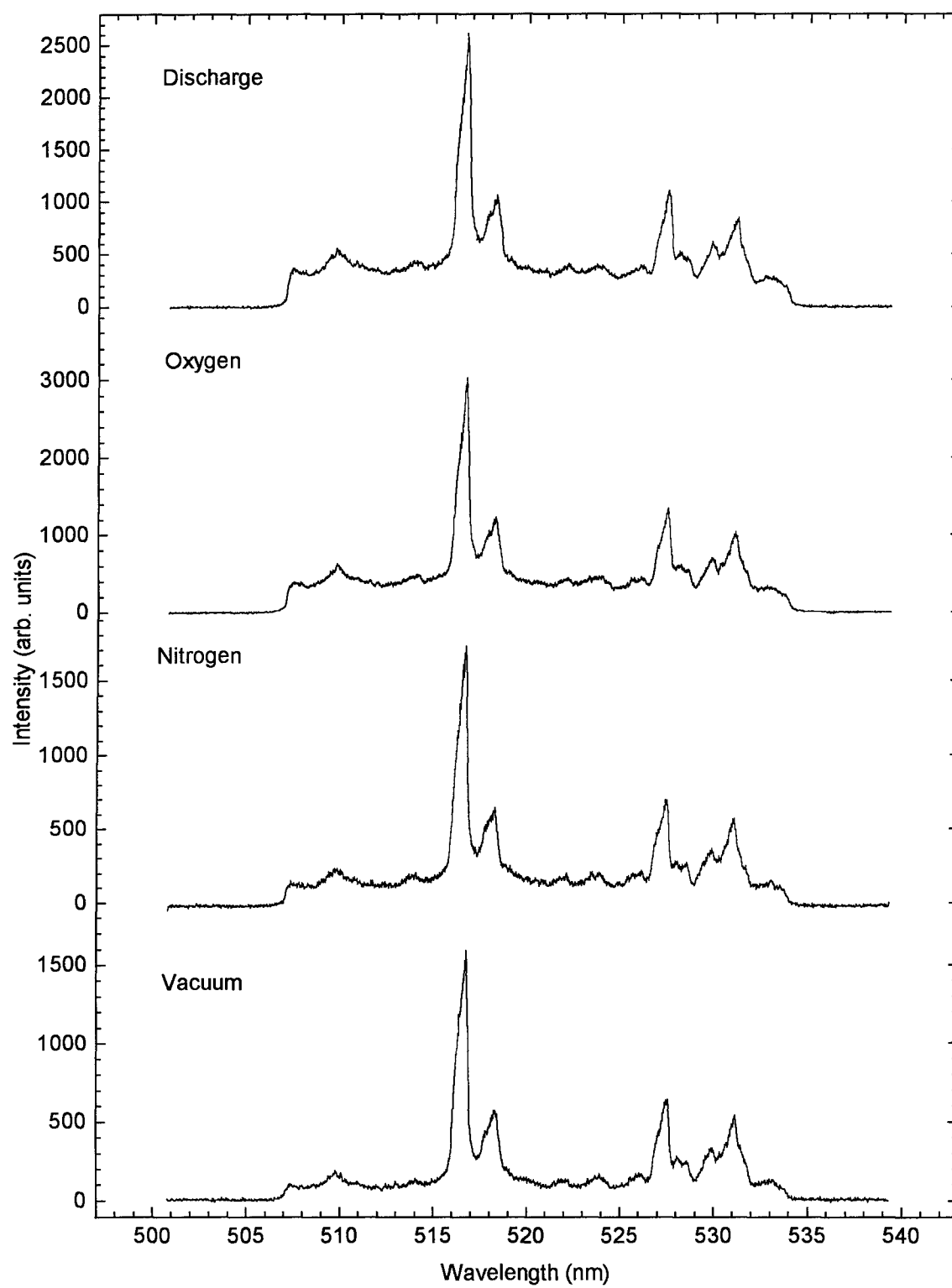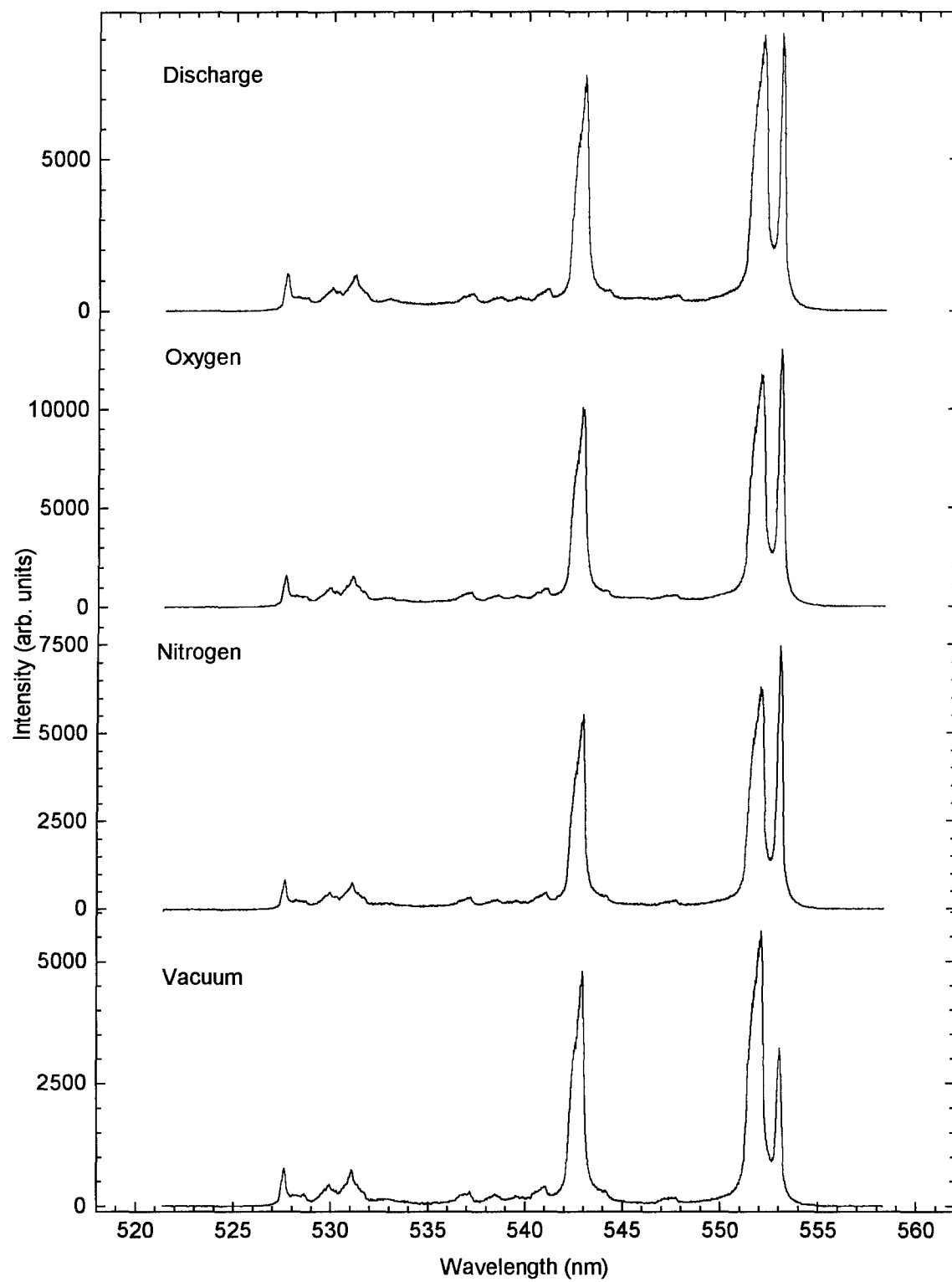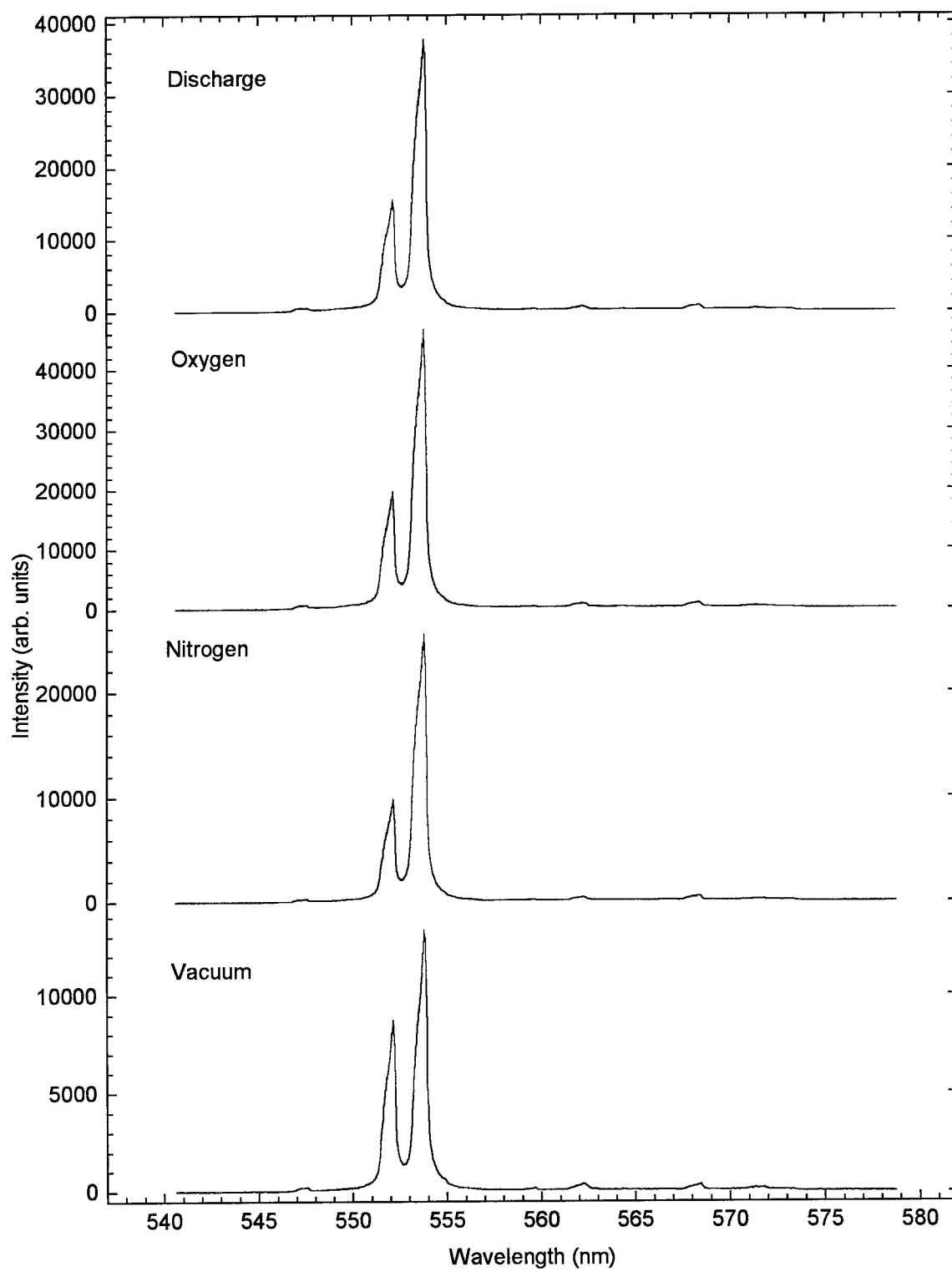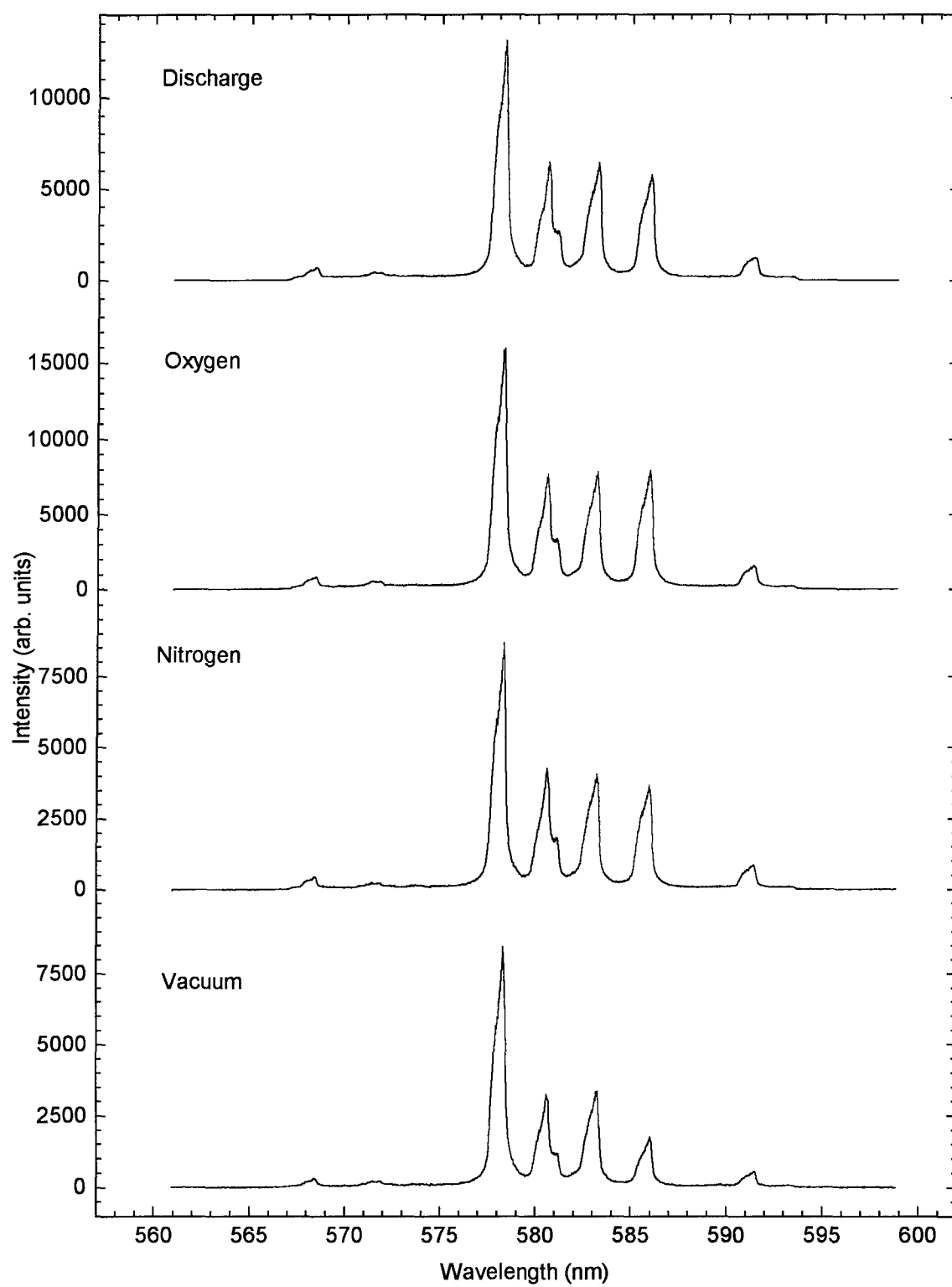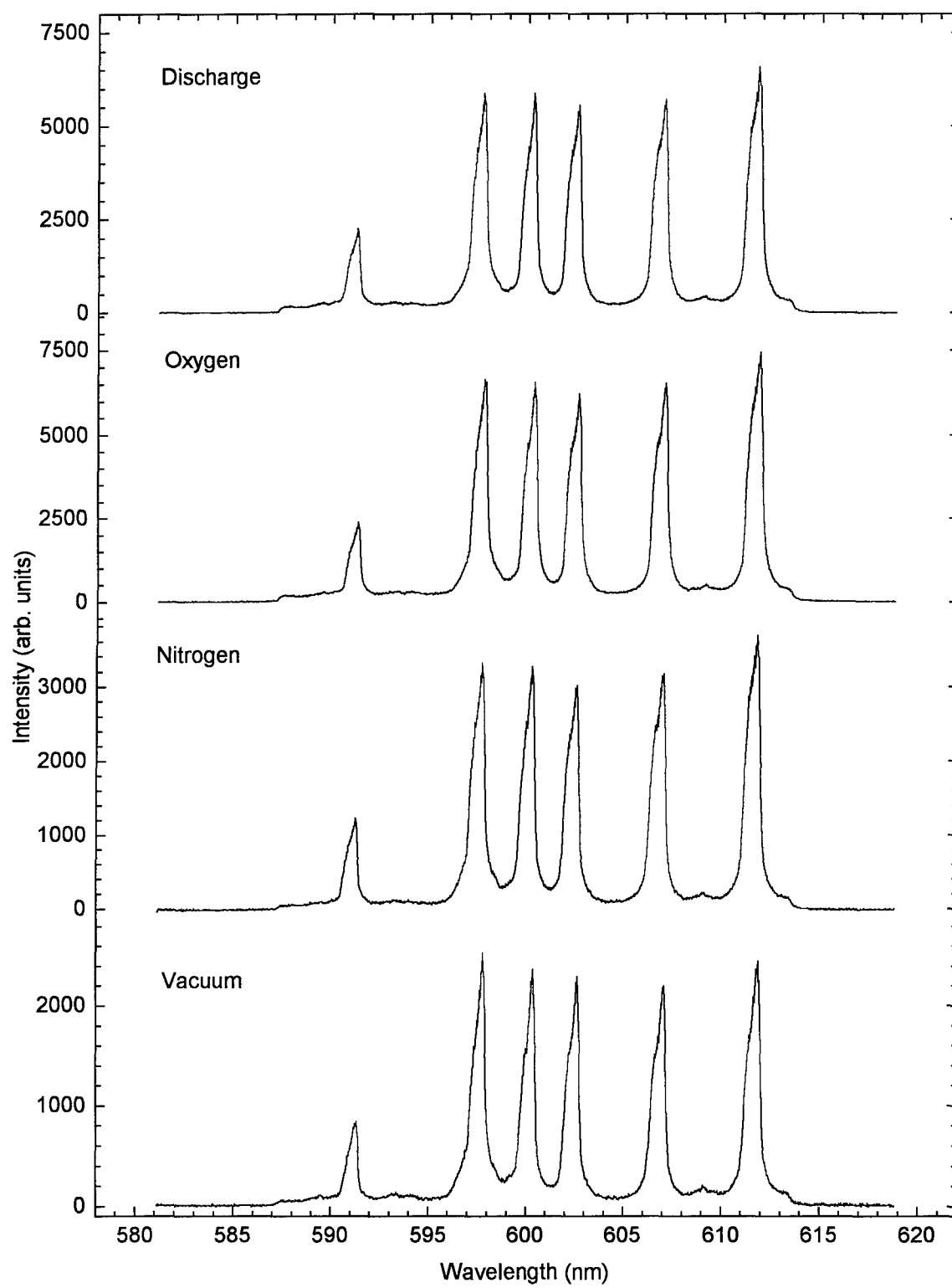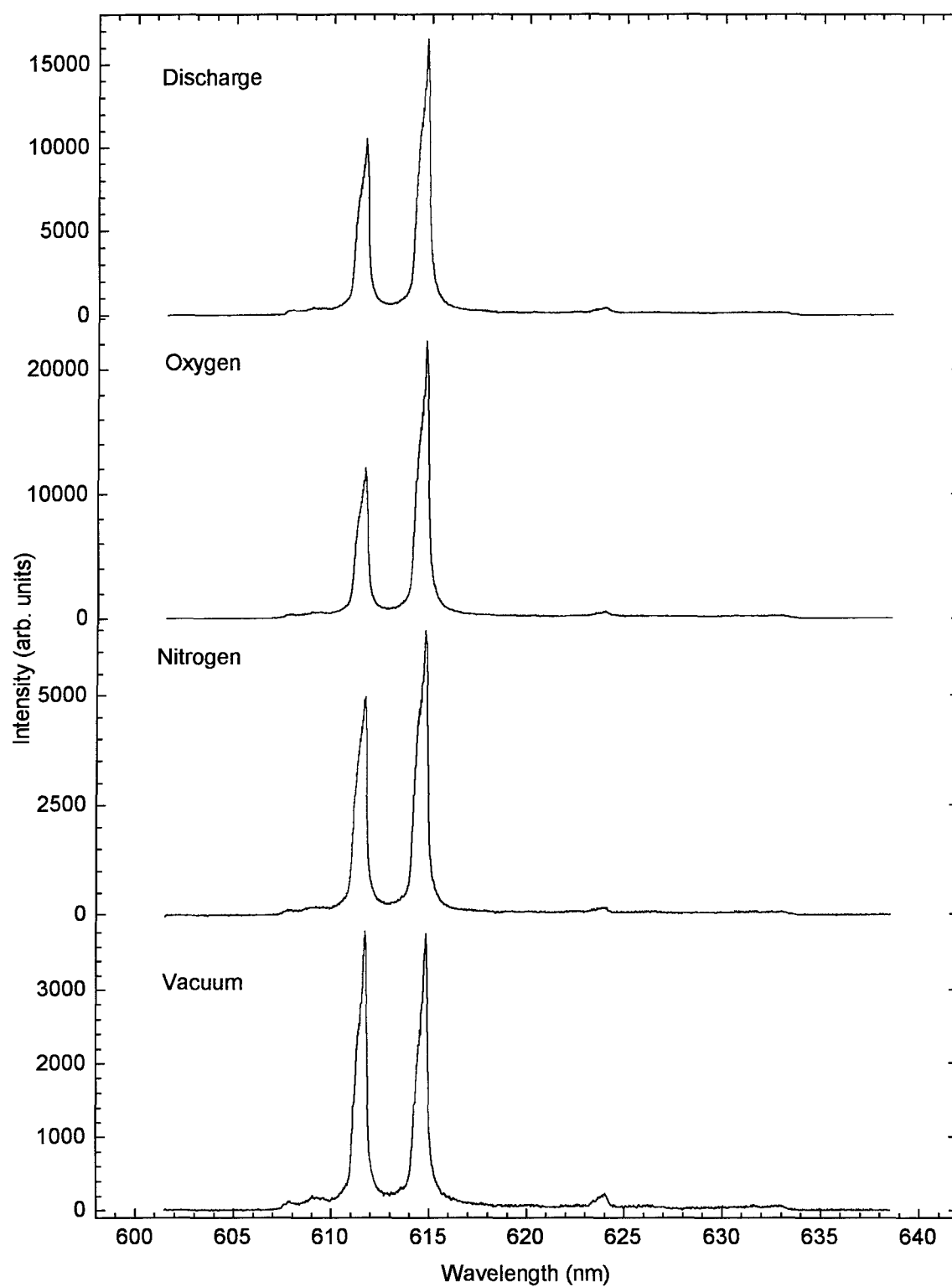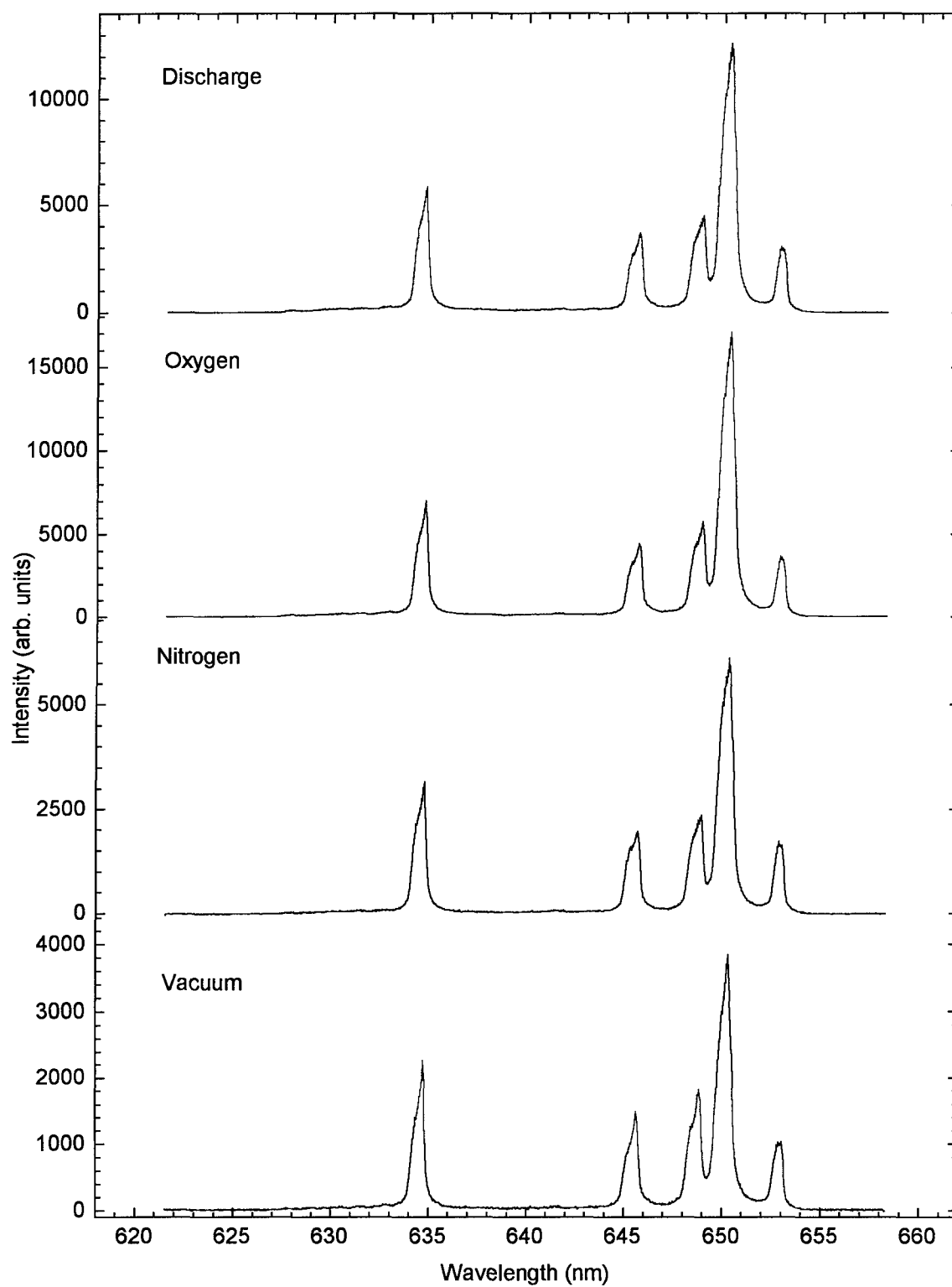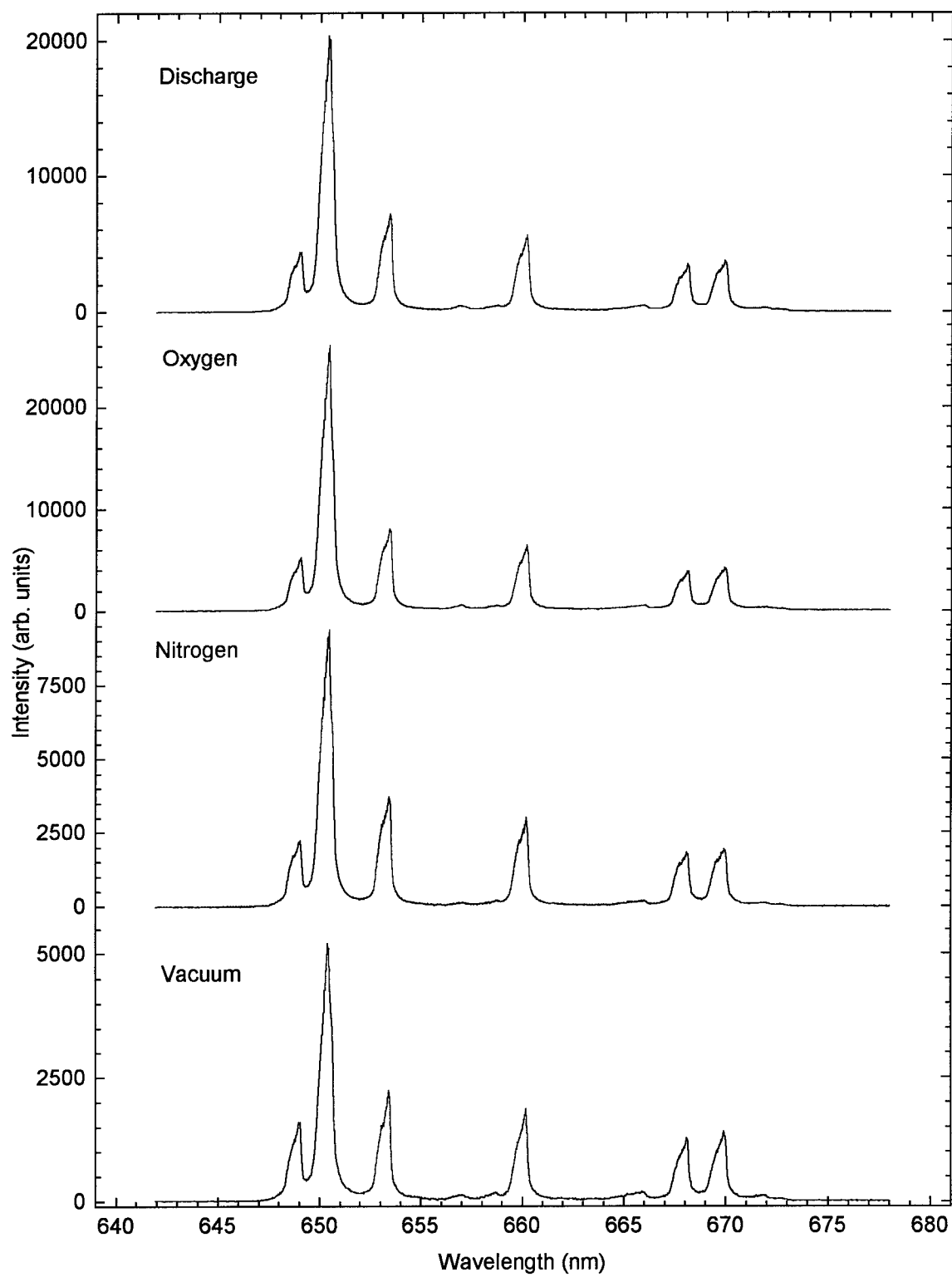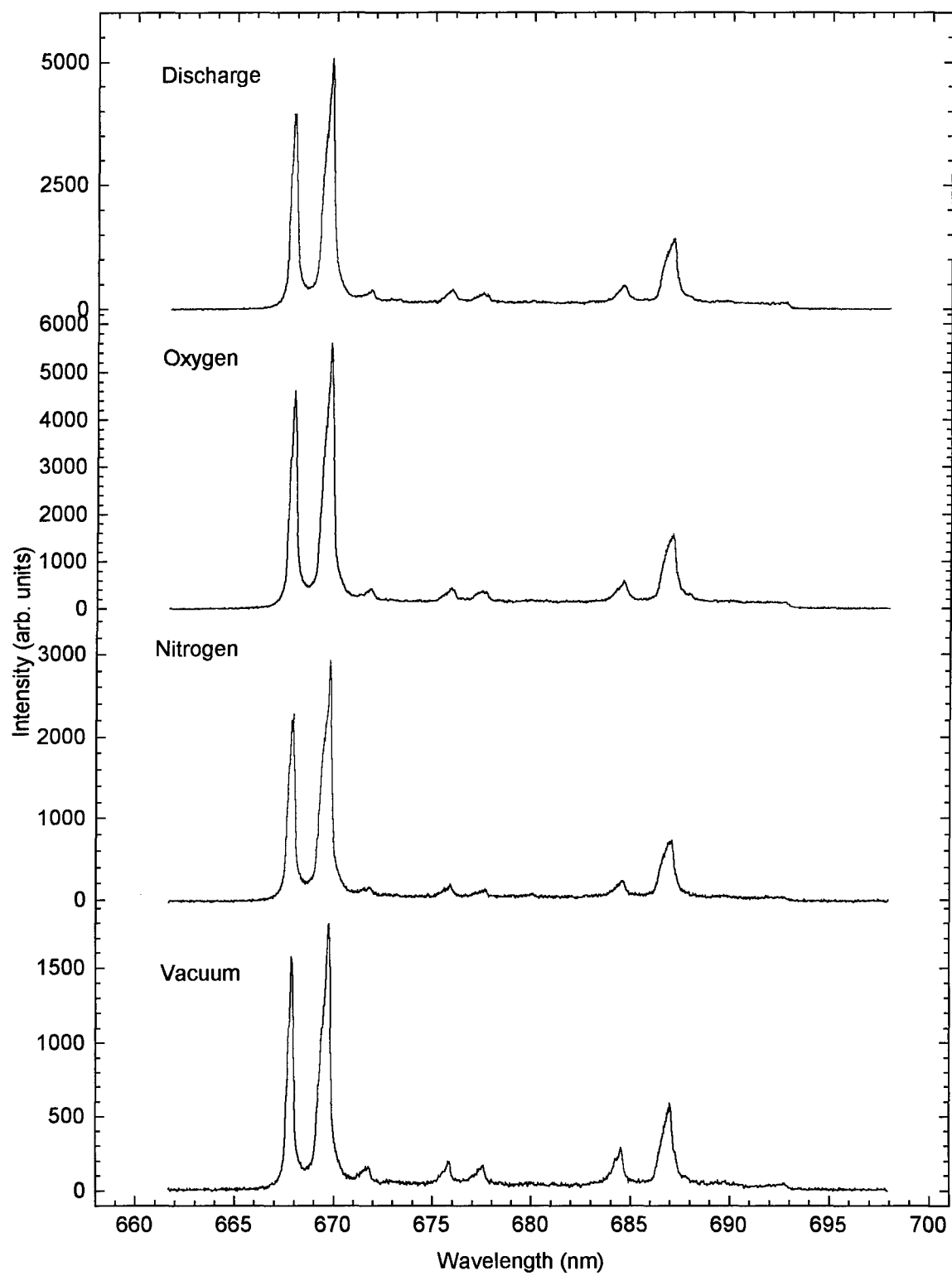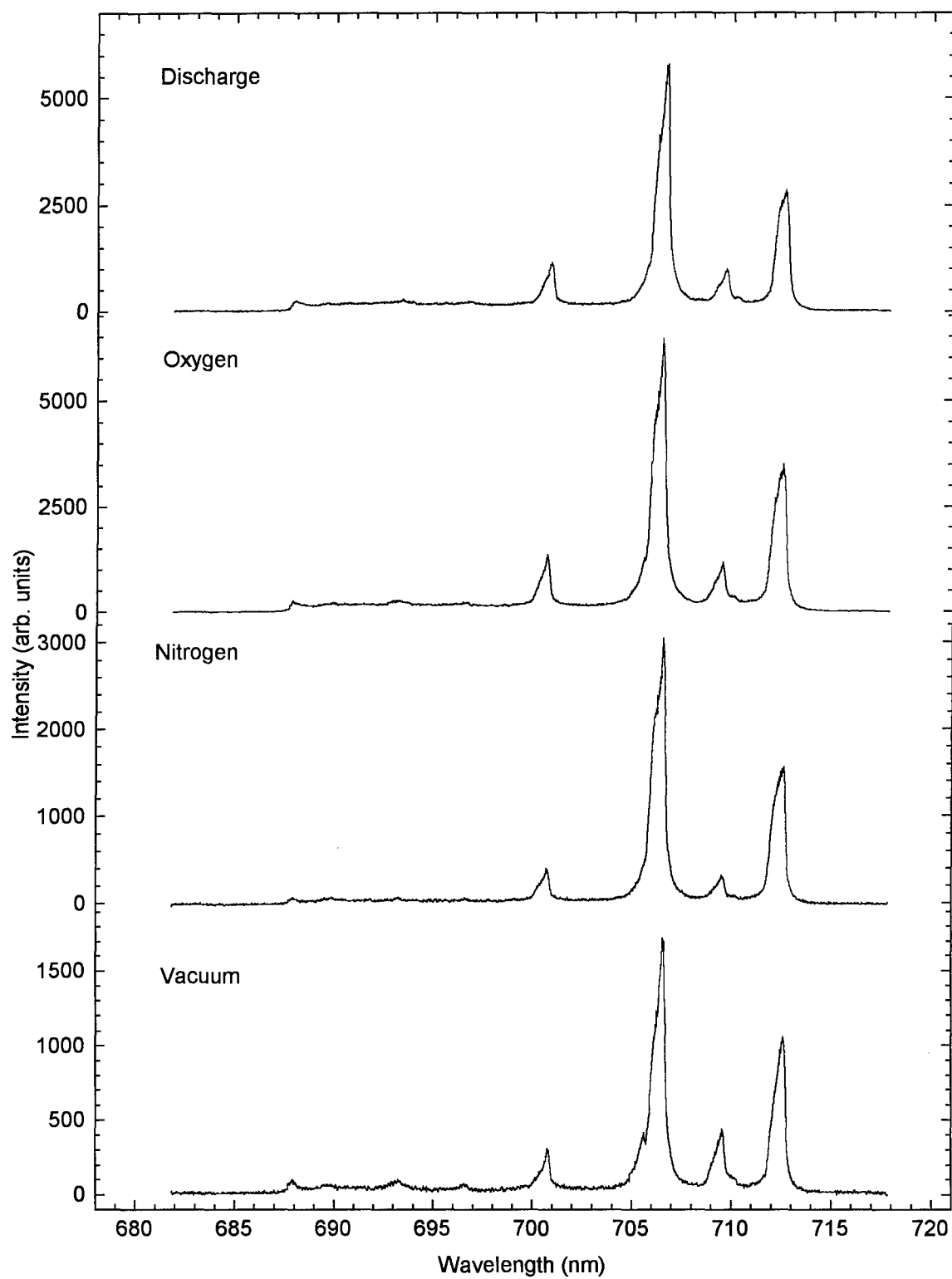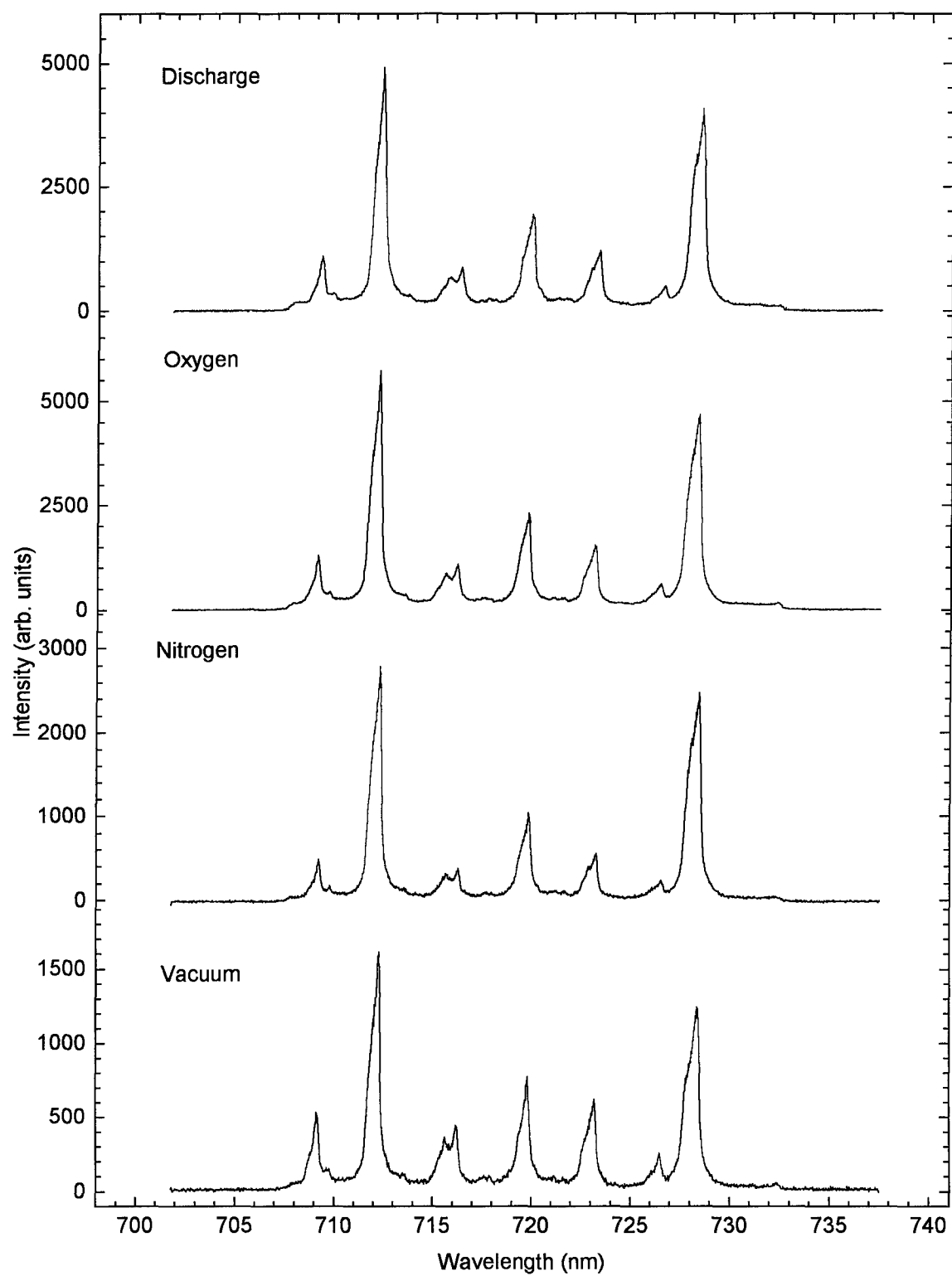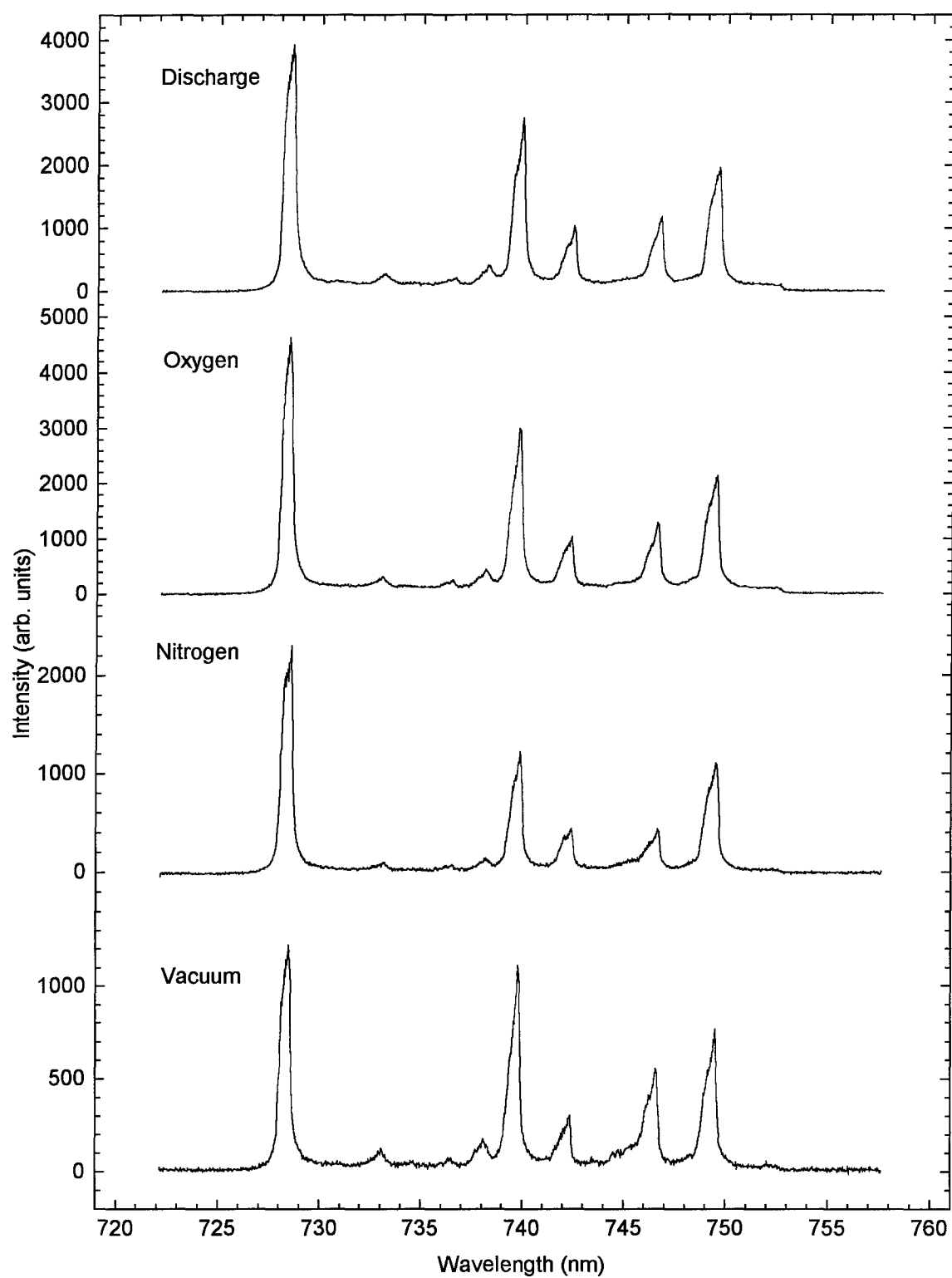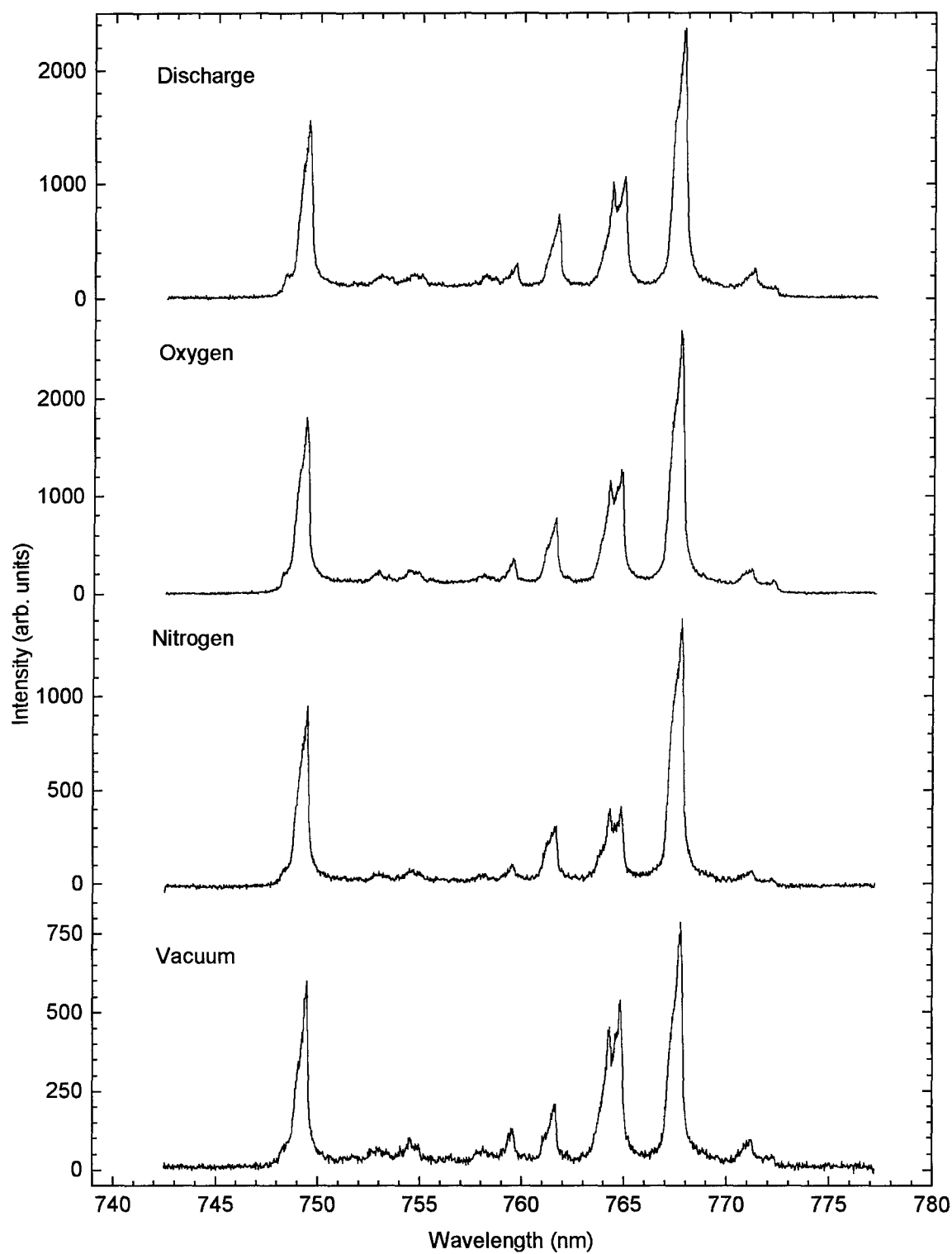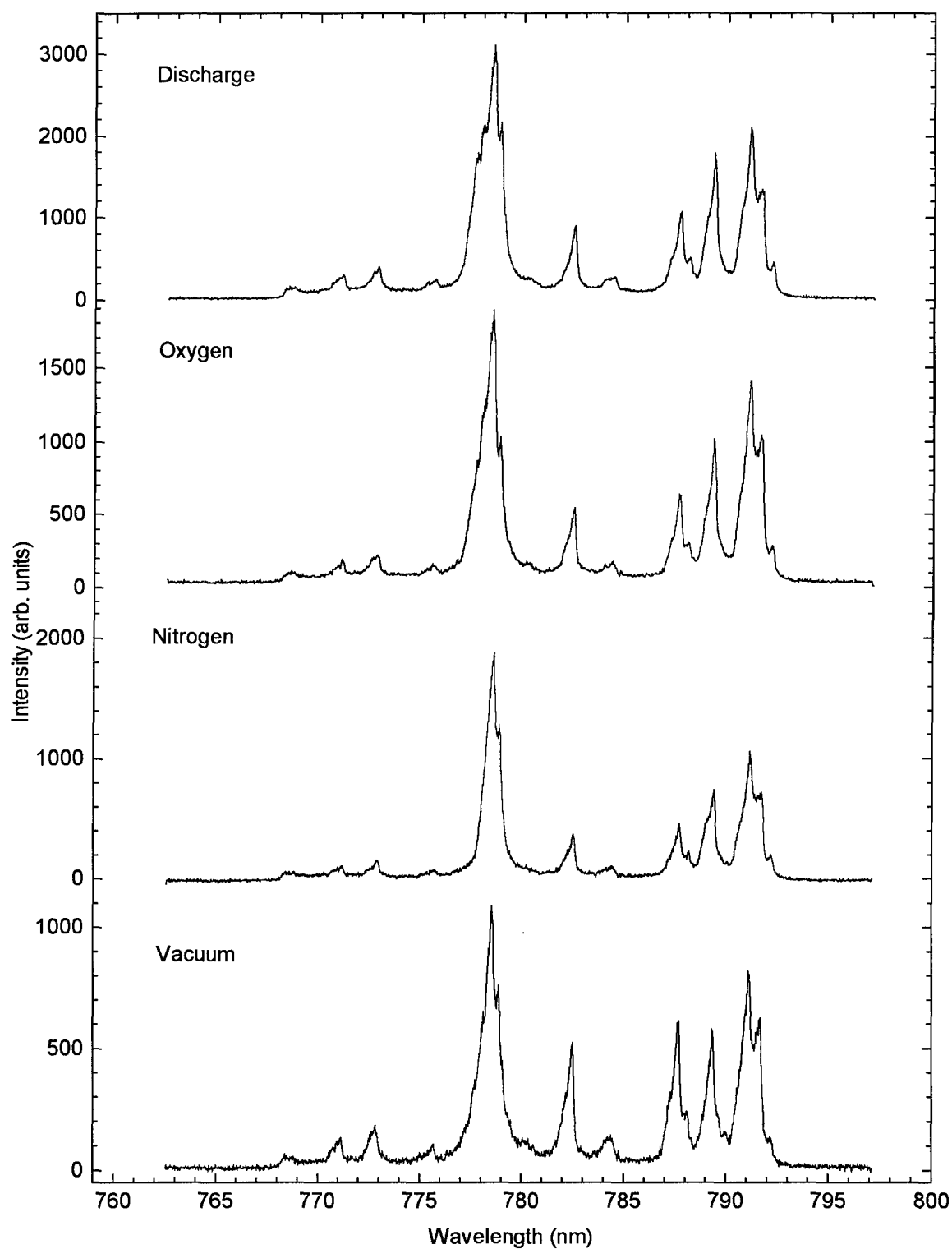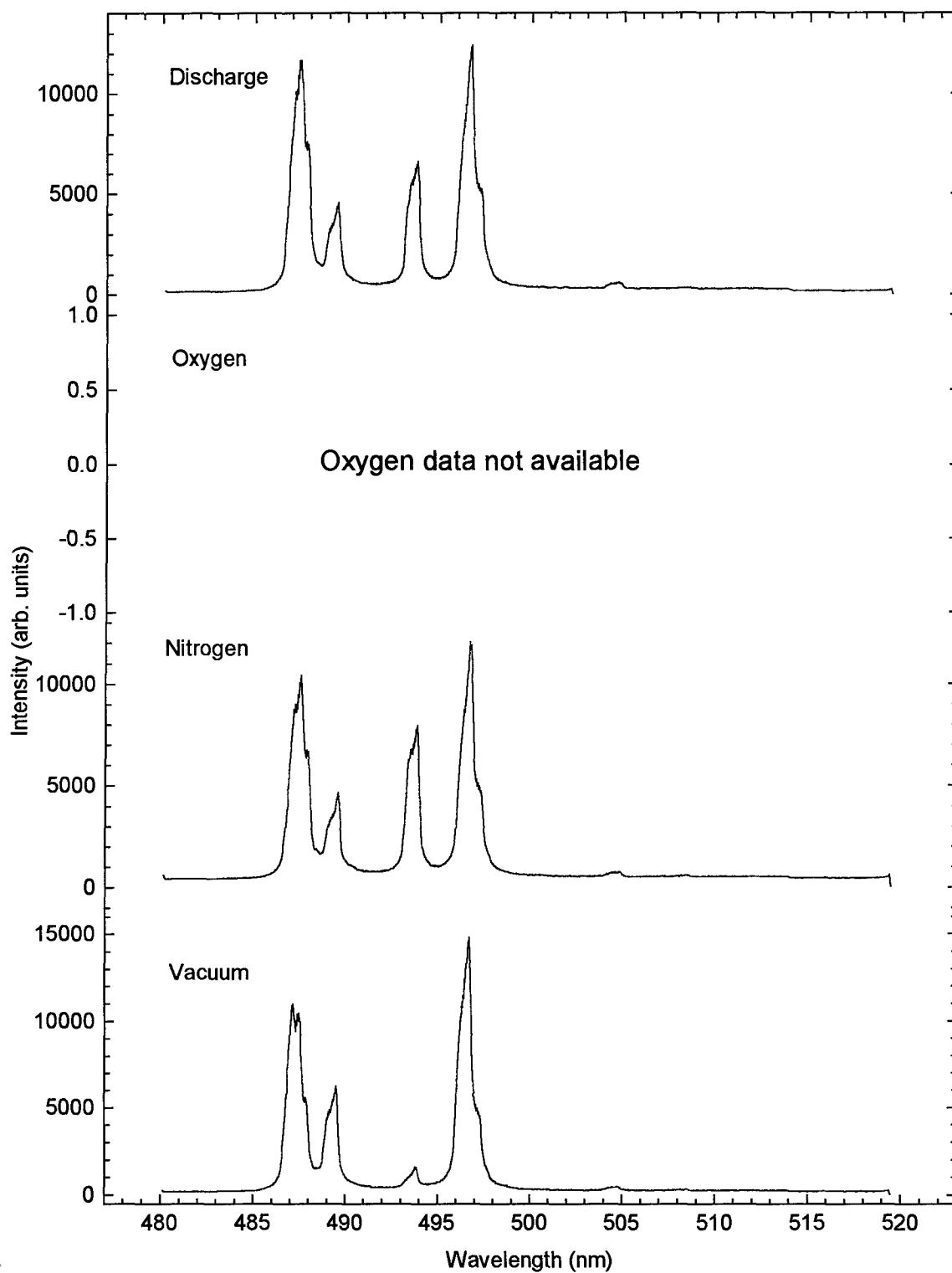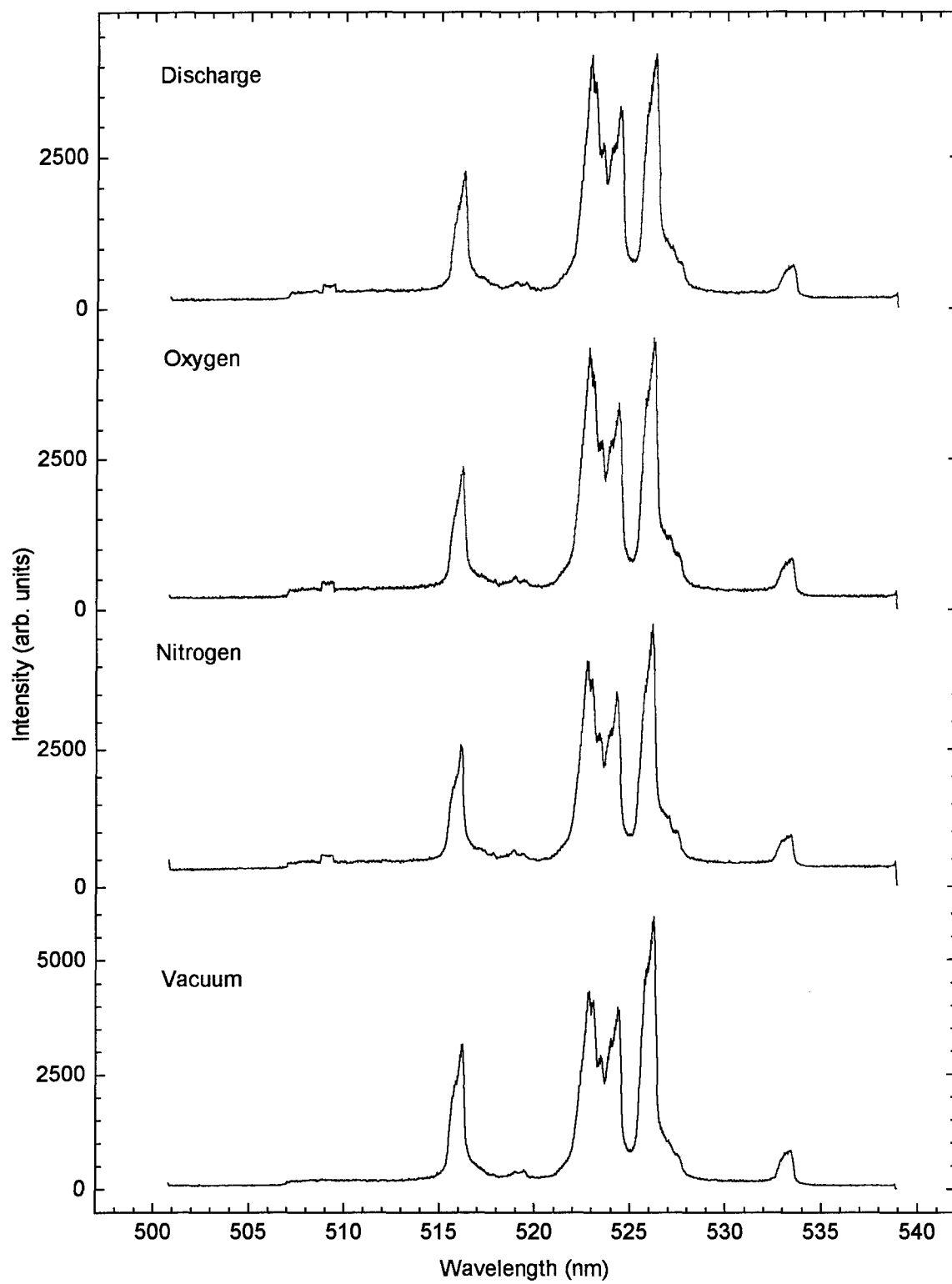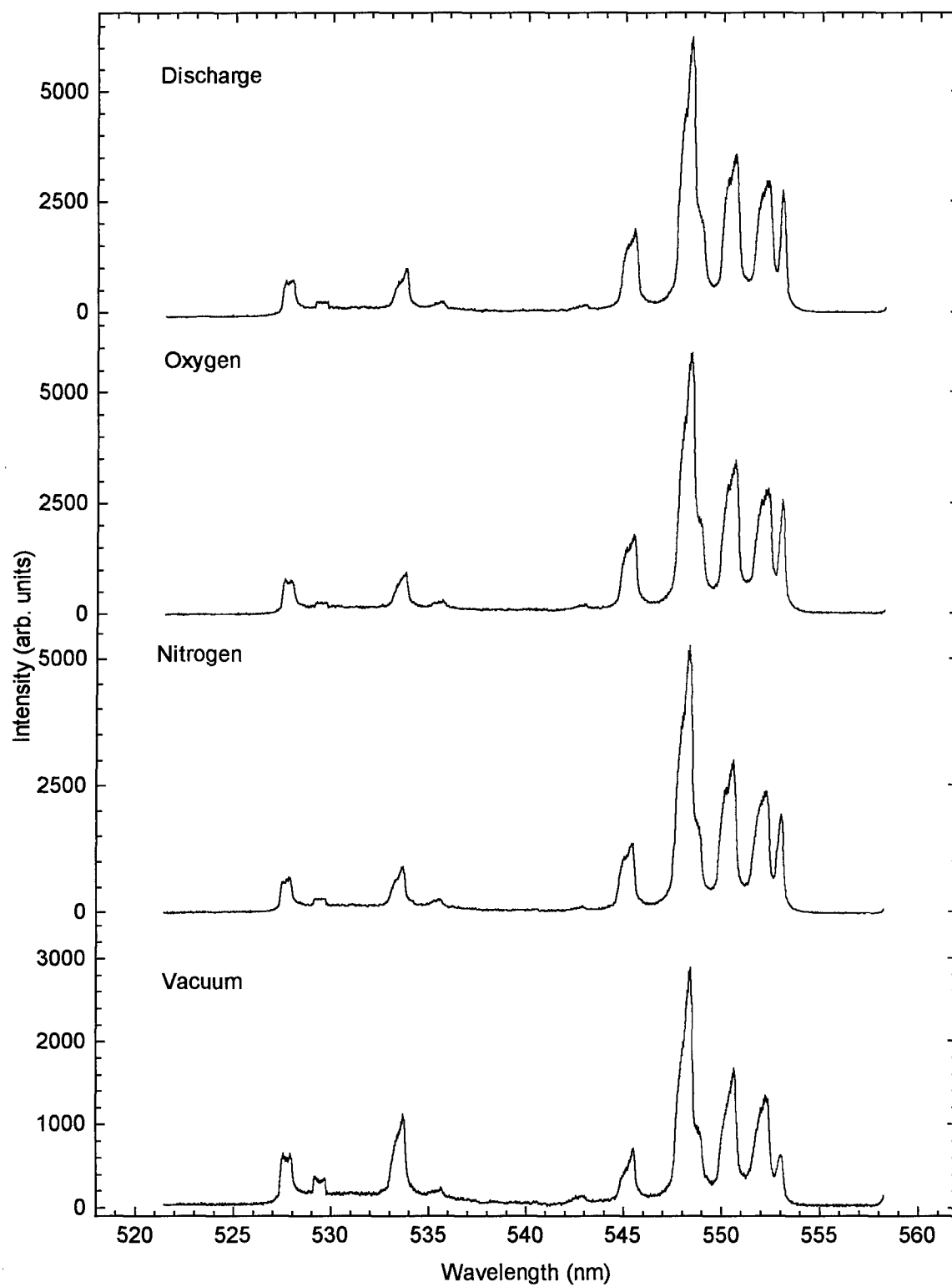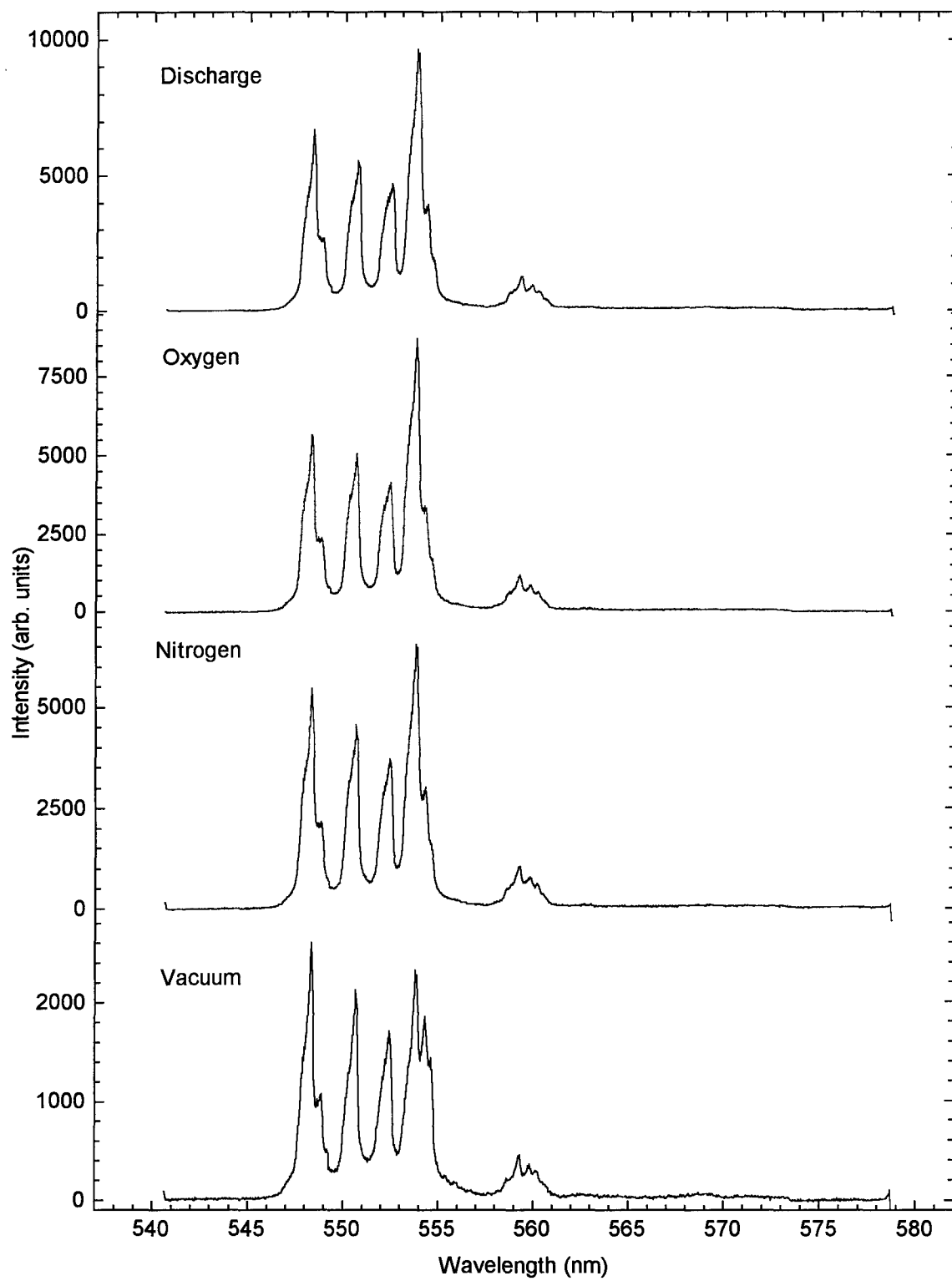
Appendix C: Spectral Data From Sr Target in O_2 and Discharged O_2 at 12.5 and 25.0 mtorr.

This section contains spectral data of laser-ablation plumes from a Sr target at 340 nm, 400 nm, 420 nm and 600 nm in vacuum and O_2 and discharged O_2 at 12.5 and 25.0 mtorr. Data was taken 1.0 cm from the target. Laser fluence was 385 mJ-cm^{-2}. Data was taken using a 0.5 m spectrometer with a 1200g/mm grating, 100μm slit and an Oma linear array. The signal was integrated over 16.6 msec and 120 pulses were summed to get this output.

Oxygen
800 mtorr

Oxygen
1.25 torr

Vacuum

Intensity (arb units)

Wavelength (nm)

Oxygen
25.0 mtorr

Oxygen
12.5 mtorr

Vacuum

127
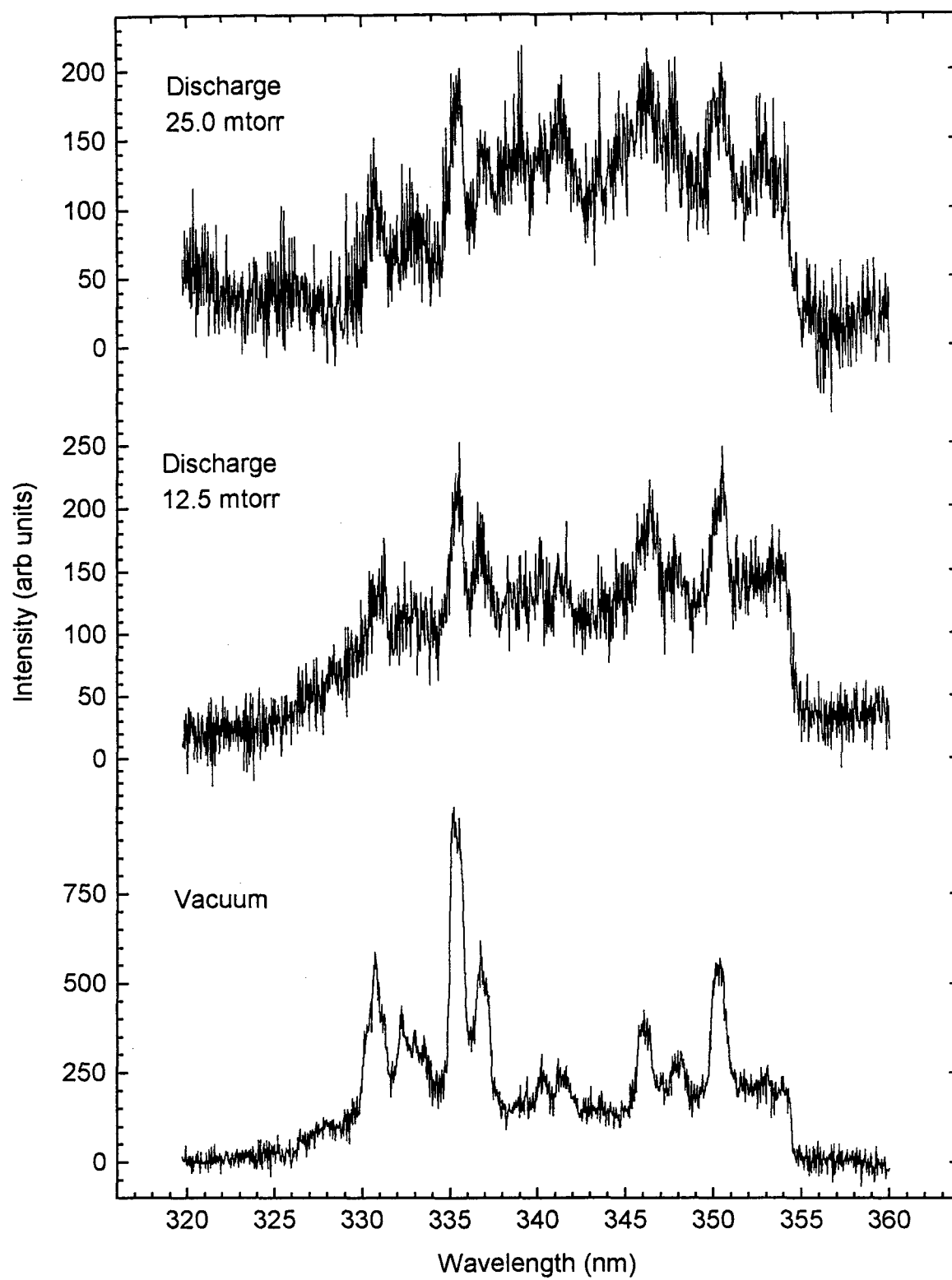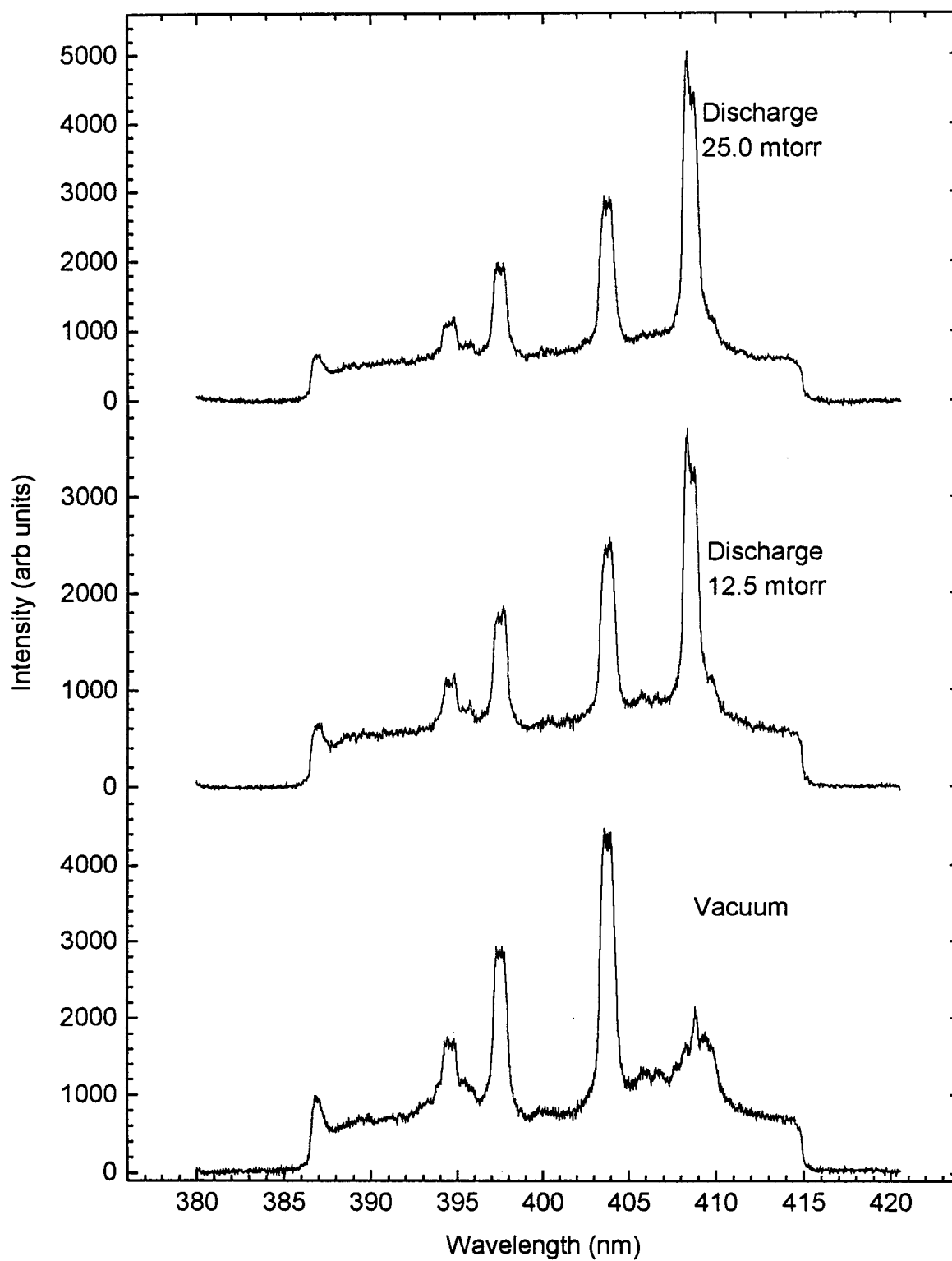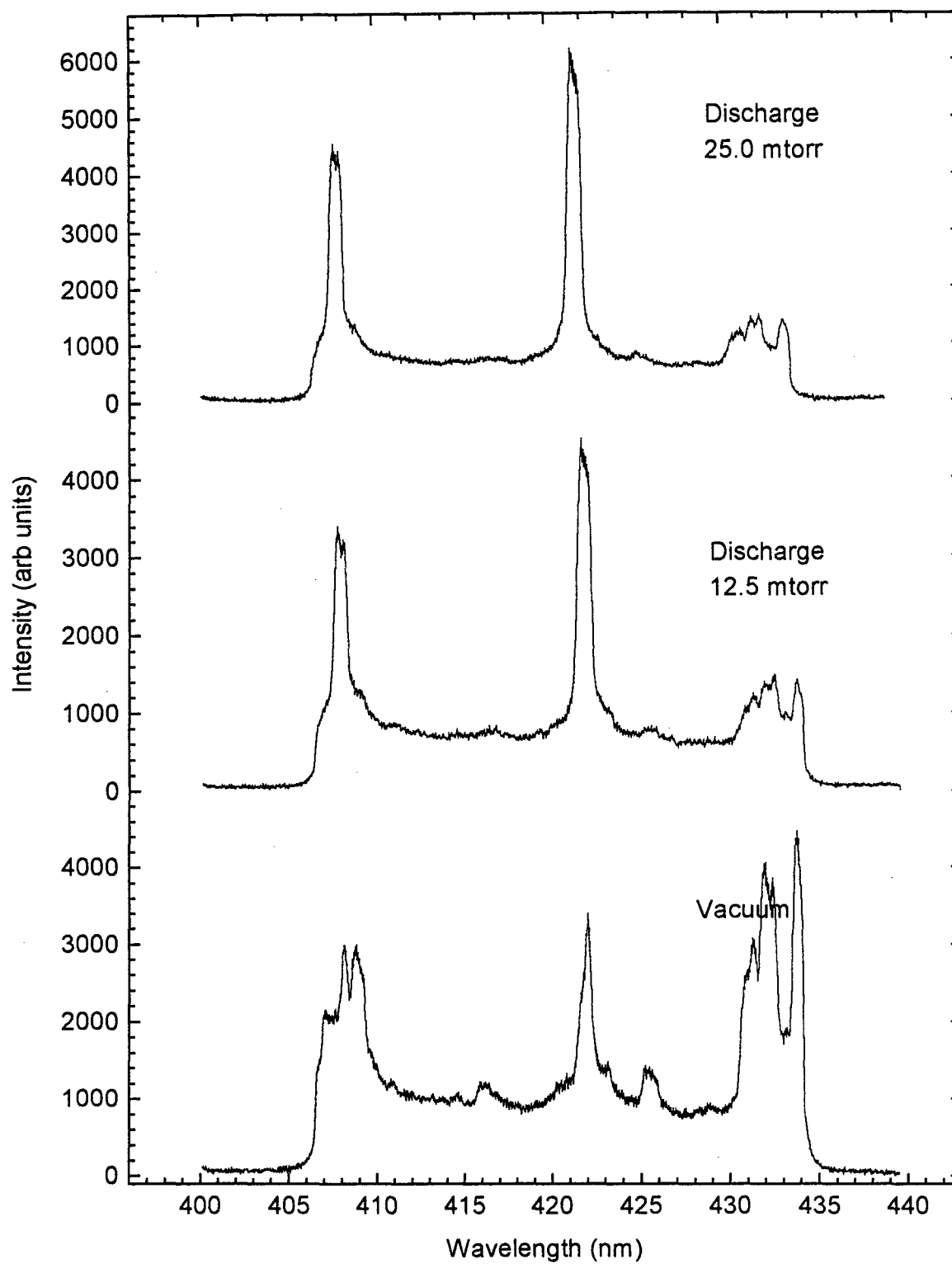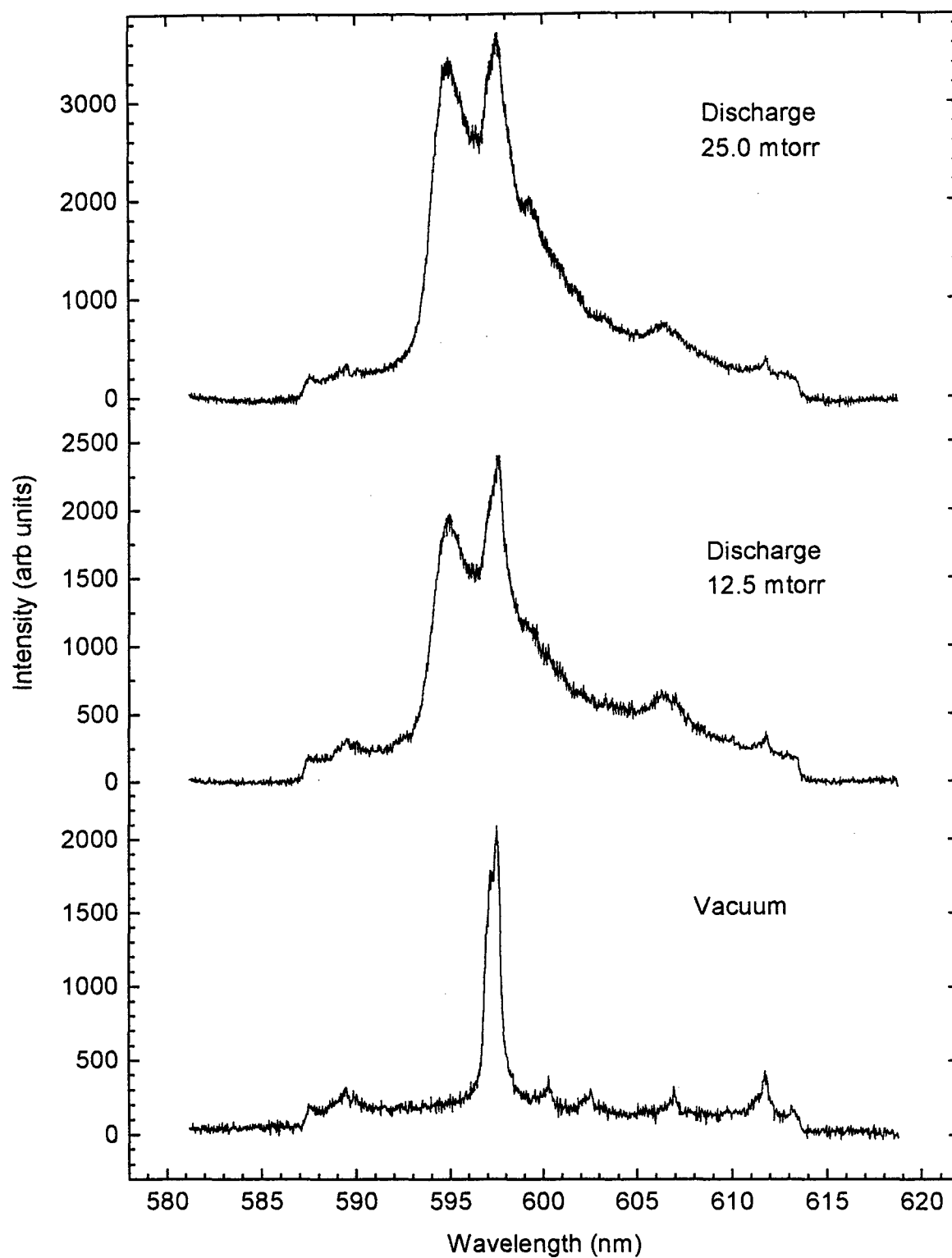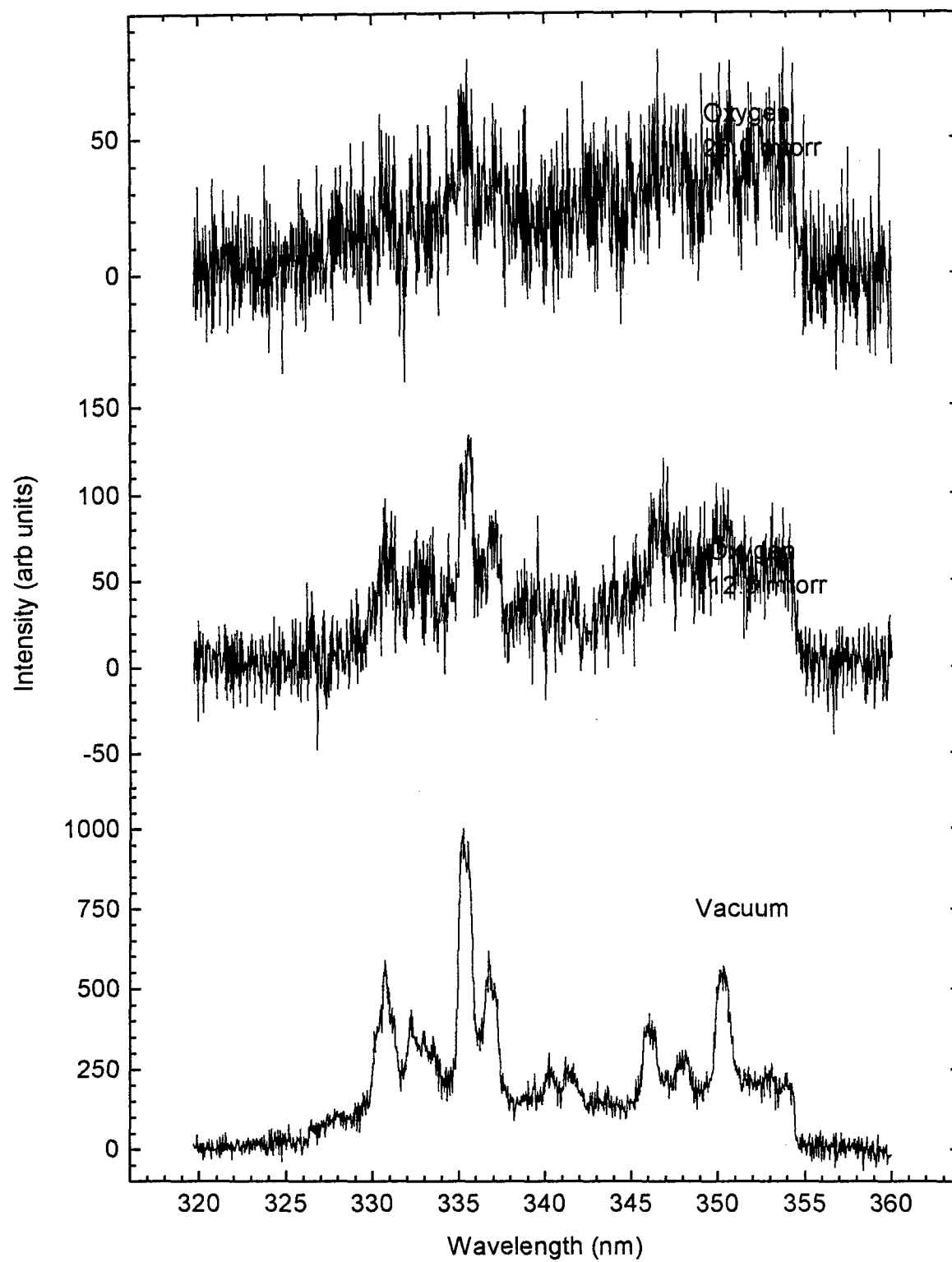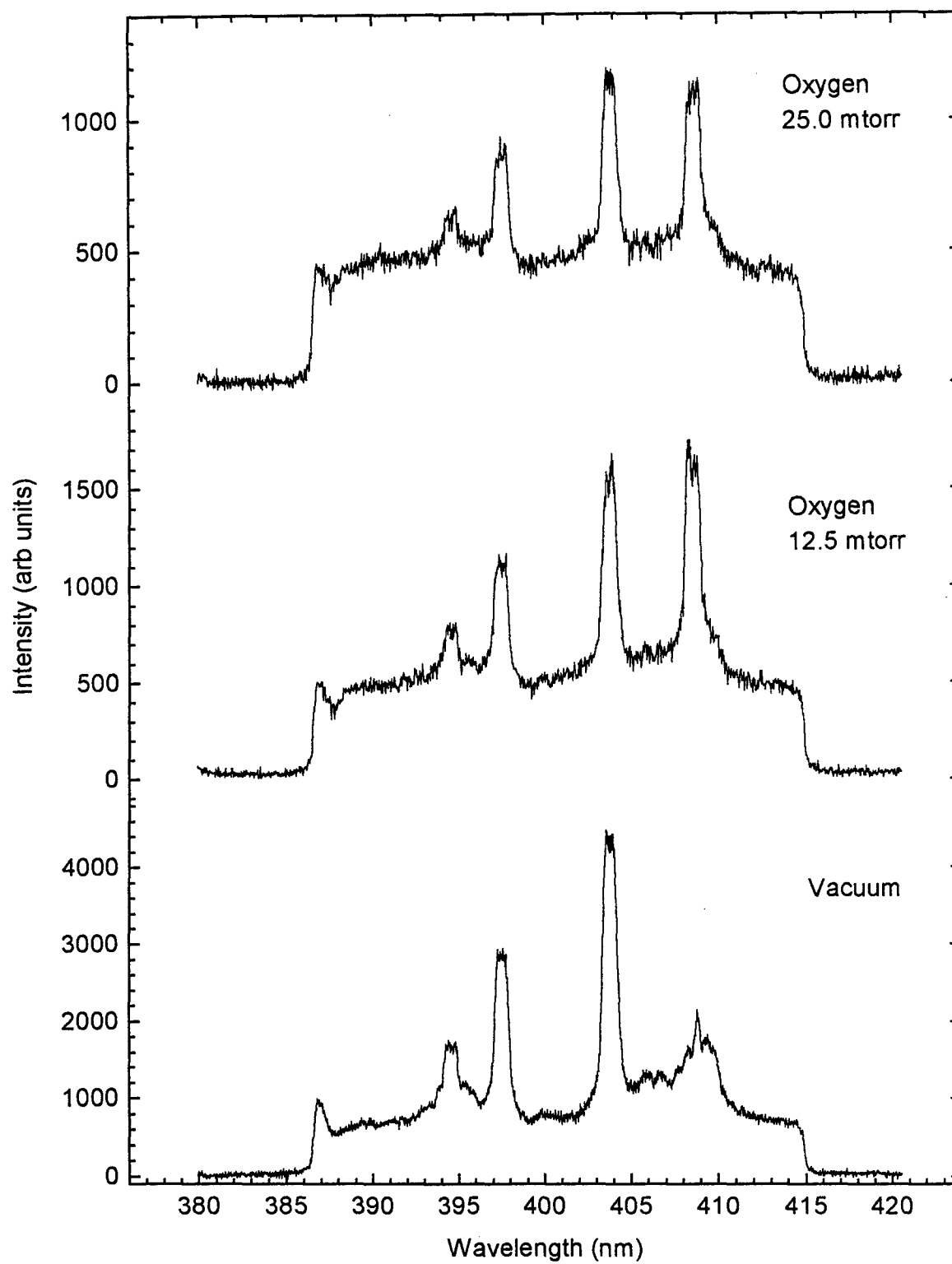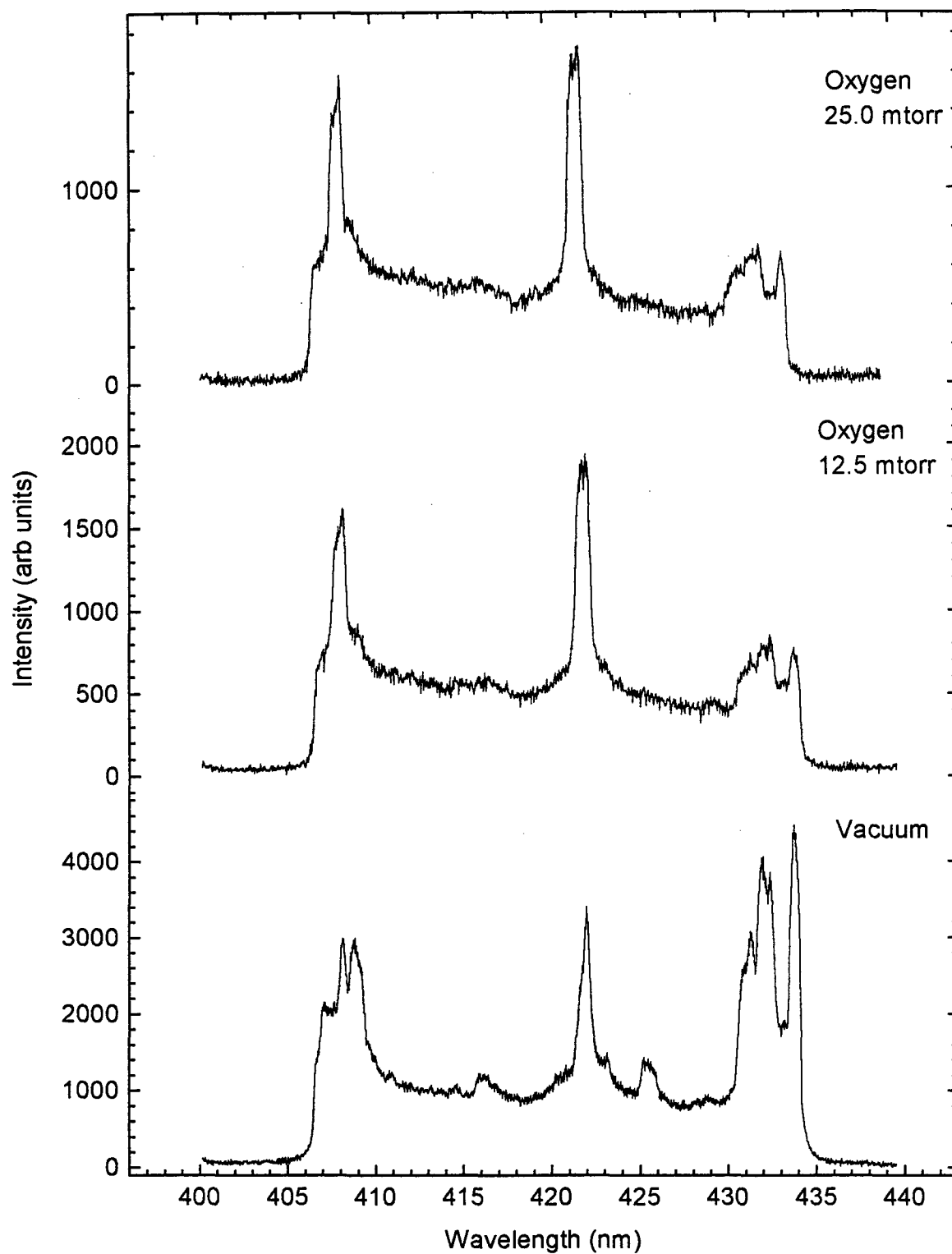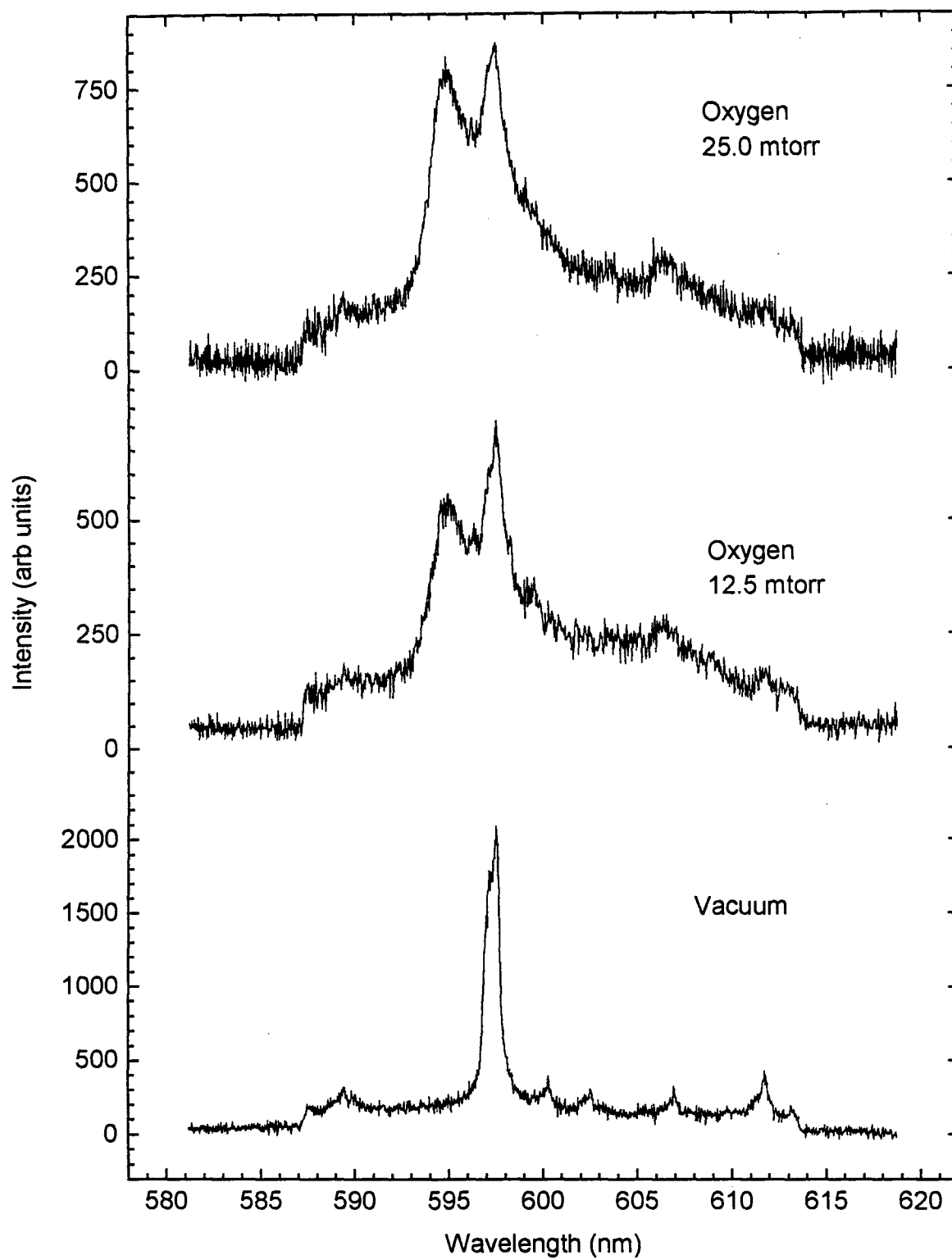
Appendix D: Spectral Data from Sr Target

This section contains spectral data of laser-ablation plumes from a Sr target. Background gases were at 25.0 mtorr. Data was taken 1.0 cm from the target. Laser fluence was 385 mJ-cm^{-2}. Data was taken using a 0.5 m spectrometer with a 1200g/mm grating, 100μm slit and an Oma linear array. The signal was integrated over 16.6 msec and 120 pulses were summed to get this output.

5000

Discharge

0

150

Oxygen

100

50

0

-50

Nitrogen

Intensity (arb. units)

500

Nitrogen data not available

0

200

Vacuum

100

0

-100

760   765   770   775   780   785   790   795   800

Wavelength (nm)
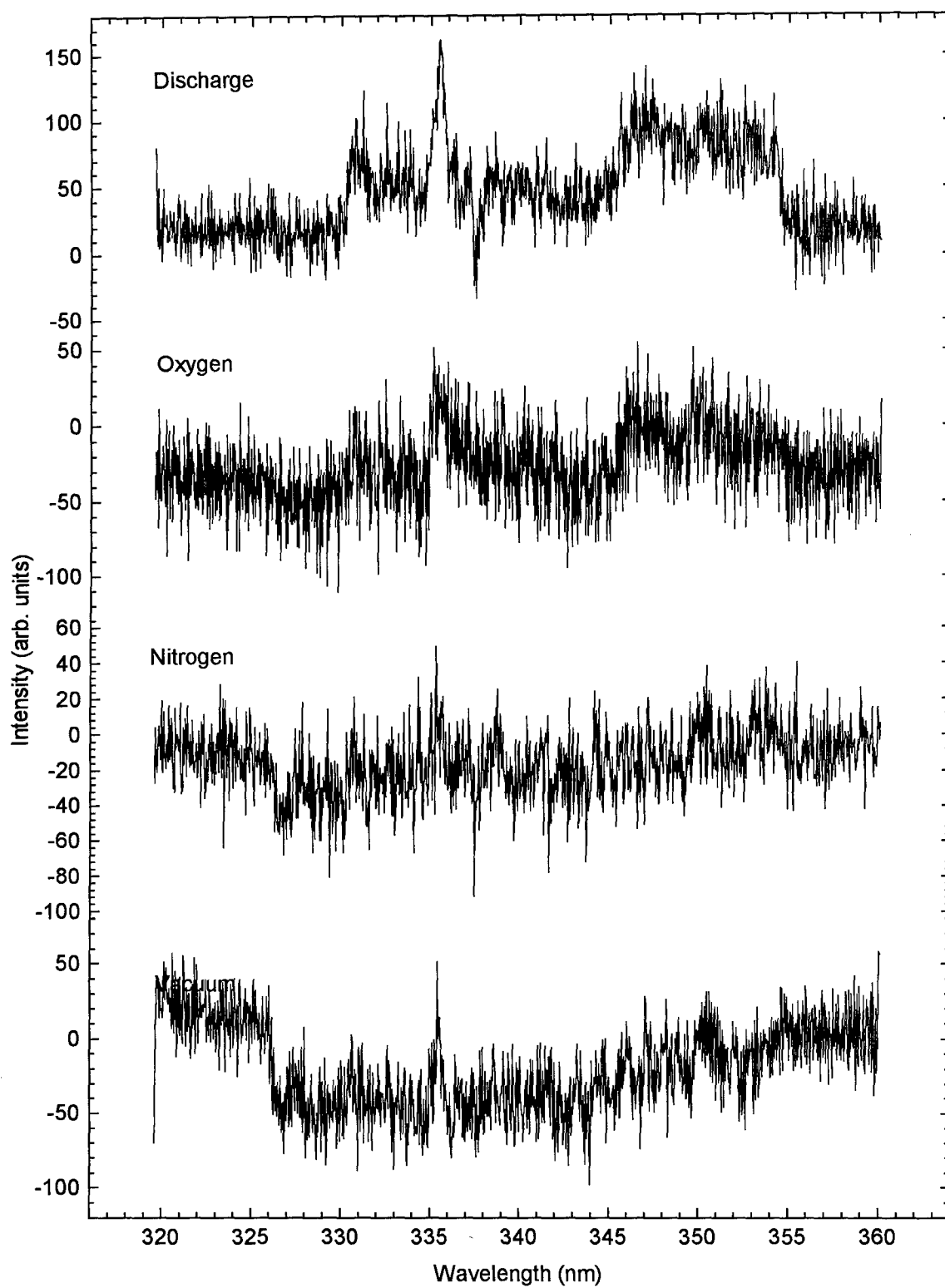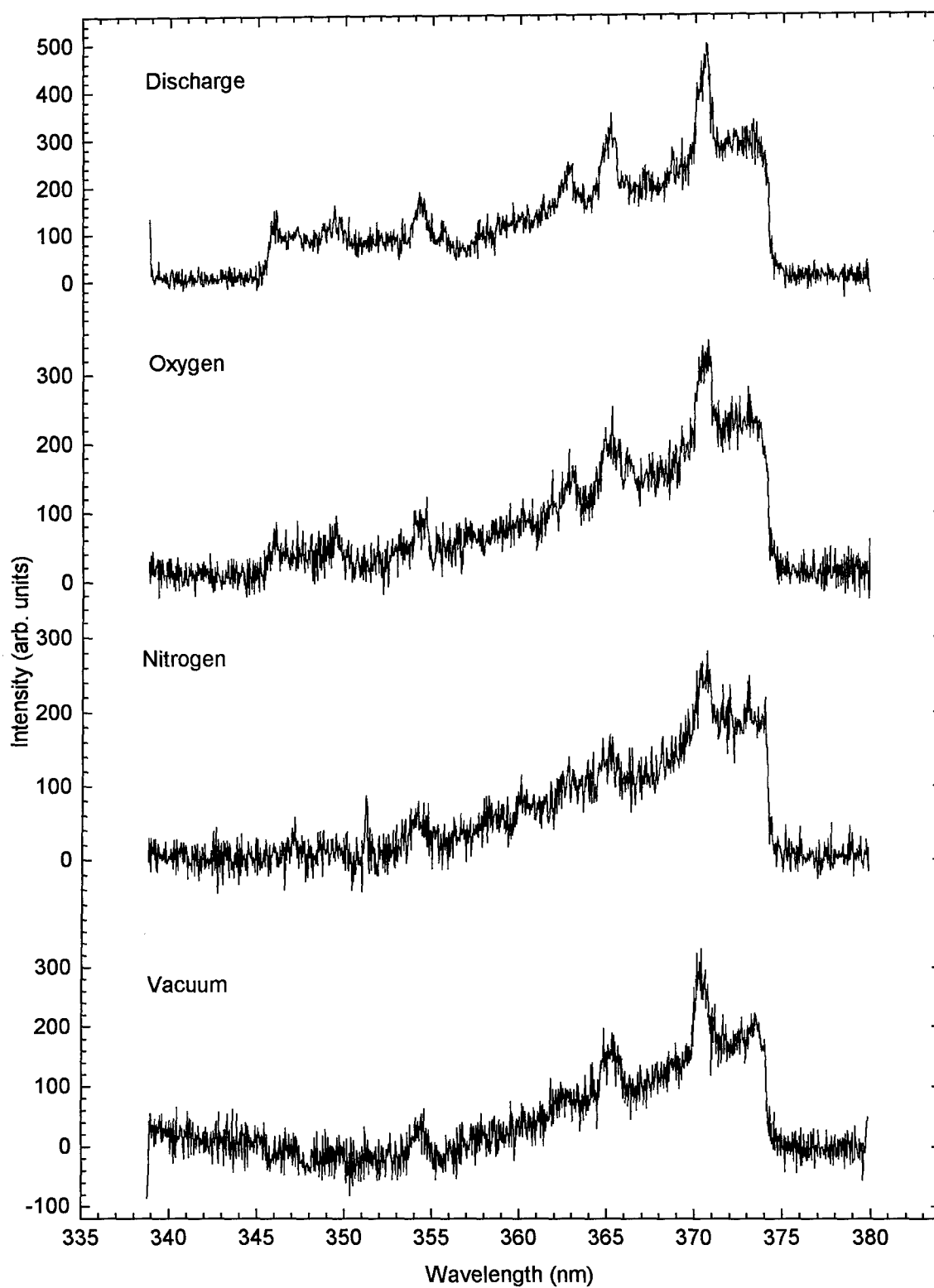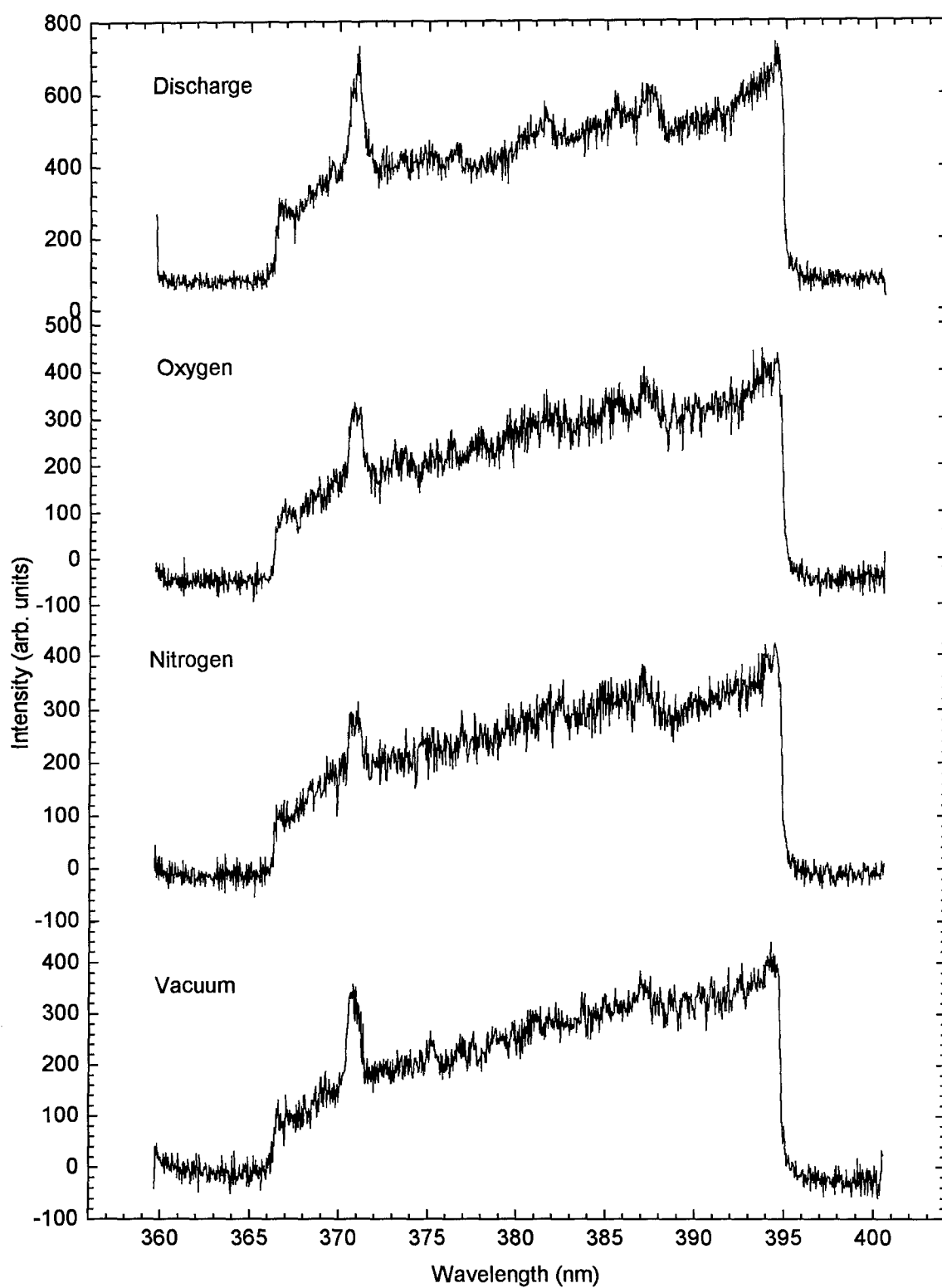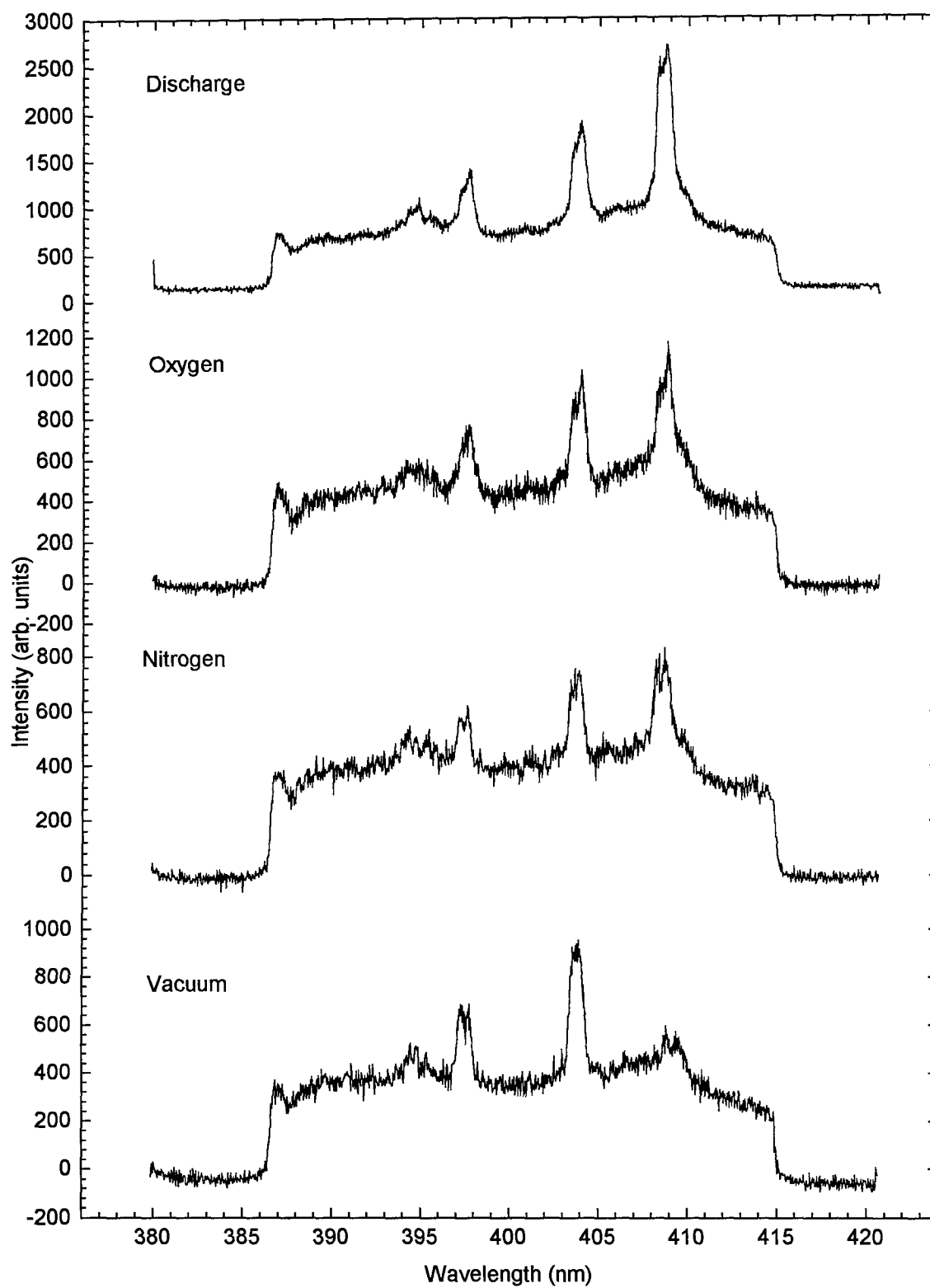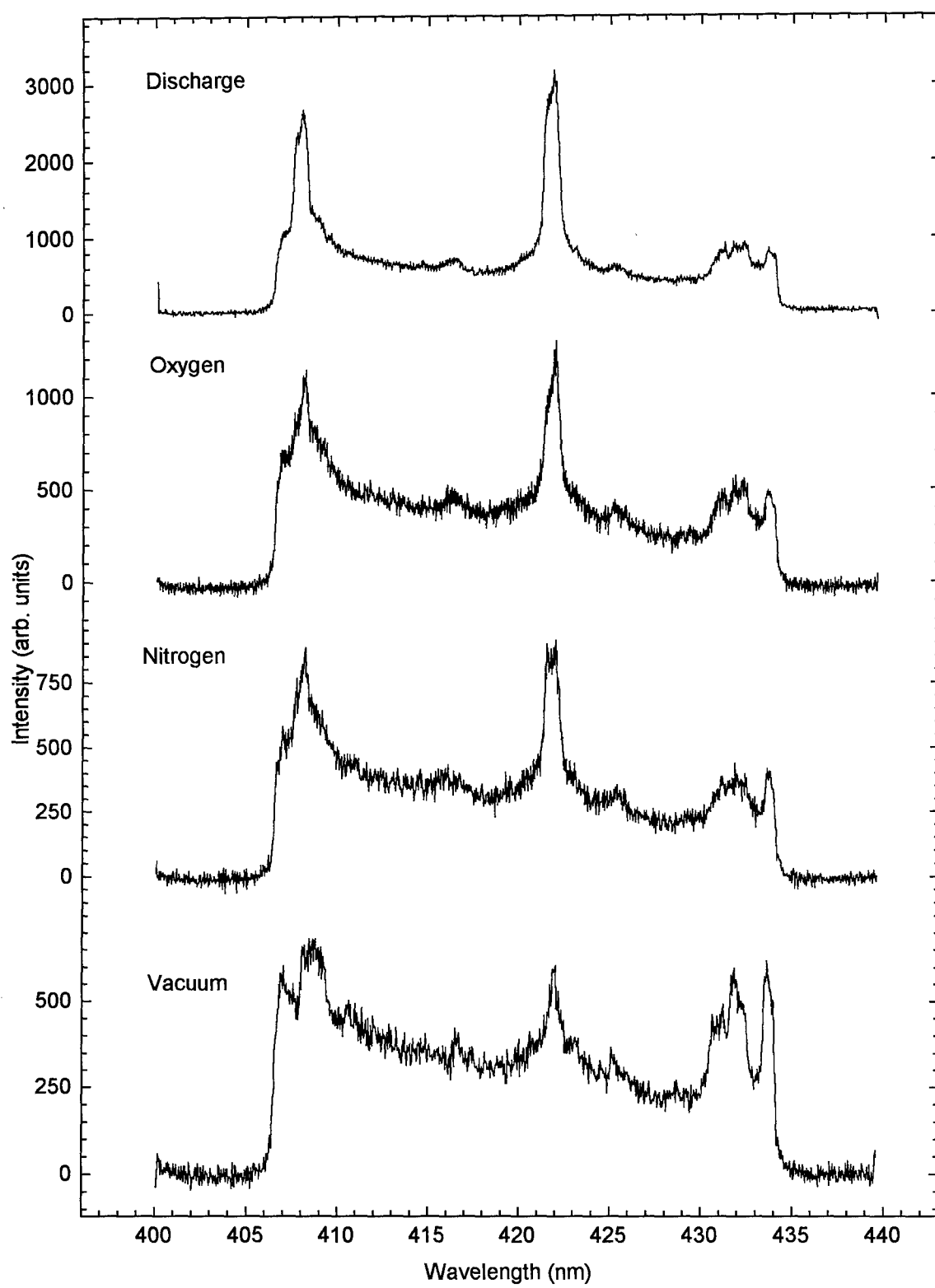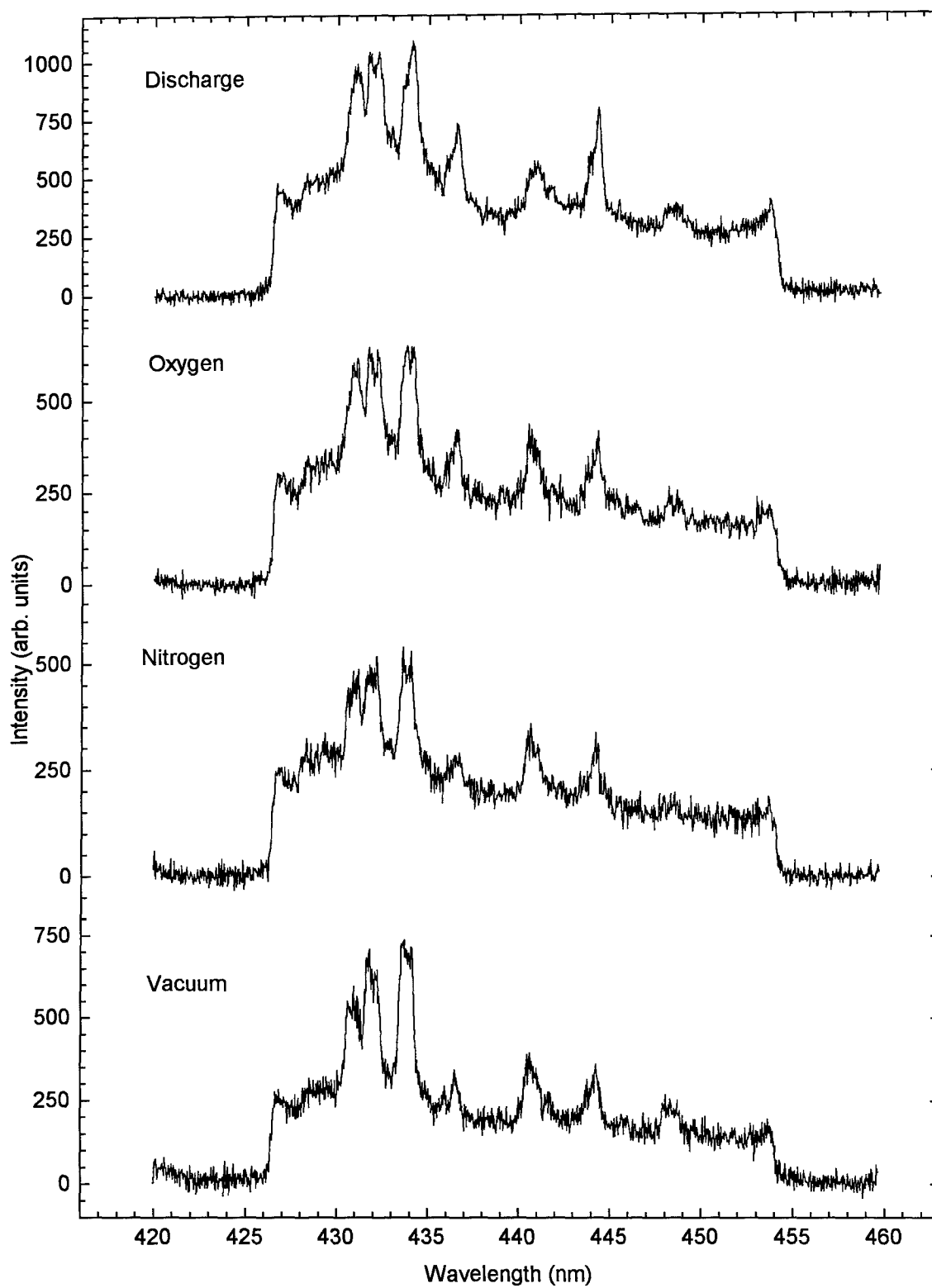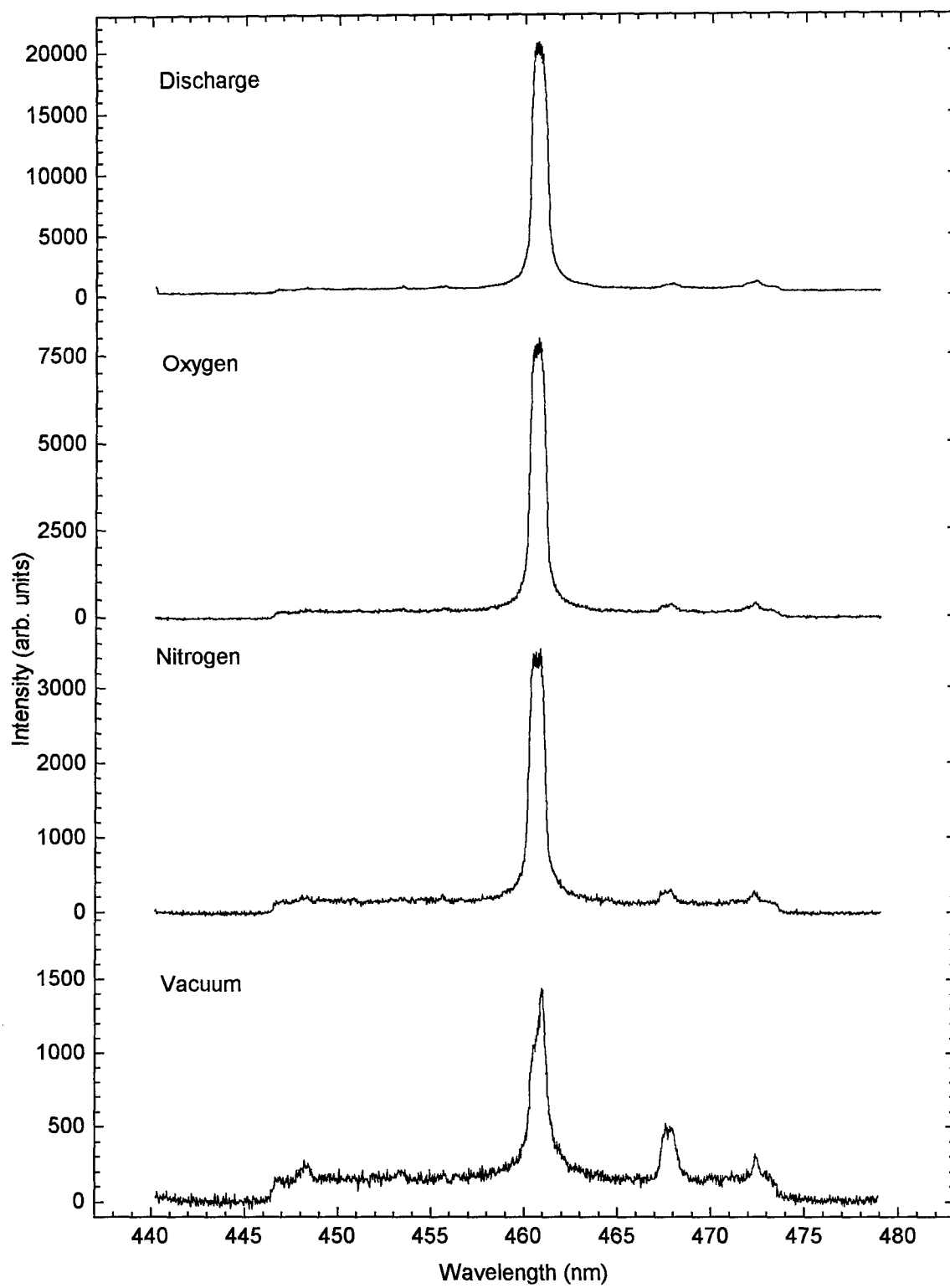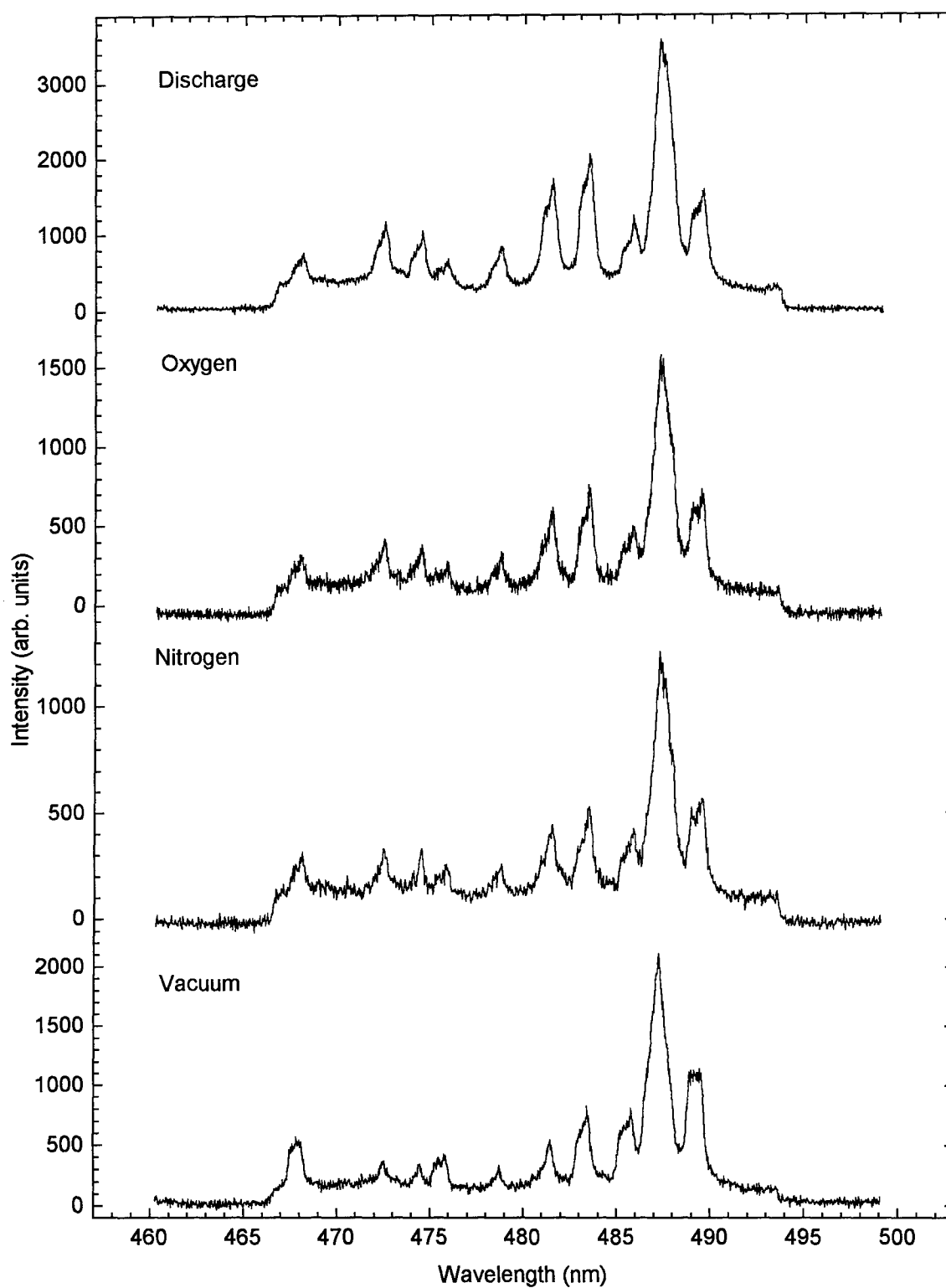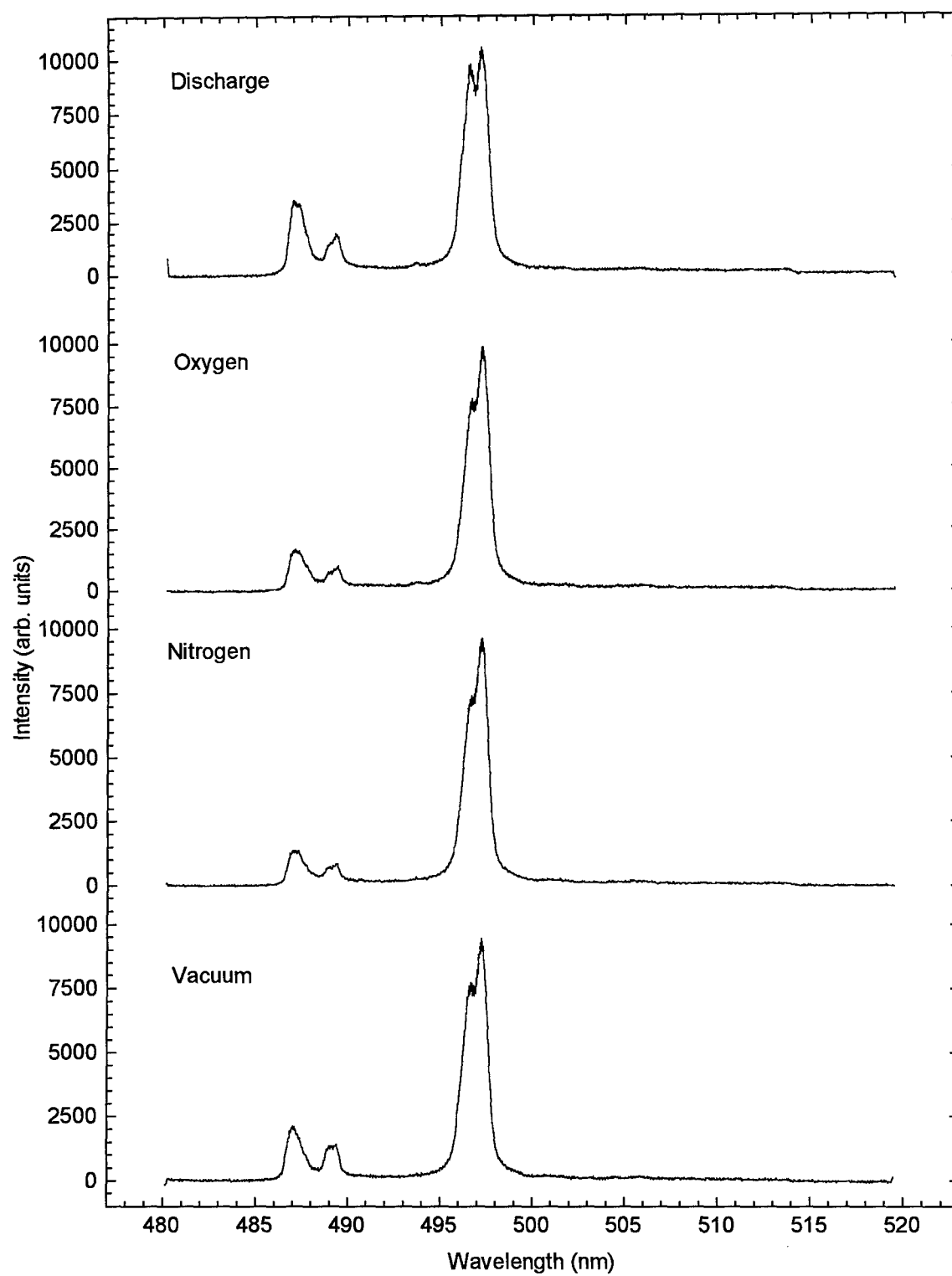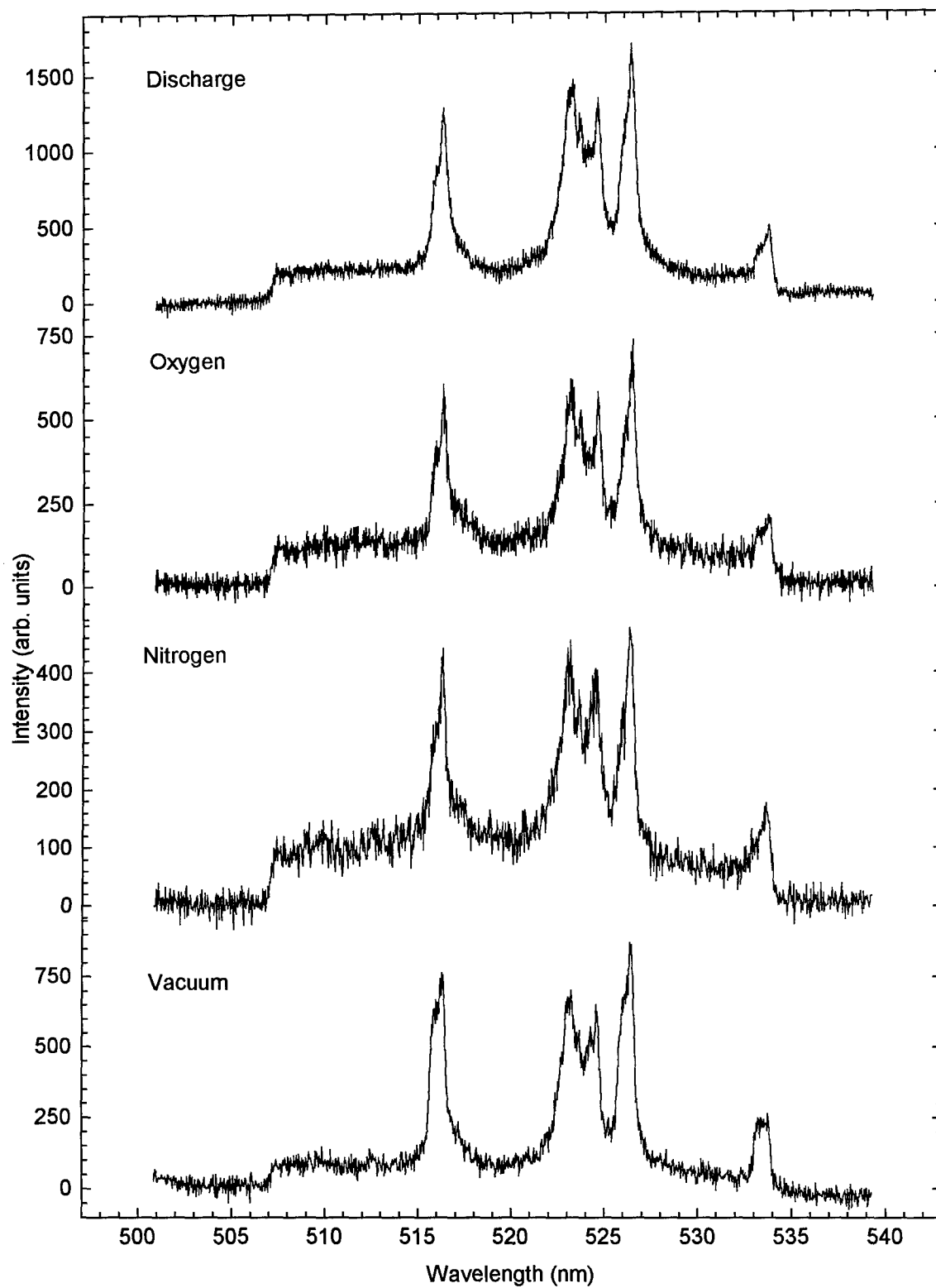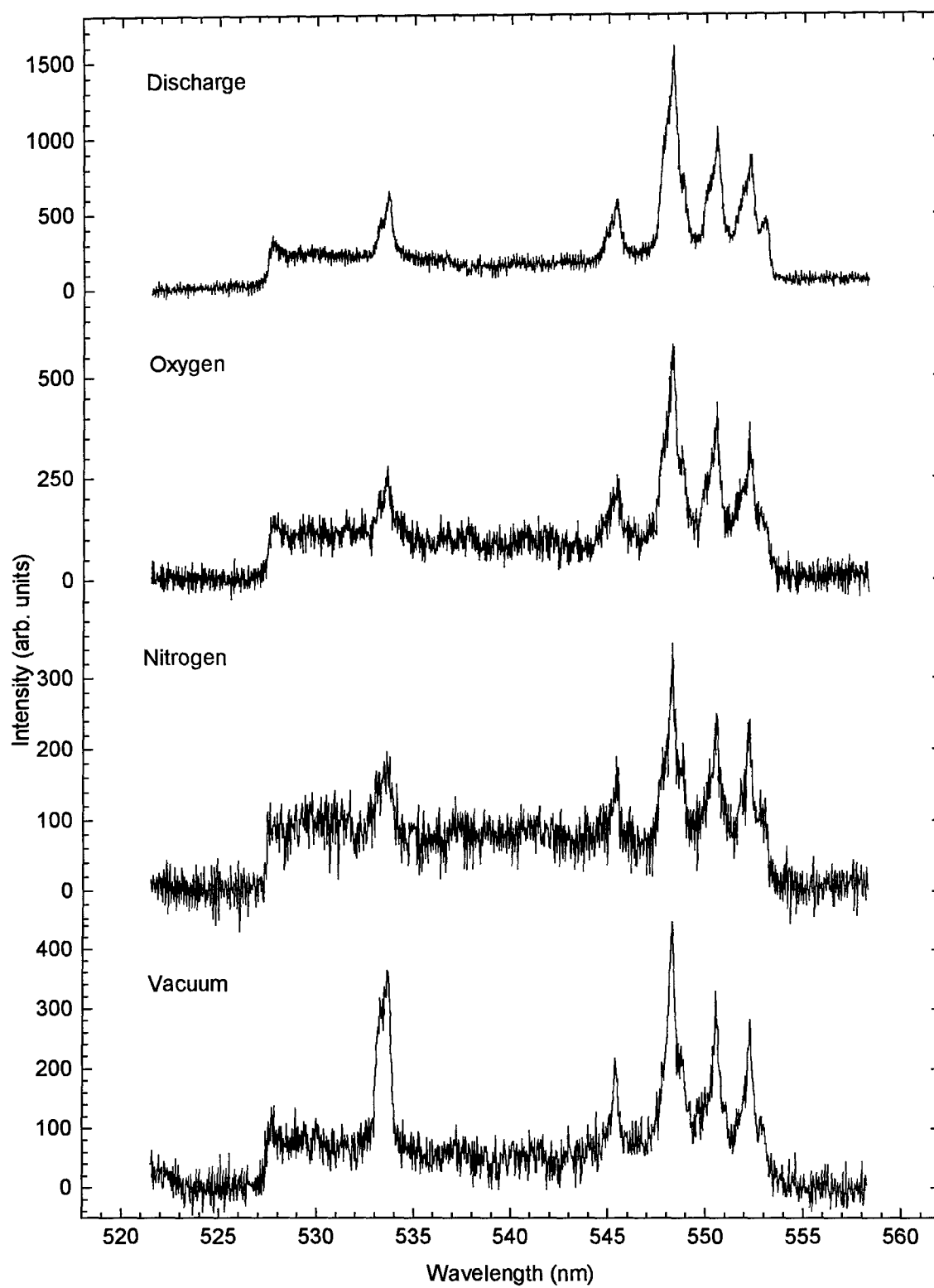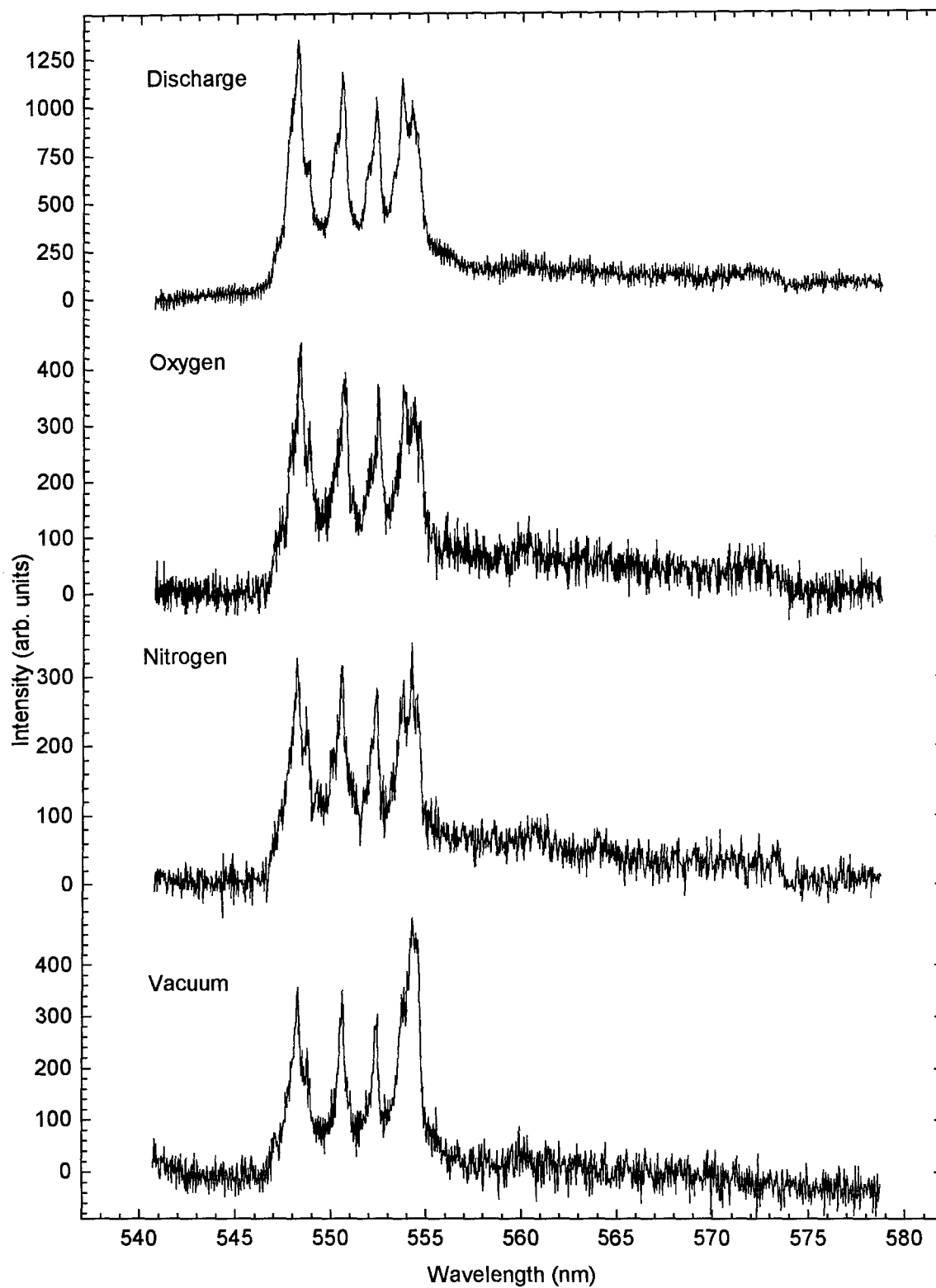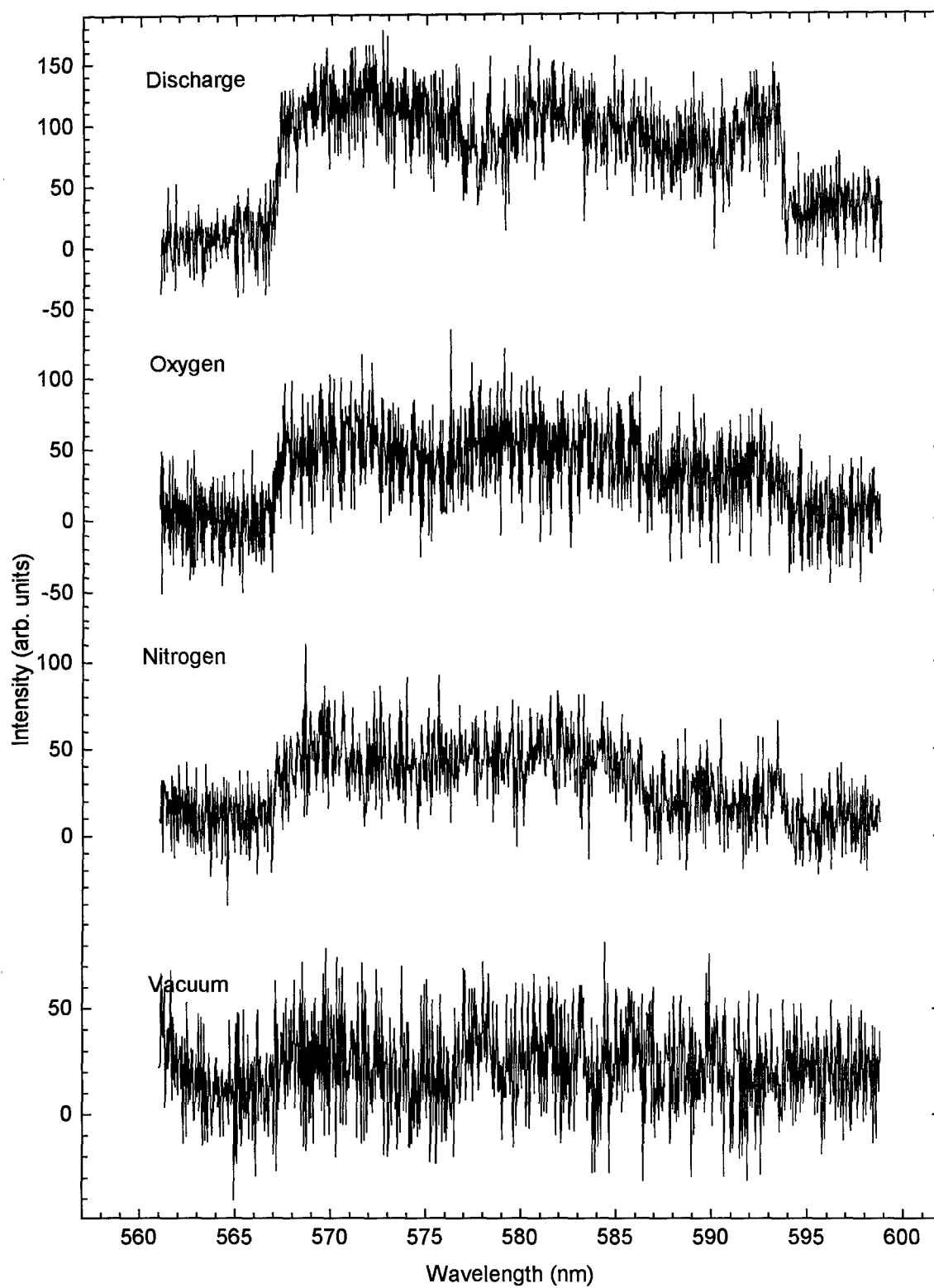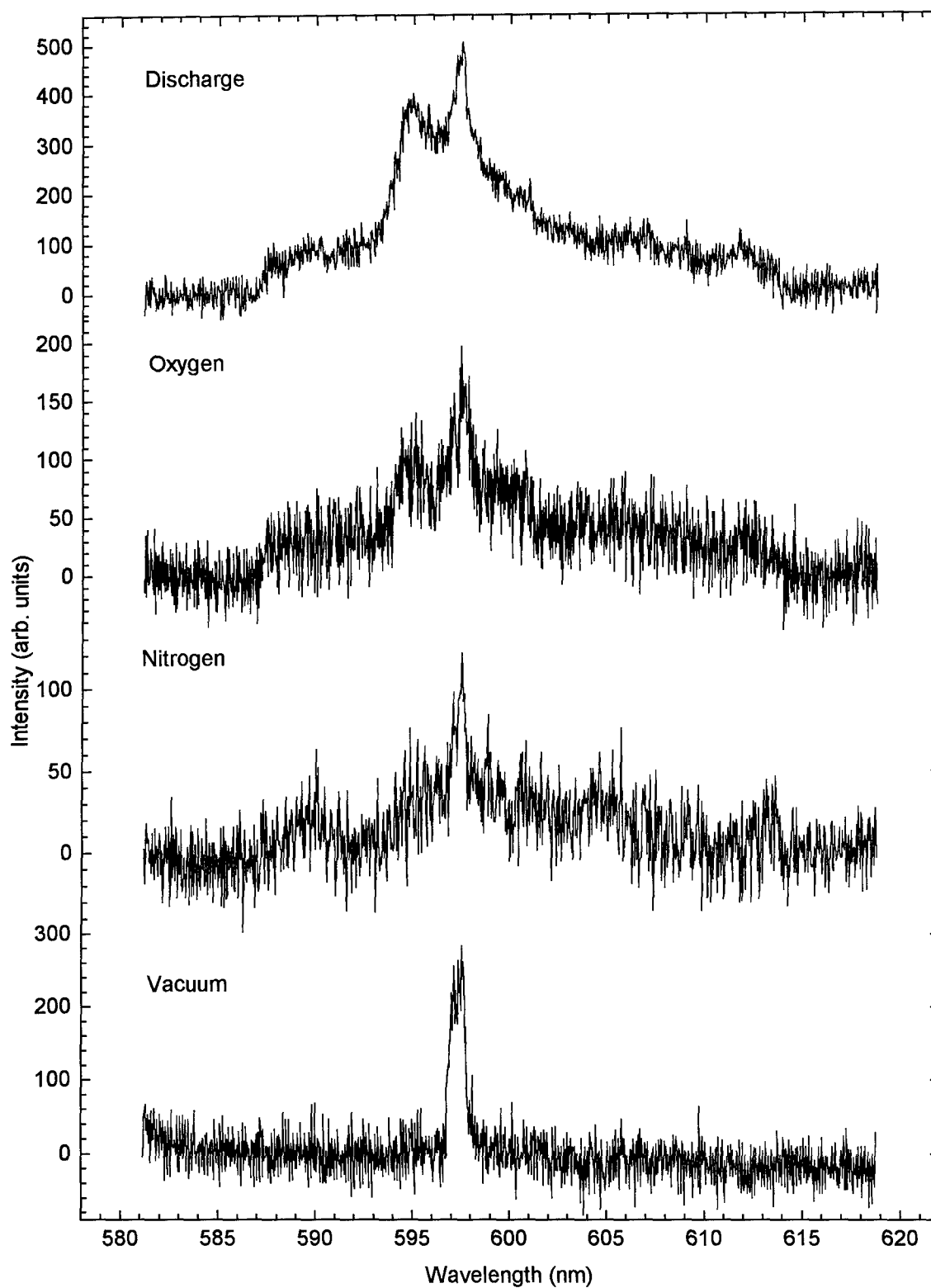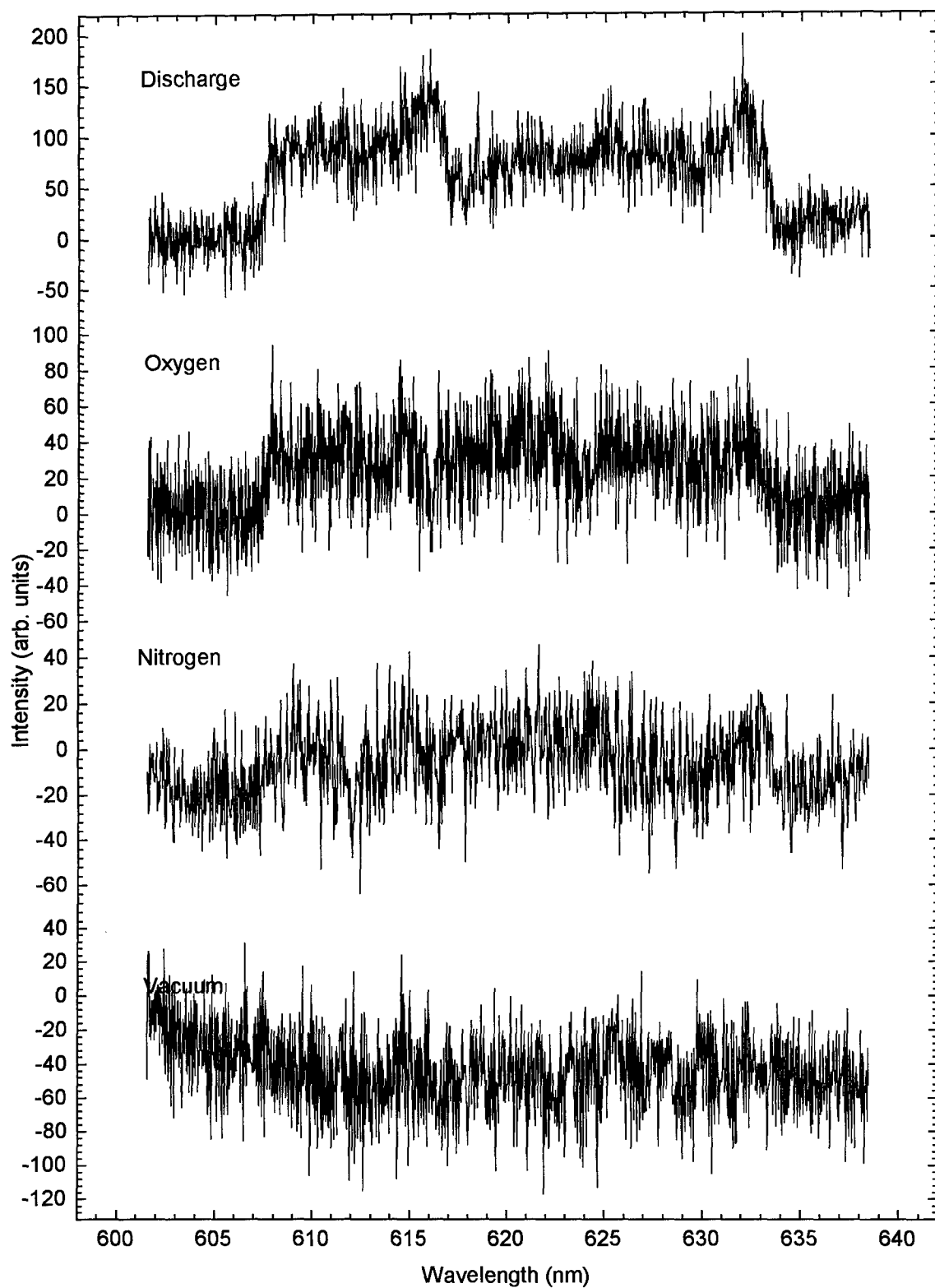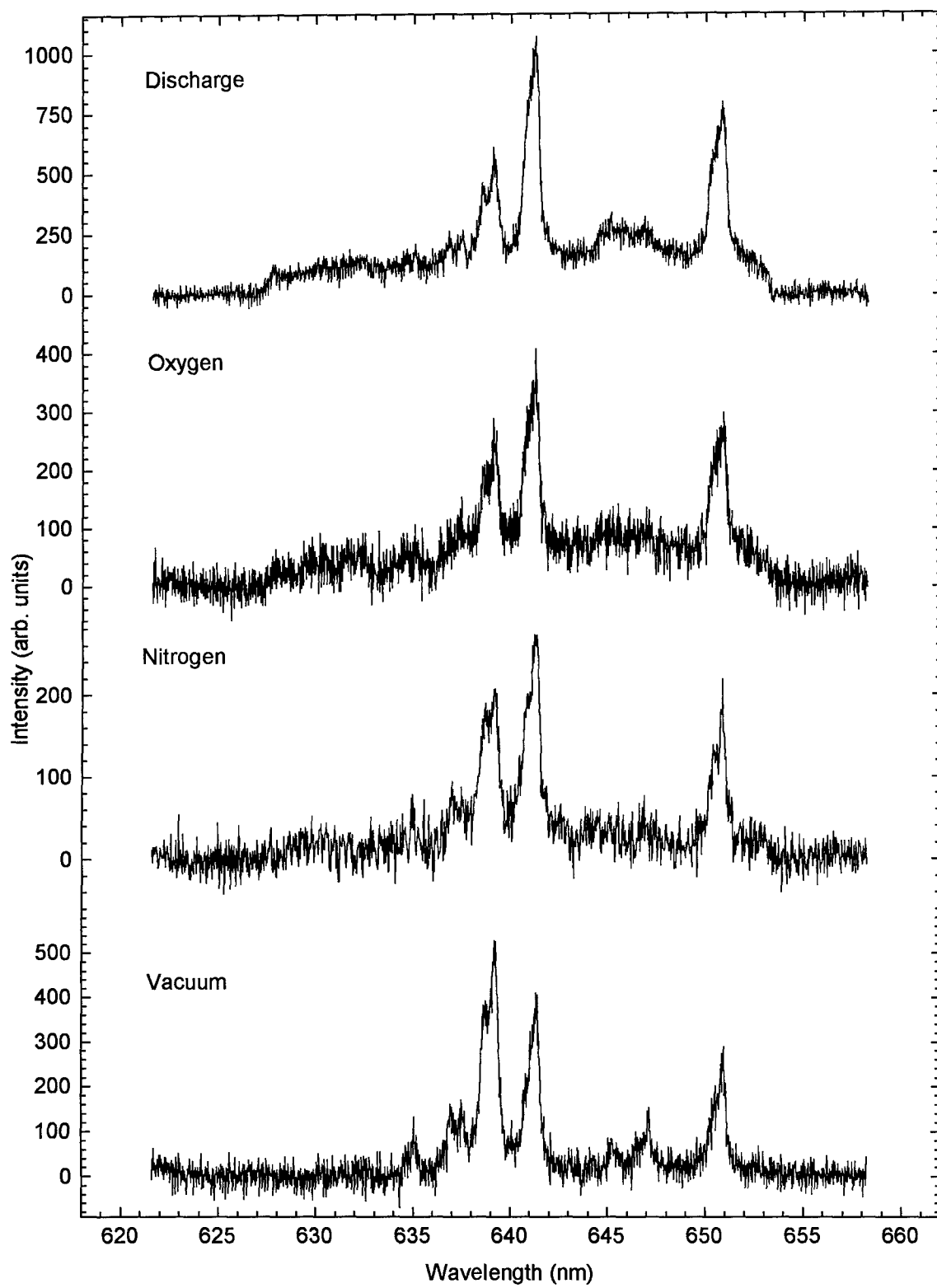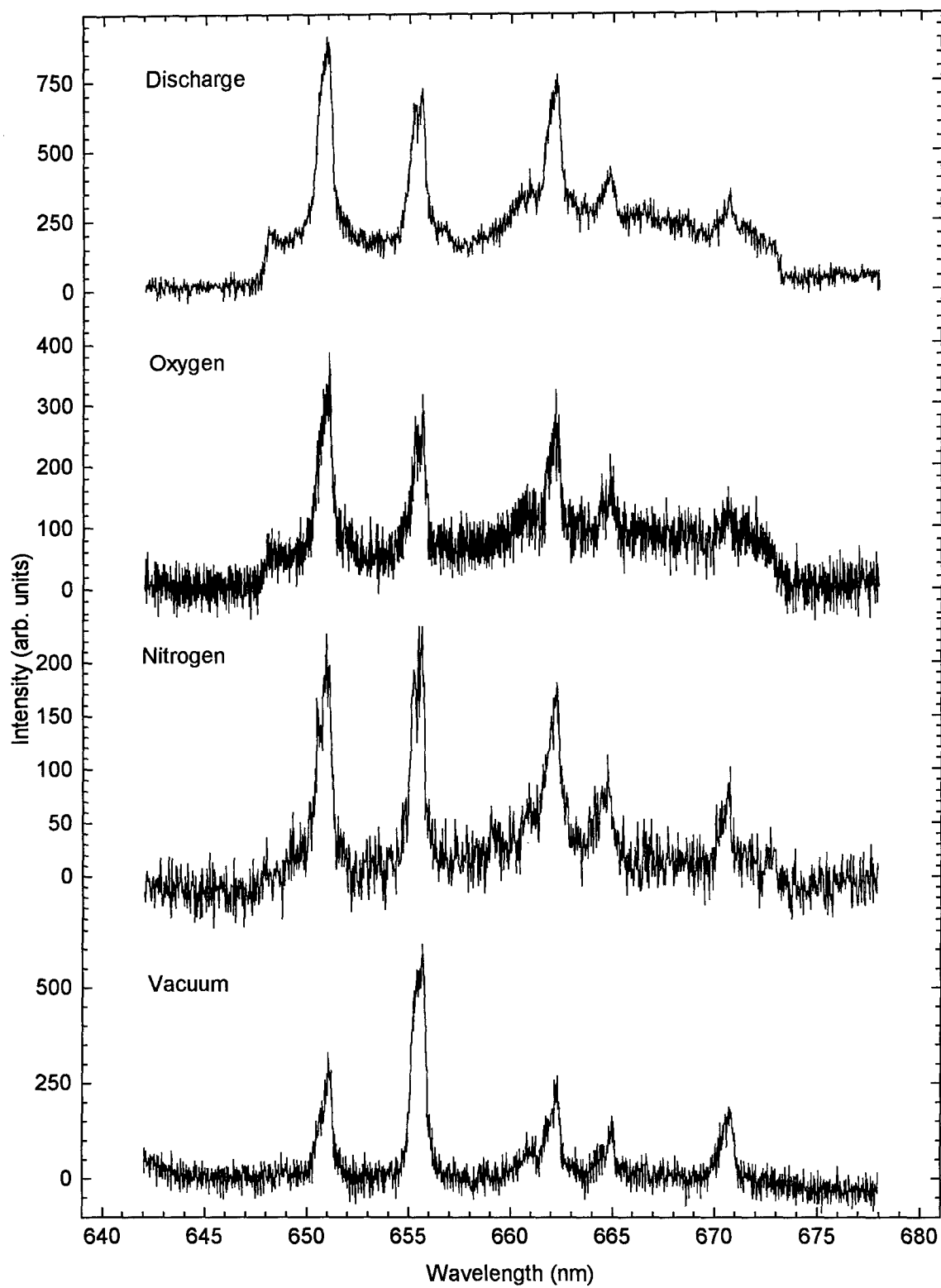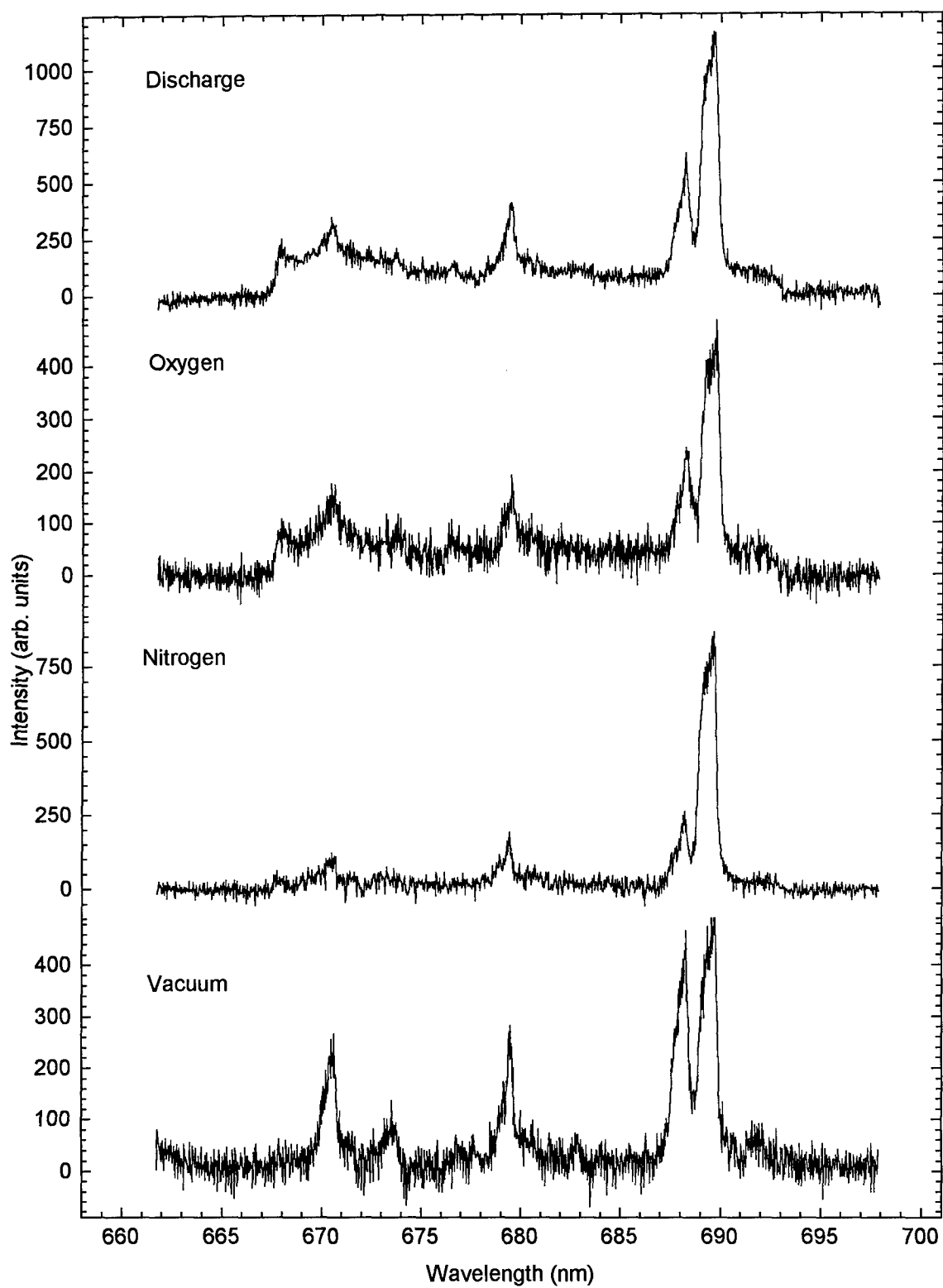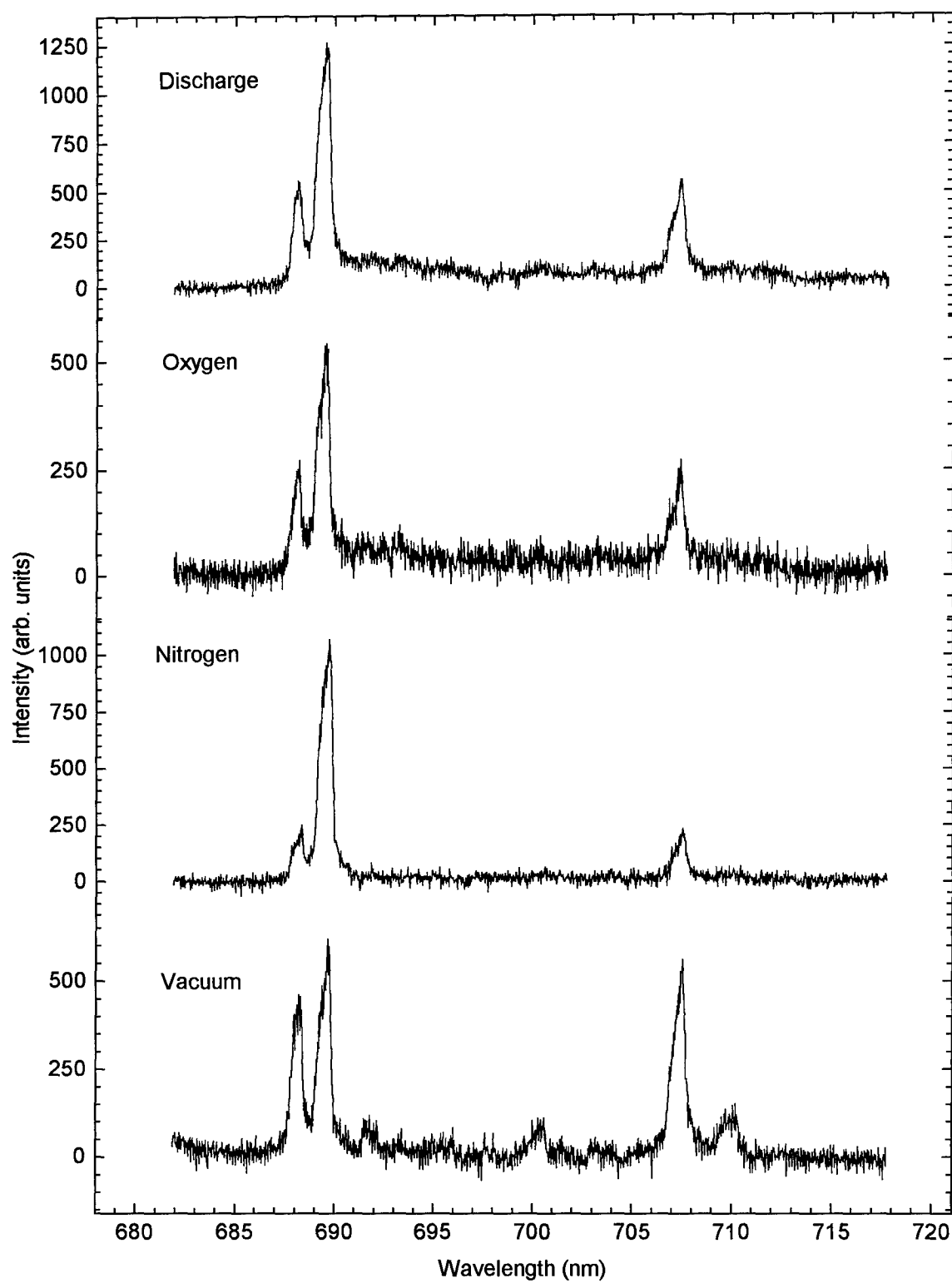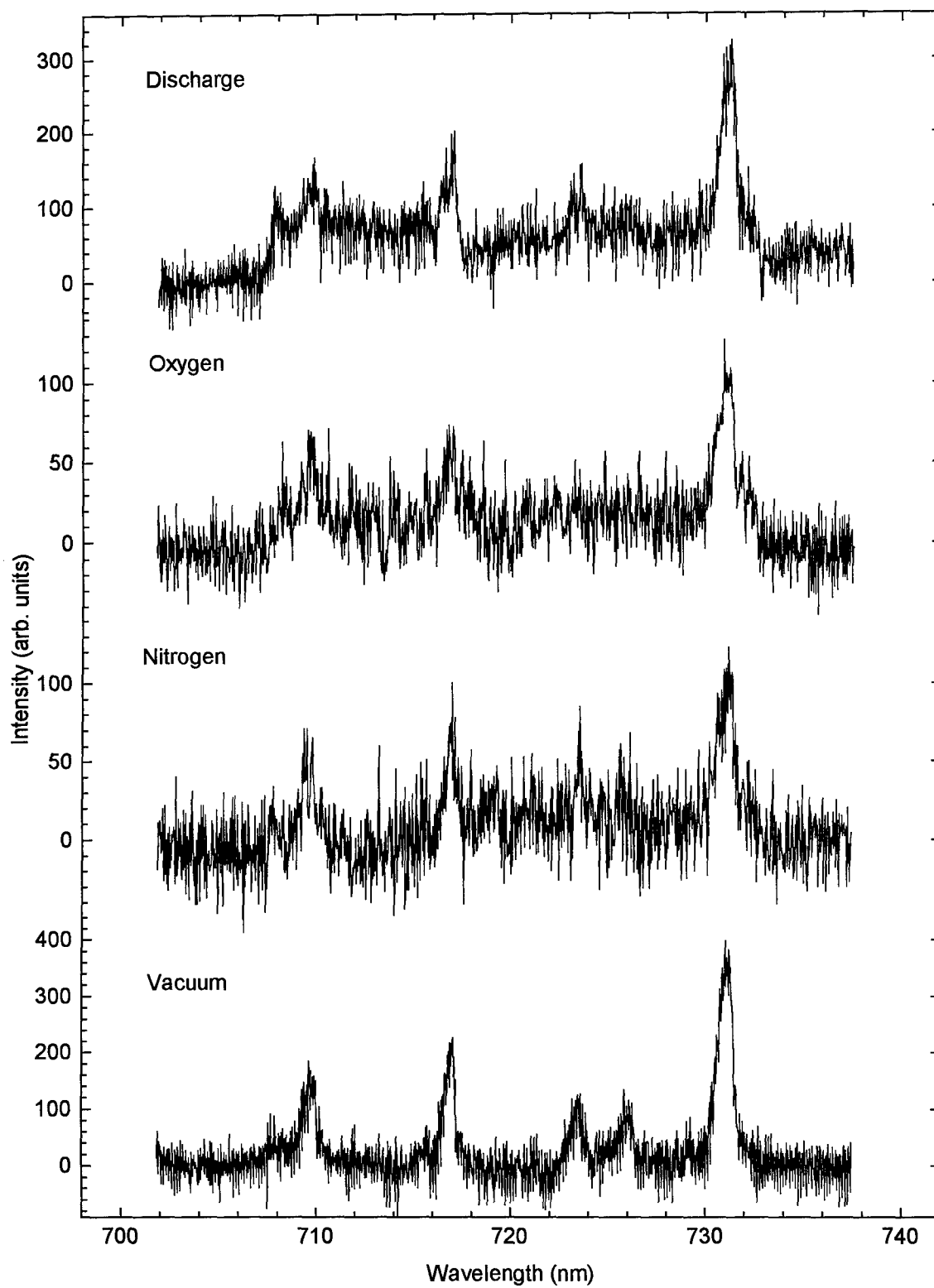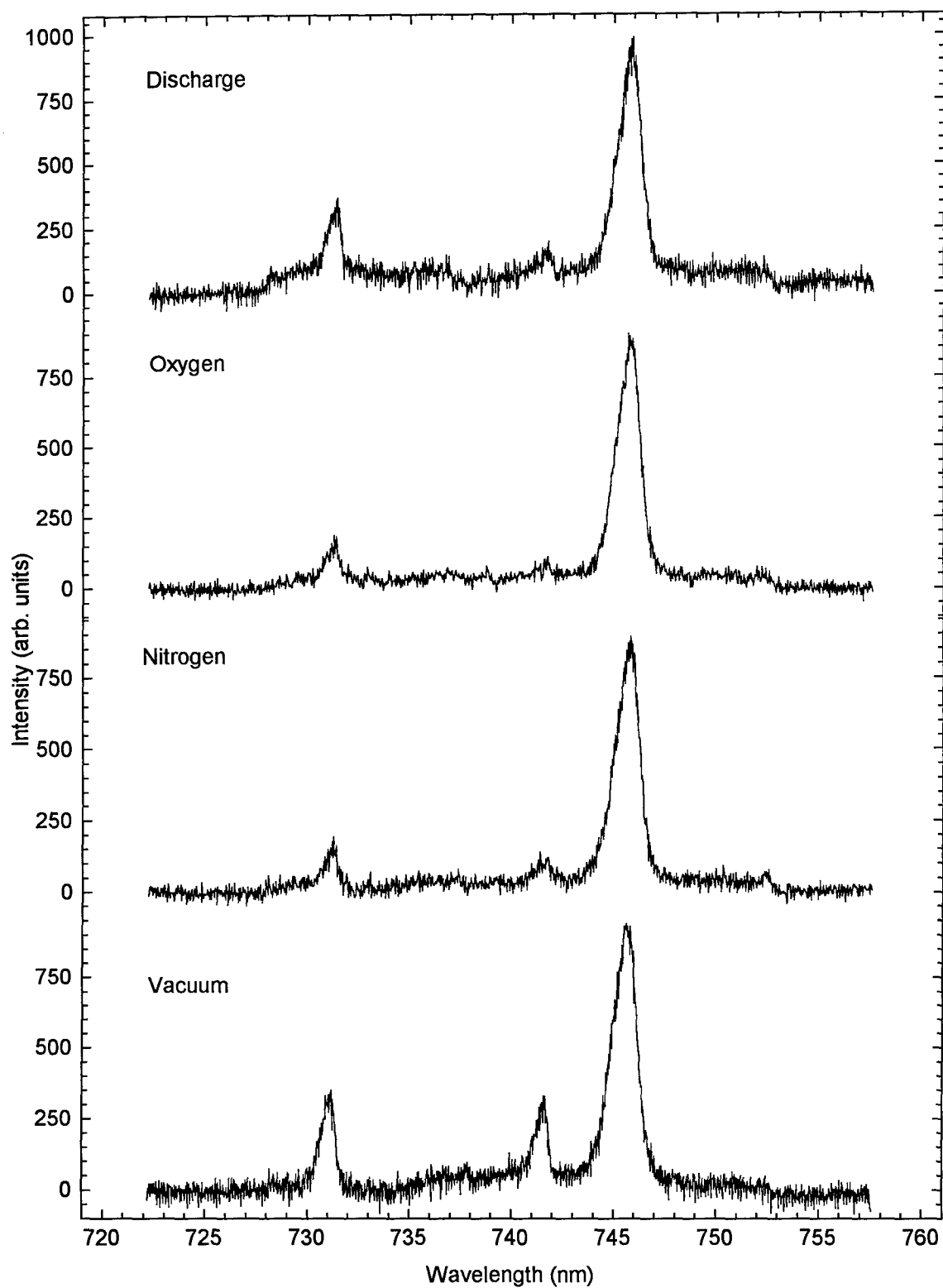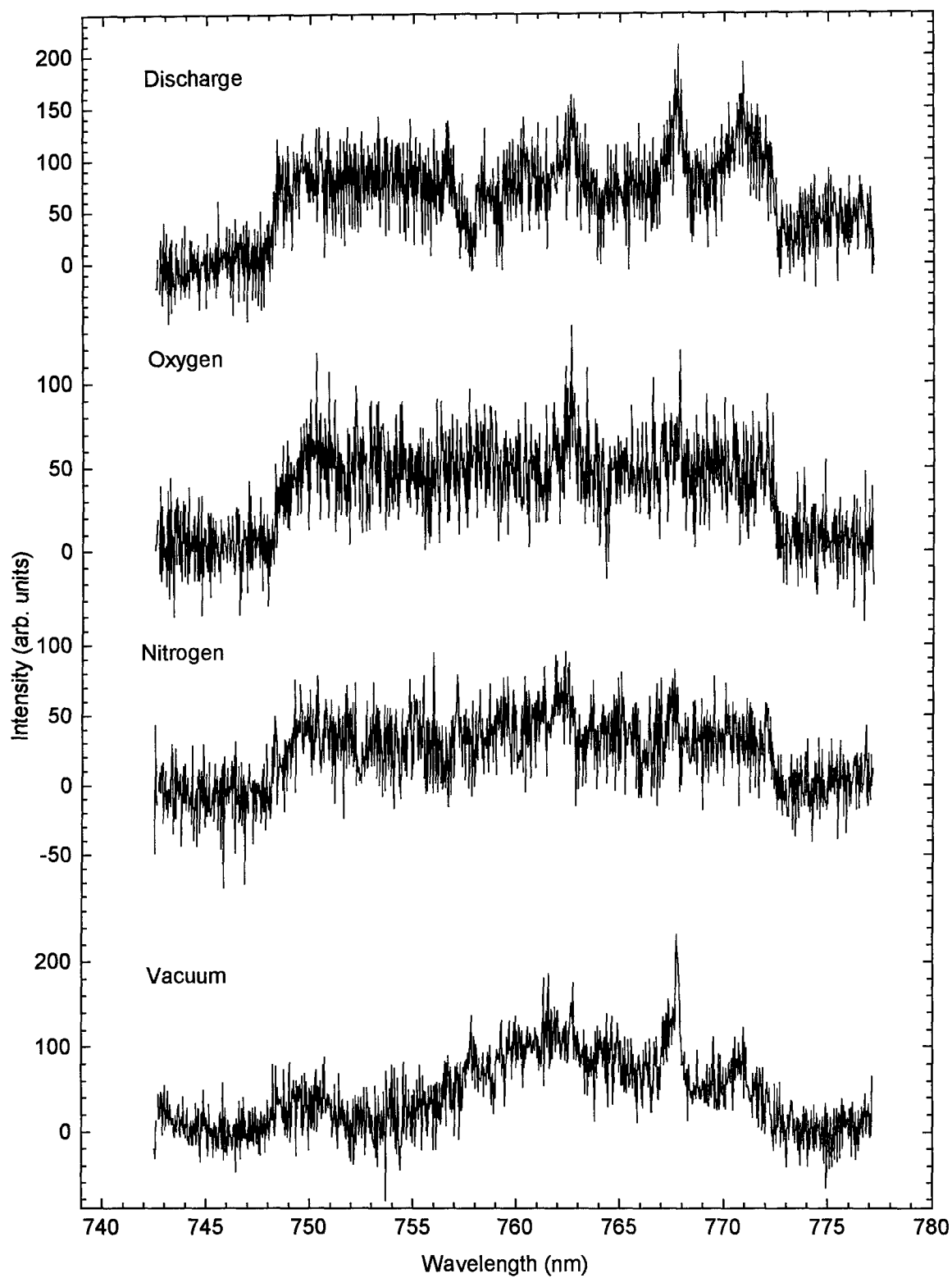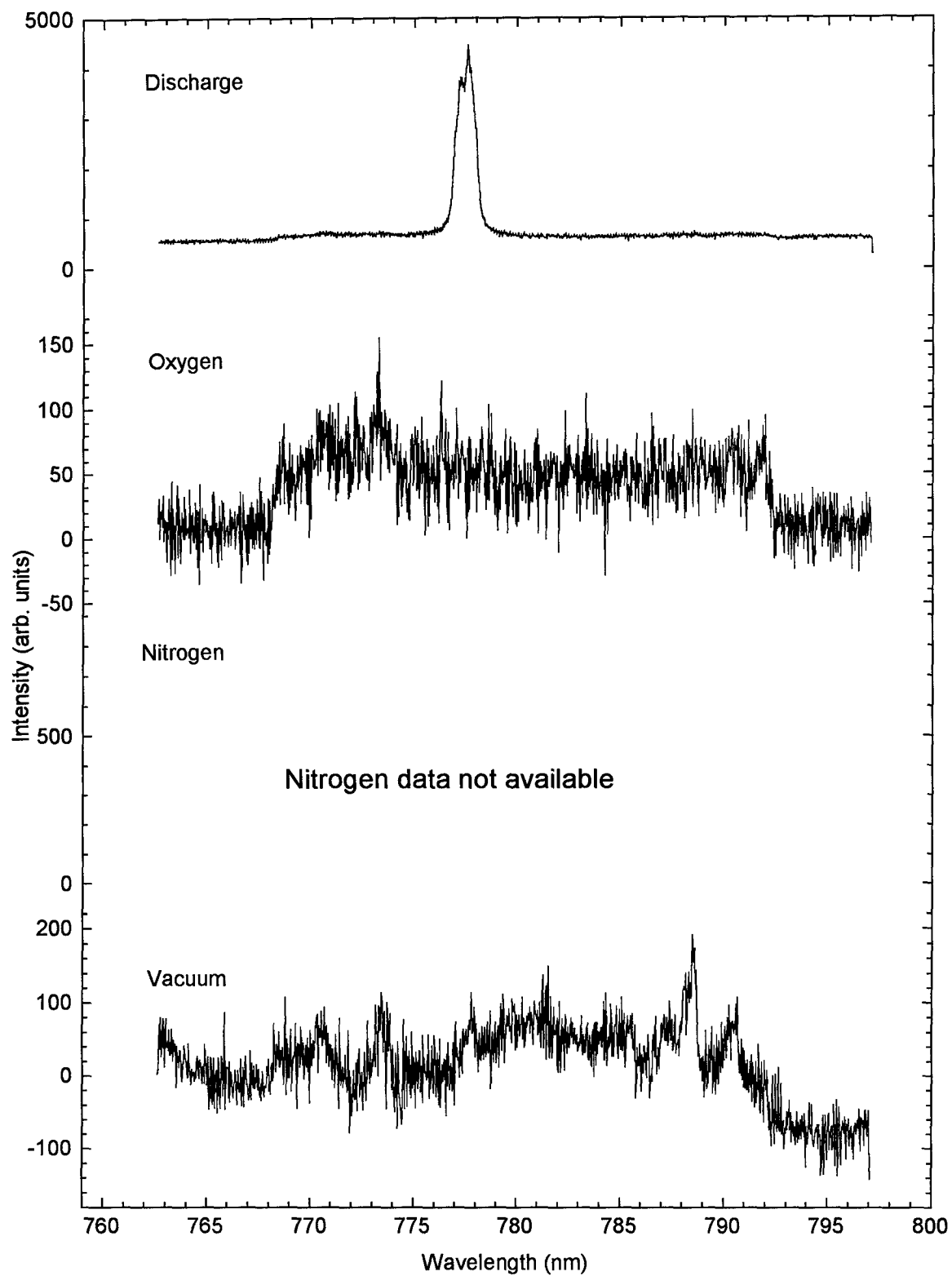
Appendix E: Spectral Data from SrO Target at 1.0 cm

Appendix E contains spectral data of laser-ablation plumes from a SrO target. Background gases were at 25.0 mtorr. Data was taken 1.0 cm from the target. Laser fluence was 575 mJ-cm^{-2}. Data was taken using a 0.5 m spectrometer with a 1200g/mm grating, 100μm slit and an Oma linear array. The signal was integrated over 16.6 msec and 120 pulses were summed to get this output.
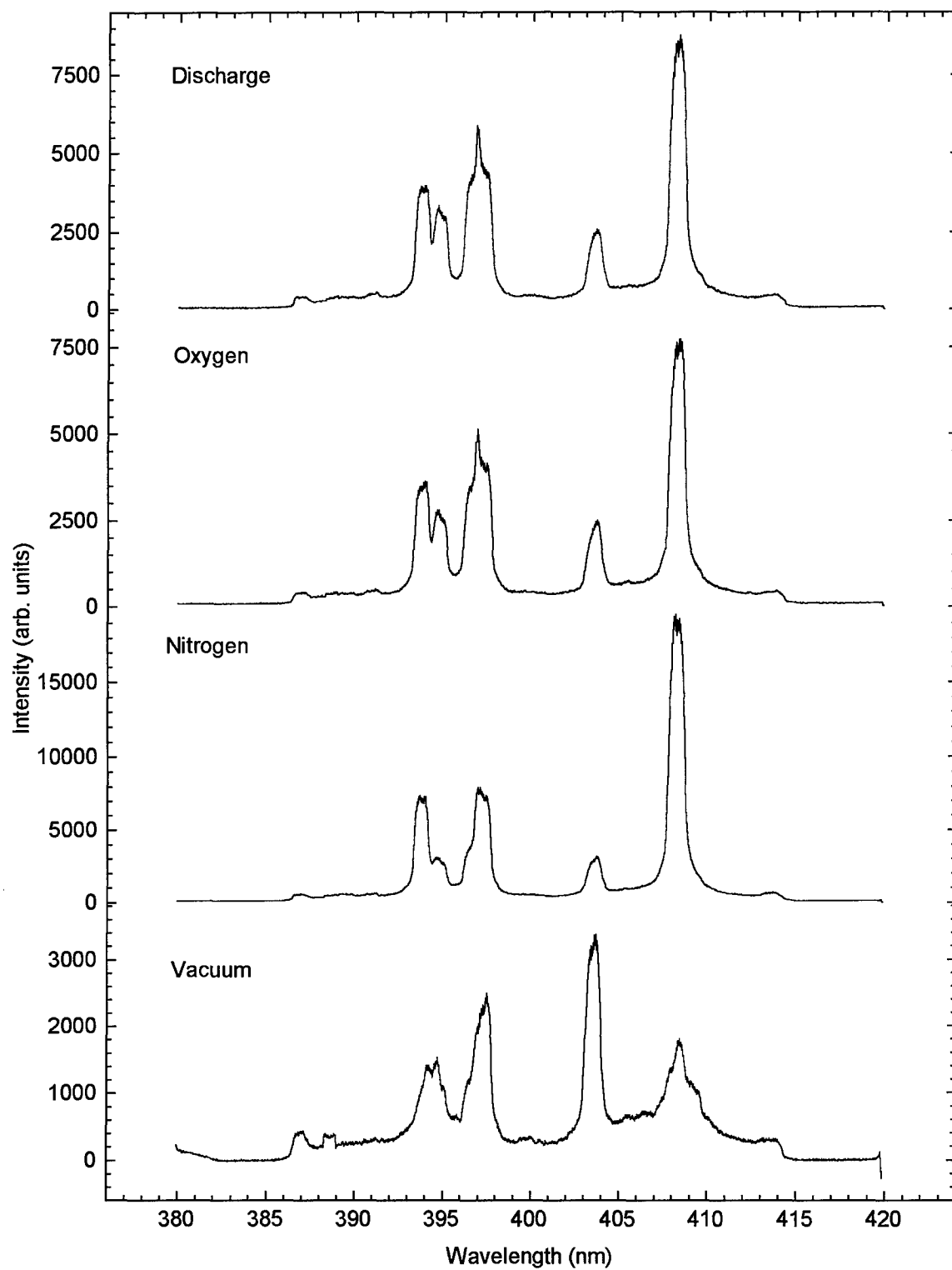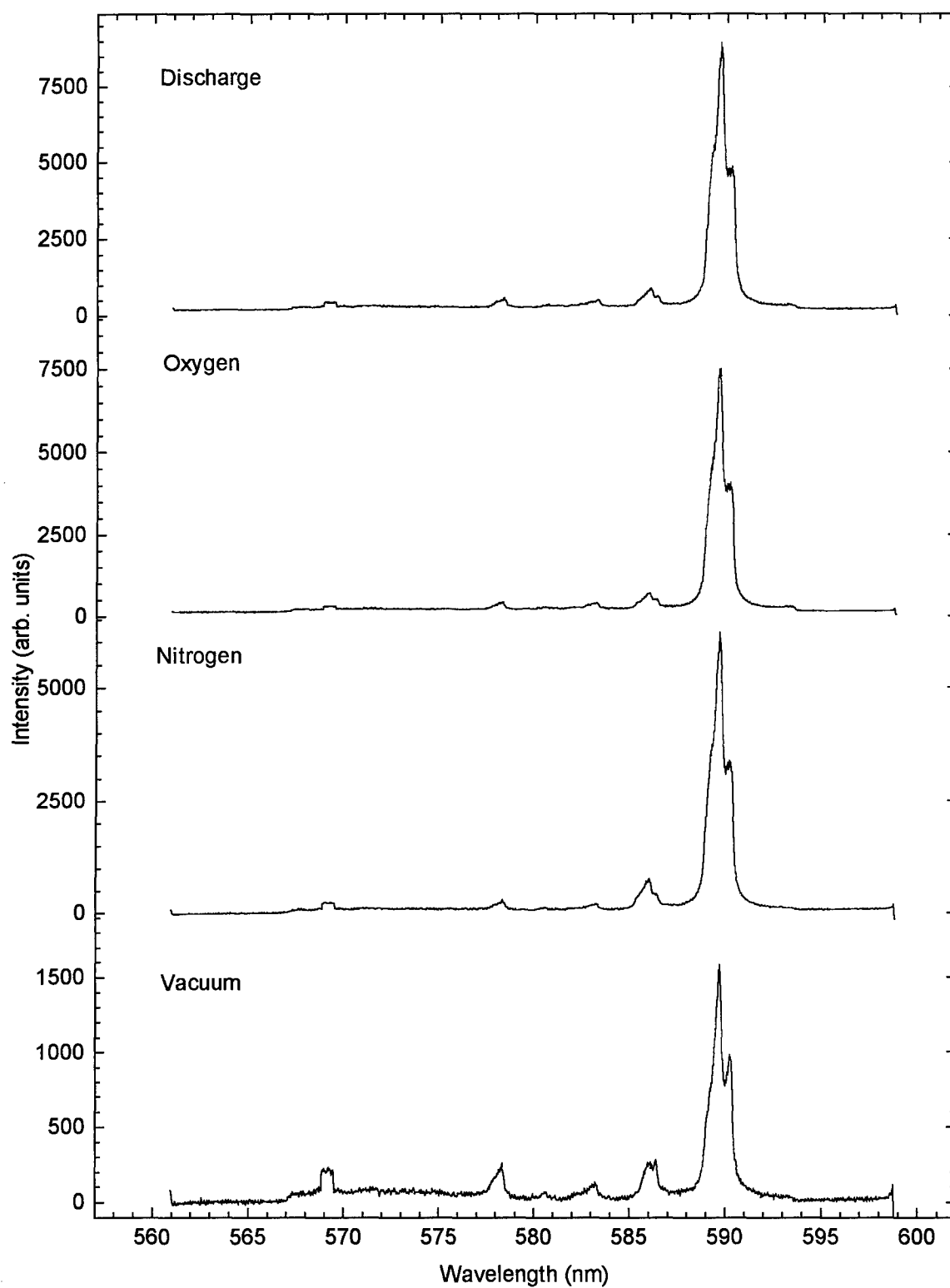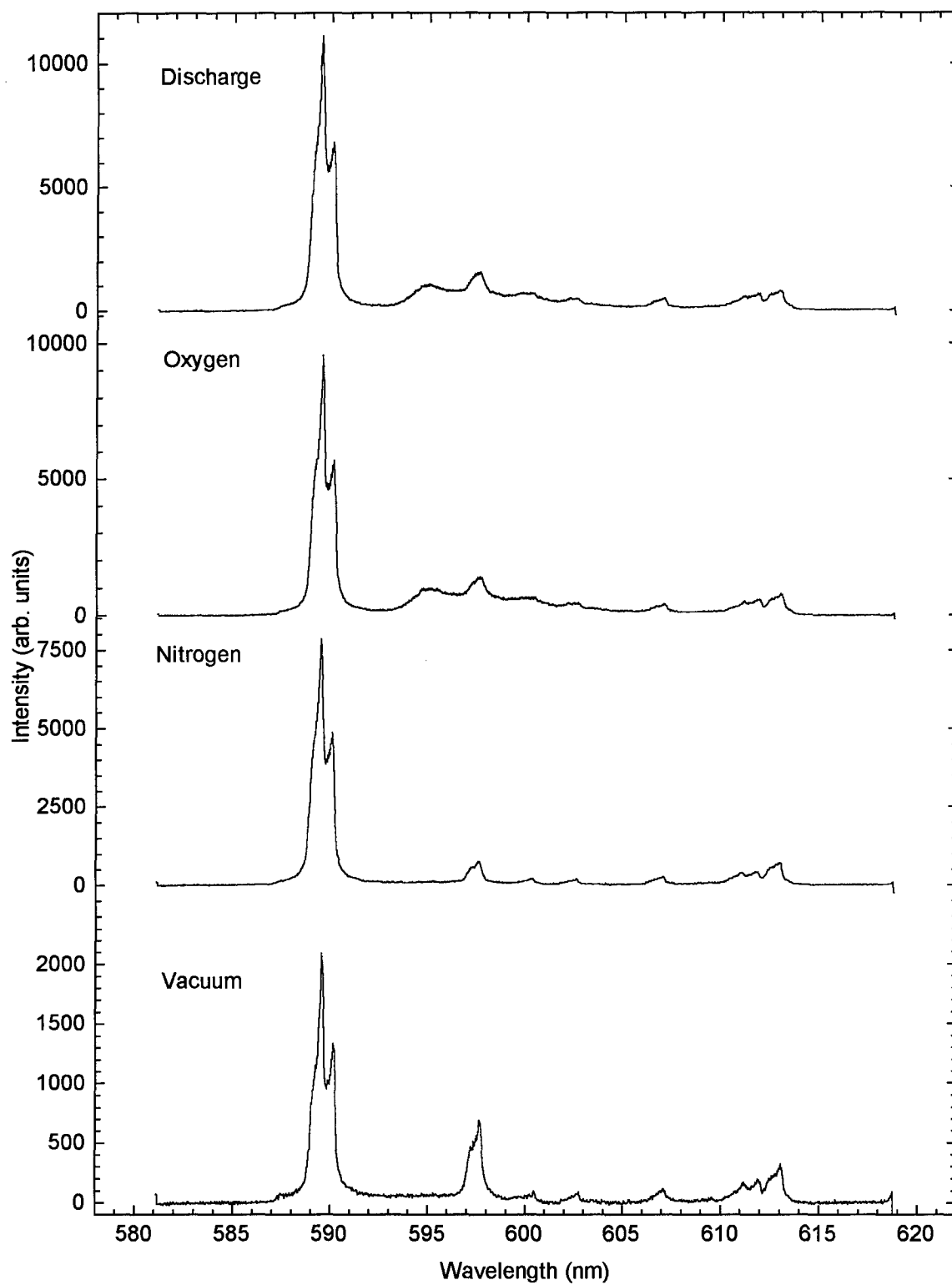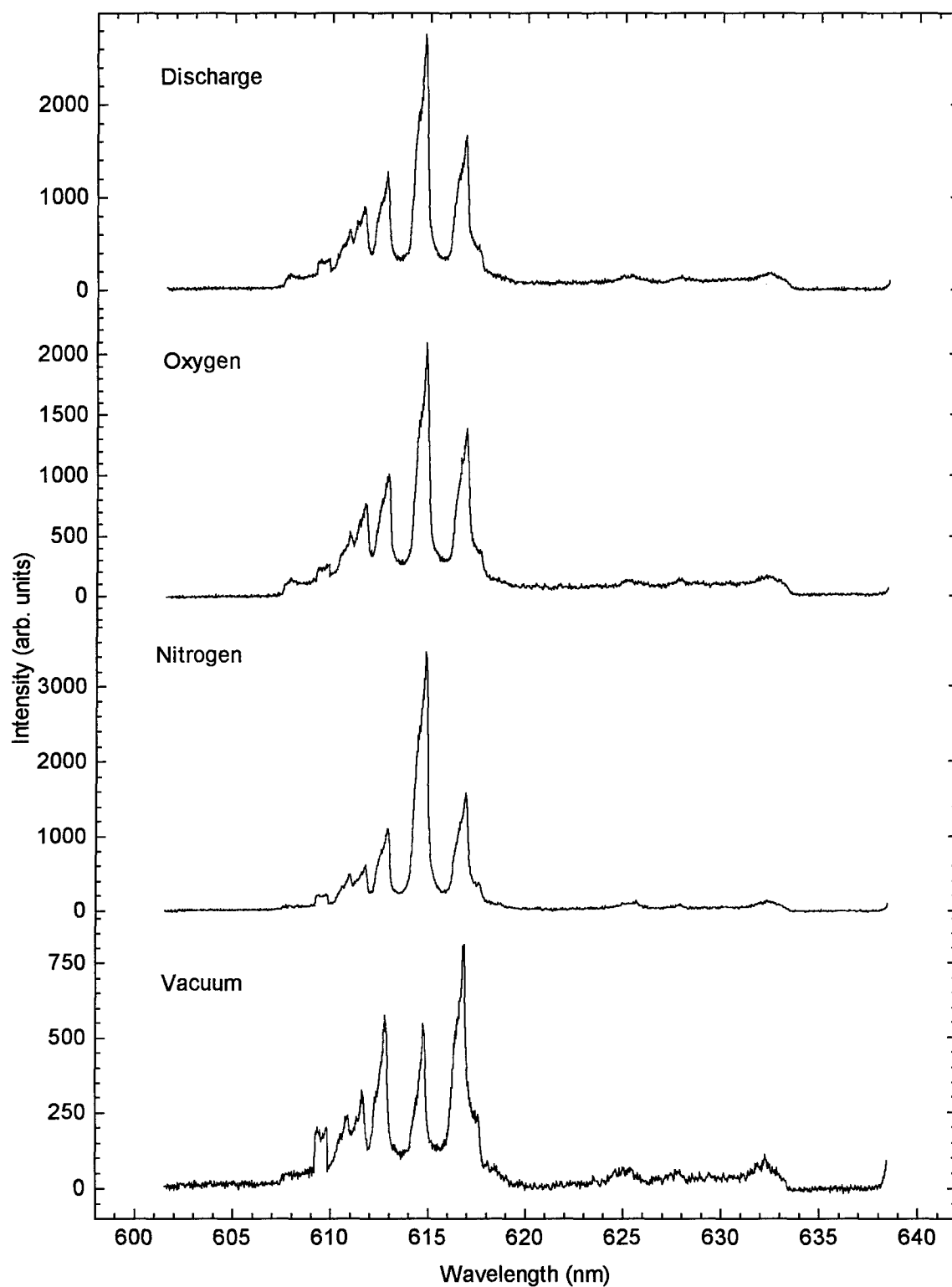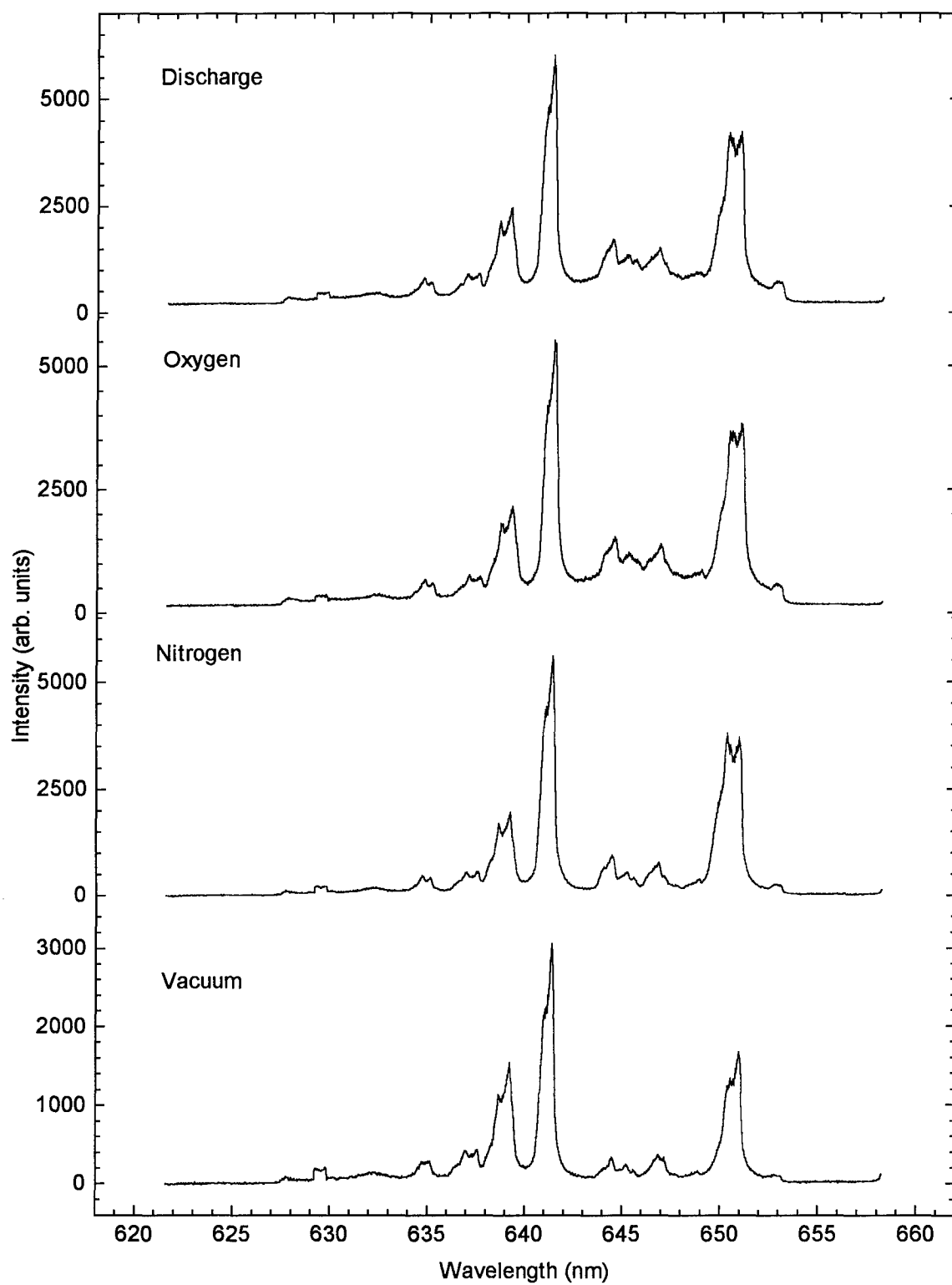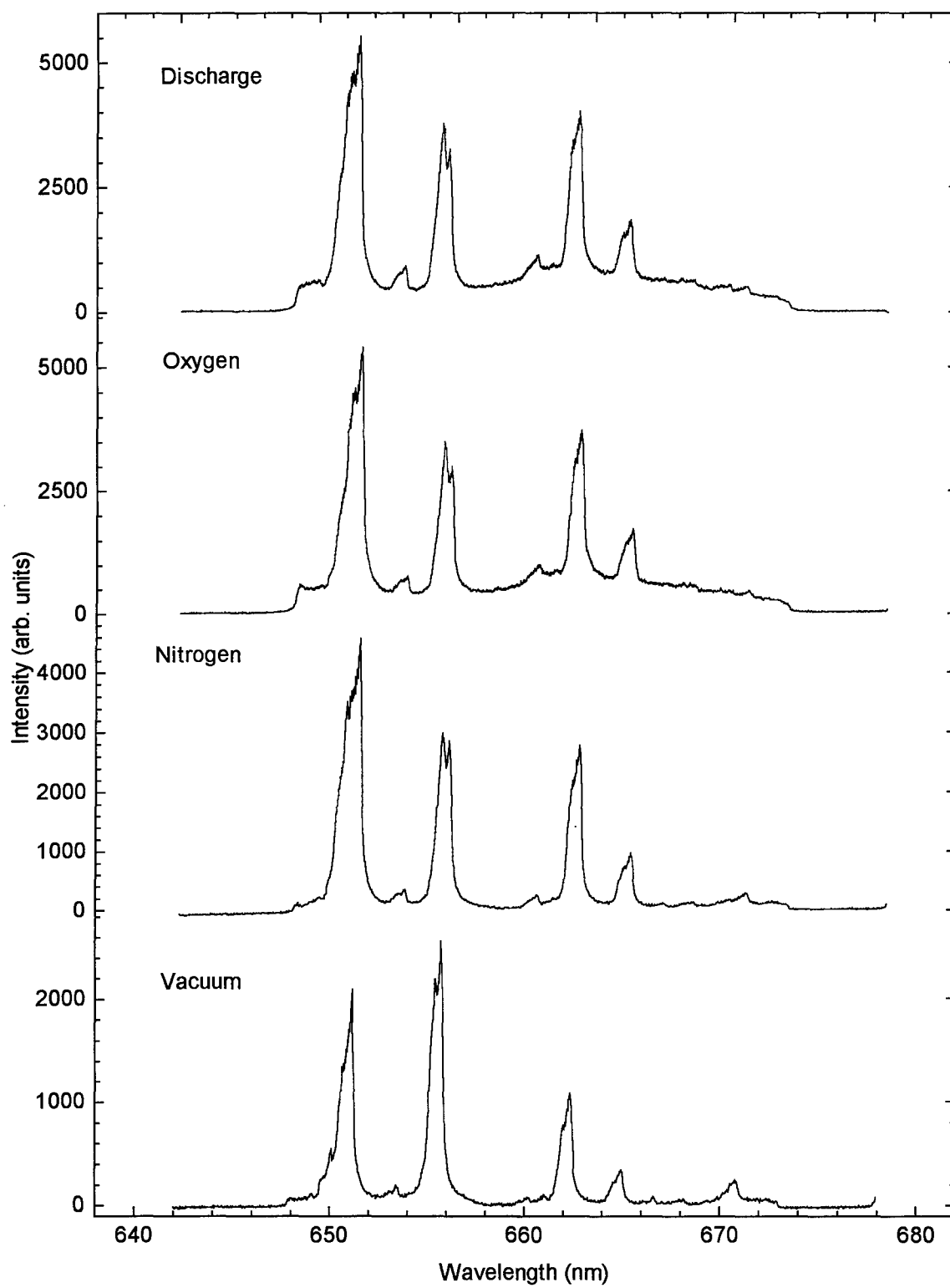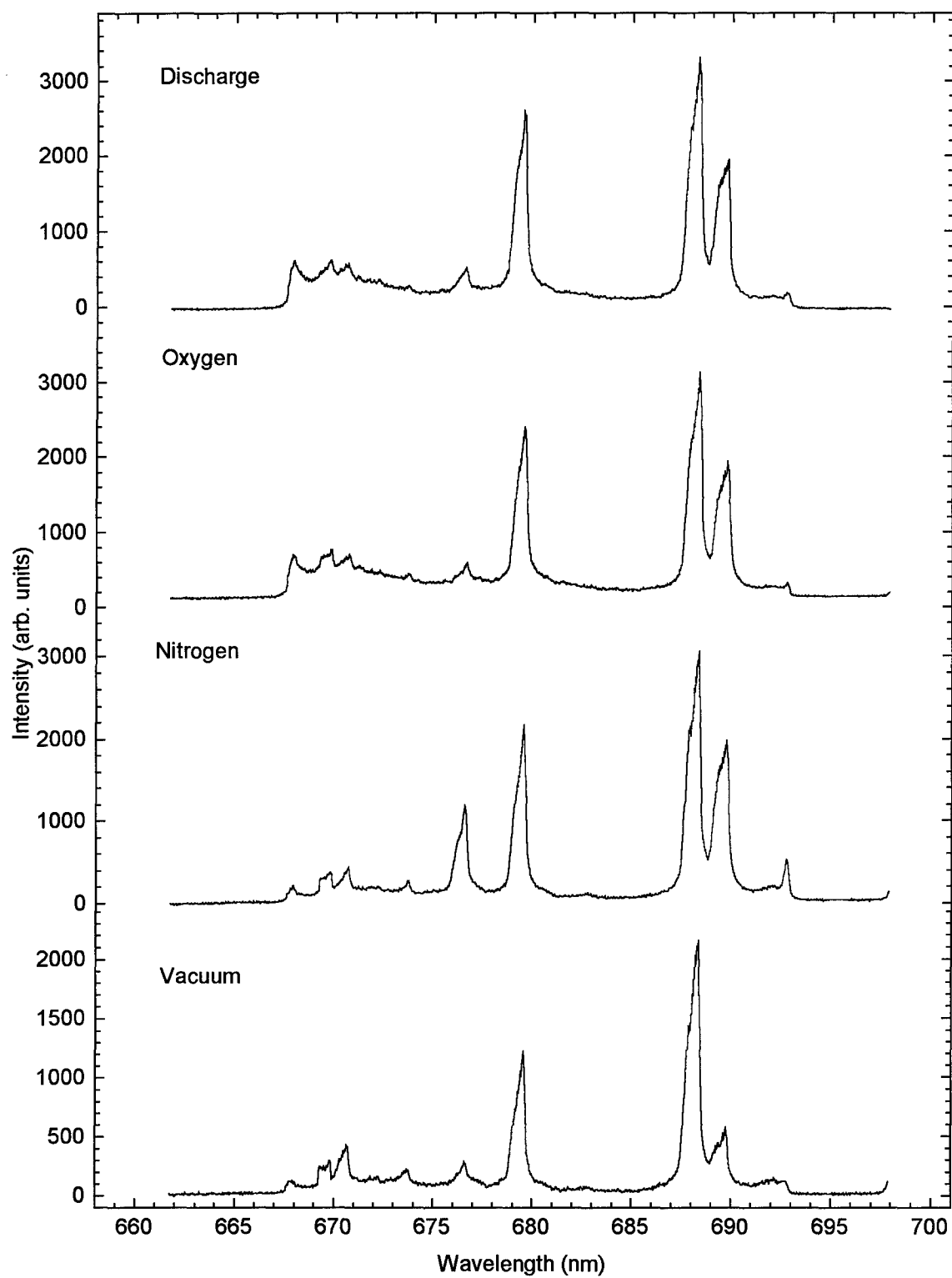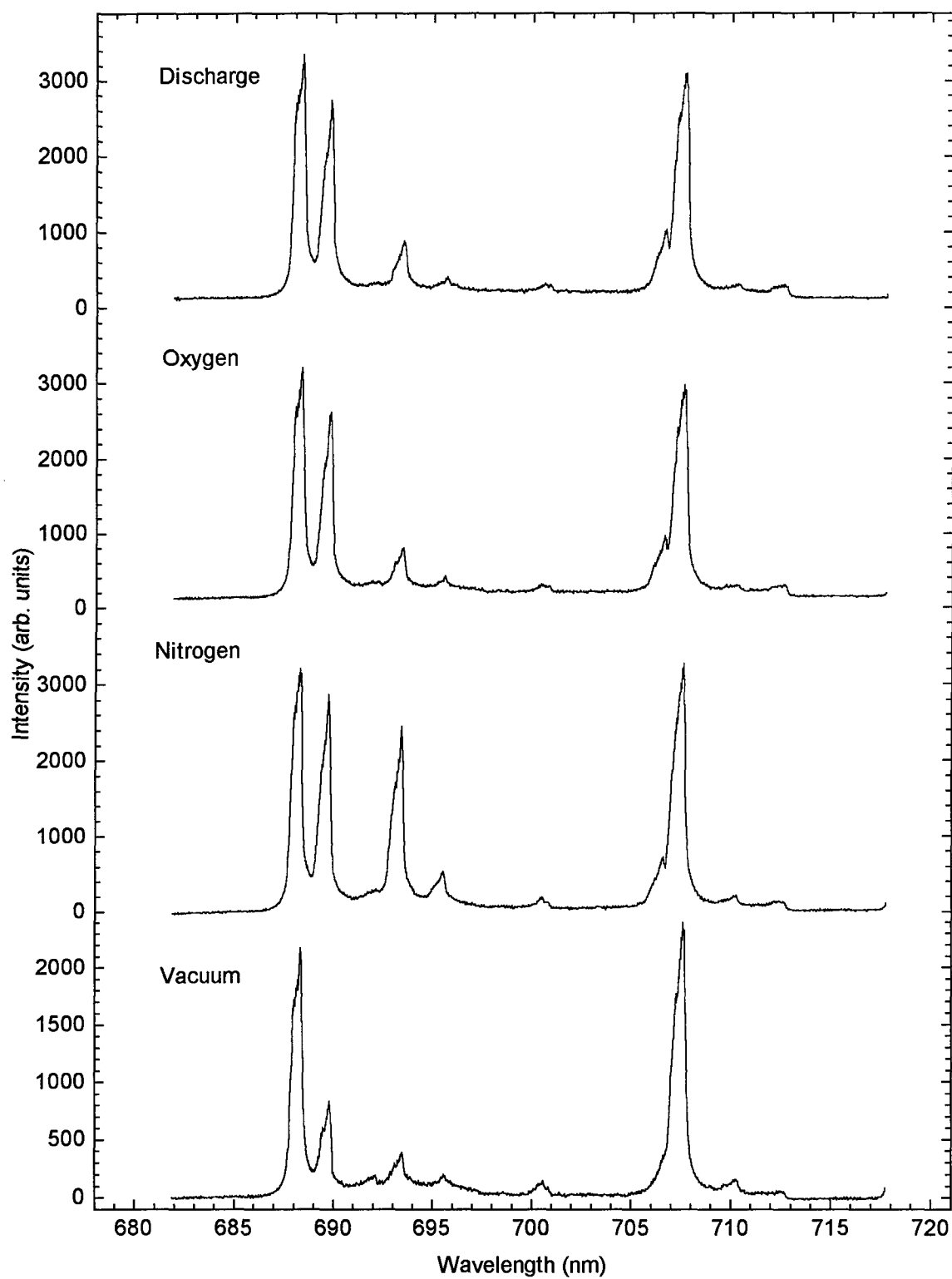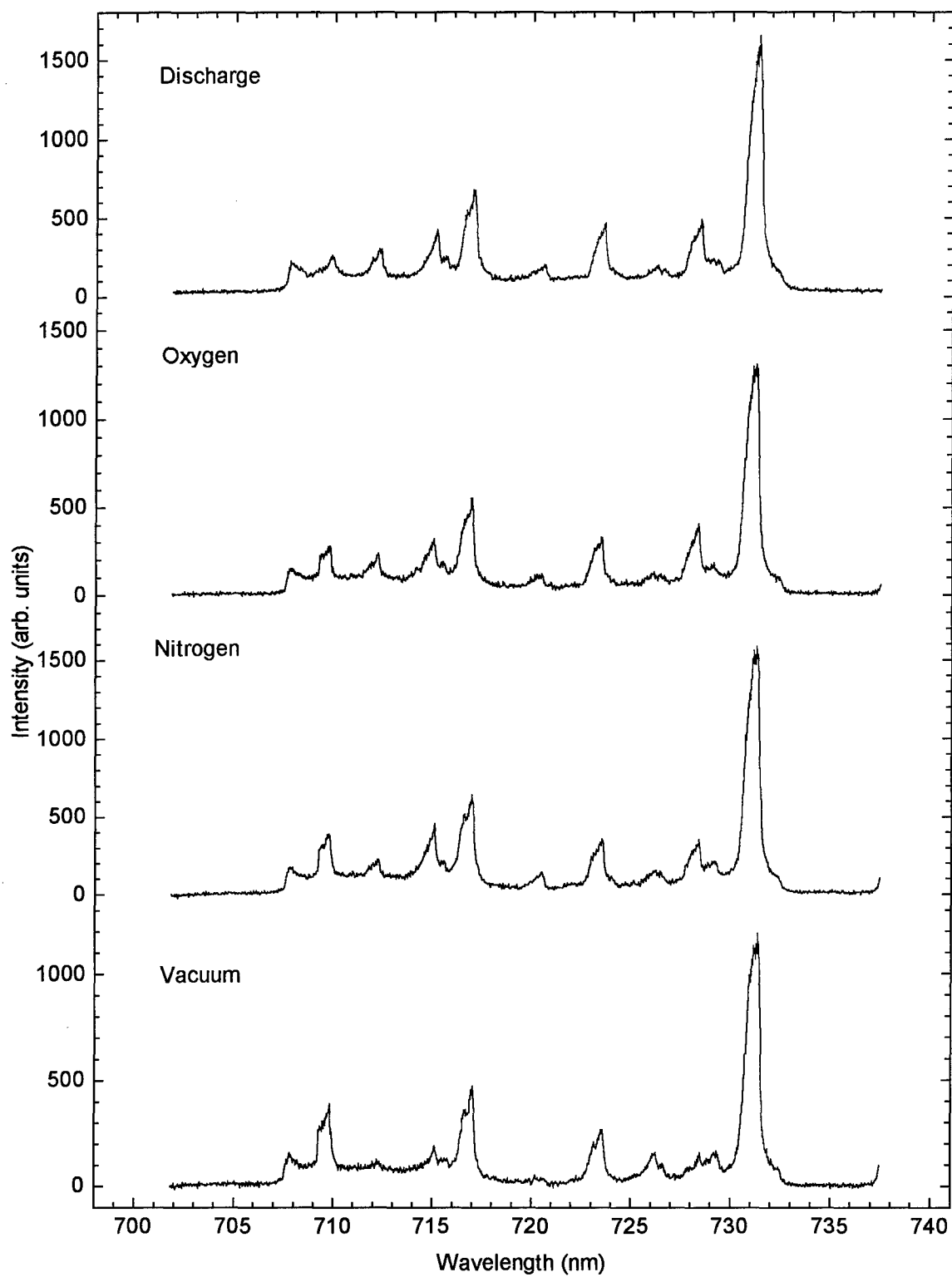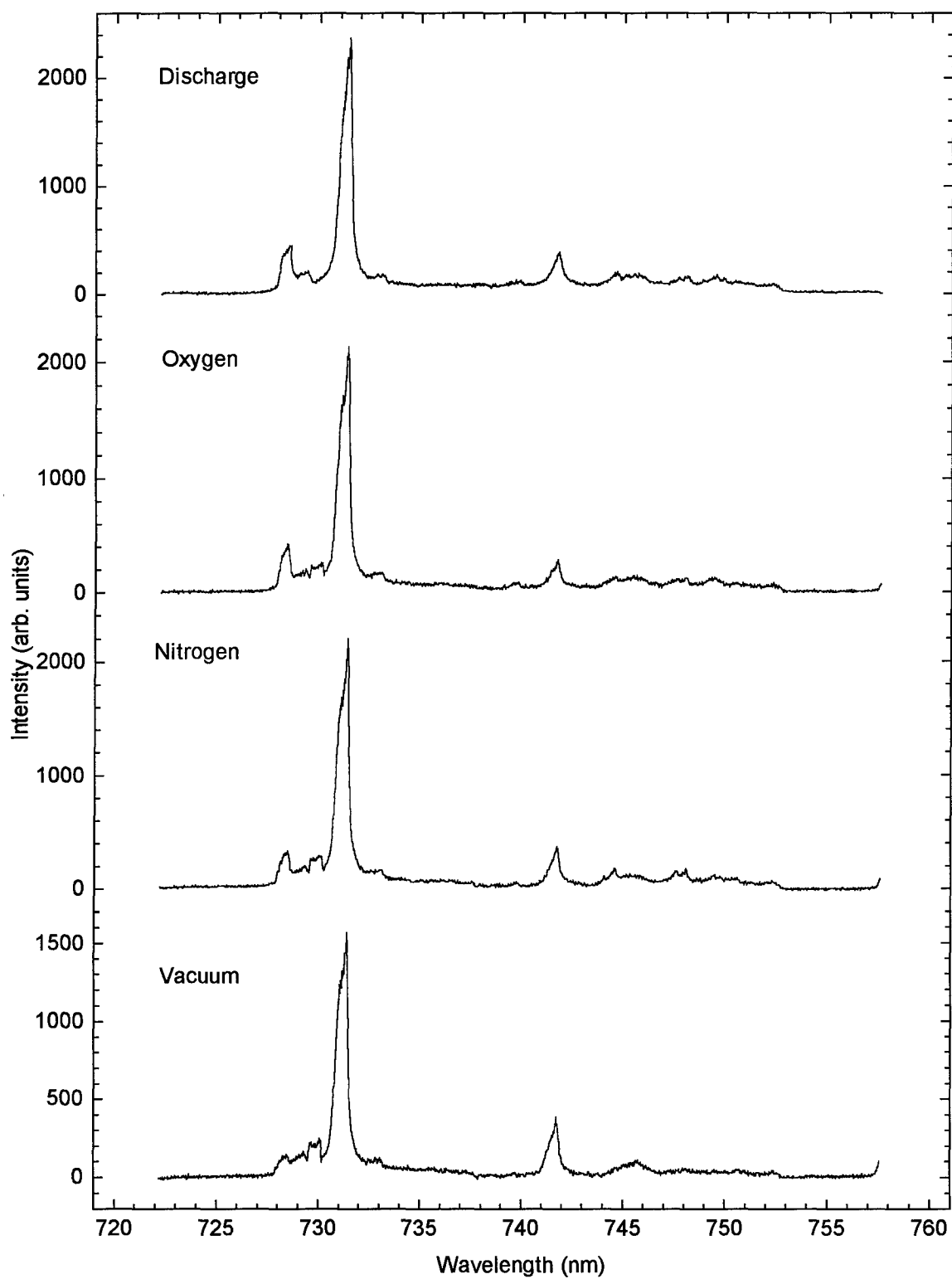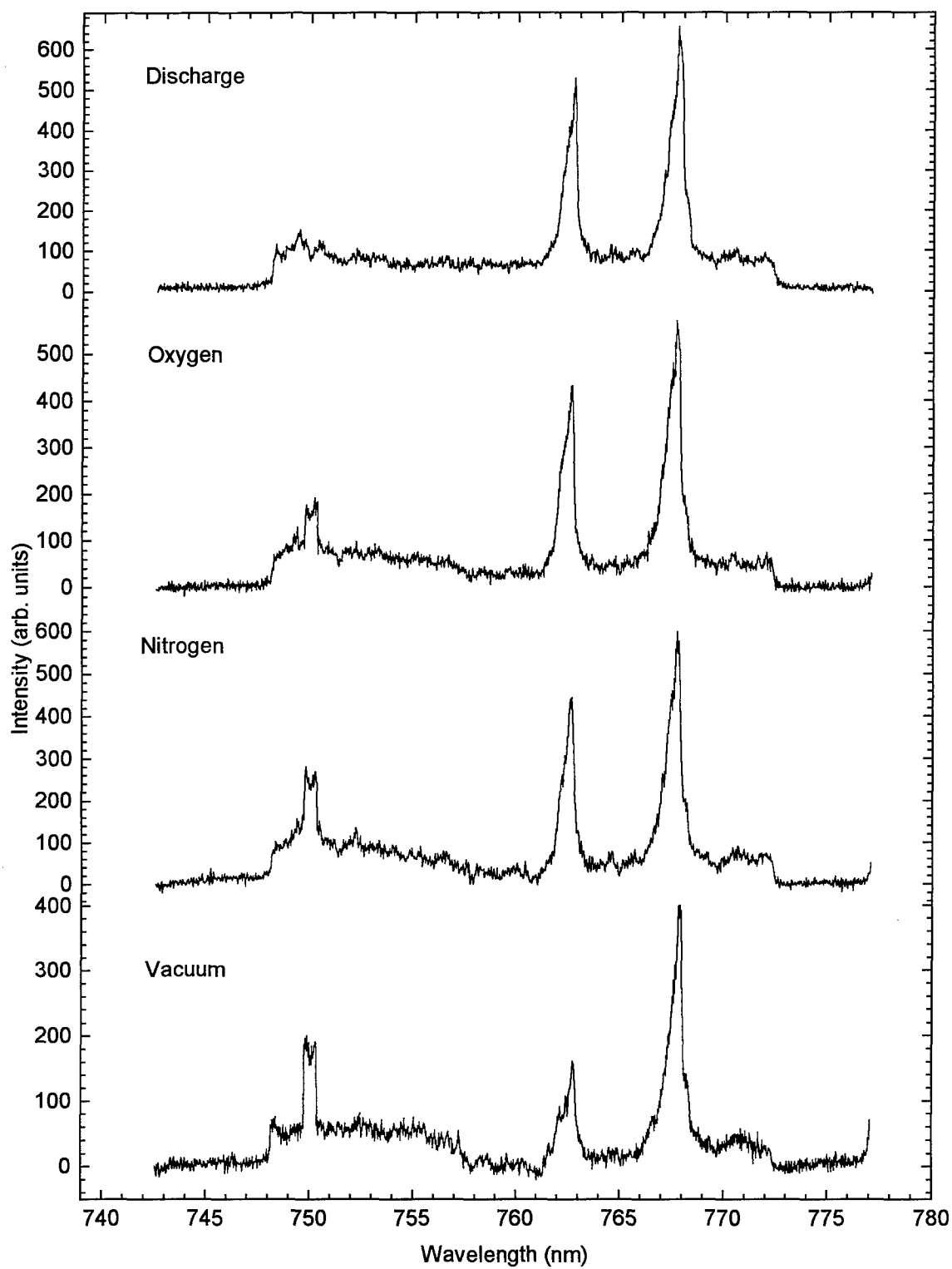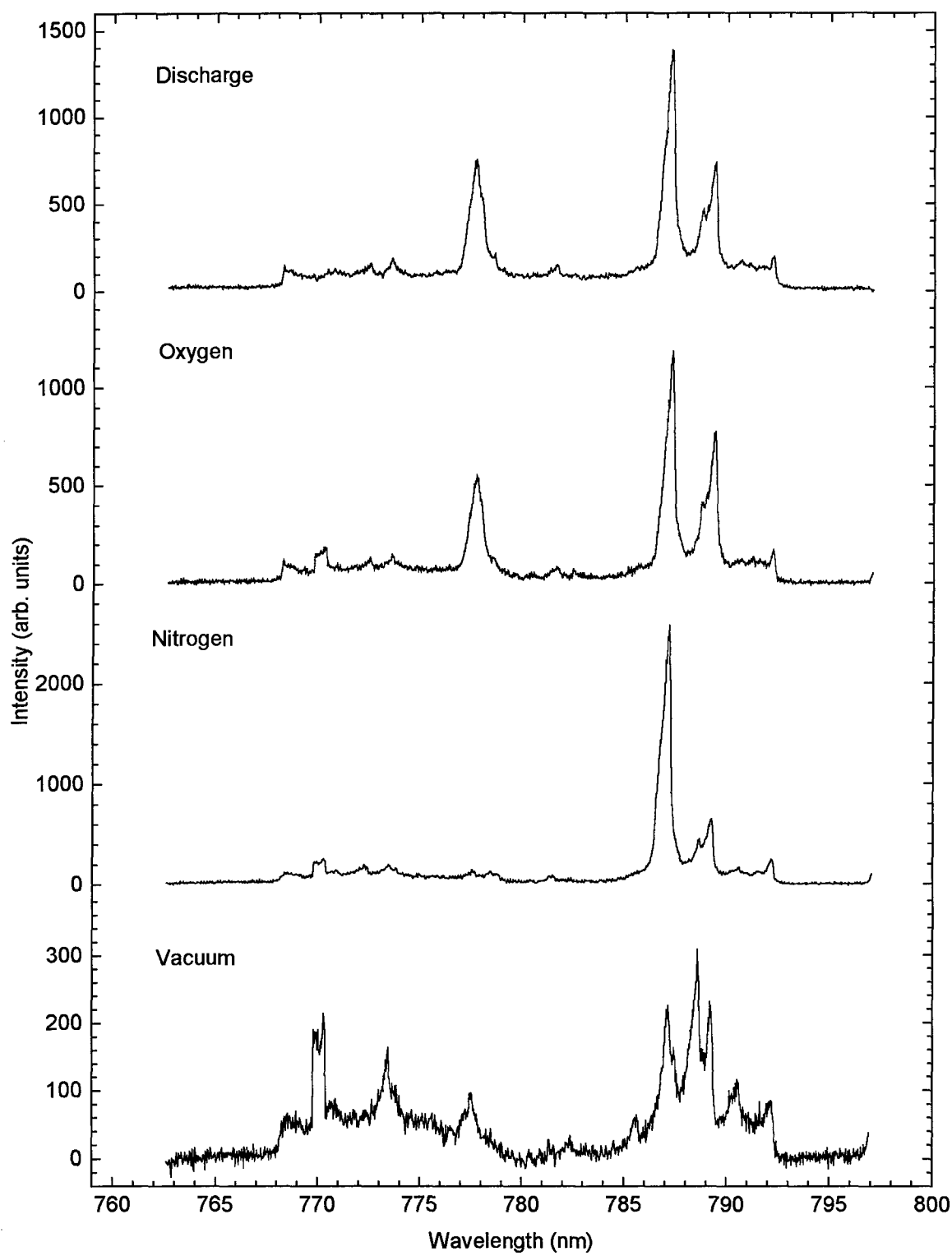
Appendix F: Spectral Data from SrO at 3.0 cm

Appendix F contain spectral data of laser-ablation plumes from a SrO target. Background gases were at 25.0 mtorr. Data was taken 3.0 cm from the target. Laser fluence was 2.0 $J-cm^{-2}$. Data was taken using a 0.5 m spectrometer with a 1200g/mm grating, 100μm slit and an Oma linear array. The signal was integrated over 16.6 msec and 20 pulses were summed to get this output.
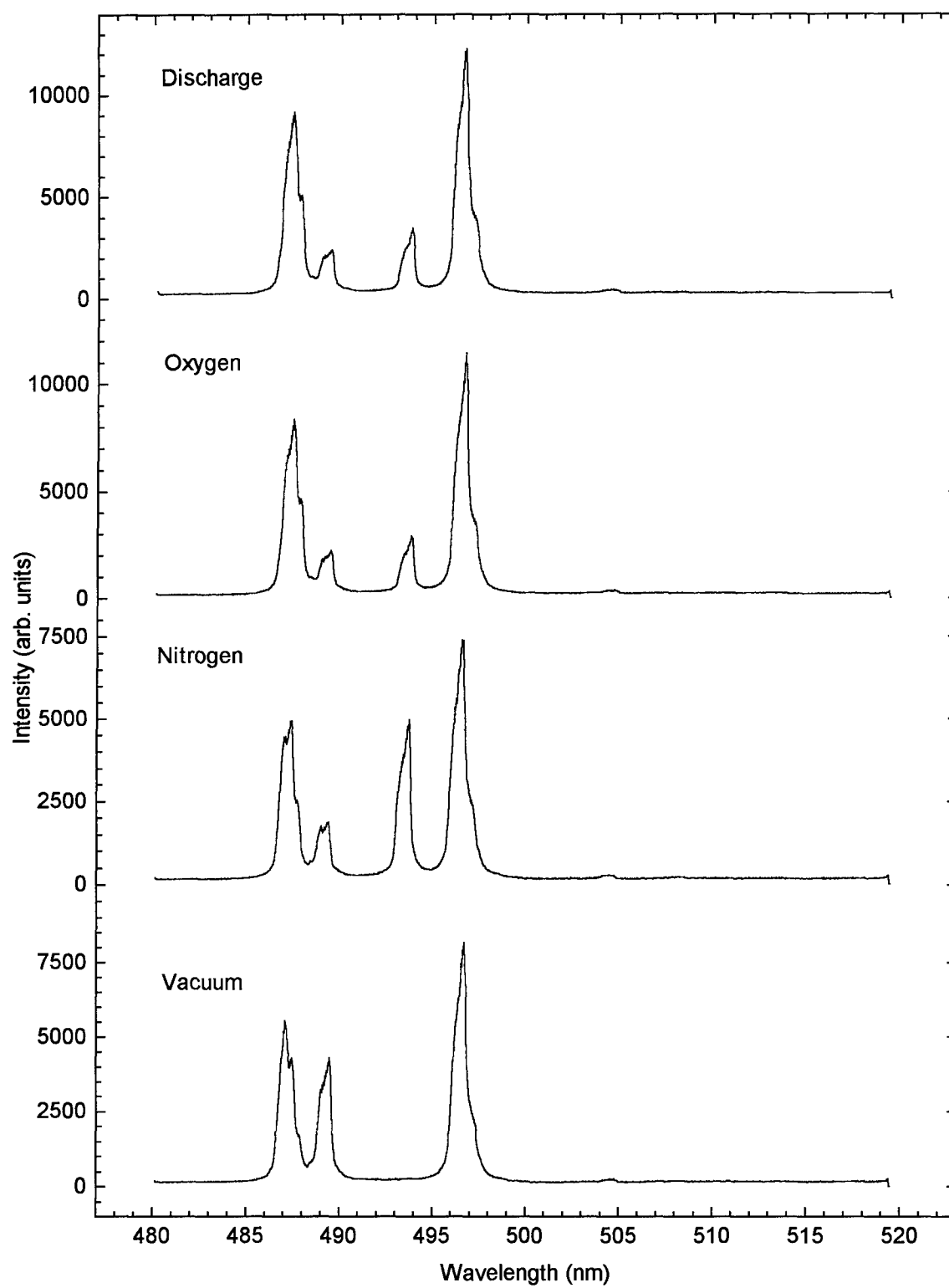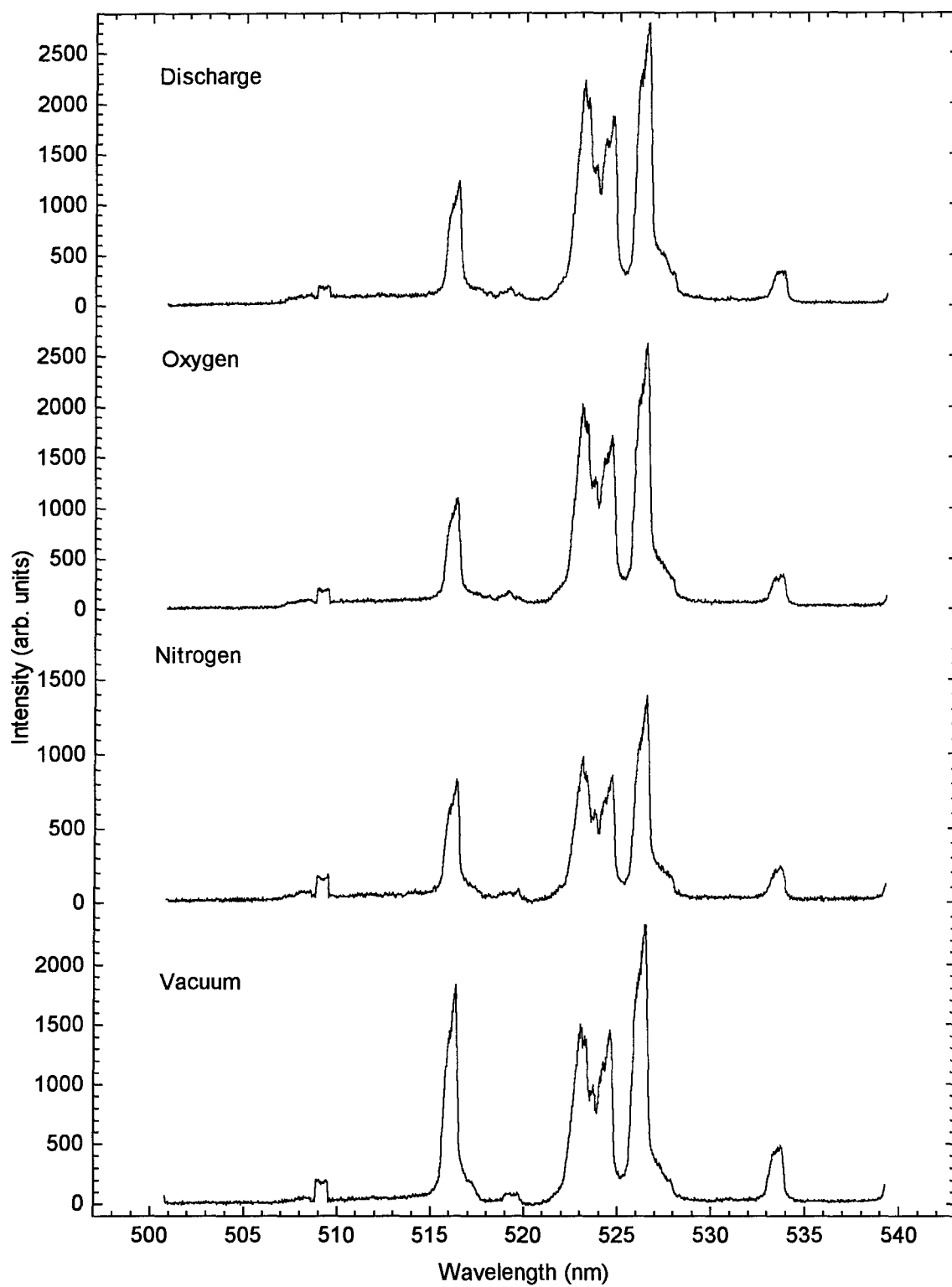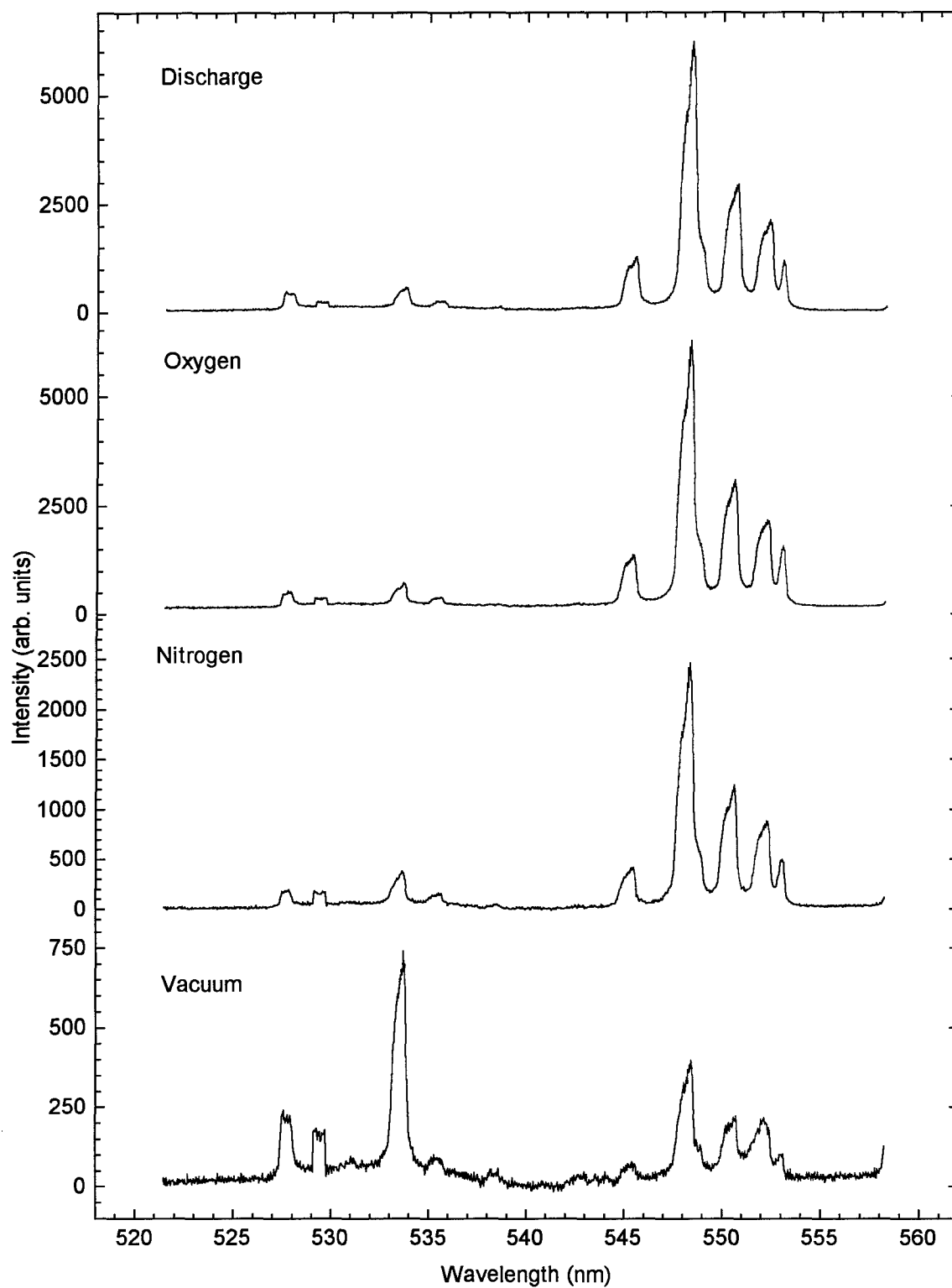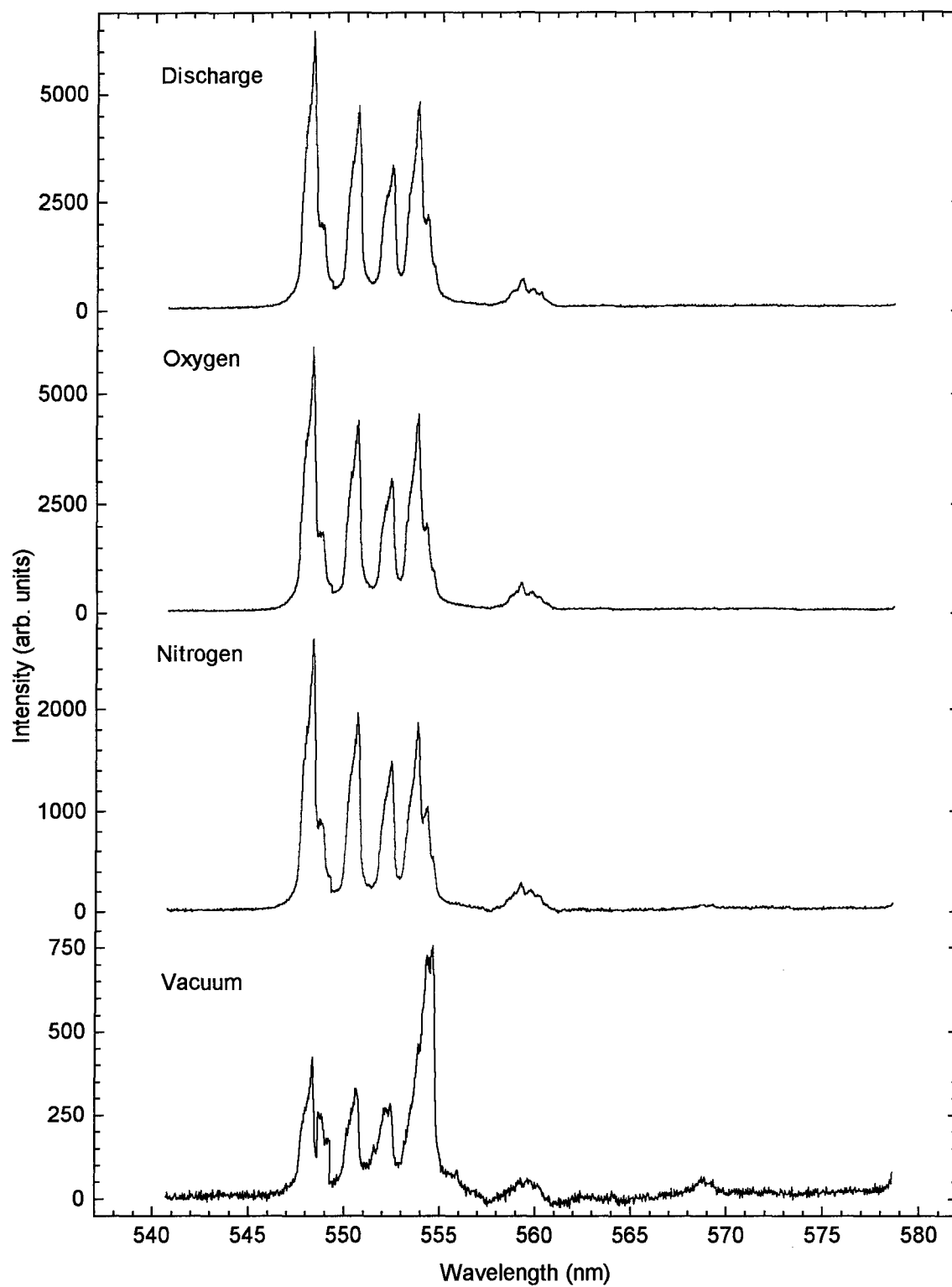
183
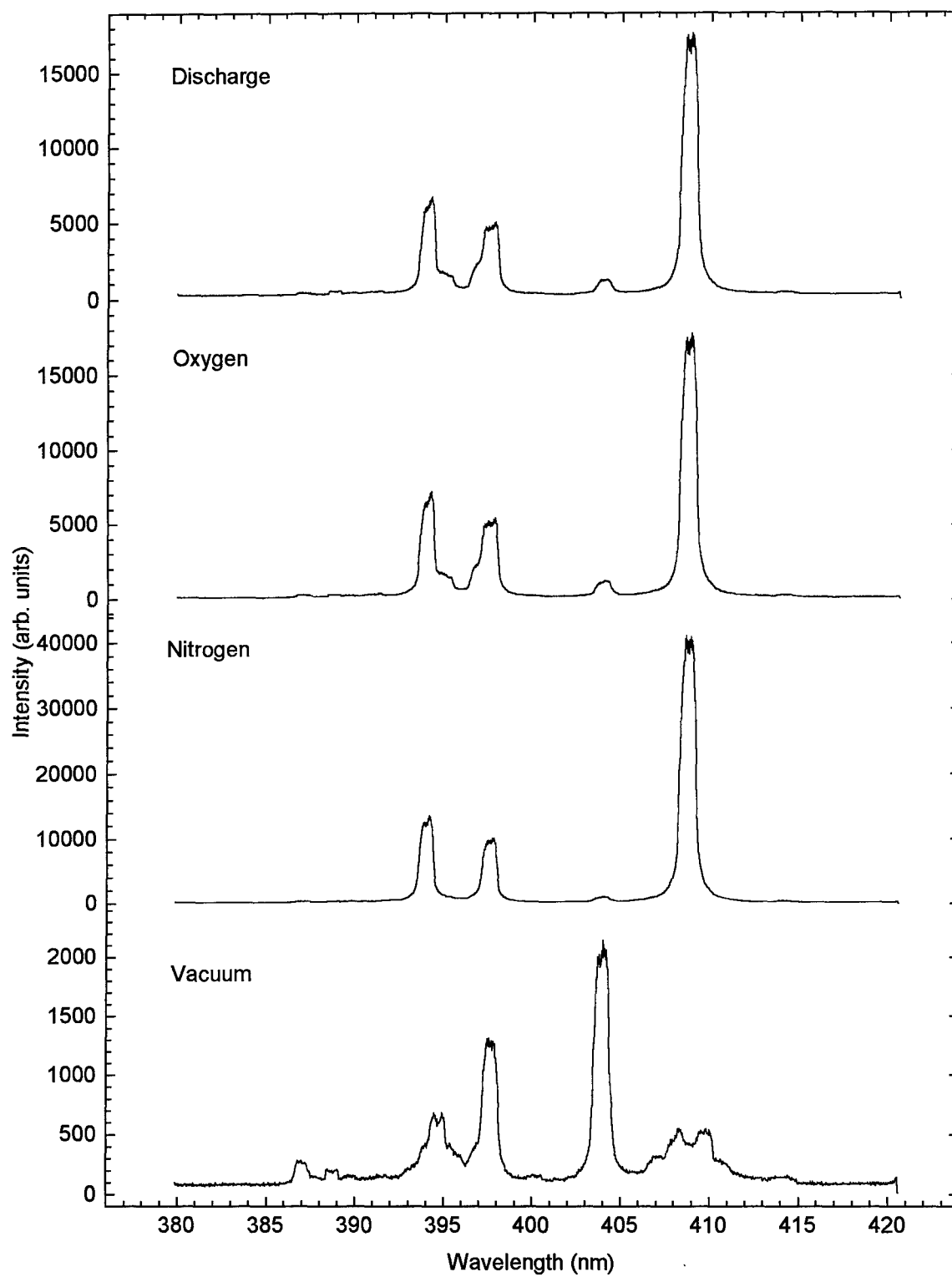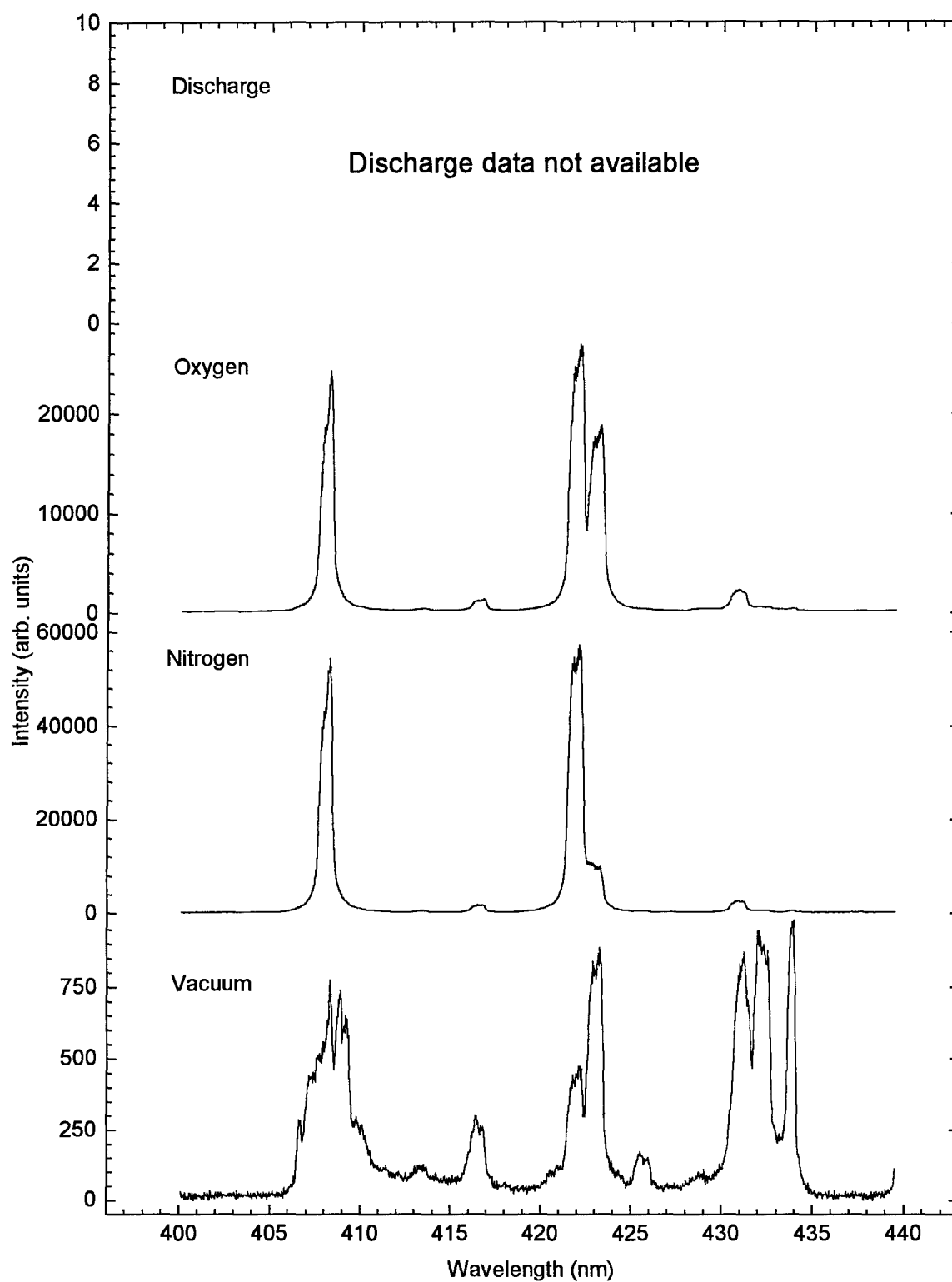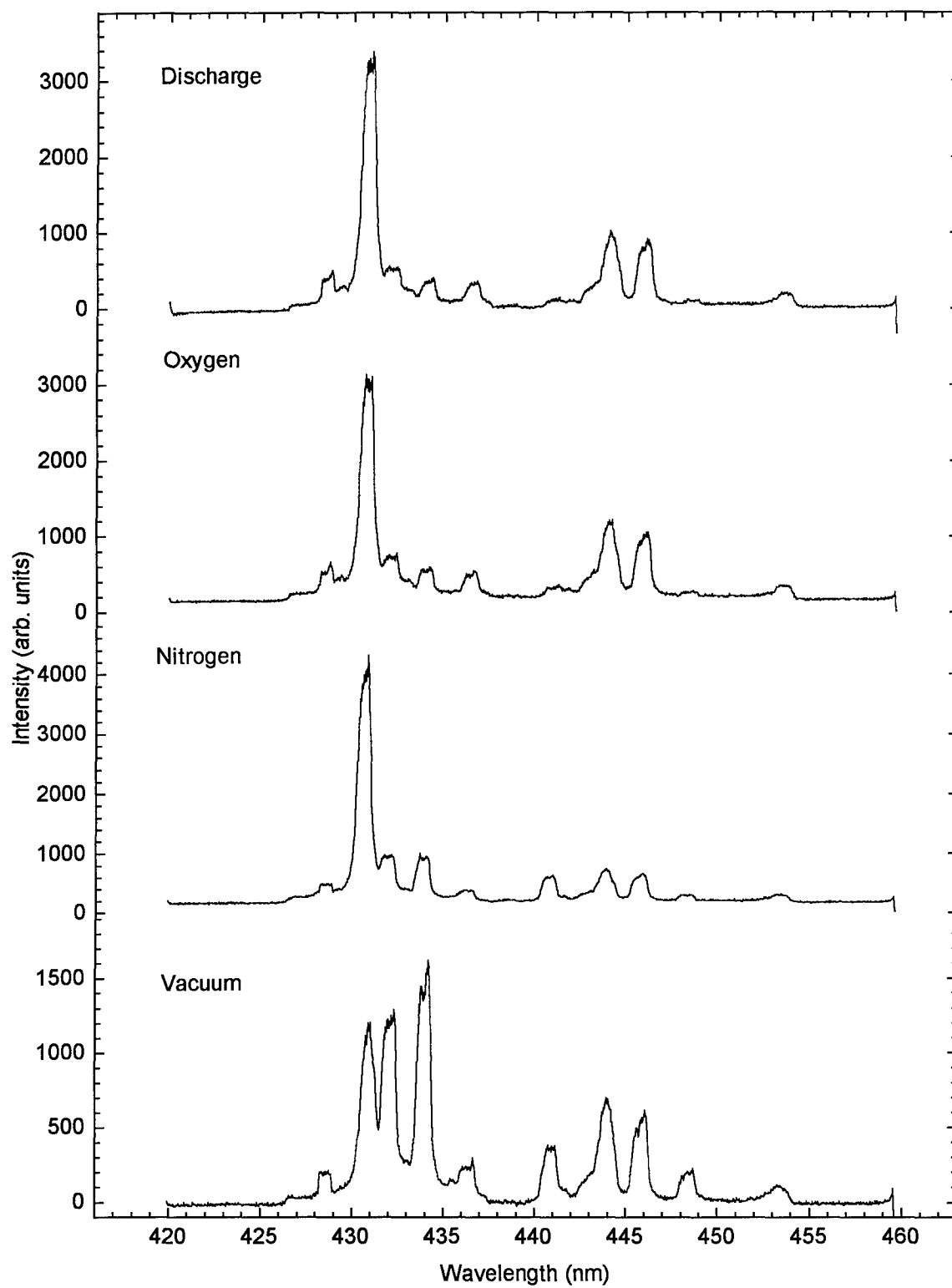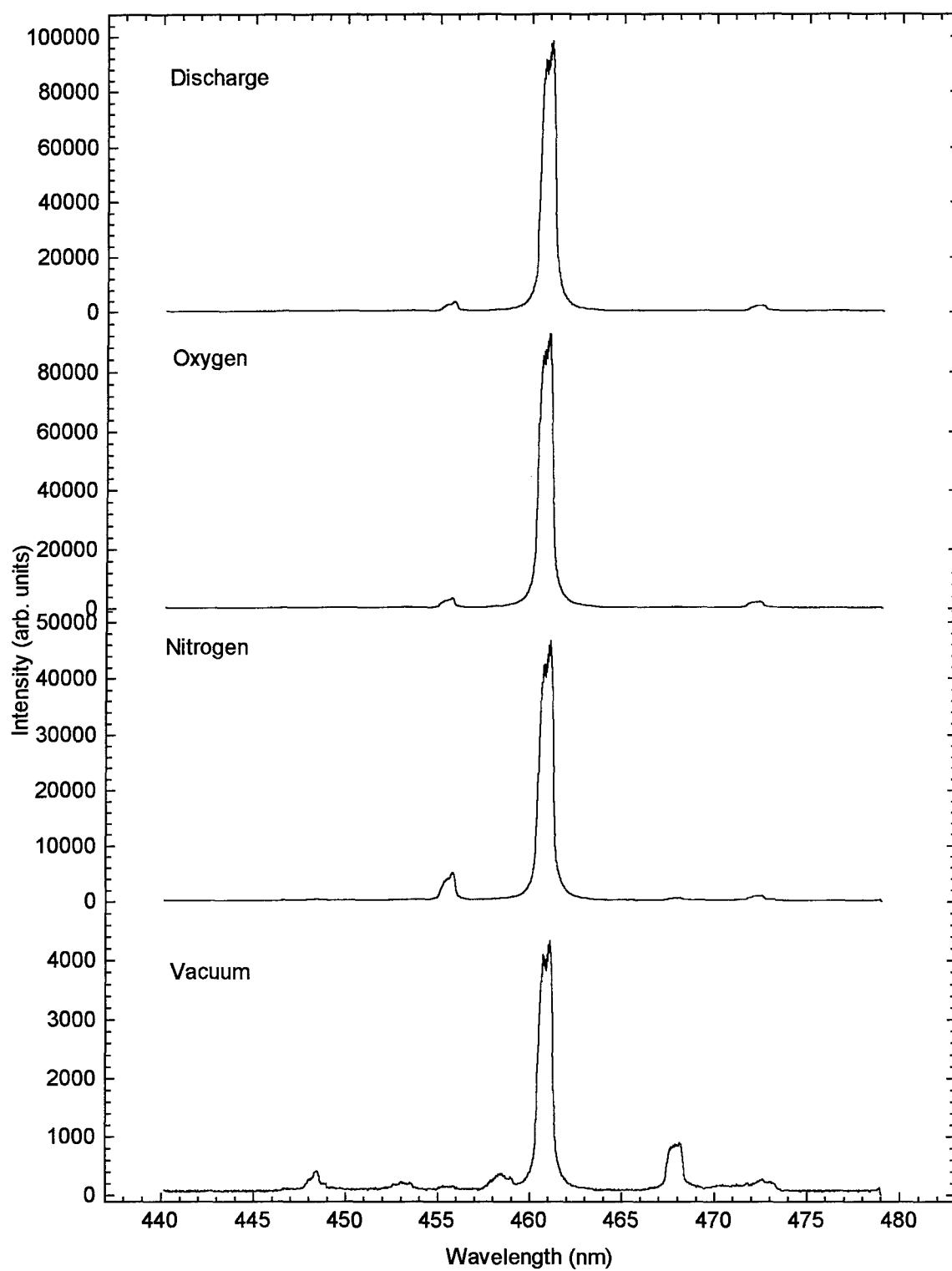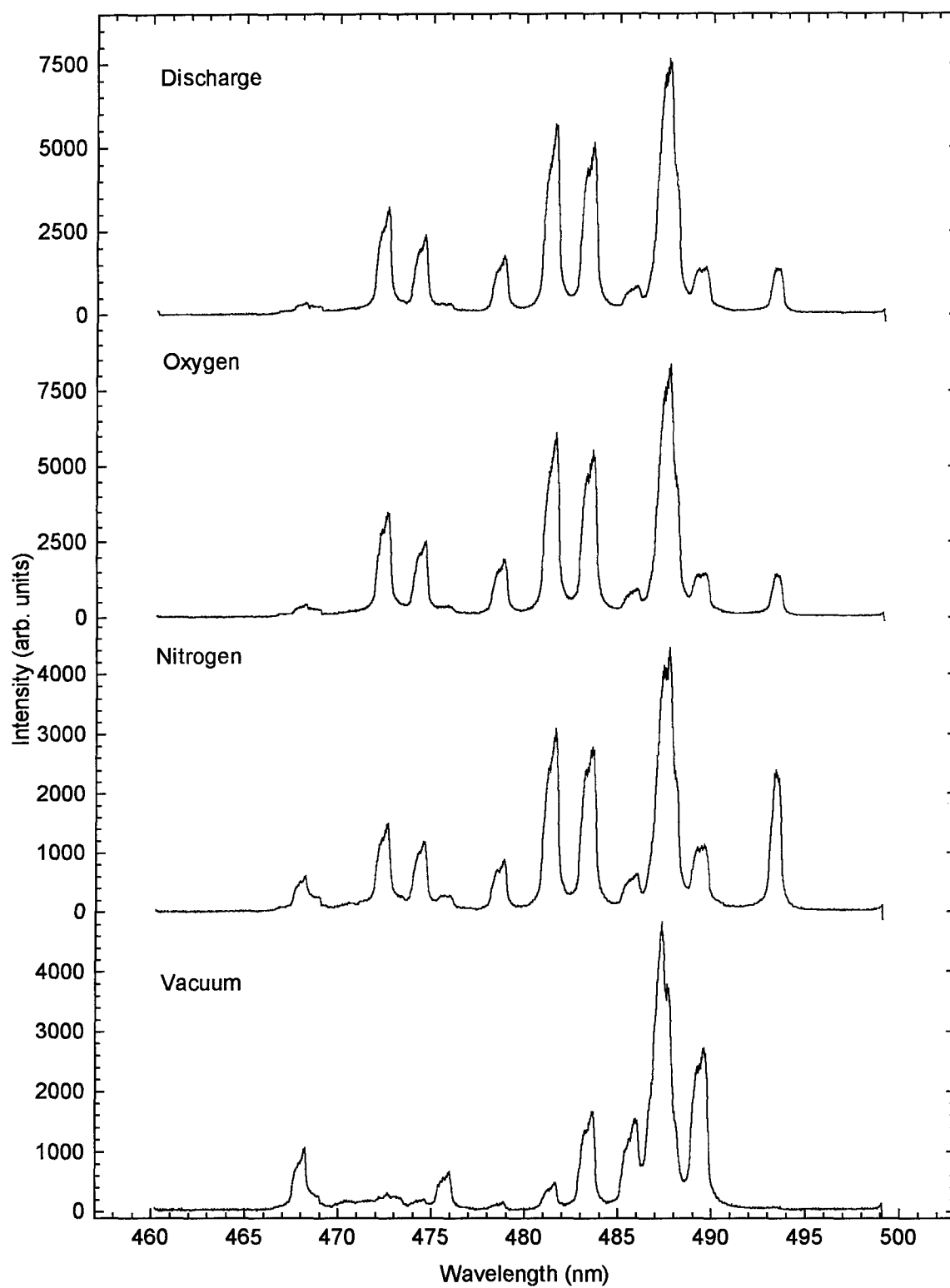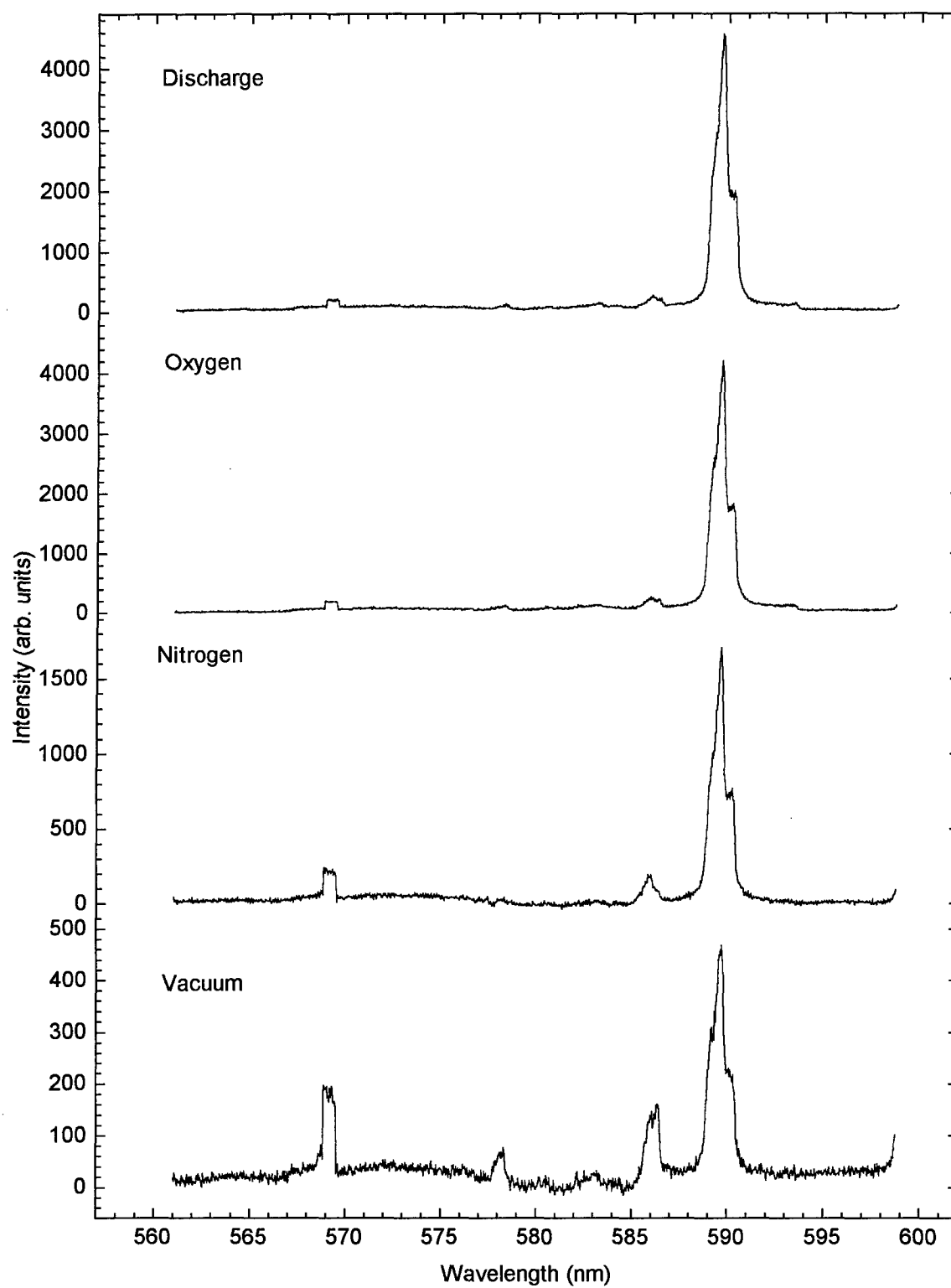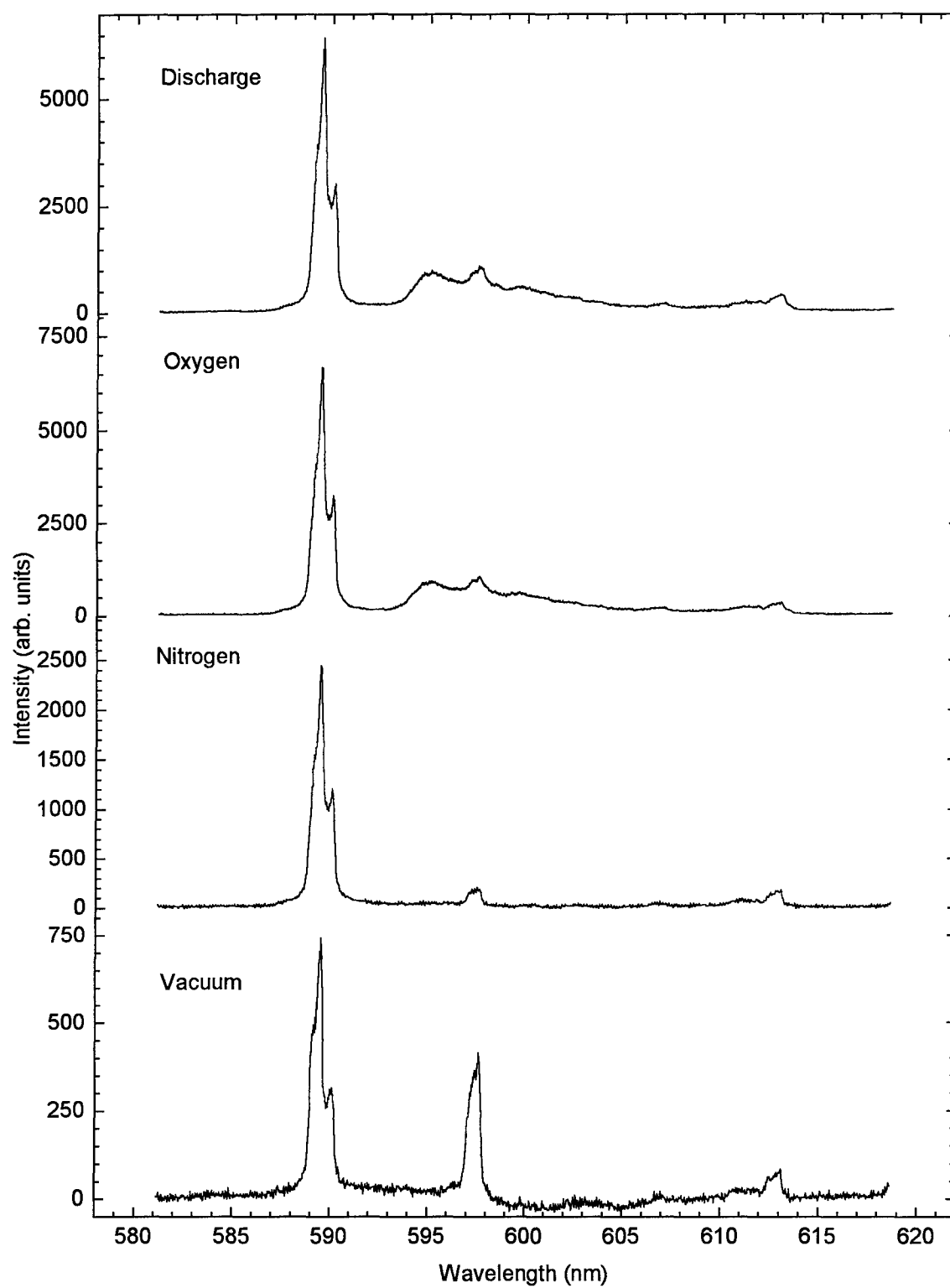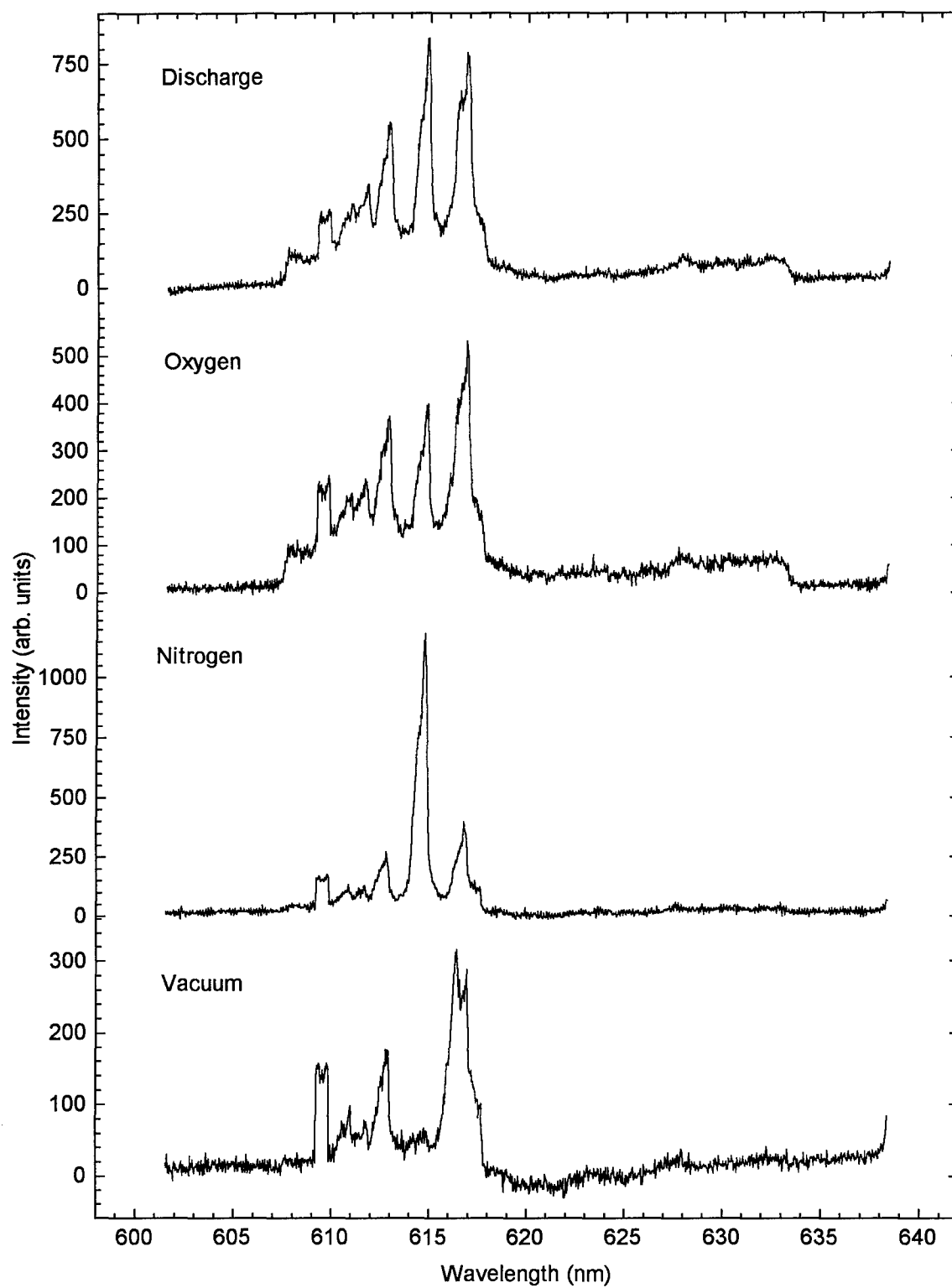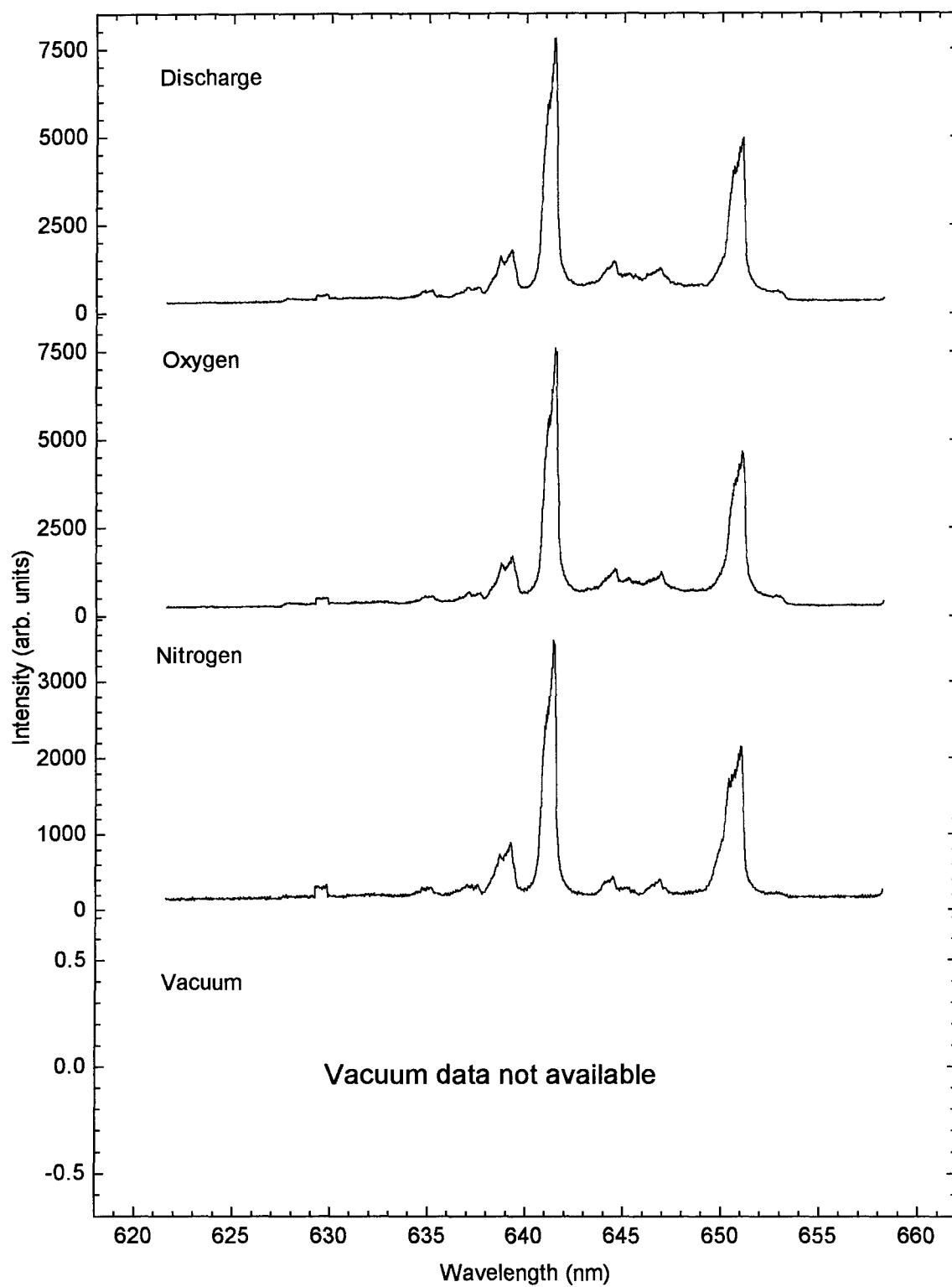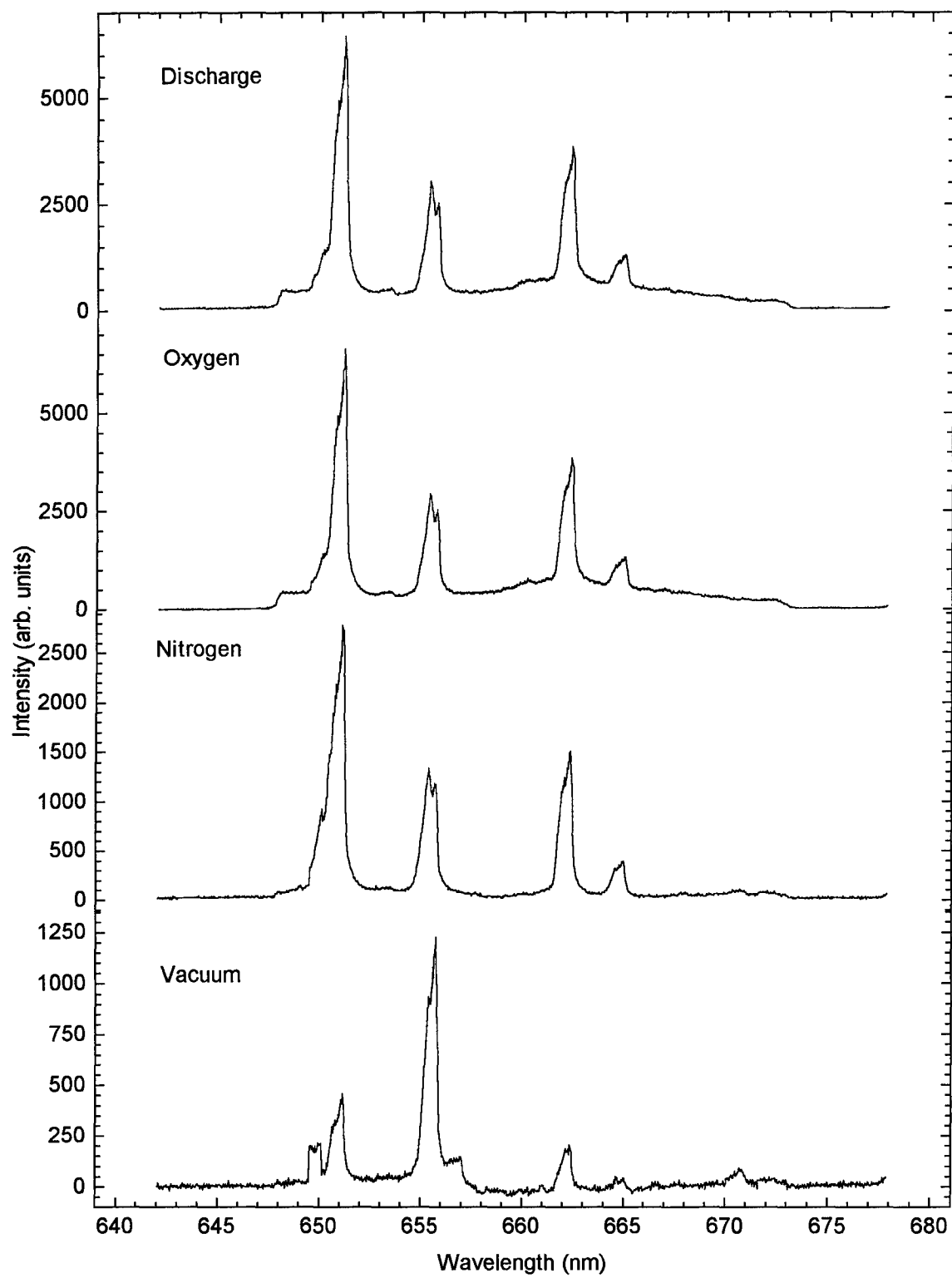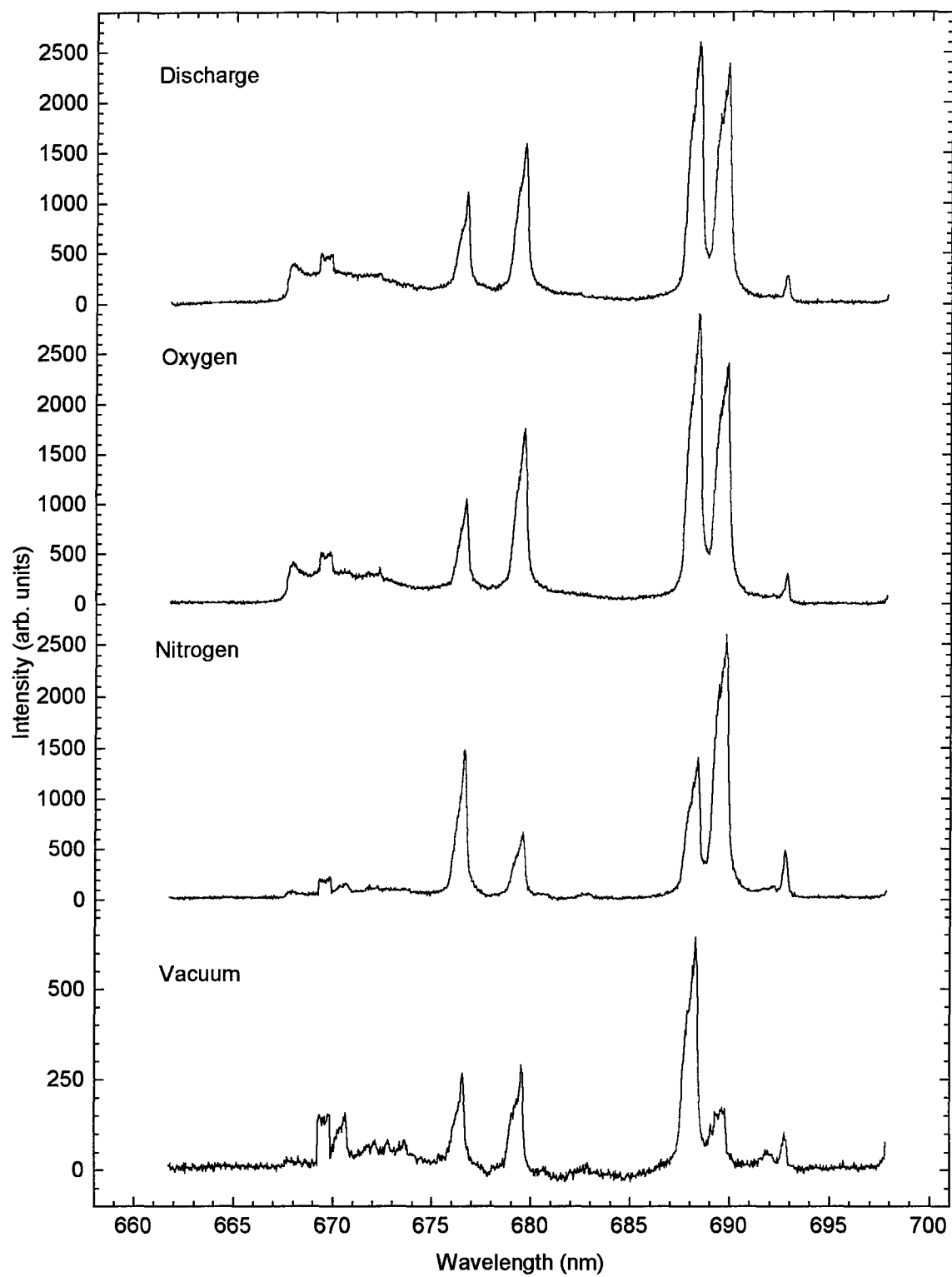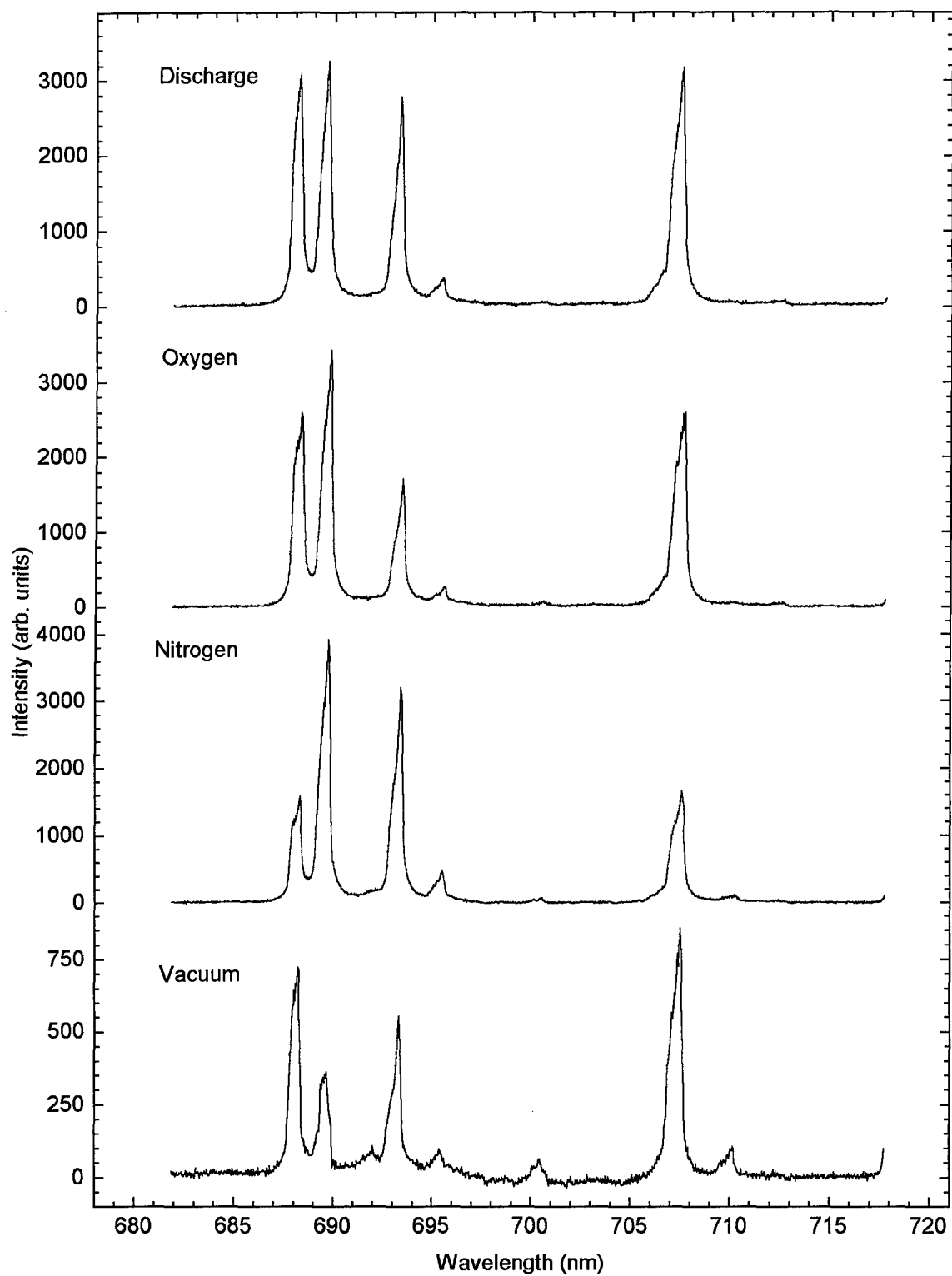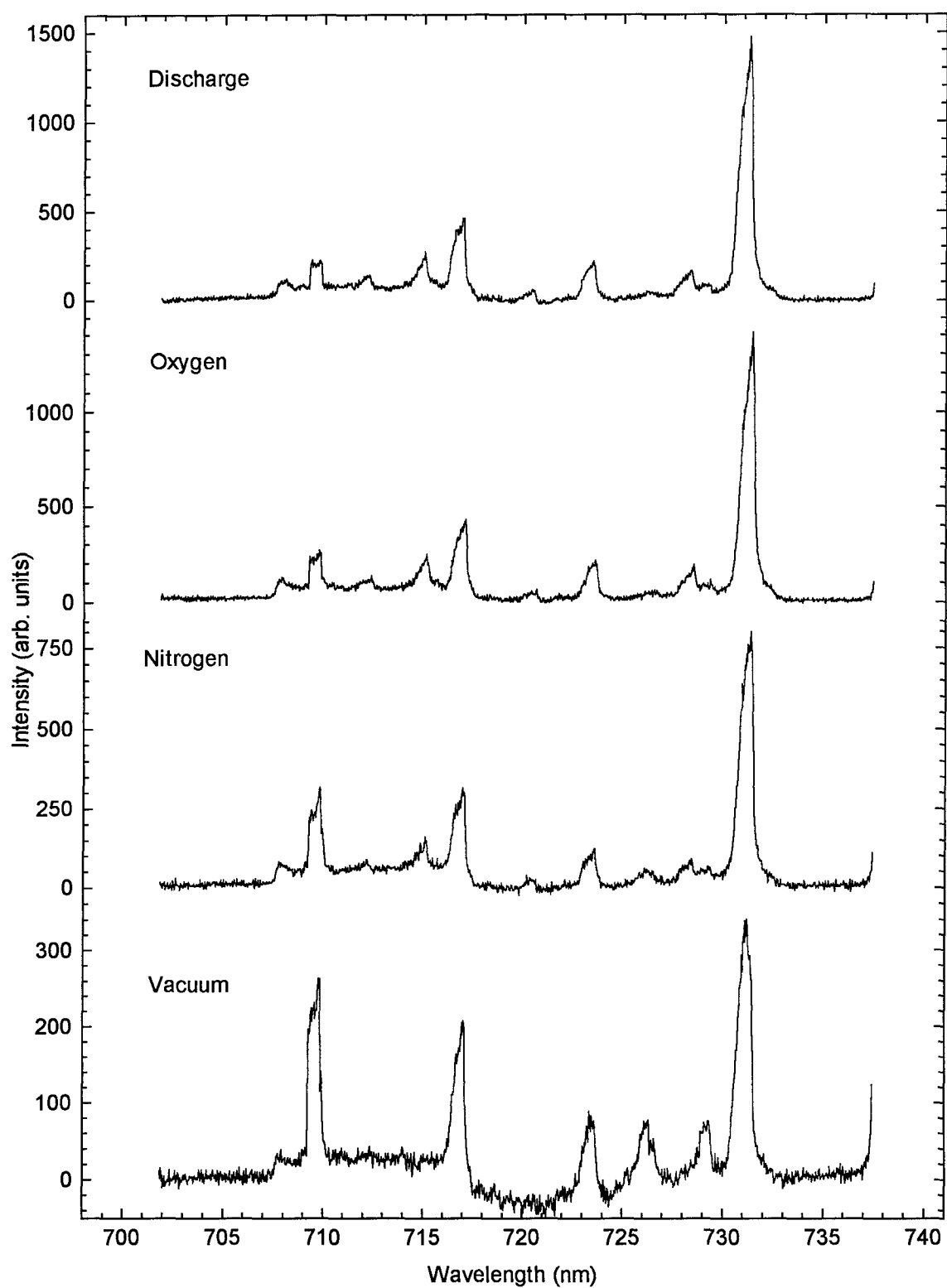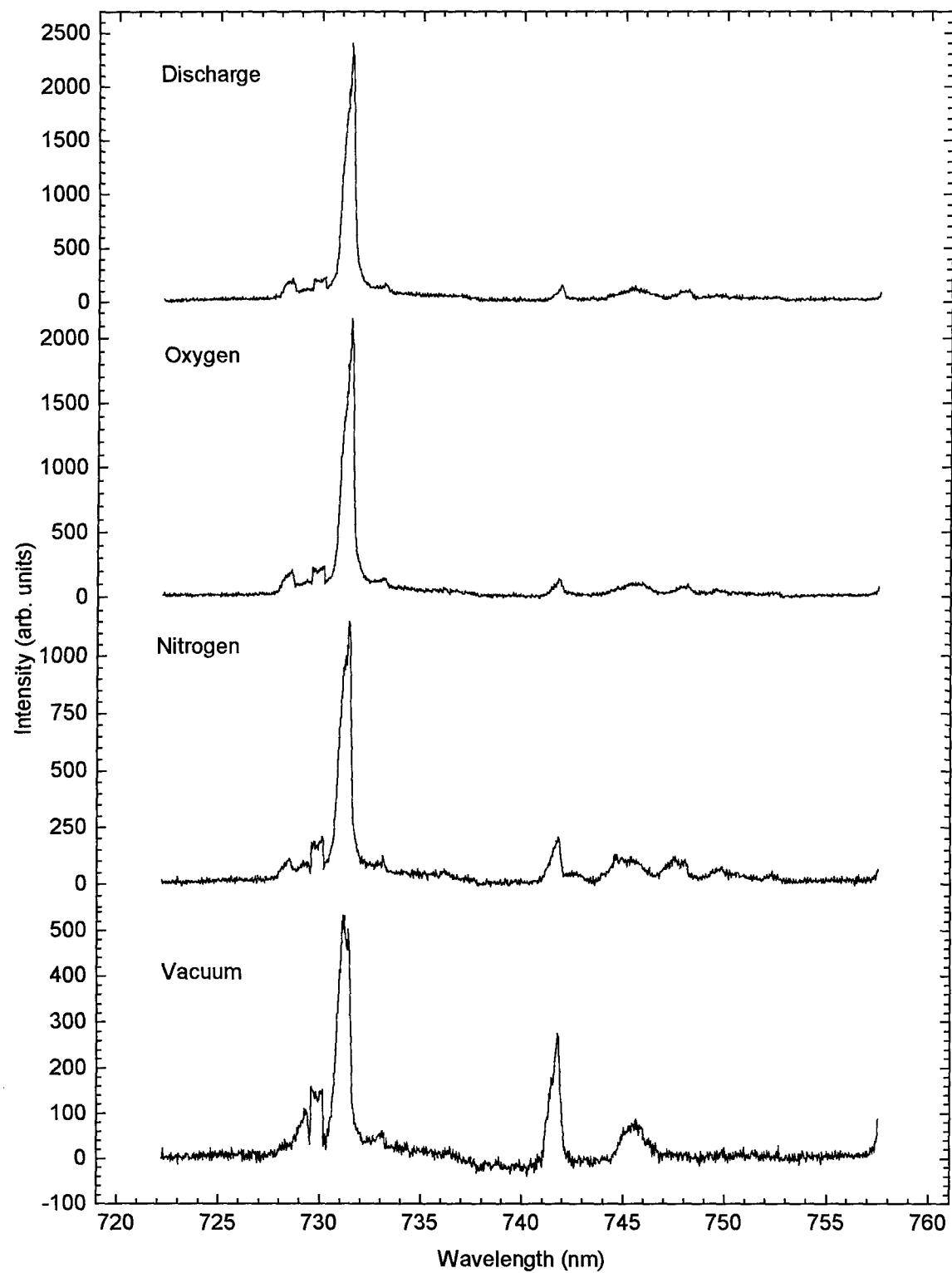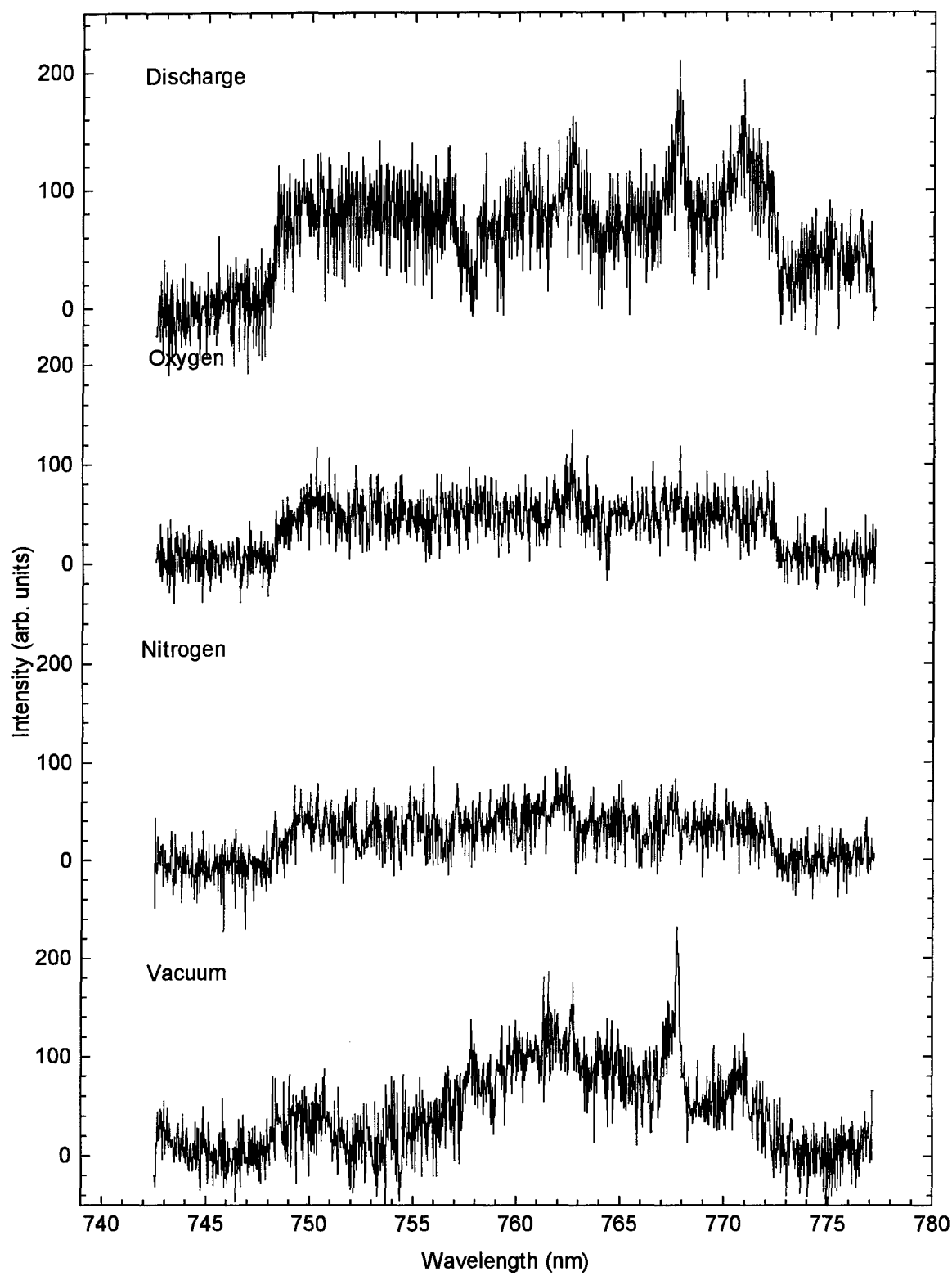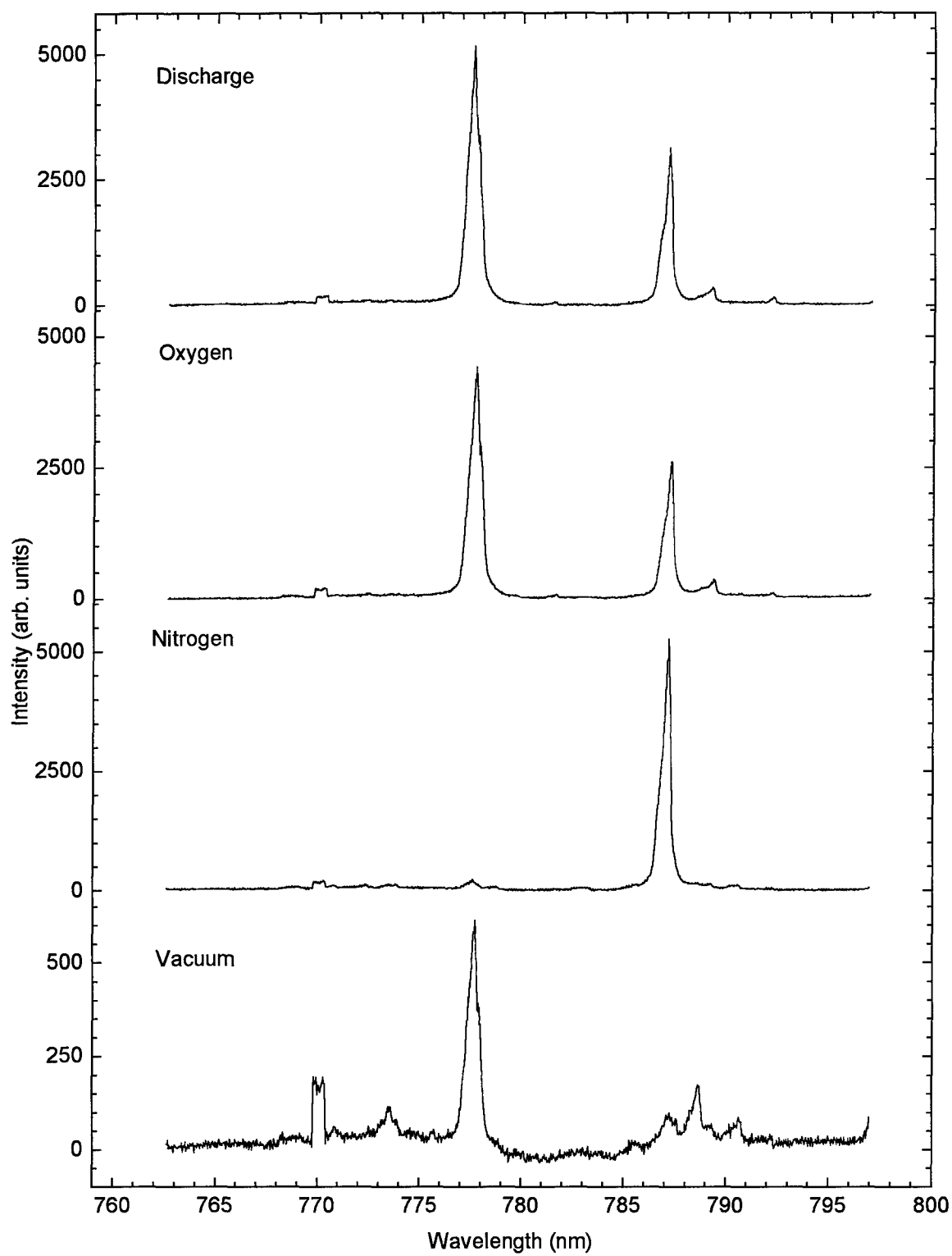
Bibliography

Baede, A.P.M. "Charge Transfer Between Neutrals at Hyperthermal Energies," *Molecular Scattering; Physical and Chemical Applications*. Ed. Lawley, K.P. Sussex, UK: 463-535, 1975.

Bernhardt, P.A. "Probing the magnetosphere using chemical releases from the Combined Release and Radiation Effects Satellite," Physics of Fluids B, Plasma: 2249-2256, July,1992.

Blair, A.J., G. Metzger and C.B. Fleddermann. "Optical absorption spectroscopic diagnostics during sputter deposition of Y-Ba-Cu-oxide," Journal of Applied Physics, 72(10): 4792-4797, 1992.

Chrisey, Douglas B. and Graham Hubler. "Diagnostics and characteristics of pulsed laser deposition laser plasmas," Pulsed Laser Deposition of Thin Films, New York: John Wiley & Sons, Inc., 1994.

Field, Robert. "Assignment of the lowest $^3\Pi$ and $^1\Pi$ states of CaO, SrO and BaO*," Journal of Chemical Physics, 60(6): 2400-2413, 1974.

Gupta, Arunava. "Gas-phase oxidation chemistry during pulsed laser deposition of $YBa_2CU_3O_{7-\delta}$ films," Journal of Applied Physics, 73(11): 7876-7887, 1993.

Huber, K.P. and G. Herzberg. Molecular Spectra and Molecular Structure IV. Constants of Diatomic Molecules. New York: Van Nostrand Reinhold Company, 1979.

Kaufman, Frederick. "Reaction of Oxygen Atoms," Progress in Reaction Kinetics, Vol. 1, Ed. G. Porter. New York: Pergamon Press, 24-27 1961.

Kaufman, Frederick. "The Air Afterglow Revisited," Chemiluminescence and Bioluminescence, Eds. M.J. Cormier, D.M. Hercules, and J. Lee. New York, New York, 1973.

Lacmann, K. "Collisional Ionization," Potential Energy Surfaces. Ed. K.P. Lawley. New York: Wiley, 513-527 1980.

Landau, L.D. and E. M. Lifshitz. Quantum Mechanics Non-relativistic Theory (Third Edition). Oxford, England: Pergamon Press, 1981.

Liou, K. and R. B. Torbert. "On Ba^+ production in the CRIT II experiment," Journal of Geophysical Research, 100: 5811-5818, April 1995.

Mashburn, D.N. and D.B. Geohegan. "$Y_1Ba_2Cu_3O_{7-x}$ laser-ablation plume dynamics measurement by nanosecond response ion probe: Comparison with optical measurements," SPIE, Vol. 1187, Processing of Films for High T_c Superconducting Electronics," 172-181, 1989.

Mukherjee, P., P. Sakthivel, K. Ahmed, and S. Witanachchi. "Study of ion activation in the in situ low-temperature laser deposition of superconducting $Yba_2Cu_3O_{7-\delta}$ films," Journal of Applied Physics, 74(2): 1205-1208, 1993.

Murad, Edmond. "The reactions of Ba^+ ions with O_2 and H_2O," Journal of Chemical Physics, 77(4): 2057-2059, 1992).

NASA HQ Public Affairs Office, NASA. "Early Findings from Tethered Satellite Mission Point to Revamping of Space Physics Theories," press release, release 96-106, 23 May 1996.

Neynaber, R. H., G. Magnuson, S. Trujillo, and B. Myers. Physical Review A, 5(1): 285-294, 1972.

Nishikawa, Hiroaki, Masaki Kanai, Tomoji Kawai and Shichio Kawai. "Laser-Ablation Mechanism of Sr Metal Investigated by Time-of-Flight Mass Spectroscopy," Journal of Applied Physics, 33: 1090-1092, 1994.

Reader, Joseph and Charles H. Corliss. Wavelengths and Transition Probabilities for Atoms and Atomic Ions, Part 1. Wavelengths. Washington: U.S. Government Printing Office, 1980.

Rees, M.H.. Physics and chemistry of the upper atmosphere. Great Britain: Cambridge University Press, 1989.

Serway, Raymond A. Physics for Scientists and Engineers with Modern Physics (second Edition). Philadelphia: Saunders College Publishing, 1986.

Shadid, Timothy M.. <u>Analysis and Interpretation of Ion Data</u>
<u>Associated with Neutral Gas Releases in the Earth's</u>
<u>Ionosphere.</u> MA thesis, AFIT/GAP/ENP/95D-12. School of
Engineering, Air Force Institute of Technology (AU),
Wright-Patterson AFB OH, December 1995.

Van Tassel, R.A. and R. E. Huffman. "Atomic oxygen
oscillator strengths in the autoionization region. I. The
absolute strength of the 5s' lines," <u>Journal of Chemical</u>
<u>Physics,</u> 59(11): 5926-5935, 1973.

Walpole, Ronald E. <u>Probability and Statistics for Engineers</u>
<u>and Scientists.</u> New York, Macmillan Publishing Company,
1985.

Witanachi, S. Department of Physic, University of South
Florida, Tampa, FL, Telephone conversation with Paul J.
Wolf, August 21, 1996.

Wolf, Paul J., "The plasma properties of laser-ablated
SiO_2," <u>Journal of Applied Physics, 72(4):</u> 1280-1289,
1992.

Wolf, Paul J., Associate Professor of Physics, Unpublished
Work, Air Force Institute of Technology, Wright
Patterson, AFB, OH, 1996.

Vita

Captain David L. Byers ▓▓▓▓▓▓▓▓▓▓▓▓▓▓▓▓▓▓▓▓▓▓

▓▓▓▓▓▓▓▓▓▓▓▓. He graduated from Rangely High

School, Rangely, Colorado in 1978 and entered the Air Force

in April 1983. While serving as an automatic tracking

radar repairman on Mountain Home AFB, Idaho, he was

selected for the Airman Education and Commissioning Program.

He graduated from the University of Arizona in May 1991,

with a Bachelor of Science Double Degree in Physics and

Atmospheric Science.

After receiving his commission on 20 November 1991,

Captain Byers was assigned as the Officer-In-Charge (OIC)

of the Cadre Weather Team on Fort Carson, Colorado. He then

went to Reese AFB , Texas in August 1993 as the 64th OSS

Weather Flight Commander. Captain Byers entered the School

of Engineering, Air Force Institute of Technology in June

1995 and, upon graduation in December 1996, will be

assigned to the 50th Space Environment Squadron on Falcon

AFB, Colorado.

▓▓▓▓▓▓▓▓▓▓▓▓▓▓▓▓▓▓▓▓▓▓▓▓▓▓▓▓

▓▓▓▓▓▓▓▓▓

1. AGENCY USE ONLY (Leave blank)	2. REPORT DATE	3. REPORT TYPE AND DATES COVERED
	December 1996	Master's Thesis

4. TITLE AND SUBTITLE	5. FUNDING NUMBERS
INVESTIGATION OF BA, BAO,SR AND SRO PULSED LASER-INDUCED VAPOR PLUMES IN O/O$_2$, O$_2$, N$_2$ AND VACUUM AT LOW LASER FLUENCY	

6. AUTHOR(S)

David L. Byers, Capt, USAF

7. PERFORMING ORGANIZATION NAME(S) AND ADDRESS(ES)	8. PERFORMING ORGANIZATION REPORT NUMBER
Air Force Institute of Technology, 2750 P Street WPAFB OH 45433-7765	AFIT/GAP/ENP/96D-3

9. SPONSORING / MONITORING AGENCY NAME(S) AND ADDRESS(ES)	10. SPONSORING / MONITORING AGENCY REPORT NUMBER
Maj. Hugh DeLong AFOSR/NL 110 Duncan Ave. Bolling AFB, DC 20332-0001	

11. SUPPLEMENTARY NOTES

12a. DISTRIBUTION / AVAILABILITY STATEMENT	12b. DISTRIBUTION CODE
Approved for public release; distribution unlimited	

13. ABSTRACT (Maximum 200 words)

Ba, BaO, Sr and SrO were ablated by 248 nm laser pulses at fluences ranging from 270 mJ-cm^{-2} to 575 mJ-cm^{-2} in vacuum and in 25 mtorr atmospheres of N$_2$, O$_2$ and microwave-discharged O$_2$. The spectral emissions of these plumes were compared for indications of ionization due to Ba or Sr collisions with each gas. The addition of a background gas increased the ion and neutral signature across the spectrum. SrO band emission was observed at 16,600-16,900 cm^{-1} and possible BaO band emissions were observed in the 18,250-18,400 cm^{-1}, 19,000-19700 cm^{-1} and 19,800-20,000 cm^{-1} regions. A screened plate ion probe was use to establish the ion content of the Ba plume. A time of flight study established low-pressure (1 to 35 mtorr) and low-fluence (40 to 160 mJ-cm^{-2} relationships on Ba$^+$ velocity and population. Observed ion velocities ranged fron 3.1 km/sec. To 4.5 km/sec. Results indicate the addition of a background gas at pressures less than 25 mtorr quenches Ba$^+$ in the plume and retards the plume expansion.

14. SUBJECT TERMS		15. NUMBER OF PAGES
Ionization,Cross Section, Collisional Ionization, Pulsed Laser Ablation, Ion Probe, Langmuir Probe, Barium, Barium Oxide, Strontium, Ablation		211
		16. PRICE CODE

17. SECURITY CLASSIFICATION OF REPORT	18. SECURITY CLASSIFICATION OF THIS PAGE	19. SECURITY CLASSIFICATION OF ABSTRACT	20. LIMITATION OF ABSTRACT
Unclassified	Unclassified	Unclassified	UL